SYNTHESIS, CHARACTERIZATION AND APPLICATIONS OF HYBRID NANOCOMPOSITES OF TiO_2 WITH CONDUCTING POLYMERS

Thesis submitted to

Cochin University of Science and Technology

in partial fulfillment of the requirements for the degree of

Doctor of Philosophy

in

Chemistry

Under the Faculty of Science

By

SANDHYA K.P.

Under the Supervision of

Dr. S. SUGUNAN

DEPARTMENT OF APPLIED CHEMISTRY
COCHIN UNIVERSITY OF SCIENCE AND TECHNOLOGY
COCHIN-682 022, KERALA, INDIA

October 2014

Synthesis, Characterization and Applications of Hybrid Nanocomposites of TiO_2 with Conducting Polymers

Ph.D. Thesis under the Faculty of Science

Author:

Sandhya K.P.
Research Fellow,
Department of Applied Chemistry,
Cochin University of Science and Technology,
Cochin - 682 022, Kerala, India.
Email: sandhyakp30@gmail.com

Supervisor:

Dr. S. Sugunan
Emeritus Professor,
Department of Applied Chemistry,
Cochin University of Science and Technology,
Cochin - 682 022, Kerala, India.
Email: ssg@cusat.ac.in

October 2014

Department of Applied Chemistry
Cochin University of Science and Technology
Kochi - 682 022, India.

Dr. S. Sugunan
Emeritus Professor

Date: 24-10 -2014

Certificate

Certified that the thesis work entitled "**Synthesis, Characterization and Applications of Hybrid Nanocomposites of TiO_2 With Conducting Polymers"** submitted by **Ms. Sandhya K.P.** is an authentic record of research work carried out by her under my supervision at the Department of Applied Chemistry in partial fulfillment of the requirements for the degree of Doctor of Philosophy in Chemistry of Cochin University of Science and Technology and has not been included in any other thesis previously for the award of any other degree. All the relevant corrections and modifications suggested by the audience and recommended by the doctoral committee of the candidate during the presynopsis seminar have been incorporated in the thesis.

Dr. S. Sugunan
(Supervising Guide)

Declaration

I hereby declare that the work presented in the thesis entitled "**Synthesis, Characterization and Applications of Hybrid Nanocomposites of TiO_2 with Conducting Polymers** " is my own unaided work under the supervision of **Dr. S. Sugunan**, Emeritus Professor in Department of Applied Chemistry, Cochin University of Science and Technology, Kochi-22, and is not included in any other thesis submitted previously for the award of any other degree.

Kochi-22 **Sandhya K.P.**
24-10-2014

This thesis is dedicated to my parents and loving brother for their love, endless support and encouragement.

The fear of the LORD is the beginning of wisdom: a good understanding have all they that do his commandments":
(Psalms: 111:10).

Acknowledgement

First of all let me thank Lord Almighty for showering enormous grace upon me, blessing me with a lot of well-wishers to support and motivate me, and for providing me enough facilities to do my work, thereby enabling me to complete the work in time.

It would not have been possible to write this doctoral thesis without the help and support of the kind people around me. It is a pleasure to convey my gratitude to them all in my humble acknowledgment. Although it should be relatively simple, this part is not the easiest part of my thesis. At the moment of approaching the finish line of my PhD study, I am very grateful for all help I have received throughout these years. After finishing the above thesis, I might forget to mention a few people…but certainly they are not forgotten and they are in my mind and memories.

First and foremost I would like to thank my supervisor, Dr. S. Sugunan, for his supervision from my undergraduate studies through to the opportunity to carry out this research. His knowledge, support and enthusiasm has been exceptional and the major factor in the success of this work. One could not ask for more from a supervisor. His intellectual insight, work discipline and personal strengths have had a positive influence on my research life, for which I am grateful.

I am grateful to Dr. N. Manoj, Head of the department for providing the necessary facilities. I express my gratitude to former heads of the department, Dr. K. Girish Kumar and Dr. K. Sreekumar for their immense help during the various stages of my research. I relish the blessings and encouragement of Dr. M.R. Prathapachandra Kurup, Dr. P.A. Unnikrishnan, Dr. P.V. Mohanan and Dr. P.M. Sabura Begum. I am grateful to Dr. S. Prathapan my doctoral committee member, for providing me academic and creative thoughts that helped me a lot on several occasions.

My honest thanks to Dr.V.P.N.Nampoori, Professor, International School of Photonics, CUSAT for his help and support in doing various application studies in his department. I salute his supporting attitude that has always led me to think and work independently. Sir, without your help I could not complete my research work.

Dr. Suja Haridas who led me to the field of photocatalysis is one person whom I would render a special word of thanks.

The peaceful and loving moments shared by the non teaching staffs of the Department of Applied Chemistry, CUSAT, is always a relaxation during the continuous hours spent in the lab. I take this opportunity to thank all them.

I really feel much honored for having come across brilliant teachers who not only taught me the academic subjects but also touched the deepest chords of my heart. I would like to convey my genuine appreciation and heart-felt gratitude to all of them.

My sincere thanks to Dr.Shibu Eapen (STIC, CUSAT) for his timely help and support. I am grateful to Dr. C.Anandan, Scientist, NAL, for his prompt and thorough collection and analysis of XPS.I would like to express my gratitude to Dr.M.K.Jayaraj, Department of Physics, CUSAT for Raman analysis, Mr.Narayanan (IIT Chennai) for various analysis. I owe my special thanks to Dr.Samuel Mathew, Professor, AMPRS, Odakkali and Dr. N. Chandramohanakumar, Department of Chemical Oceanography for HPLC analysis. I would like to thank Mr. Vishnu (Alpha Chemicals), Mr.Jamal. Mr. Suresh (Chemito) for their help in various junctures.

Especially to all the colleagues of the laboratory, with whom I've had the pleasure to work during all these years, for all the good times we've had together in the lab and outside of it and for every wonderful day we've spent together. A word of appreciation for my seniors Dr.Rajesh K.M., Dr.Reni George, Dr.Ambili V.K.,Dr.Dhanya, Dr.Rose Philo K.J., Dr.Cimi A. Daniel, Nissam E, Soumini C, Mothi Krishna Mohan and Temi Robert for their judicious advice and whole hearted cooperation during my initial stages of research. I would be doing injustice to myself if I forget to convey my gratitude to my juniors Soumya and Honey. They were always with me....love u all.

Reni is like my elder sister and is always with me with her love and advice. Her support and inspiration helped me a lot during my research carrier. Special thanks to Nissam and Cimi for their constant help and encouragement. Thank you Soumini for her support, help and inspiration. Special thanks to Mothi for the research discussions, warm friendship and encouraging suggestions.

My heartful thanks to Hasna, Geetha chechi (Dept. Of Physics, CUSAT), Divya, Indhu, Sr.Rosmin, Mathew chettan (ISP, CUSAT), Saritha (Dept.of Chemical Oceanography), and friends of Biotechnology department for various analyses.

Loving thanks to Soumya H., Department of Instrumentation, CUSAT. You are with me in all the circumstances in my life.

To my friends for always being there, listening, helping me and providing me a lot of joy. Their kind cooperation, friendly company, suggestions and invaluable help during my research work has provided a stimulating and amicable environment to learn and grow. Thanks again to all of them for their memorable, pleasant and perpetual refreshment while working together in the lab. I will cherish the memories of all these years spent together as labmates. I would as well wish to express my untoward appreciations to my dear friends Jiby, Reshma, Mridula, Jisha and Jinsa for their sensible help and support.

To my family because I am who I am because of them, for being part of everything I do and of my daily life. And because they are the most important and the best of my life. To whom I dedicate this thesis. The last words are dedicated to my parents! You were always there for me, loving me and encouraging me all the time. Without you in my life I could not have accomplished it. Words are too poor to express all my love for and gratitude to you! My heartiest love for my brother Sanoop, for his constant support and inspiration. Their love provided my inspiration and was my driving force. I owe them everything and wish I could show them just how much I love and appreciate them. I also want to thank my in-laws for their unconditional support. Also I thank my sister-in-law Anu for her support and encouragement. In them, I got another family. They always inspired me to do my best. I am forever grateful to my grandparents, uncles and aunts, for their foresight and values paved the way for a privileged education and support at each turn of the road.

Words can never express my love and warmest thanks to my husband. It is with a thankful heart only I could remember the silent pain taken by my dearest husband Ratheesh E.R., who stood with me always by my side, encouraged me, wanted me to

be authentically myself, supported me to enjoy freedom in all aspects- in acquiring knowledge and in shaping my academic life.

For the financial support in carrying out this research and participation at national and international conferences, CSIR is gratefully acknowledged.

There are many others whom I didn't manage to mention in this short acknowledgement. I want to say 'Thank you' to all of you. Because of your support, I managed to reach the finish line. The work of this thesis also belongs to you.

To all and every one of you thanks for everything.

Sandhya K.P.

Preface

A nanocomposite is a multiphase solid material where one of the phases has one, two or three dimensions of less than 100 nanometers (nm), or structures having nano-scale repeat distances between the different phases that make up the material. In the broadest sense this definition can include porous media, colloids, gels and copolymers, but is more usually taken to mean the solid combination of a bulk matrix and nano-dimensional phase(s) differing in properties due to dissimilarities in structure and chemistry. The mechanical, electrical, thermal, optical, electrochemical, catalytic properties of the nanocomposite will differ markedly from that of the component materials. Size limits for these effects have been proposed, <5 nm for catalytic activity, <20 nm for making a hard magnetic material soft, <50 nm for refractive index changes, and <100 nm for achieving superparamagnetism, mechanical strengthening or restricting matrix dislocation movement. Conducting polymers have attracted much attention due to high electrical conductivity, ease of preparation, good environmental stability and wide variety of applications in light-emitting, biosensor chemical sensor, separation membrane and electronic devices. The most widely studied conducting polymers are polypyrrole, polyaniline, polythiophene etc.

Conducting polymers provide tremendous scope for tuning of their electrical conductivity from semiconducting to metallic region by way of doping and are organic electro chromic materials with chemically active surface. But they are chemically very sensitive and have poor mechanical properties and thus possessing a processibility problem. Nanomaterial shows the presence of more sites for surface reactivity, they possess good mechanical properties and good dispersant too. Thus nanocomposites formed by combining conducting polymers and inorganic oxide nanoparticles, possess the good properties of both the constituents and thus enhanced their utility. The properties of such type of nanocomposite are strongly depending on concentration of nanomaterials to be added.

Conducting polymer composites is some suitable composition of a conducting polymer with one or more inorganic nanoparticles so that their desirable properties are combined successfully. The composites of core shell metal oxide particles-conducting polymer combine the electrical properties of the polymer shell and the magnetic, optical, electrical or catalytic characteristics of the metal oxide core, which could greatly widen their applicability in the fields of catalysis, electronics and optics. Moreover nanocomposite material composed of conducting polymers & oxides have open more field of application such as drug delivery, conductive paints, rechargeable batteries, toners in photocopying, smart windows, etc

The thesis is organized into eight chapters. Chapter 1 gives concise introduction and literature survey to the topic of study. Second chapter focuses the materials and method adopted for the present work. Third chapter deals with the physico-chemical characterization of the prepared nanocomposite systems. Chapter 4-7 elucidates the application s of the prepared nanocomposite systems towards various applications. Last chapter includes the summary of the investigations and conclusions drawn from the work.

Contents

…..ஜ۞ஜ…..

Chapter 1

INTRODUCTION AND LITERATURE SURVEY

Contents

Nanocomposites, a high performance material exhibit unusual property combinations and unique design possibilities. Polymeric materials containing metal oxide particles constitute a new class of polymer composites materials. The main purpose of the preparation of the nanocomposite is to obtain the synergic effect of the polymer and the inorganic compound. Nanocomposites have a peculiar structure, i.e. a phase separated structure, with a nanoscale interface between the polymer matrix and the inorganic compound (nanophase separated structure). This phase separated structure plays a very important role in the production of a molecular-level synergic effect between the organic and inorganic compounds in nanocomposites. Conducting polymers are combined with metal oxides because of their enhanced physical and electronic properties. Nanocomposite material composed of conducting polymers & oxides have open more field of application such as drug delivery, conductive paints, rechargeable batteries, toners in photocopying, smart windows, etc.

1.1. Introduction

Progress in the field of materials science has taken a new lead since the advent of the nanocluster-based materials or nanocomposites. Nanoclusters are ultrafine particles of nanometer dimensions and whose characteristics are size dependent and are different from those of the atomic and bulk counterparts [1]. Recently nanocomposite materials have become one of the most extensively studied material all over the world as they have shown to possesses several technological application such as effective quantum electronic devices, magnetic recording materials sensors etc [2]. Nanocomposites are as multiphase materials, where one of the phases has nanoscale additives and are originating from suitable combinations of two or more such nanoparticles or nanosized objects in some suitable technique, resulting in materials having unique physical properties and wide application potential in diverse areas [1,3]. Novel properties of nanocomposites can be derived from the successful combination of the characteristics of parent constituents into a single material. Materials scientists very often handle such nanocomposites, which are an effective combination of two or more inorganic nanoparticles. They are expected to display unusual properties emerging from the combination of each component [3]. Organic-inorganic composites have attracted considerable attention as they can combine the advantages of both components and may offer special properties through reinforcing or modifying each other [4]. To exploit the full potential of the technological applications with good processability which has ultimately guided scientists toward using conventional polymers as one component of the nanocomposites, resulting in a special class of hybrid materials termed “polymeric nanocomposites”[1]. Significant scientific and technological interest has focused on polymer-inorganic nanocomposites (PINCs) over the last two decades. The use of

inorganic nanoparticles into the polymer matrix can provide high-performance novel materials that find applications in many industrial fields. As a result of the development in nanotechnology, inorganic nanostructured materials have been designed/discovered and fabricated with important cooperative physical phenomena such as superparamagnetism, size-dependent band-gap, ferromagnetism, electron and phonon transport. Yet, they typically suffer from high manufacture expense, and the shaping and further processing of these materials is often difficult and demanding or impossible [5]. These materials are also intimate combinations (up to almost molecular level) of one or more inorganic nanoparticles with a polymer so that unique properties of the former can be taken together with the existing qualities of the latter. Many investigations [6] regarding the development of the incorporation techniques of the nanoparticles into the polymeric matrices have been published. In most of the cases [7] such combinations require blending or mixing of the components, taking the polymer in solution or in melt form.

According to their matrix materials, nanocomposites can be classified as ceramic matrix nanocomposites (CMNC), metal matrix nanocomposites (MMNC), and polymer matrix nanocomposites (PMNC). Organic polymer-based inorganic nanoparticle composites have attracted increasing attention because of their unique properties emerging from the combination of organic and inorganic hybrid materials. Generally, the resultant nanocomposites display enhanced optical, mechanical, magnetic and optoelectronic properties. Therefore, these composites have been widely used in the various fields such as military equipment, safety, protective garments, automotive, aerospace, electronics and optical devices [3]. Moreover nanocomposite material composed of conducting polymers & oxides have open more field of application such as drug

delivery, conductive paints, rechargeable batteries, toners in photocopying, smart windows etc [8, 9].

Synthesis of polymer composites of core shell inorganic particle-polymer has attracted much research attention in recent years because of its properties [10, 11]. In particular, the composites of core shell metal oxide particles-conducting polymer combine the electrical properties of the polymer shell and the magnetic, optical, electrical or catalytic characteristics of the metal oxide core, which could greatly widen their applicability in the fields of catalysis, electronics and optics [12].

Polymers are already widely used in the optoelectronics industry and are playing important roles in various applications. Therefore, the drawbacks of using inorganic nanostructured materials can be overcome by employing a polymer matrix to embed a relatively small content of inorganic nanoparticles. The integration of inorganic nanoparticles into a polymer matrix allows both properties from inorganic nanoparticles and polymer to be combined/enhanced and thus advanced new functions can be generated to the PINCs [13]. The PINCs are one kind of composite materials comprising of nanometer-sized inorganic nanoparticles, typically in the range of 1-100 nm, which are uniformly dispersed in and fixed to a polymer matrix. In this way, the inorganic nanoparticles are acting like 'additives' to enhance polymer performance and thus are also termed 'nano-fillers' or 'nano-inclusions' [14, 15].

Among various PINCs, there is a new class of PINCs comprised of a polymer matrix with 'transparent nano-fillers' that is usually fabricated by in-situ polymerization for the formation of nanocomposite and sol-gel methods for the formation of nano-fillers. This class of material is also sometimes called polymer-inorganic 'hybrid/nanohybrid' [16, 17].

These nanocomposite materials are especially important due to their bridging role between the world of conducting polymers and that of inorganic materials. Inorganic nanoparticles of different nature and size can be combined with the conducting polymers, giving rise to a host of nanocomposites with interesting physical properties and important application potential. Inorganic materials used for this purpose are generally of two types: nanoparticles and some nanostructured materials or templates. Depending upon the nature of association between the inorganic and organic components, nanocomposites are also classified into two categories: one in which the inorganic particle is embedded in organic matrix and the other where organic polymer is confined into inorganic template. However, in each case the composite formation demands some entrapment or encapsulation (Scheme 1) rather than simple blending or mixing [1].

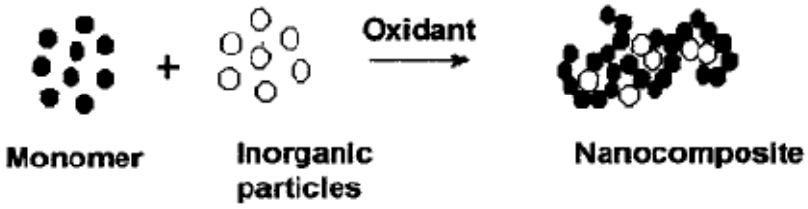

Scheme 1.1. Formation of Nanocomposite from the Constituents

Inorganic nanoparticles can be introduced into the matrix of a host-conducting polymer either by some suitable chemical route or by an electrochemical incorporation technique. These two synthesis techniques have given birth to materials that are widely different from one another in common physical properties. However, each synthesis route opens a way to a group of materials with complementary behaviour between two components. Chemical origins as well as the special properties of the incorporated materials viz. its

catalytic property, magnetic susceptibility, colloidal stability, etc. always add new dimensions to the characteristics of the resulting composites and have accordingly divided them into different subgroups [1].

Table 1.1. shows relevant categorization of the nanocomposites as followed here [1].

Table 1.1. Categorization of the nanocomposites

Conducting Polymer Nanocomposites

Inorganic-in-Organic | Organic –in-Inorganic

Chemical Preparation	**Electrochemical Preparation**
1) Nanocomposites with Colloidal stability (SiO_2, SnO_2, $BaSO_4$) etc are core materials). 2) Nanocomposites with improved physical and mechanical properties (Fe_2O_3, ZrO_2, TiO_2 etc are incorporated materials). 3) Nanocomposites with magnetic susceptibility (using Fe_3O_4, γ-Fe_2O_3 etc as magnetic particles). 4) Nanocomposites with dielectric, energy storage, piezoresitive and catalytic activities (with BT, POM, PtO_2, TiO_2, Pt, Pd etc incorporation) 5) Nanocomposites with surface functionalization (-NH_2/-COOH functional groups on surface and colloidal silica as core).	1) Nanocomposites with charge storage, optical and electrochromic activities (Incorporation of MnO_2, SnO_2, CB, PB, WO_3, SiO_2 etc). 2) Nanocomposites with catalytic activities (incorporation of catalytically active Pd, Pt, Cu etc. microparticles and some bimetallic couples like Pd/Cu etc). 3) Nanocomposites with magnetic susceptibility (γ-Fe_2O_3, magnetic macro anion).

1.2. Hybrid Materials and Nanocomposites

The term hybrid material is used for many different systems spanning a wide area of different materials, such as crystalline highly ordered coordination polymers, amorphous sol–gel compounds, materials with and without interaction between the inorganic and organic units. The most wide-ranging definition is the following: a hybrid material is a material that includes two moieties blended on the molecular scale. Commonly one of these compounds is inorganic and the other one organic in nature. A more detailed definition distinguishes between the possible interactions connecting the inorganic and organic species. *Class I* hybrid materials are those that show weak interactions between the two phases, such as Van der Waals, hydrogen bonding or weak electrostatic interactions. *Class II* hybrid materials are those that show strong chemical interactions between the components. Because of the gradual change in the strength of chemical interactions it becomes clear that there is a steady transition between weak and strong interactions. For example there are hydrogen bonds that are definitely stronger than for example weak coordinative bonds [18].

The so-called hybrid organic–inorganic materials [19] are not simply physical mixtures. They can be broadly defined as nanocomposites with organic and inorganic components, intimately mixed. Indeed, hybrids are either homogeneous systems derived from monomers and miscible organic and inorganic components, or heterogeneous systems (nanocomposites) where at least one of the components' domains has a dimension ranging from some A° to several nanometers [20]. It is obvious that properties of these materials are not only the sum of the individual contributions of both phases, but the role of the inner interfaces could be predominant. The nature of the interface has

been used to divide these materials grossly into two distinct classes [20]. In class I, organic and inorganic components are embedded and only weak bonds (hydrogen, van der Waals or ionic bonds) give the cohesion to the whole structure. In class II materials the two phases are linked together through strong chemical bonds (covalent or iono-covalent bonds) [19]. Maya blue is a beautiful example of a remarkable quite old man-made class I hybrid material whose conception was the fruit of an ancient serendipitous discovery. Maya blue is a hybrid organic–inorganic material with molecules of the natural blue indigo encapsulated within the channels of a clay mineral known as palygorskite. It is a man made material that combines the color of the organic pigment and the resistance of the inorganic host, a synergic material, with properties and performance well beyond those of a simple mixture of its components. Paints are a good link between Mayas and modern applications of hybrids [19].

Different chemical interactions and their respective Strength [18]

Type of Interaction	Strength (kJ/mol)	Range	Character
Van der Waals	ca.50	Short	Nonselective, Nondirectional
H-bonding	5-65	Short	Selective, Directional
Coordination bonding	50-200	Short	Directional
Ionic	50-250[a]	Short	Nonselective
Covalent	350	Short	Predominantly irreversible

[a] **Depending on solvent and ion solution; data are for organic media**

In addition to the bonding characteristics, structural properties can also be used to distinguish between various hybrid materials. An organic moiety containing a functional group that allows the attachment to an inorganic network, e.g. a trialkoxysilane group, can act as a network modifying

compound because in the final structure the inorganic network is only modified by the organic group. The situation is different if two or three of such anchor groups modify an organic segment; this leads to materials in which the inorganic group is afterwards an integral part of the hybrid network

Blends are formed if no strong chemical interactions exist between the inorganic and organic building blocks. One example for such a material is the combination of inorganic clusters or particles with organic polymers lacking a strong (e.g. covalent) interaction between the components (Scheme 1.2a). In this case a material is formed that consists for example of an organic polymer with entrapped discrete inorganic moieties in which, depending on the functionalities of the components, for example weak cross linking occurs by the entrapped inorganic units through physical interactions or the inorganic components are entrapped in a cross linked polymer matrix. If an inorganic and an organic network interpenetrate each other without strong chemical interactions, so called interpenetrating networks (IPNs) are formed (Scheme 1.2b), which is for example the case if a sol–gel material is formed in presence of an organic polymer or vice versa. Both materials described belong to class I hybrids. Class II hybrids are formed when the discrete inorganic building blocks, e.g. clusters, are covalently bonded to the organic polymers (Scheme 1.2c) or inorganic and organic polymers are covalently connected with each other (Scheme 1.2d) [18].

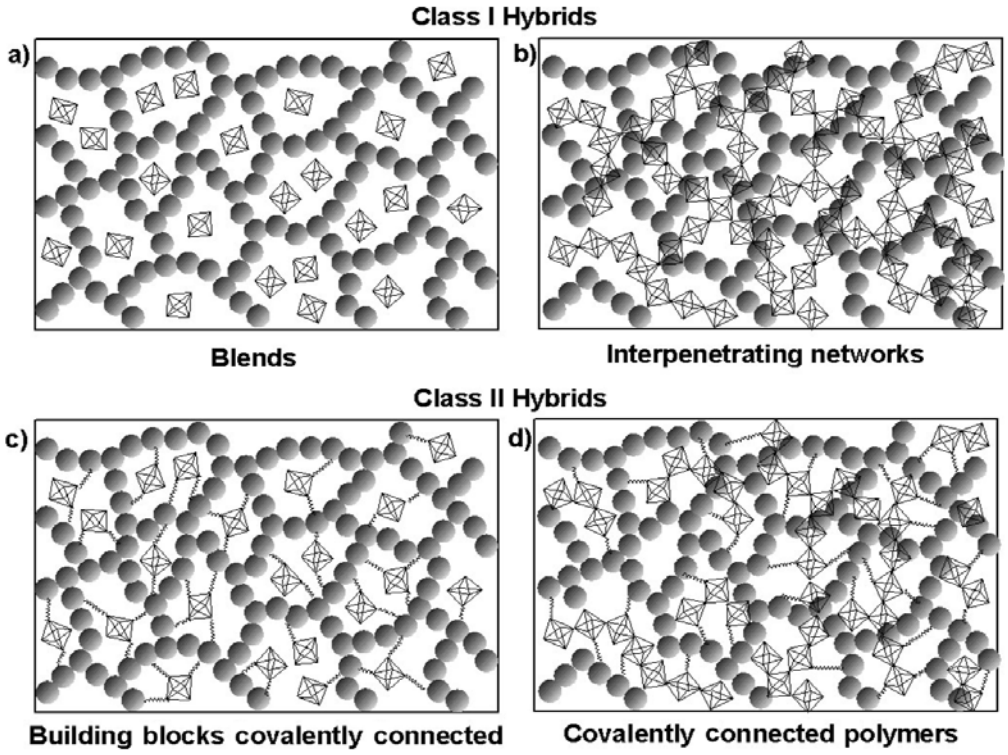

Scheme 1.2. The different types of hybrid materials.

In fact there is no clear borderline between these materials. The term nanocomposite is used if one of the structural units, either the organic or the inorganic, is in a defined size range of 1–100 nm.

There is a gradual transition between hybrid materials and nanocomposites, because large molecular building blocks for hybrid materials, such as large inorganic clusters, can already be of the nanometer length scale. Commonly the term nanocomposites is used if discrete structural units in the respective size regime are used and the term hybrid materials is more often used if the inorganic units are formed *in situ* by molecular precursors, for example applying sol–gel reactions. Examples of discrete inorganic units for nanocomposites are nanoparticles, nanorods, carbon nanotubes and galleries of clay minerals.

Usually a nanocomposite is formed from these building blocks by their incorporation in organic polymers [18].

1.3. Synthetic Strategies towards Hybrid Materials

In principle two different approaches can be used for the formation of hybrid materials: Either well-defined preformed building blocks are applied that react with each other to form the final hybrid material in which the precursors still at least partially keep their original integrity or one or both structural units are formed from the precursors that are transformed into a novel (network) structure.

1.3.1. Building block approach

Building blocks at least partially keep their molecular integrity throughout the material formation, which means that structural units that are present in these sources for materials formation can also be found in the final material. At the same time typical properties of these building blocks usually survive the matrix formation, which is not the case if material precursors are transferred into novel materials. Representative examples of such well-defined building blocks are modified inorganic clusters or nanoparticles with attached reactive organic groups.

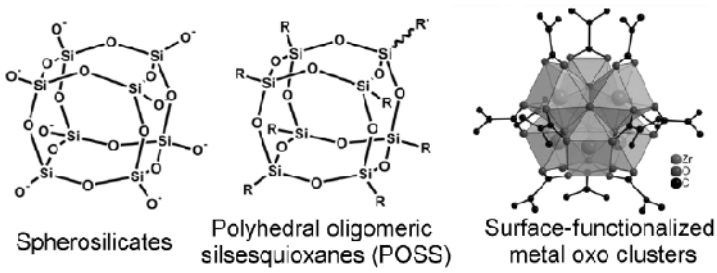

Fig.1.1. Typical well-defined molecular building blocks used in the formation of hybrid materials.

1.3.2. Insitu formation of the components

Contrary to the building block approach the *in situ* formation of the hybrid materials is based on the chemical transformation of the precursors used throughout materials' preparation. Typically this is the case if organic polymers are formed but also if the sol–gel process is applied to produce the inorganic component. In these cases well-defined discrete molecules are transformed to multidimensional structures, which often show totally different properties from the original precursors. The insitu formation method can be any one of the following: (1) Insitu Formation of Inorganic Materials (2) Formation of Organic Polymers in Presence of Preformed Inorganic Materials (3) Hybrid Materials by Simultaneous Formation of Both Components. Here we are interested in Formation of Organic Polymers in Presence of Preformed Inorganic Materials.

1.3.2.1. Formation of Organic polymers in presence of preformed inorganic materials

If the organic polymerization occurs in the presence of an inorganic material to form the hybrid material one has to distinguish between several possibilities to overcome the incompatibility of the two species. The inorganic material can either have no surface functionalization but the bare material surface; it can be modified with nonreactive organic groups (e.g. alkyl chains); or it can contain reactive surface groups such as polymerizable functionalities. Depending on these prerequisites the material can be pre-treated, for example a pure inorganic surface can be treated with surfactants or silane coupling agents to make it compatible with the organic monomers, or functional monomers can be added that react with the surface of the inorganic material. If the inorganic component has nonreactive organic

groups attached to its surface and it can be dissolved in a monomer which is subsequently polymerized, the resulting material after the organic polymerization is a blend. In this case the inorganic component interacts only weakly or not at all with the organic polymer; hence, is a class I material formed.

If a porous 3-D inorganic network is used as the inorganic component for the formation of the hybrid material a different approach has to be employed depending on the pore size, the surface functionalization of the pores and the stiffness of the inorganic framework. In many cases intercalation of organic components into the cavities is difficult because of diffusion limit. The composites obtained can be viewed as host–guest hybrid materials. There are two possible routes towards this kind of hybrid material; (a) direct threading of preformed polymer through the host channels (soluble and melting polymers) which is usually limited by the size, conformation, and diffusion behaviour of the polymers and (b) the *in situ* polymerization in the pores and channels of the hosts. The latter is the most widely used method for the synthesis of such systems. Of course, diffusion of the monomers in the pores is a function of the pore size; therefore the pores in zeolites with pore sizes of several hundred picometers are much more difficult to use in such reactions than mesoporous materials with pore diameters of several nanometers. Two methods proved to be very valuable for the filling of the porous structures with monomers: one is the soaking of the materials in liquid monomers and the other one is the filling of the pores in the gas phase. A better uptake of the monomers by the inorganic porous materials is achieved if the pores are pre-functionalized with organic groups increasing the absorption of monomers on the concave surface [18].

1.4. Properties and Applications

There is almost no limit to the combinations of inorganic and organic components in the formation of hybrid materials. Therefore materials with novel composition– property relationships can be generated that have not yet been possible. Based on the increased importance of optical data transmission and storage, optical properties of materials play a major role in many high-tech applications. The materials used can reveal passive optical properties, which do not change by environmental excitation, or active optical properties such as photochromic (change of color during light exposure) or electrochromic (change of color if electrical current is applied) materials. Silica is preferred as the inorganic component in such applications because of its low optical loss. Other inorganic components, for example zirconia, can incorporate high refractive index properties, or titania in its rutile phase can be applied for UV absorbers. Functional organic molecules can add third order nonlinear optical (NLO) properties and conjugated polymers, conductive polymers can add interesting electrical properties. The enhancement of mechanical and thermal properties of polymers by the inclusion of inorganic moieties, especially in the form of nanocomposites, offers the possibility for these materials to substitute classical compounds based on metals or on traditional composites in the transportation industry or as fire retardant materials for construction industry [18].

Organic–inorganic hybrid materials do not represent only a creative alternative to design new materials and compounds for academic research, but their improved or unusual features allow the development of innovative industrial applications. Nowadays, most of the hybrid materials that have already entered the market are synthesised and processed by using conventional soft chemistry based routes developed in the eighties. Looking to

the future, there is no doubt that these new generations of hybrid materials, born from the very fruitful activities in this research field, will open a land of promising applications in many areas: optics, electronics, ionics, mechanics, energy, environment, biology, medicine for example as membranes and separation devices, functional smart coatings, fuel and solar cells, catalysts, sensors, etc [19, 20].

1.5. Photocatalysis

From the beginning of the 21st century there has been an increasing demand for the implementation of clean energy technologies rendering little or no environmental footprint. However, until such time that clean, non-carbon based energy becomes a reliable and affordable commodity, environmental pollution abatement for a multitude of everyday industrial and domestic activities remains a crucial responsibility. Amongst the many abatement strategies known, semiconductor mediated photocatalysis has been a subject of vigorous academic research for the past 20 years. Due to the largely insoluble nature of the catalysts during application, the area of semiconductor photocatalysis (SP) invariably constitutes a heterogeneous catalytic system that adheres to the five discrete processes associated with conventional heterogeneous catalysis:

1) Transfer of liquid or gaseous phase reactants to the catalytic surface
2) Adsorption of at least one reactant
3) Reaction in the adsorbed phase
4) Desorption of product(s).
5) Removal of products from the interface region [21].

Photocatalysis is a rapidly developing field of research with a high potential for a wide range of industrial applications, which includes mineralisation of organic pollutants, disinfection of water and air, production of renewable fuels and organic synthesis. A great deal of attention has been devoted in the last years to photocatalytic processes both in the homogeneous phase and in heterogeneous systems. In its broadest sense, photocatalysis concerns the use of light to induce chemical transformations on organic or inorganic substrates that are transparent in the wavelength range employed. Radiation is absorbed by a photocatalyst whose electronically excited states induce electron- or energy-transfer reactions able to trigger the chemical reactions of interest [22-24].

Photocatalysis process, as an environmental application is a relatively novel subject with tremendous potential in the near future. It can be defined as the acceleration of photoreaction in the presence of a catalyst. The initial interest in the heterogeneous photocatalysis was started when Fujishima and Honda discovered in 1972 the photochemical splitting of water into hydrogen and oxygen with TiO_2 [25]. From this date extensive work has been carried out to produce hydrogen from water by this novel oxidation reduction reaction using a variety of semiconductors. In heterogeneous photocatalysis two or more phases are used in the photocatalytic reaction. A light source with semiconductor material is used to initiate the photoreaction. The catalysts can carry out substrate oxidations and reductions simultaneously. UV light of long wavelengths can be used, possibly even sunlight [26].

The concept photocatalysis and, of greater importance here, heterogeneous photocatalysis were first introduced in the second decade (1910–1920) of the 20^{th} century. In his introductory remarks into the origins of photocatalysis,

Teichner affirmed that the study of photocatalytic reactions began in the early part of the 1970s, and that the concept and the term heterogeneous photocatalysis (or photocatalyse hétérogène) was introduced and developed at the Institut de Catalyse and at the Université Claude Bernard in Lyon (France) in 1970 to describe the partial oxidation of alkanes and olefinic hydrocarbons, the photoinduced reactions of CO, SO_2, and NO in the presence of TiO_2, the partial photooxidation of various paraffins to aldehydes and ketones also in the presence ofTiO_2, as well as an exhaustive study into the reactivity of various carbon atoms for photooxidation reactions [27,28].

Heterogeneous photocatalysis is an advanced oxidation process which is the subject of a huge amount of studies related to environment recovery, such as air cleaning and water purification, in which organic and inorganic pollutants are totally degraded to innocuous substances over mainly TiO_2 photocatalysts [25, 29].

It also includes a large variety of reactions: mild or total oxidations, dehydrogenation, hydrogen transfer, oxygen-18 and deuterium isotopic exchange, metal deposition, water detoxification, gaseous pollutant removal, bactericidal action etc. In line with the last point, it can be considered as one of the new ‘‘Advanced Oxidation Technologies’’ (AOT) for air and water purification treatments [30].

Attributes of an ideal photocatalyst for heterogeneous photocatalysis

1) Stability and sustained photoactivity
2) Biologically and chemically inert, non toxic
3) Low cost
4) Suitability towards visible or near UV light

5) High conversion efficiency and high quantum yield

6) Can react with wide range of substrate and high adaptability to various environments

7) Good adsorption in solar spectrum [31].

During the last two decades much attention has been paid to the reactions that take place on the illuminated surface of semiconductor metal oxides and sulfides. These compounds, mainly TiO_2, ZnO, CdS, WO_3, etc., are semiconductors, i.e. they have a moderate band-gap between their valence and conduction bands. Under illumination by photons of energy greater than band-gap energies, the valence band electrons can be excited to the conduction band, creating highly reactive electron-hole pairs. After migration to the solid surface, these may undergo electron-transfer processes with adsorbates of suitable redox potentials. In this way, these semiconductor compounds act (if the reaction exhibits a positive free energy gain), or catalytic photoassisted reactions (negative gain).

Among semiconductor photocatalytic materials, TiO_2 becomes a most important one because of its advantages of high photocatalytic activity, strong ultraviolet radiation shielding, good thermal conductivity, good dispersibility, cheap, non-toxic, and no secondary pollution etc.

1.5.1. Photocatalysis by TiO_2

Titanium dioxide (TiO_2) is an n-type semiconductor [32]. Photocatalysis technology with titanium dioxide (TiO_2) photocatalyst has attracted extensive attention because of its low cost, nontoxicity, and structural stability. TiO_2 photocatalyst could be activated only by UV light due to its large energy band gap (ca. 3.2 eV for anatase). On the other hand, TiO_2 has a small surface area

and low adsorbability, which results in low photocatalytic efficiency in much diluted solutions [33-37]. The actual efficiency of titanium dioxide depends not only on its phase composition, but also on the particle size, morphology, and porosity [38]. Anatase form has been found to exhibit higher activity compared to the rutile. Although the mechanism responsible for this is a controversial subject, at present there are four hypotheses seeking explanation for this behaviour are (1) crystal size, surface area, defect population and porosity (2) higher Fermi level (3) indirect band gap and (4) excitation electron mass [40]. Higher photocatalytic activity of anatase is usually attributed to its larger specific surface area. Poor adsorption and low surface area properties lead to great limitations in exploiting the photocatalyst to the best of its photoefficiency. On the other hand, lower photocatalytic activity of the rutile sample is probably related to the lower specific surface area due to calcination at temperatures above 950°C [38]. TiO_2 photocatalysis has shown great promise as an innovative and "green" technology due to its ability to generate electron and holes under UV illumination, which can produce radicals and/or initiate redox reactions to degrade trace level environmental pollutants. Starting in the late 1960s, we had involved in an unfolding story whose main character is the fascinating material titanium dioxide (TiO_2) [41]. In 1972, Fujishima and Honda discovered the phenomenon of photocatalytic splitting of water on a TiO_2 electrode under ultraviolet (UV) light [25, 32, 42]. Since then, enormous efforts have been devoted to the research of TiO_2 material, which has led to many promising applications in areas ranging from photovoltaics and photocatalysis to photo-electrochromics and sensors [43-46]. Even though titanium dioxide is the most widely used photocatalyst, there are several limitations that make its activity far from optimum [26, 47]. Particularly, the wide band gap of TiO_2 restricts photoexcitation of this

semiconductor to the UV region with onset about 350 nm. Also, the electron–hole recombination of the photoinduced charge separated state represents an energy wastage that is detrimental for the photocatalytic activity. It has been estimated that the amount of solar energy reached on the earth every day is more than that mankind could use for 30 years. In whole energy of incoming solar spectrum, ultraviolet radiation ($\lambda < 400$ nm) accounts to only less that 4%, while the visible light is more than 50%. Hence, effective utilization of the visible light of solar radiation, as in the photosynthesis of plants, is a long ''dream'' of the photochemical researchers. Visible light activated TiO_2 can be prepared by several methods, including metal-ion implantation, reducing of TiO_2, sensitizing of TiO_2 with dyes, or non-metal doping by incorporation of various dopants into the TiO_2 lattice [48,49]. Hence, doping a foreign element into TiO_2 has been performed since the early 1980s. For example, studies, which substitute d transition metal ions for Ti sites, have been performed. In 2001, N-doped TiO_2 in which a nitrogen atom is substituted for a lattice oxygen site was reported as a visible light sensitive photocatalyst, and has attracted a lot of attention. Since then, various types of TiO_2 doped with anions such as sulphur, carbon, etc. have been extensively studied. In the N-doped TiO_2, the localized N 2p level in the forbidden band is the origin of the visible light sensitivity. The hole mobility in the localized N 2p level should be very low. Moreover, the oxidation power of holes produced in the N 2p level by visible light is low due to its potential of 2.25 V (vs. SHE). Thus, we concluded that the photo-produced holes in the valence band of TiO_2 with high mobility and oxidation power should be utilized to obtain high activity even under visible light.

1.5.2. Characteristics of TiO_2 photocatalyst.

1. High oxidizing ability

   As oxidative OH radicals produced by TiO_2 photocatalysis have high oxidation potential, TiO_2 photocatalyst exhibits high oxidizing ability.

2. Chemical stability

   TiO_2 is chemically stable and not dissolved in water; although some other semiconductive photocatalytic compounds are dissolved when irradiated in water. TiO_2 is so chemically stable that it is not dissolved in almost all acidic, basic and organic solvent.

3. Safety

   A safe and inert material in general.

1.5.3. Potential Applications

- Wastewater & potable water treatment
- Air toxics abatement
- Disinfection & Self Cleaning Devices
- Hydrogen production (water splitting) [50]

1.5.4. Advantages of TiO_2 Photocatalyst

- Photostable, cheap & reusable
- Chemically & biologically inert
- High Activity
- Operate at ambient temperature
- Ideal to treat trace level pollutants

1.5.5. Titanium dioxide

Pure titanium dioxide does not occur in nature but is derived from ilmenite or leuxocene ores. It is also readily mined in one of the purest forms,

rutile beach sand [51]. Titanium Dioxide (TiO_2) has a wide range of applications. Since its commercial production in the early twentieth century, it is used as a pigment in paints, coatings, sunscreens, ointments and toothpaste. TiO_2 is considered as a "quality–of–life" product with demand affected by gross domestic product in various regions of the world. Titanium dioxide pigments are inorganic chemical products used for imparting whiteness, brightness and opacity to a diverse range of applications and end–use markets. TiO_2 as a pigment derives value from its whitening properties and opacifying ability (commonly referred to as hiding power). As a result of TiO_2's high refractive index rating, it can provide more hiding power than any other commercially available white pigment [52].

1.5.5.1. Structure of TiO_2

Titanium dioxide is a polymorphic compound having three polymorphous structures; anatase, rutile and brookite. Both anatase and rutile are tetragonal, whereas brookite is orthorhombic. Rutile is the preferred polymorph of TiO_2 in such environments because it has the lowest molecular volume of the three polymorphs; it is thus the primary titanium bearing phase in most high pressure metamorphic rocks, chiefly eclogites. Brookite and anatase are typical polymorphs of rutile formed by retrogression of metamorphic rutile.

In all the three modifications, each titanium atom is coordinated to six almost equidistant oxygen atoms and each oxygen atom to three titanium atoms [53]. The octahedra differ however in rutile anatase and brookite with respect to their spacing relative to each other. In the case of anatase TiO_6 octahedron is slightly distorted, with two Ti-O bonds slightly greater than the other four and with some of the O-Ti-O bond angles deviating from 90^o. Distortion is greater in anatase compared to rutile. The structure of anatase and

rutile has been described frequently in terms of chains of TiO_6 octahedra having common edges. Two or four edges are shared in rutile and anatase respectively. In brookite the interatomic distance and Ti-O- Ti bond angles are similar to those of rutile and anatase. Brookite is formed by joining together the distorted TiO_6 octahedra sharing three edges.

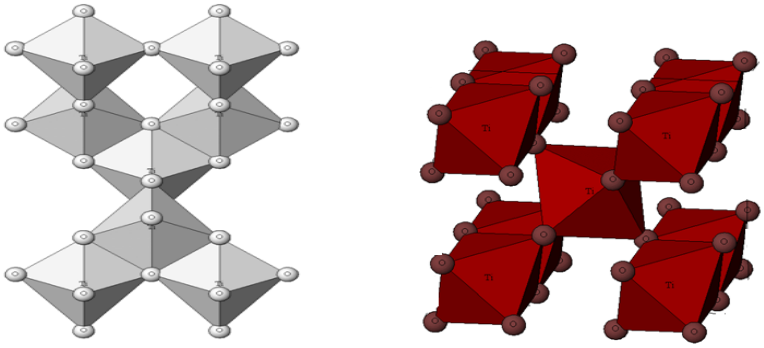

Anatase **Rutile**

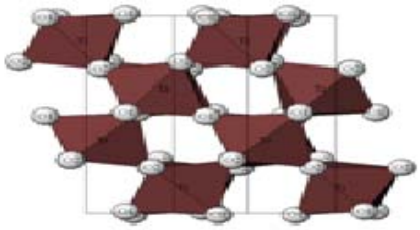

Brookite

Fig.1.2. Structures of Anatase, Rutile and Brookite

Rutile has a primitive tetragonal unit cell, with unit cell parameters a=4.584Å, c=2.953Å and Z=2.It is having the space group 136 and point group 4/m 2/m 2/m. The titanium cations have a co-ordination number of 6 meaning they are surrounded by an octahedron of 6 oxygen atoms. The oxygen anions have a co-ordination number of 3 resulting in a trigonal planar

co-ordination. In rutile there is hexagonal close packing of oxygen atoms, in which half of the octahedral spaces are filled with titanium atoms [54].

Anatase belongs to tetragonal crystal system with unit cell parameters a = 3.7845 Å, c = 9.5143 Å; Z = 4. It is having the point group: 4/m 2/m 2/m and space group I41/amd. In the case of anatase, (cubic close packing of oxygen atoms) half of tetrahedral spaces are filled with titanium atoms.

Brookite belongs to the orthorhombic dipyramidal crystal class 2/m 2/m 2/m (also designated mmm). The space group is Pcab and the unit cell parameters are a = 5.4558 Å, b = 9.1819 Å, c = 5.1429 Å and Z= 8. Brookite TiO_2 has an orthorhombic unit constructed by an octahedron of oxygen ions arranged about a single titanium ion. Each octahedron shares three edges with adjoining octahedra.

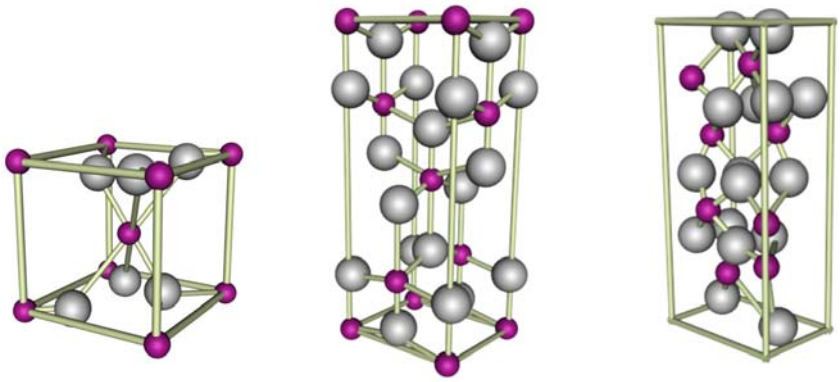

Fig.1.3. Unit cells of (A) rutile, (B) anatase and (C) brookite. Grey and red spheres represent oxygen and titanium, respectively

1.5.6. Mechanism of Photocatalysis

Photocatalytic processes involve the initial absorption of photons by a molecule or the substrate to produce highly reactive electronically excited

states. The efficiency of the photoinduced chemistry is controlled by the system's light absorption characteristics. In a compound semiconductor consisting of different atoms, the valence band and conduction band formation processes are complicated, but the principles involved are the same [55]. Unlike metals which have a continuum of electronic states, semiconductors possess a void energy region where no energy levels are available to promote recombination of an electron and hole produced by photoactivation in the solid. The void region which extends from the top of the filled valence band to the bottom of the vacant conduction band is called the band gap. The initial process for heterogeneous photocatalysis of organic and inorganic compounds by semiconductors is the generation of electron-hole pairs in the semiconductor particles [56]. The valence band of titanium oxide is comprised of the 2p orbital of oxygen (O), while the conduction band is made up of the 3d orbital of titanium (Ti). Photocatalytic mechanism is initiated by the absorption of the photon of energy *hv* which is equal to or greater than the band gap of TiO_2 (~3.3 eV for the anatase phase) producing an electron-hole pair on the surface of TiO_2. An electron is promoted to the conduction band (CB) while a positive hole is formed in the valence band (VB). Excited-state electrons and holes can recombine and dissipate the input energy as heat, get trapped in metastable surface states, or react with electron donors and electron acceptors adsorbed on the semiconductor surface or within the surrounding electrical double layer of the charged particles. After reaction with water, these holes can produce hydroxyl radicals with high redox potential [57].

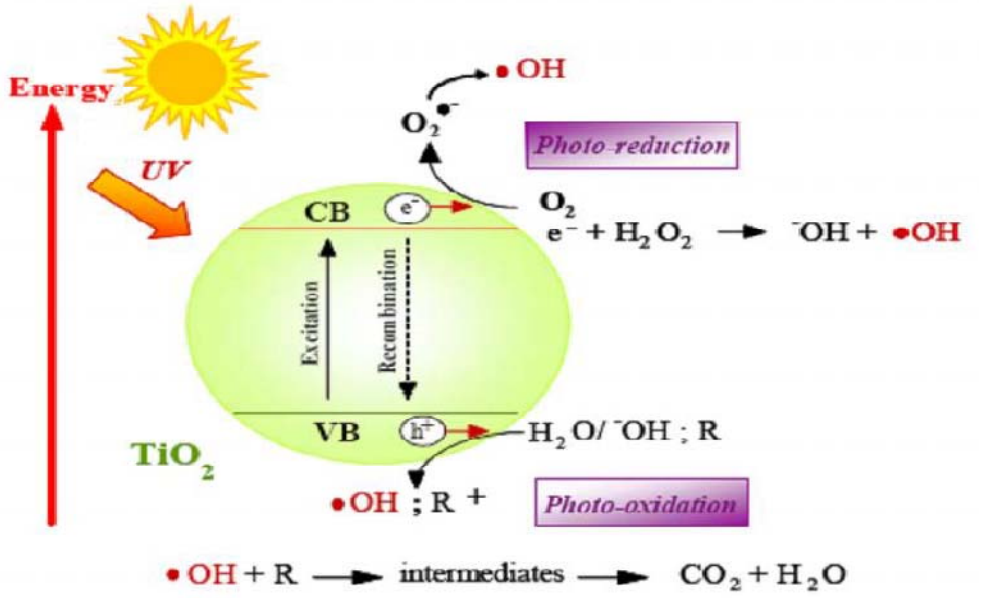

Fig.1.4. General Mechanism of Photocatalytic degradation

1.6. Hybridization with Conducting Polymers-A Fine way to tune the Photocatalytic Activity in the Visible Region

Polymers that conduct electric currents without the addition of conductive (inorganic) substances are known as "intrinsically conductive polymers" (ICP). Conducting polymers is a prospective class of new materials that combine solubility, processability, and flexibility of plastics with electrical and optical properties of metals and semiconductors. The discovery of conducting polymers opened up many new possibilities for devices combining unique optical, electrical, and mechanical properties [58]. Conductive polymers or, more precisely, intrinsically conducting polymers (ICPs) are organic polymers that conduct electricity [59]. Such compounds may have metallic conductivity or can be semiconductors. The biggest advantage of conductive polymers is their processability, mainly by dispersion. Conductive polymers are generally not thermoplastics, i.e., they are not thermo formable. But, like insulating polymers,

they are organic materials. They can offer high electrical conductivity but do not show similar mechanical properties to other commercially available polymers [60]. Intrinsically conducting polymers, also known as "synthetic metals", are polymers with a highly conjugated polymeric chain [61-63]. For the discovery of conducting polymers, Alan J. Heeger, Alan G. MacDiarmid and Hideki Shirakawa were awarded the Nobel Prize in Chemistry in 2000. Typical conducting polymers include polyacetylene (PA), polyaniline (PANI), polypyrrole (PPy), polythiophene (Pth), poly (para-phenylene) (PPP), poly (phenylenevinylene) (PPV), polyfuran (PF), etc [64].

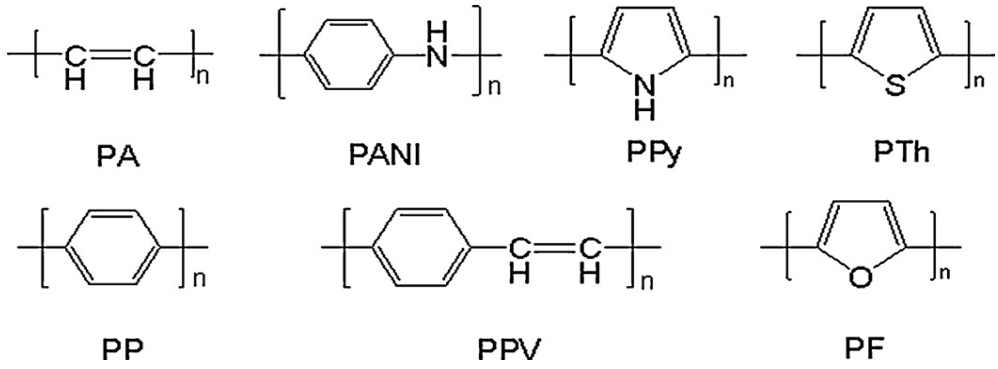

Fig.1.5. The chemical structures and their abbreviations of several kinds of conducting polymers.

Conducting polymers are generally wide band gap semiconducting materials, which can be chemically doped, with resulting electronic properties ranging from insulating to near metallic [65]. Environmental, energy sources and materials sciences are the three key projects of 21th century. One of them is the photocatalysis using oxide semiconductor, which is closely associated with those topics. Since 1977, conducting polymers (CPs) have drawn considerable interest because of their unusual electrical, optical and photoelectrical properties and

their numerous applications in various fields. Recently, the preparation for the nanocomposites of CPs with inorganic nanoparticles has attracted many researchers' attention, aiming to obtain the materials with synergetic or complementary behaviours between the CPs and the inorganic nanoparticles. Because of their semiconductor energy level structure, broad absorption spectra and very high stability under irradiation of solar light, CPs can be used to photosensitize semiconductor oxides and to obtain the novel photocatalysts response to the visible light [66]. Conjugated polymers (CP's) with extend π-conjugated electron systems such as polyaniline, polythiophene, polypyrrole, and their derivatives, etc have shown great promises due to their high absorption coefficients in the visible part of the spectrum, high mobility of charge carriers, and good stability [67]. The properties of delocalized conjugated structures in electron-transfer processes have been widely studied to show that they could effectively active a rapid photo-induced charge separation and a relatively low charge recombination. Furthermore, many CPs in their doped or undoped states are efficient electron donor and good holes transporter upon visible light excitation [68].

1.6.1. Polyaniline

Among conducting polymers, polyaniline has been a significant interest due to its high conductivity, good redox reversibility, and swift change in film colour with potential and high stability in air. Polyaniline is one of the most important conducting polymers because of excellent electrical properties, number of intrinsic redox states, possible processability, good environmental stability, successful combination of chemical & physical properties, as well as its numerous applications in practice. Polyaniline (PANI) is the first polymer of this kind to achieve world-wide commercial availability.

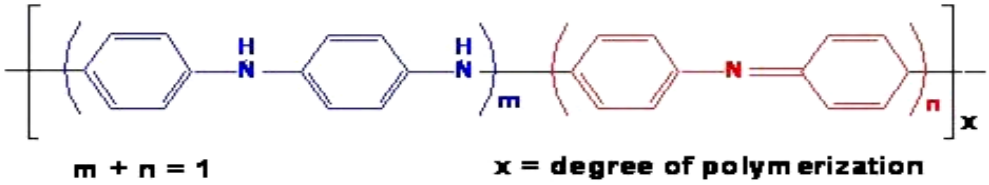

Fig.1.6. Structure of Polyaniline

Polyaniline (PANI) exists in a variety of forms that differ in chemical and physical properties [69-72]. The most common green protonated emeraldine has conductivity on a semiconductor level of the order of 100 S cm^{-1}, many orders of magnitude higher than that of common polymers (<10^{-9} S cm^{-1}) but lower than that of typical metals (>104 S cm^{-1}). Protonated PANI, (e.g., PANI hydrochloride) converts to a non conducting blue emeraldine base when treated with ammonium hydroxide [73].

Polymerized from the inexpensive aniline monomer, polyaniline can be found in one of three idealized oxidation states:

leucoemeraldine – white/clear & colourless $(C_6H_4NH)_n$

emeraldine – green for the emeraldine salt, blue for the emeraldine base $(\{[C_6H_4NH]_2[C_6H_4N]_2\}_n)$

(per)nigraniline – blue/violet $(C_6H_4N)_n$

In Fig.1.6. *x* equals half the degree of polymerization (DP). Leucoemeraldine with n = 1, m = 0 is the fully reduced state. Pernigraniline is the fully oxidized state (n = 0, m = 1) with imine links instead of amine links. Studies have shown that most forms of polyaniline are one of the three states or physical mixtures of these components. The emeraldine (n = m = 0.5) form of polyaniline, often referred to as emeraldine base (EB), is neutral, if doped (protonated) it is called emeraldine salt (ES), with the imine nitrogens protonated by an acid.

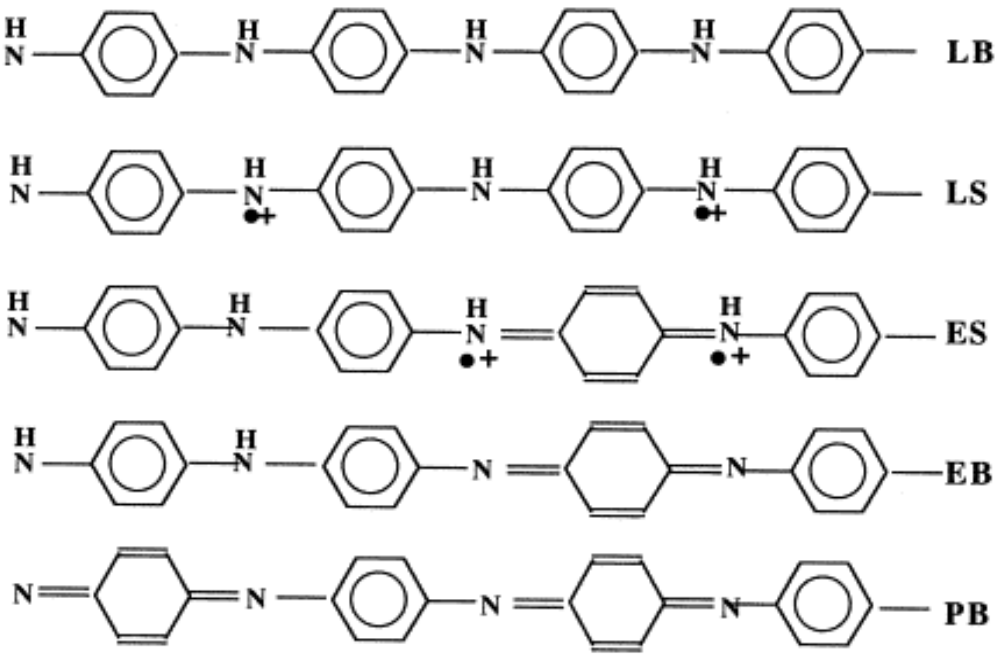

Fig.1.7. Different forms of polyaniline: LB: leucoemeraldine base; LS: leucoemeraldine salt, (radical cation); ES, emeraldine salt (bipolaronic form); EB, emeraldine base; PB, pernigraniline base [74].

Polyaniline can be used for batteries [75] electrochromic devices, [76] photo electrochemical conversion of light to electricity, [77,78] light-emitting diode [80] and immobilization of enzymes [81,82].

1.6.2. Polypyrrole

Polypyrrole (PPy) is a chemical compound formed from a number of connected pyrrole ring structures. Polypyrroles are conducting polymers of the rigid-rod polymer host family, all basically derivatives of polyacetylene. Polypyrrole was the first polyacetylene-derivative to show high conductivity. Polypyrroles are also called pyrrole blacks or polypyrrole blacks. Polypyrroles also exist naturally, especially as part of a mixed copolymer with polyacetylene and polyaniline in some melanins. Polypyrrole is a conducting polymer that has

attractive characteristics for the use as a radar absorbing material [83]. Polypyrrole (PPy) is a p-type semiconducting polymer that has proven to be relatively highly conductive, easy to synthesize, and environmentally stable. PPy can be prepared by chemical [84-86], electrochemical [85-87], plasma [88, 89] and vapor phase [90, 91] polymerization. In applications like coating dielectric materials (in this case optical plastic) the most suitable process is the in situ chemical polymerization, because it provides relatively high conductivity as well as suitable thickness and uniformity of the film. The main drawbacks of other methods are poor conductivity (plasma); need for conductive substrate, finite size of substrate, porosity, and uneven thickness of films (electrochemical); problematic adhesion of oxidant solution with substrate (vapour phase) [92].

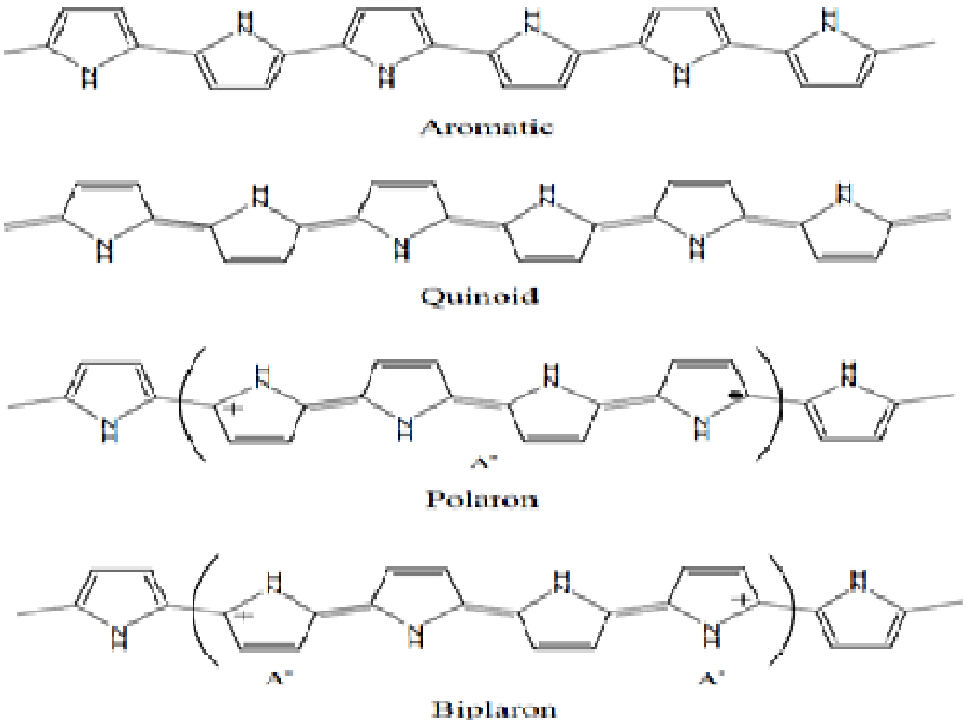

Fig.1.8.Chemical structures of polypyrrole in neutral aromatic and quinoid forms and in oxidised polaron and bipolaron forms.

Applications

Applications of PPy were essentially extended during last years and include now such different fields of science and technology as corrosion protection of metals, development of individual electronic devices e.g. diodes, metallization, electromagnetic interference shielding, biosensors, tissue engineering scaffolds, neural probes, drug-delivery devices, and bio-actuators [93-95].

(1) It has been studied as a material for artificial muscles--a technology that would offer numerous advantages over traditional motor actuating elements [96].(2) Used to coat silica and reverse phase silica to yield a material capable of anion exchange and exhibiting hydrophobic interactions [97]. (3) Used in the microwave fabrication of multiwalled carbon nanotubes, a new method that allows to obtain CNTs in a matter of seconds [98]. (4) polypyrrole (PPy) was synthesized by vapour phase polymerization (VPP) and electropolymerization (EP) and these PPys were employed as counter electrodes in dye-sensitized solar cells [99].

1.6.3. Polythiophene

Polythiophenes and other conjugated polymers have attracted attentions because of their electronic and photonic properties [100-102]. The π-conjugated electronic structure of these polymers facilitates the delocalization of the charge carriers upon doping and imparts high charge mobility. This delocalized electronic structure also leads to characteristic strong absorptions and emissions, in most cases in the UV-Vis. region. Since the original unsubstituted conjugated polymers are not solution- or melt processable, flexible side chains are attached to improve processibility. In addition to solubility and fusibility, the

attachment of various substituents can modify other physical properties of conjugated polymers, and lead phenomena which are not observed in the original unsubstituted polymers [103].

Polythiophenes consist of a chain of alternating double- and single-bonds like polyacetylene, however, each first and forth carbon atoms are connected by a sulfur atom forming a thionyl ring. Therefore the bond between the second and the third carbon atom get more single bond character than the other C-C bonds and consequently also the bonds connecting the thionyl rings are more of single-bond character. Due to this weaker mesomerization than in polyacetylene the band-gaps of polythiophenes are shifted to the blue and UV. Beside of their structure defining function the sulfur atoms will have also a direct influence on the electronic and optical properties of a polythiophene. Nevertheless the conjugation of the C-atoms will dominate the spectroscopic properties of the polythiophenes.

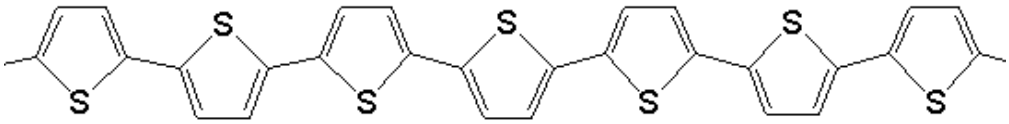

Fig.1.9. Structure of Polythiophene

Polythiophenes (Pth's) result from the polymerization of thiophenes, a sulfur heterocycle, that can become conducting when electrons are added or removed from the conjugated π-orbitals via doping.

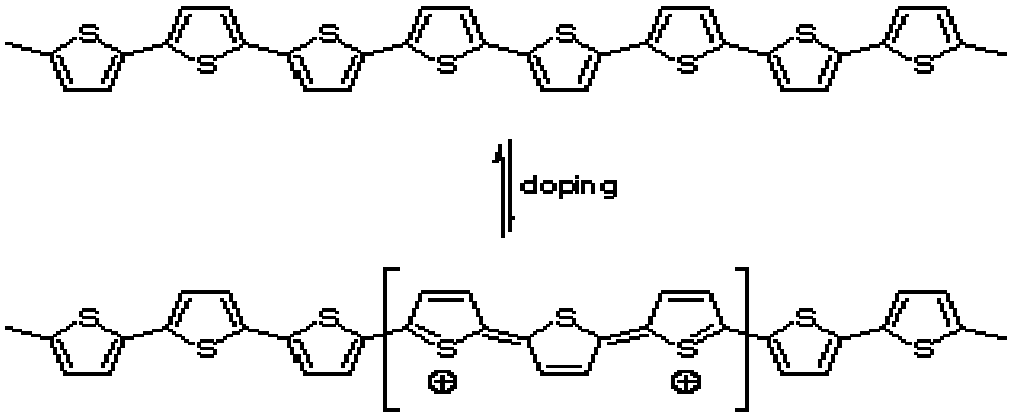

Fig.1.10. Polythiophenes Bipolaron Structure

Delocalised electrons along the conjugated backbone of polythiophene result in an extended π-system which is filled with valence electrons. Adding or removing electrons from the π-system (doping) produces a charged unit called a bipolaron unit. Polythiophene is insoluble in organic solvents [104-106].

Therefore, recently, conjugated polymers act as stable photo-sensitizer combined with wide band gap inorganic semiconductors (e.g., TiO_2, CdS, and CdSe) was an emerging area of research for optical, electronic, and photoelectric conversion applications [107-109]. And various composites with different combinations of the two components composition have been reported in the literature. In a conjugated polymer/TiO_2 system, polymer, bound to TiO_2, can actively harvest the visible light matching the semiconductor energy levels, and then inject electrons into the conduction band (CB) of TiO_2. Polyaniline (PANI), can generate π–π* transition under visible light, delivering the excited electrons into the conduction band of TiO_2, and then the electrons transferred to an adsorbed electron acceptor to yield oxygenous radicals to degrade pollutants .

The photocatalytic activity of conducting polymers modified TiO_2 under visible light irradiation resulted from the visible light absorption of conducting polymers and effective charge separation of photogenerated carriers owing to the heterojunction built between TiO_2 and the conducting polymers. Zhang etal. and Li etal. prepared PANI modified TiO_2 and other inorganic semiconductors photocatalyst via chemisorptions and insitu polymerization method, respectively [110-114]. The resulting composite photocatalyst exhibited significantly higher photocatalytic activity than that of neat semiconductors on degradation of dye or aqueous solution of phenol under visible light irradiation. Wang and Min [115] have pointed out that PANI/TiO_2 photocatalyst plays an efficient role for the degradation of the dye methylene blue over that of free TiO_2. This behaviour is owing to the ability of PANI to sensitize TiO_2 by absorbing both ultraviolet and visible light (190–800 nm), whereas the pure TiO_2 only absorbs ultraviolet light ($\lambda < 380$ nm). Li and co-workers reported that [116] on using PANI/TiO_2 composite sample prepared via self assembling and graft polymerization for degradation of methyl orange under sunlight, the composite exhibits superior photocatalytic activity for the degradation of dye over the neat TiO_2. Min etal reported Polyaniline (PANI) sensitized nanocrystalline TiO_2 composite photocatalyst (PANI/TiO_2) with high activity and easy separation was facilely prepared by insitu chemical oxidation of aniline from the surfaces of TiO_2 nanoparticles. PANI was able to sensitize TiO_2 efficiently and the composite photocatalyst could be activated by absorbing both the ultraviolet and visible light (λ = 190–800 nm), whereas pure TiO_2 absorbed ultraviolet light only (λ=400 nm). Photocatalytic experiments showed that under natural light irradiation, methylene blue could be degraded more efficiently on the PANI/TiO_2 than on the pure TiO_2, due to the charge transfer from PANI to TiO_2 and efficient separation of e^-- h+ pairs

on the interface of PANI and TiO_2 in the excited state [115]. Wang etal reported a series of polypyrrole–TiO_2 (PPy–TiO_2) nanocomposites with different PPy: TiO_2 ratios were prepared by 'insitu' deposition oxidative polymerization of polypyrrole, and their photocatalytic activities were evaluated by photocatalytic degradation of aqueous solution of methyl orange (MeO) under sunlight. According to them the PPy–TiO_2 nanocomposites showed higher photocatalytic activity than neat TiO_2 nanoparticles on the degradation of MeO under sunlight irradiation due to the sensitizing effect of PPy [117]. Shoubin Xu et al reported the visible light photocatalytic degradation of methyl orange (MeO) using TiO_2/Polythiophene composites [118]. Dan Yi etal in 2010 also reported the degradation of methyl orange under visible light using the TiO_2/Polythiophene (Pth) composites. According to them, the introduction of Pth into the composites provides an apparently additive effect on their adsorption capacities. A strong adsorption of MeO on the composite particles results from the electrostatic attraction of the positively charged composite particle surfaces with the MeO molecules. Under UV light irradiation, Pth/TiO_2 composites with a certain content of Pth exhibit higher photocatalytic activities than TiO_2 because of the high electron mobility of Pth with its p-conjugated structure. Under visible light irradiation, Pth adsorbed on the surface of TiO_2 acts as a sensitizer and charge transport layer; Pth/TiO_2 composites absorb visible light and photocatalytically degrade MeO [119]. Yi Dan and Yunfeng Zhu also showed that the Poly (3-hexylthiophene) (P3HT) sensitized TiO_2 shows fairly good activity towards the degradation of methyl orange under both UV and visible light irradiation [120]. In 2011, according to Qing Lin Liu etal the composites of poly (N-isopropyl acrylamide-co-acrylic acid)/ titanium dioxide (TiO_2) prepared via UV-initiated free radical polymerization shows comparatively

better photocatalytic activity under UV irradiation at various under various pHs and temperatures [121].

Yi Dan etal in 2008 synthesized Polythiophene/titanium dioxide (Pth/TiO_2) composites by the insitu chemical oxidative polymerization method. They showed that the prepared composites exhibited good photocatalytic activity under UV light illumination. The Pth/TiO_2 composites showed good adsorption properties and were more efficient in removing dye from solution than pure Pth and pure TiO_2. The maximum adsorption capacity of the Pth/TiO_2 composites was achieved when the mass percentage of Pth based on total composites was 40 % [122]. According to Liang etal the mechanism of polythiophene sensitized TiO_2 is shown below [123].

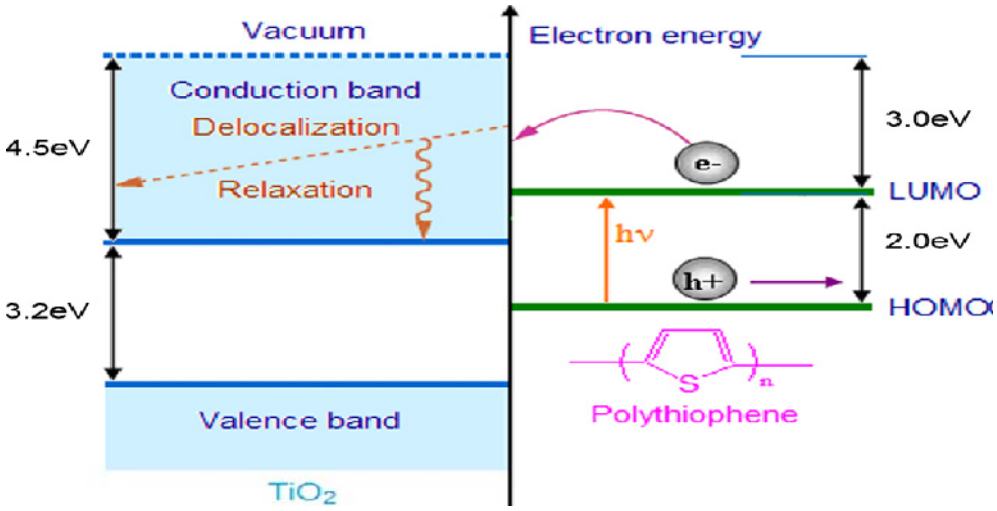

Fig.1.11.Mechanism of photocatalysis by polythiophene sensitized TiO_2

1.7. Mechanism of the photocatalysis under UV and Visible light irradiation

The Pth/TiO_2 composites induce the generation of electron-hole pairs under UV light irradiation, which yields radical and hole oxidants. It is well

known that TiO_2 particles are not excited by visible light. The surface hybridization of the Pth/TiO_2 composite particles will induce visible light photon absorption. The conduction band (CB) position of TiO_2 is lower than that of the LUMO of PTh in the Pth/TiO_2 composite particles. The Pth layer absorbs visible light, which induces excited-state electrons and these photoexcited electrons are readily injected into the CB of TiO_2 and subsequently transferred to the photocatalyst's surface [124]. These electrons react with water and oxygen to generate hydroxyl radicals and superoxide radicals [125], which are able to oxidize the pollutants. From these results, it is clear that the hole and the radical oxidants compete although only one of these is the main element.

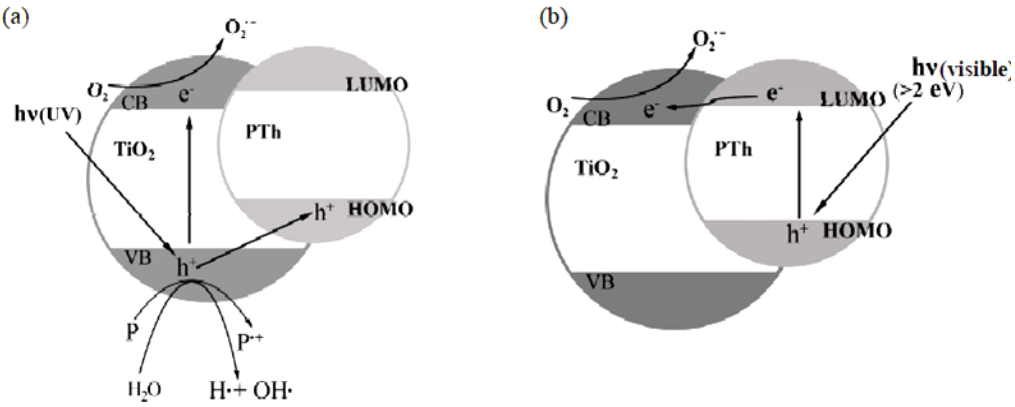

Fig.1.12. Schematic diagram illustrating the photocatalysis process of the PTh/TiO_2 composites under UV light (a) and visible light (b).

1.8. Measurement of Thermal diffusivity of a sample using Thermal lens technique

The evaluation of thermal properties of new materials is quite important. For several of their engineering applications in microscopic or macroscopic structures for instance, we need to know how they are able to dissipate heat. The same is true for those systems suitable for the recover or storage of energy

[126]. Photothermal spectroscopy belongs to a class of highly sensitive techniques, which can be used to measure optical absorption and thermal characteristics of a sample. The basis of photothermal spectroscopy is photo-induced changes in the thermal state of the sample due to optical absorption by molecules and the subsequent nonradiative relaxation processes that result in heating of the sample, which in turn modifies its thermal state. Photothermal signals will not be affected by scattered or reflected light unlike conventional optical signal detection. Hence photothermal spectroscopy measures optical absorption more precisely in scattering solutions, solids and at interfaces. The large signal to noise ratio of thermo-optic techniques makes it 'an effective tool to study the surface and absorption properties of materials, particularly for solids.

The first photothermal spectroscopic method to be applied for sensitive chemical analysis was photothermal lens spectroscopy. The thermal lens effect was discovered when Gordon, et al. (1964) observed transient power and beam divergence changes in the output of a helium-neon laser after placing "transparent" samples in the laser cavity. It is a photothermal effect and results when energy from a laser beam passing through a sample is absorbed, causing heating of the sample along the beam path. The lens is created through the temperature dependence of the sample refractive index. The lens usually has a negative focal length since most materials expand upon heating and the refractive index is proportional to the density. This negative lens causes beam divergence and the signal is detected as a time dependent decrease in power at the center of the beam.

Thermal Lens Spectroscopy (TLS) is a powerful and well-established tool for material characterization. TLS can be applied to the measurement of

analyte concentrations [127,128], characterization of trace elements in gases [129], measurement of absolute absorption coefficients [130], and spectrometry for liquid chromatography [131,132]. In particular, TLS has been established as an accurate technique to evaluate quantum yield, diffusivity and thermal conductivity of liquid and transparent solid media [133].

Thermal lens spectrometry is based on the measurement of the temperature rise that is produced in an illuminated sample by nonradiative relaxation of the energy absorbed from a laser. It is one of the most sensitive techniques for trace determination.

Light energy absorbed and not lost by subsequent emission results in sample heating, [134] and this heating result in a temperature change. The thermally perturbed sample can act as a lens. Light transmitted through an aperture placed beyond the photothermal lens will vary the strength of the lens. Photothermal methods based on measurement of the strength of this lens are called photothermal lensing spectroscopy. The procedure for the thermal lens technique is as follows. An excitation light beam passes through the sample that contains the analyte, the light is tuned to an absorption line of this, and the energy is absorbed by the analyte. The molecules are excited into vibrational, rotational, or electronic states; the excited molecules lose the energy in the form of heat through nonradiative relaxation processes, the heat generated equals the excitation energy. The heating of the sample causes a change of the refractive index, detecting this fact by convergence or divergence through to the sample.

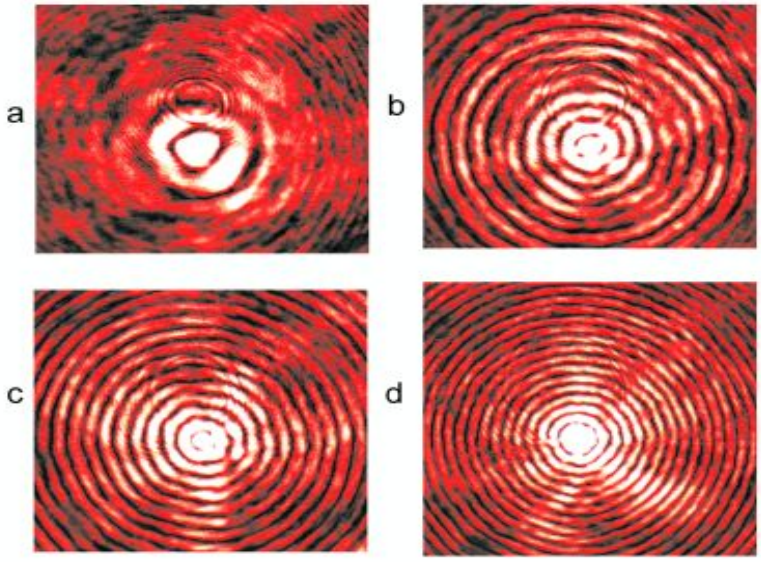

Fig.1.13. Thermal lensing behaviour in PLZT ceramics showing diffraction rings [135].

Particularly in high power lasers, the heating of the gain medium (e.g. a Laser crystal) often causes a significant thermal lens through the following mechanisms: The gain medium is hotter on the beam axis, compared with the outer regions, typically causing some transverse gradient of the refractive index (thermo optic effect, quantified with the coefficient dn/dT). Further index change can be caused by thermally induced mechanical stress (photoelastic effect, quantified with photoelastic coefficients ρij and the thermal expansion coefficient a). Mechanical stress can also lead to bulging of the end faces of the gain medium, so that these also cause lensing. This effect can be important for short laser crystals. Depending on the situation, these effects can have different relative strength and even sign. In many cases, the first mentioned effect (temperature dependence of the refractive index) is most important [136].

Another interesting aspect of thermal lens is that the heating and subsequent lens formation is not instantaneous. It takes a finite time to develop, depending on the laser power and the thermal properties of the sample. In solution, the thermal properties of the solvent (heat capacity and thermal conductivity) determine the time for blooming to occur (typically milliseconds). To best observe the "grow-in" of the thermal lens effect, laser light is focused with a lens at a precise position in the sample. The pump laser is turned off and on with a rotating chopper. By correct choice of components, lens formation will occur during the "on" cycle of the pump laser through the chopper, and it will dissipate by cooling during the "off" cycle, so that the effect can be observed repetitively. During the formation of the lens, the probe beam is deflected and it comes back when the lens is destroyed. The variation of the intensity of the probe beam during lens formation is something like shown in Fig.1.14.

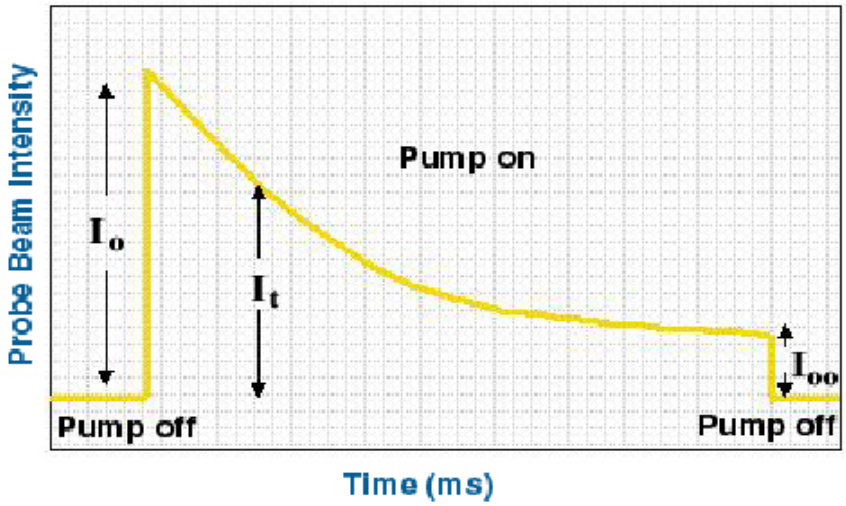

Fig.1.14. Trace of probe beam intensity variation during thermal lens formation

1.9. Nonlinearity Studies Using Z-scan Techniques: Optical limiting Applications

Nonlinear optics is a study that deals mainly with various new optical effects and novel phenomena arising from the interactions of intense coherent optical radiation with matter. Nonlinear optics is the study of phenomena that occur as a consequence of the modification of the optical properties of a material system by the presence of light. Typically, only laser light is sufficiently intense to modify the optical properties of a material system. The beginning of the field of nonlinear optics is often taken to be the discovery of second-harmonic generation by Franken *et al.* (1961), shortly after the demonstration of the first working laser by Maiman in 1960. Nonlinear optical phenomena are "nonlinear" in the sense that they occur when the response of a material system to an applied optical field depends in a nonlinear manner on the strength of the optical field. In order to describe more precisely what we mean by an optical nonlinearity, let us consider how the dipole moment per unit volume, or polarization$\tilde{P}(t)$, of a material system depends on the strength $\tilde{E}(t)$of an applied optical field. In the case of conventional (i.e., linear) optics, the induced polarization depends linearly on the electric field strength in a manner that can often be described by the relationship

$$\tilde{P}(t) = \epsilon_0 \chi^{(1)} \tilde{E}(t)$$

Where the constant of proportionality $\chi^{(1)}$ is known as the linear susceptibility and ϵ_0 is the permittivity of free space. In nonlinear optics, the optical response can often be described by generalizing the above Eq. by expressing the polarization $\tilde{P}(t)$ as a power series in the field strength $\tilde{E}(t)$ as

$$\begin{aligned}\tilde{P}(t) &= \epsilon_0[\chi^{(1)}\tilde{E}(t) + \chi^{(2)}\tilde{E}^2(t) + \chi^{(3)}\tilde{E}^3(t) + \cdots \\ &= \tilde{P}^{(1)}(t) + \tilde{P}^{(2)}(t) + \tilde{P}^{(3)}(t) + \cdots\end{aligned}$$

The quantities $\chi^{(2)}$ and $\chi^{(3)}$ are known as the second and third-order nonlinear optical susceptibilities, respectively. We shall refer to $\tilde{P}^{(2)}(t) = \epsilon_0 \chi^{(2)} \tilde{E}^2(t)$ as the second-order nonlinear polarization and to $\tilde{P}^{(3)}(t) = \epsilon_0 \chi^{(3)} \tilde{E}^3(t)$ as the third-order nonlinear polarization.

1.9.1. Z-Scan Measurements

Reliable methods for determining the nonlinear optical properties of materials (i.e. nonlinear absorption and nonlinear refraction) have been developed for wide ranging applications such as optical limiting1, multi-photon polymerization as well as optical switching. Of these methods, the "Z-scan", introduced in 1985 by Sheik Bahae etal [137,138] and later developed by Eric Van Stryland remains the standard technique. This is a simple and sensitive single beam technique to measure the sign and magnitude of both real and imaginary part of third order nonlinear susceptibility, $\chi^{(3)}$. The Z-scan technique is performed by translating a sample through the beam waist of a focused beam and then measuring the power transmitted through the sample. Z-scan has many possible configurations (e.g. "E Z-Scan", "White Light Z-scan", "Excite-Probe Z-scan"). The two measurable quantities connected with the Z-scan are nonlinear absorption (NLA) and nonlinear refraction (NLR) [139]. These parameters are associated with the imaginary and real part of the third order nonlinear susceptibility, and provide important information about the properties of the material. The Z-scan method is an easy and relatively simple way for measuring nonlinear absorption coefficients as well as nonlinear refractive indices for a wide variety of optically interesting materials.

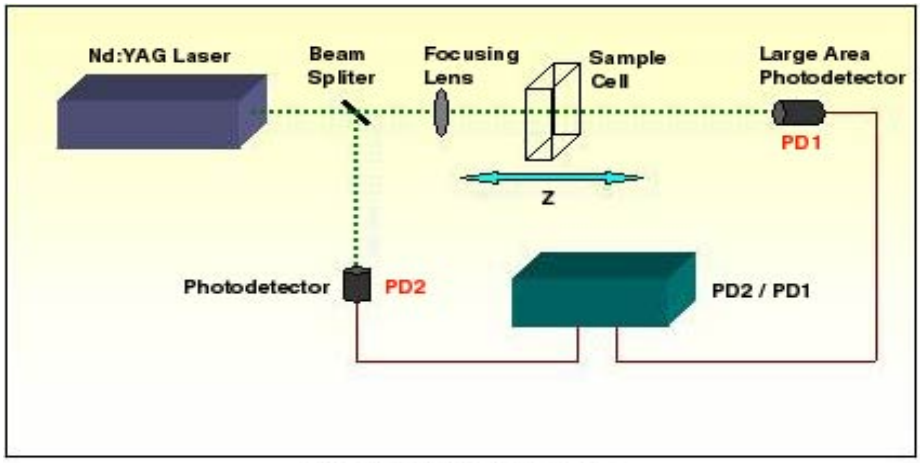

Fig.1.15. Z scan experimental set-up

In the original single beam configuration, the transmittance of the sample is measured, as the sample is moved, along the propagation direction of a focussed Gaussian laser beam. A laser beam propagating through a nonlinear medium will experience both amplitude and phase variations. If transmitted light is measured through an aperture placed in the far field with respect to focal region, the technique is called closed aperture Z-scan experiment [137,138]. In this case, the transmitted light is sensitive to both nonlinear absorption and nonlinear refraction. In a closed aperture Z-scan experiment, phase distortion suffered by the beam while propagating through the nonlinear medium is converted into corresponding amplitude variations. On the other hand, if transmitted light is measured without an aperture (in this case the entire light is collected), the mode of measurement is referred to as open aperture Z-scan [138]. In this case, the throughput is sensitive only to the nonlinear absorption. Closed and open aperture Z-scan graphs are always normalized to linear transmittance i.e. transmittance at large values of |z |.

In the Z-scan set-up, the transmittance of the sample is measured, using a large area photodetector, as the sample is moved along the propagation direction (z) of a focussed Gaussian laser beam. The measurement is done using a 532 nm Gaussian laser beam of a frequency doubled Nd: YAG laser. A portion of the laser beam is sampled out to monitor the input energy. Laser energy is measured and averaged using a commercial energy meter and a ratio meter respectively. From open aperture Z-scan experimental data, nonlinear absorption coefficient is calculated using two-photon absorption (TPA) model. It is obtained by fitting the experimental data to the normalized transmittance equation.

1.9.2. Optical limiting Application

There are three basic requirements for a material to be good optical limiter viz. (1) An excited state absorption cross-section that exceeds the ground state absorption cross-section, (2) fast response and (3) high damage threshold. Magnitude of effective nonlinear absorption coefficient is an indication of the usefulness of a sample to act as good optical limiter. Samples with higher value of effective nonlinear absorption coefficient are obviously better optical limiters.

1.10. Lasing

Lasers (light amplification by stimulated emission of radiation) are radiation sources for coherent, quasi-monochromatic and sharply bundled radiation in the visible region and in the adjacent regions of the electromagnetic spectrum (far infrared, infrared, ultraviolet and X-rays). Lasers are employed in all areas of science and technology. The most important applications use laser light having a wavelength in the range from 300 to 1800 nm.

In principle, all lasers consist of three components: an active medium or laser medium (for example a gas, a solid, for example a crystal or diode, or a

liquid), which substantially determines the optical properties of the laser; a pump source (for example a flash lamp, a pump laser or an electrically operated gas discharge), which-supplies energy-to the active medium, and finally a feedback medium or laser resonator, which provides the feedback and thus induced emission of the radiation. In the present application, the terms laser medium and active medium are used synonymously. The term "amplifying medium" here is taken to mean the system comprising active medium and feedback medium.

Lasers are usually classified according to the active medium used, for example as gas, dye, solid-state or semiconductor lasers.

Dye lasers are of particular interest in many areas of industry since lasers of this type are distinguished by a large continuous tuning range of the wavelength of the emitted laser radiation. In addition, high outputs can be achieved with narrow line widths. The pumping mechanisms, i.e. the processes for exciting the activatable particles of the active medium, are very flexible. The dye is usually excited by so-called optical pumping, with the energy source used being, for example, a flash lamp or a pump laser. Typical pump lasers are nitrogen, argon ion and frequency-doubled Nd: YAG (neodymium/yttrium aluminum garnet) lasers. Dye lasers are operated either continuously or in pulsed mode with pulse energies of up to 1J and pulse durations in the femto second region.

Laser action in random structures where light is multiply scattered and amplified becomes a subject of intense theoretical and experimental studies because of its important potential applications [140]. Following the pioneering theoretical work by Letokhov in the late 1960s [141], experiments by

Markushe *etal.* on powdered $Na_5La_{1-x}Nd_x(MoO_4)_4$ [142] and Lawandy *etal* on solutions containing an organic dye Rhodamine 640, and TiO_2 particles [143] demonstrated scattering-assisted optical gain upon laser pumping.

A dye laser is a laser which uses an organic dye as the lasing medium, usually as a liquid solution. Compared to gases and most solid state lasing media, a dye can usually be used for a much wider range of wavelengths. The wide bandwidth makes them particularly suitable for tunable lasers and pulsed lasers. Moreover, the dye can be replaced by another type in order to generate different wavelengths with the same laser, although this usually requires replacing other optical components in the laser as well [144].

The first broadly tunable laser was the organic dye laser discovered in 1966 by Sorokin [145] and Lankard and Schafer et al.[146]. Dye doped polymer gain media for tunable lasers were introduced shortly afterward by Soffer and McFarland [147] and Peterson and Snavely [148].

1.11. Scope of the present work

The current area of research interest includes the synthesis, characterization and applications of hybrid nanocomposites of TiO_2 with conducting polymers. Nanocomposite material composed of conducting polymers & oxides have open more field of application such as drug delivery, conductive paints, rechargeable batteries, toners in photocopying, smart windows, etc. The composites of core shell metal oxide particles-conducting polymer combine the electrical properties of the polymer shell and the magnetic, optical, electrical or catalytic characteristics of the metal oxide core, which could greatly widen their applicability in the fields of catalysis, electronics and optics The hybrid nanocomposites are prepared via hydrothermal technique

and characterized using various physico chemical techniques. The application studies include photocatalysis, thermal diffusivity measurements, nonlinear optics and lasing studies.

1.12. Objectives of the Present work

- Prepare mesoporous TiO_2 and TiO_2-conducting polymer (Polyaniline, Polypyrrole and Polythiophene) hybrid nanocomposites via hydrothermal technique.
- Prepare different compositions of the conducting polymer-TiO_2 hybrid nanocomposites.
- Physico chemical characterization of the prepared nanocomposites via XRD,UV-Vis. DRS, Raman spectra, FT-IR Spectra, SEM-EDX,TG-DTG analysis, XPS,TEM and conductivity measurements.
- The prepared nanocomposites were used in the field of photocatalysis, thermal diffusivity measurement, nonlinear optics and lasing.
- The photocatalytic efficiency of the prepared systems was evaluated by monitoring the degradation dyes, phenol, 4-nitrophenol, the endocrine disruptor Bisphenol- A, and the antibiotic Sulfamethoxazole.
- The Antibacterial activity of the composites were analysed using the typhoid causing bacteria Salmonella typhi.
- The thermal diffusivity measurements were carried out using thermal lens technique.
- Non-linear Optical properties (3^{rd} order non linearity) were studied using Z-scan technique.
- Study the Light amplification in dye doped nanocomposites: The polyaniline-TiO_2 hybrid nanocomposites were used as a potential dye laser gain medium.

References

[1]. R. Gangopadhyay, A. De, Chem. Mater. 12, (2000) 609.

[2]. A. Anderson, O. Hunderi, C. G. Granqvist , J. Appl. Phys. 57(1980)75.

[3]. In-Yup Jeon, J.B. Baek, Materials 3(2010)3654.

[4]. B. I. Nandapure, S. B. Kondawar, M.Y. Salunkhe, A. I. Nandapure, Adv. Mat. Lett. 4(2013)134.

[5]. H. Althues, J. Henle, S. Kaskel, Chem Soc Rev. 36(2007)1454.

[6]. Special Issue on Nanostructured Materials. Chem. Mater. 1996, 8 (8), 1569.

[7]. H.L. Tasi, J. L. Schindler, C. R. Kannewurf, M.G. Kanatzidis, Chem. Mater. 9(1997) 875.

[8]. O. Jarjayes, P. H. Fries, G. Bidan, Synthetic metals 69(1995)343.

[9]. M.D. Butter worth, R. Corradi, J. Johal, S.F. Lascelles, S.Maeda, S.P. Armes, J Colloid Interface sci. 174(1995)510.

[10]. B. Govindraj, N. V. Sastry, A. Venkataraman, J. Appl. Poly. Sci. 92(2004) 1527.

[11]. S. Khasim, S.C.Raghvendra, M. Revansiddappa, M.V.N. Ambika Prasad, Ferroelectrics 325(2005) 111.

[12]. R. Sinha, Outlines of polymer technology, New Delhi: Prentice Hall of India private Limited, (2002).

[13]. S. Li, M. M. Lin, M. S. Toprak, Do K. Kim, M. Muhammed, Nano Reviews 1(2010) 5214.

[14]. T.Ramanathan, S Stankovich, D.A. Dikin, H.Liu, H.Shen, S.T. Nguyen, J Polymer Sci B Polymer Phys 45(2007)2097

[15]. L.Vaisman, E. Wachtel, H.D.Wagner, G.Marom, Polymer 48(2007)6843.

[16]. J. Zhang, S. Luo, L. Gui, J Mater Sci. 32(1997)1469.

[17]. A.H. Yuwono, B.Liu, J. Xue, J. Wang, H.I. Elim, W.Ji, J Mater Chem. 14(2004)2978.

[18]. Guido Kickelbick, Hybrid Materials. Synthesis, Characterization, and Applications. Edited by Guido Kickelbick Copyright © 2007 Wiley-VCH Verlag GmbH & Co. KGaA, Weinheim ISBN: 978-3-527-31299-3.

[19]. C.Sanchez, B.Julia´n, Philippe Belleville, M. Popall, J. Mater. Chem. 15 (2005)3559.

[20]. C. Sanchez, F. Ribot, New J. Chem. 18(1994)1007.

[21]. Energeia Vol. 17, No. 3, 2006 © UK Centre for Applied Energy Research.

[22]. A.Albini, J. Chem. Educ. 63(1986) 383.

[23]. H.Hennig, R.Billing, H. Knoll, In Photosensitization and Photocatalysis Using Inorganic and Organometallic Compounds; Kalyanasundaram, K., Gratzel, M., Eds.; Kluwer Academic Publishers: Dordrecht, The Netherlands, 1993; p 51

[24]. H. Kisch, In Photocatalysis-Fundamentals and Application; Serpone, N., Pelizzetti, E., Eds.; Wiley-Interscience: New York, 1989; p 1.

[25]. A. Fujishima, K. Honda, Nature 37(1972)238.

[26]. M.A.Fox, M.T. Dulay, Chemical Reviews 93(1993)341.

[27]. N.Serpone, A.V.Emeline, S.Horikoshi, V.N. Kuznetsov, V.K. Ryabchuk, Photochem. Photobiol. Sci. 11 (2012)1121.

[28]. V. Augugliaro, V. Loddo, G. Palmisano, L. Palmisano, M. Pagliaro, Clean by Light Irradiation. Practical Applications of Supported TiO_2, The Royal Society of Chemistry, Cambridge (2010).

[29]. J.M. Herrmann, Topics in Catalysis 34(2005) 49,DOI: 10.1007/s11244-005-3788-2

[30]. D.S. Bhatkhande, V.G. Pangarkar, A.A.Beenackers, Journal of Chemical Technology and Biotechnology 77(2001)102.

[31]. A. Fujishima, T.N. Rao, D. A. Tryk, Journal of Photochemistry and Photobiology C: Photochemistry Reviews 1 (2000) 1.

[32]. J. C. Yu, W. K. Ho, J.G. Yu, H.Yip, P.Wong, J. C. Zhao, Environ. Sci. Technol. 39(2005) 1175.

[33]. D. M. Chen, Z.Y Jiang, J.Q.Geng, Q.Wang, D. Yang, Ind.Eng. Chem. Res. 46(2007) 2741.

[34]. Y.Cong, J. L Zhang, F.Chen, M. Anpo, J. Phys. Chem. C. 111(2007) 10618

[35]. C.Hu, X. X. Hu, L. S. Wang, J. H. Qu, A. M. Wang, Environ. Sci. Technol. 40(2006) 7903.

[36]. S.Kim, W. Choi, J. Phys. Chem. B. 109(2005) 5143.

[37]. M.M. Mohamed, Appl. Catal. A. 267 (2004) 135.

[38]. V. Stengl, J. Subrt, Zp°usob v´yroby fotokatalyticky aktivn´ı titanov´eb˘eloby, PV 2000–2814, The way of production of photocatalytically active titanium white, Czech patent.

[39]. www.coatingssys.com-- Physics and chemistry of photocatalytic titanium dioxide: Visualization of bactericidal activity using atomic force microscopy; S.Banerji, Muraleedharan,Tyagi,Raj;Current Science 90No.10,2006.

[40]. A. Fujishima, T. N. Rao, D. A. Tryk, J. Photochem. Photobiol. C 1 (2000)1.

[41]. D. A.Tryk, A.Fujishima, K. Honda, Electrochim. Acta. 45(2000)2363.

[42]. M. Gra¨tzel, Nature 414(2001)338.

[43]. A. Hagfeldt, M. Gra¨tzel, Chem. ReV. 95(1995) 49.

[44]. L. Linsebigler, G.Lu, J. T. Yates Jr., Chem. ReV. 95 (1995) 735.

[45]. A. Millis, S. Le Hunte, J. Photochem. Photobiol., A. 108(1997) 1.

[46]. A. Wold, Chem.Mater. 5(1993) 280.

[47]. A.W. Y Choi, A.Termin, M. R. Hoffmann, Angew. Chem. 106(1994) 1148.

[48]. C. Burda, Y. B.Lou, X. B Chen, A. C. S. Samia, J.Stout, J. L. Gole, Nano Lett. 3(2003) 1049.

[49]. IESE Research Advanced Oxidation Technology for Environmental Application: TiO_2 Photocatalysis.

[50]. http://www.greatvistachemicals.com industrial and specialty chemicals titanium-dioxide.html

[51]. www.worldscibooks.com/etextbook/8325/8325chap01.pdf--Nanostructured Titanium Dioxide Materials: Properties, Preparation.

[52]. R.J.H. Clark, The chemistry of Titanium and vanadium, Amsterdam: Elsevier (1968) 269.

[53]. Titanium dioxide (book)-Jochen Winkler –European coatings literature.

[54]. Three Bond Technical News Issued January 1, (2004) 62.

[55]. L. Linsebigler, G. Lu, and J. T. Yates, Jr., Chemical Reviews, 1995, Vol. 95, No.3 741.

[56]. A.Zaleska, Recent Patents on Engineering, 2(2008) 157.

[57]. http://inprom-file.s3.amazonaws.com/213 ormation about polyaniline.pdf.

[58]. Inzelt, György (2008). "Chapter 1: Introduction". In Scholz, F. Conducting Polymers: A New Era in Electrochemistry. Monographs in Electrochemistry. Springer. pp. 1–6.ISBN 978-3-540-75929-4.

[59]. http://en.wikipedia.org/wiki/Conductive_polymer

[60]. H. Shirakawa, Angew Chem Int Ed. 40(2001)2575.

[61]. A.G. MacDiarmid, Angew Chem Int Ed. 40(2001)2581.

[62]. A.J. Heeger, Angew Chem Int Ed. 40(2001)2591.

[63]. X. Lu, W. Zhang, C. Wang, T.C.Wen, Y. Wei, Progress in Polymer Science 36 (2011) 671

[64]. T.A. Skotheim (Ed.), Handbook of Conducting Polymers, Marcel Dekker, New York, 1986

[65]. LiShengYing, Preparation of Conducting Polymer/Semiconductor Nanocomposites and Their photocatalytic Activities, PhD thesis (2006)

[66]. Pron, P. Rannou, Prog Polym Sci. 27(2002) 135.

[67]. S.E. Shaheen, C.J. Brabec, F. Padinger, T. Fromherz, J.C. Hummelen, N.S.Sariciftci, Appl Phys Lett. 78(2001)841.

[68]. G. MacDiarmid, A. J. Epstein. Faraday Discuss. Chem. Soc. 88 (1989)317.

[69]. J. Stejskal, P. Kratochvil, A. D. Jenkins. Polymer 37(1996) 367.

[70]. C. Trivedi, In Handbook of Organic Conductive Molecules and Polymers, H. S. Nalwa (Ed.), Wiley, Chichester 2 (1997) 505.

[71]. N. Gospodinova, L. Terlemezyan. Prog. Polym. Sci. 23(1998) 1443.

[72]. J. Stejskal, P. Kratochvil, A. D. Jenkins. Polymer 37(1996) 367.

[73]. M.C. Bernard, Susana Cordoba de Torresi, Anne Hugot-Le Goff,Volume 44, Issue 12, 1 January 1999, Pages 1989–1997.

[74]. G. MacDiarmid, S. L. Mu, N. L. D. Somasiri, Mol.Cryst.Liq.Cryst., 121(1985) 187.

[75]. T. Kobayashi, N. Yonevama, H. J. Tamura, Electroanal. Chem., 177(1984) 281.

[76]. D. Batich, H. A. Laitinen, H. C. J. Zhou, Electrochem. Soc. 137(1990)883.

[77]. J. Desilvestro, O. J. Hass, Chem.Soc.Chem.Commun. (1985)346.

[78]. Y. H. Dong, S.L. Mu. Electrochim. Acta. 36(1991) 2015.

[79]. S. Karg, J. C. Scott, J. R. Salem, Synth.Met. 80(1996)111.

[80]. P. N. Bartlett, R. G. Whitaker, Biosensor 88(1987)359.

[81]. Y.F.Yang, S.L. Mu., J.Electroanal.Chem 432(1997)71.

[82]. L.Olmedo, P. Hourquebie, P. Buvat, Antec 952(1997)1320.

[83]. R.V. Gregory, W.C. Kimbrell, H.H. Kuhn, Synth. Met. 28 (1989) 823.

[84]. M. Sak-Bosnar, M.V. Budimir, S. Kovac, D. Kukulj, L. Duic, J. Polym. Sci., A, Polym. Chem. 30 (1992) 1609.

[85]. J. Wang, K.G. Neoh, E.T. Kang, Thin Solid Films 446 (2004) 205.

[86]. P.A. Kilmartin, G.A. Wright, Electrochim. Acta. 46 (2001) 2787.

[87]. G.J. Cruz, J. Morales, R. Olayo, Thin Solid Films 324 (1999) 119.

[88]. K. Hosono, I. Matsubara, N. Murayama, W. Shin, N. Izu, Mater. Lett. 58 (2004) 1371.

[89]. S.N. Tan, H. Ge, Polymer 37 (1996) 965.

[90]. J. Kim, D. Sohn, Y. Sung, E.R. Kim, Synth. Met. 132 (2003) 309.

[91]. M.Ferenets, A. Harlin, Thin Solid Films 515 (2007) 5324.

[92]. M. Angelopoulos, IBM J. Res. & Dev. 45(2001)57.

[93]. N.K. Guimard, N.Gomez, C.E. Schmidt, Prog. Polym. Sci. 32(2007)876.

[94]. Yfantis, Development and characterization of corrosion resistant layers of conducting polymers on Aluminium alloys. PhD thesis, BTU-Cottbus, Germany (2000)

[95]. http:// atmsp. whut. edu.cn/resource/pdf/4987.pdf

[96]. http://www.sciencedirect.com/science/article/pii/002196739185003X

[97]. pubs.rsc.org/en/content/article landing/2011/CC/C1CC13359D

[98]. J. Xia, L. Chen, S.Yanagida, J. Mater. Chem. 21(2011) 4644.

[99]. Handbook of Conducting Polymers, 2nd ed. (Eds: T. Skotheim, R.L Reynolds, R. L.Elsenbaume) Marcel Dekker, New York (1997).

[100]. R. D. McCullough, Adv. Mater. 10(1998) 93.

[101]. M.Leclerc, K. Faid, Adv. Mater. 9(1997) 1087.

[102]. F.Garnier, Angew. Chem. Int. Ed. 28(1989) 513.

[103]. A.Iraqi, D. Clark, D. Jones, A. Krier, Synth. Metals 102(1999) 1220.

[104]. T. Bjornholm, T. Hassenkam, D. R.Greve, R. D. McCullough,. M.Jayaraman, S.M. Savoy, C. E. Jones, J. T. McDevitt, Adv. Mater. 11(1999) 1218.

[105]. N. Reitzel, D. R. Greve, K. Kjaer, P. B. Howes, M. Jayaraman, S.Savoy, R. D. McCullough, J. T. McDevitt, T. J. Bjornholm, Am. Chem. Soc. 122(2000) 5788.

[106]. L.B. Roberson, M.A. Poggi, J. Kowalik, G.P. Smestad, L.A. Bottomley, L.M. Tolbert, Coordin. Chem. Rev. 248 (2004) 1491.

[107]. W.J.E. Beek, M.M. Wienk, M. Kemerink, X. Yang, R.A.J. Janssen, J. Phys. Chem. B 109 (2005) 9505.

[108]. S.X. Min, F. Wang, Y.Q. Han, J. Mater. Sci. 42 (2007) 9966.

[109]. H. Zhang, R.L. Zong, J.C. Zhao, Y.F. Zhu, Environ. Sci. Technol. 42 (2008)3803.

[110]. H. Zhang, Y.F. Zhu, J. Phys. Chem. C. 114 (2010) 5822.

[111]. H. Zhang, R.L. Zong, Y.F. Zhu, J. Phys. Chem. C 114 (2009) 4605.

[112]. M. Shang, W.Z. Wang, S.M. Sun, J. Ren, L. Zhou, L. Zhang, J. Phys. Chem. C 113(2009) 20228.

[113]. X.Y. Li, D.S. Wang, G.X. Cheng, Q.Z. Luo, J. An, Y.H. Wang, Appl. Catal. B: Environ.81 (2008) 267.

[114]. F.Wang, S.X. Min, Chin. Chem. Lett. 18 (2007) 1273.

[115]. J. Li, L. Zhu, Y. Wu, Y. Harima, A. Zhang, H. Tang, Polymer 47 (2006) 7361.

[116]. D. Wang, Y.Wang, X. Li, Q.Luo, J.An, J.Yue, Catalysis Communications 9 (2008) 1162.

[117]. S. Xu, Y. Zhu, L. Jiang, Y.Dan, Water Air Soil Pollut. 213(2010)151.

[118]. Y. Zhu, S. Xu, Y. Dan, Reactive & Functional Polymers 70 (2010) 282.

[119]. Y. Zhu, Y. Dan, Solar Energy Materials & Solar Cells 94 (2010) 1658.

[120]. S. Q. Wang, Q. L.Liu, A. M.Zhu, European Polymer Journal 47 (2011) 1168.

[121]. Y. Zhu, S. Xu, L. Jiang, K. Pan, Y.Dan ,Reactive & Functional Polymers 68 (2008) 1492

[122]. H.C. Liang, X.Z. Li, Applied Catalysis B: Environmental 86 (2009) 8.

[123]. X. M. Peng, L. Zhang, Y. W. Chen, F. Li, W. H. Zhou, Appl Surf Sci, 256(2010) 2948

[124]. A. Fujishima, X. T. Zhang, D. A. Tryk, Surf Sci Rep, 63(2008) 515.

[125]. A.C Sparavigna, S. Giurdanella, M. Patrucco,. Energy and Power Engineering, 3(2011) 150.

[126]. N. J. Dovichi, J. M. Harris, Anal. Chem.51 (1979) 728.

[127]. T. Imasaka, K. Miyaishi, N. Ishibashi, Anal. Chim. Acta. 115(1980) 407.

[128]. C. Nieman , S. D. Colson, J. Chem. Phys. 68(1978) 2994.

[129]. J. R. Whinnery, Acc. Chem. Res. 7(1974) 225.

[130]. E. Buffett, M. D. Morris, Anal. Chem. 54(1982)1824.

[131]. R. A. Leach, J. M. Harris, J. Chromatogr. A 218(1981) 15.

[132]. R. Snook, R. D. Lowe, Analyst (Lond.) 120(1995) 2051.

[133]. S.E Bialkowski, Photothermal Spectroscopy methods for Chemical Analysis in Chemical Analysis: A series of Monographs on Analytical Chemistry and its Applications; Vol. 134, John Wiley & sons, Inc., (1996).

[134]. http://www.rmc.ca/aca/phy/rdp/fom-mfo/index-eng.php)

[135]. http://www.timbercon.com/Thermal-Lensing.html

[136]. M. S. Bahae, A. A. Said, E. W .Van Stryland, optics Opt. Lett. 14 (1989) 955.

[137]. M.S.Bahae, A.A.Said, T. H. Wei, D. J. Hagan, E. W. V. Stryland.,IEEE J. Quantum Electroinics 26 (1990) 760.

[138]. http://www.newport.com/Z-Scan-for-the-Characterization-of-Transparent-Optical materials/609410/1033/info. aspx# tab- Overview

[139]. S. Wiersma, Nature Physics 4(2008) 359.

[140]. V. S. Letokhov, Journal of Experimental and Theoretical Physics Letters, 5(1967) 212.

[141]. V. M. Markushev, V. F. Zolin and C. M. Briskina, Soviet Journal of Quantum Electronics 16(1986) 281.

[142]. N. M. Lawandy, R. M. Salachandran, A. S. L. Gomes , E. Sauvain, Nature 368(1994) 436.

[143]. en. Wikipedia.org/wiki/dyelaser

[144]. P.P.Sorokin, J.R. Lankard, IBM J.Res .Dev.10 (1966)162.

[145]. F.P.Schafer, W.Schmidt, J.Volze, Appl.Phys.Lett.9 (1966)306.

[146]. B.H.Soffer, B.B. McFarland, Appl.Phys.Lett.10 (1967)266.

[147]. O.G. Peterson, B.B.Snavely, Appl.Phys.Lett.12(1968)238.

.....ꕥ.....

Chapter 2

MATERIALS AND METHODS

Contents

The synthesis and characterization of material is the first and foremost important step during the experimental research. This chapter describes the preparation of various nanocomposites and the experimental techniques employed for their physico-chemical characterization. This chapter will focus on the most effective and widely used techniques available to characterize solid-state compounds. The primary objective of this chapter is to provide a practical description of the methods used to characterize a broad range of materials.

2.1. Introduction

Characterization of materials regarding composition, trace impurities, structural phase and crystallographic perfection is vital for repeated reproduction of materials with stringently defined specifications, their applications as well as for fundamental research [1, 2]. The synthesis and characterization of material is the first and foremost step during the experimental research in materials science. The quality of samples depends to a great extent on the synthesis method used. In addition, the proper selection of synthesis parameters helps to carry out desired properties in the samples to be characterized along with desired potentials. Structure, surface morphology,

grain growth, transport of electrons within material and magnetic properties depend on material synthesis. When a material is fabricated in the lab, how are we able to assess whether our method was successful? Depending on the nature of the material being investigated, a suite of techniques may be utilized to assess its structure and properties. Whereas some techniques are qualitative, such as providing an image of a surface, others yield quantitative information such as the relative concentrations of atoms that comprise the material.

2.2. Synthesis of the Hybrid Nanocomposite

2.2.1. Chemicals used for the synthesis

The chemicals used for the synthesis are listed below in Table 2.1.

Table 2.1. Chemicals used for Synthesis

SI.No.	Chemical	Company
1	Titanium tetra Isopropoxide	Sigma Aldrich
2	Glacial Acetic acid	MERCK
3	Ammonia solution (28%)	Qualigen
4	P-123- poly(ethylene oxide)-poly(propylene oxide)- poly(ethylene oxide)Pluronic 123	Sigma Aldrich
5	Con.HCl	SDFCL
6	Aniline	SD Fine Chemicals
7	Pyrrole	SPECTROCHEM
8	Thiophene	SPECTROCHEM
9	Ammonium peroxodisulphate(APS)	MERCK
10	Anhydrous $FeCl_3$	MERCK
11	Acetonitrile	SPECTROCHEM
12	Methanol	SPECTROCHEM

2.2.2. Synthesis of mesoporous TiO_2

Pure titania is prepared by surfactant assisted hydrothermal route. In this method a fixed amount of the surfactant, P123 is dissolved in a calculated amount of distilled water. Titania sol is prepared by taking 10 ml of titanium

tetraisopropoxide along with 20 ml of acetic acid in a beaker with addition of 100 ml of distilled water dropwise and the system is under stirring. The titania sol is then added to the surfactant solution dropwise under stirring. The mixture is then sonicated for one hour. It is then transferred into an autoclave and kept in an oven at 110ºC for overnight. After that the mixture is filtered, washed with water, dried at 110ºC and calcined at 500ºC for 5 hrs. It is then powered to get mesoporous titania.

2.2.3. Synthesis of Polyaniline - TiO_2 hybrid nanocomposite

Titania-Polyaniline Composites(TP)

2 g TiO_2 was taken in a beaker along with 100 ml 1 M HCl solution and 3.3 ml of distilled aniline. The mixture was kept under stirring in an ice bath with a magnetic stirrer and ammonium peroxodisulphate solution (12.5 g in 100 ml distilled water) was added drop by drop. The mixture was sonicated for about 1 hour and then transferred to an autoclave and placed in an oven for overnight at 110ºC. It was filtered, washed with water and acetone to remove unreacted aniline, dried in an oven at 110ºC.Different compositions were prepared by changing the amount of aniline (TP1, TP2 and TP3).

2.2.4. Synthesis of Polypyrrole- TiO_2 hybrid nanocomposite

Titania-Polypyrrole Composites (TPpy)

2 g TiO_2 was taken in a beaker along with 3.6 ml of distilled pyrrole in 10 ml of distilled water. The mixture was kept under stirring in an ice bath with a magnetic stirrer and $FeCl_3$ solution (8.415g in 100 ml distilled water) was added drop by drop. The mixture was sonicated for about 1 hour and then transferred to an autoclave and placed in an oven for overnight at 110º C. It was filtered, washed with water and acetone to remove unreacted pyrrole,

dried in an oven at 110ºC.Different compositions were prepared by changing the amount of pyrrole (TPpy1, TPpy2 and TPpy3).

2.2.5. Synthesis of Polythiophene- TiO_2 hybrid nanocomposite

Titania-Polythiophene Composites (TPth)

2 g TiO_2 was taken in a beaker along with 3.1 ml of distilled thiophene in 5 ml of acetonitrile. The mixture was kept under stirring in an ice bath with a magnetic stirrer and $FeCl_3$ solution (6.275g in 100 ml acetonitrile) was added drop by drop. The mixture was sonicated for about 1 hour and then transferred to an autoclave and was kept in an oven for overnight at 110ºC. It was filtered, washed with water and acetone to remove unreacted thiophene, dried in an oven at 110ºC. Different compositions were prepared by changing the amount of thiophene (TPth1, TPth2 and TPth3).

The nanocomposite systems prepared for the present work with its notations are listed in Table 2.2.

Table 2.2. Nanocomposite systems prepared

SI.No.	System	Notation
1	TiO_2	T
2	Polyaniline- TiO_2 (1:4 molar ratio of aniline and TiO_2)	TP1
3	Polyaniline- TiO_2 (1:2 molar ratio of aniline and TiO_2)	TP2
4	Polyaniline- TiO_2 (1:1 molar ratio of aniline and TiO_2)	TP3
5	Polypyrrole- TiO_2 (1:4 molar ratio of pyrrole and TiO_2)	TPpy1
6	Polypyrrole- TiO_2 (1:1 molar ratio of pyrrole and TiO_2)	TPpy2
7	Polypyrrole- TiO_2 (1:1 molar ratio of pyrrole and TiO_2)	TPpy3
8	Polythiophene- TiO_2 (1:1 molar ratio of thiophene and TiO_2)	TPth1
9	Polythiophene- TiO_2 (1:1 molar ratio of thiophene and TiO_2)	TPth2
10	Polythiophene- TiO_2 (1:1 molar ratio of thiophene and TiO_2)	TPth3
11	Polyaniline	PANI
12	Polypyrrole	Ppy
13	Polythiophene	Pth

2.3. Material Characterization Techniques

The properties of hybrid nanocomposites results from the complex cooperation between the organic and inorganic species constituting the nanocomposites. Continuously, increasing demand of the detailed knowledge of such properties at the nanoscale has contributed to the development of the characterisation techniques. By using appropriate combination of analysis techniques, the desired characterisation on the atomic as well as bulk scale is certainly possible. A thorough characterization of the prepared nanocomposites was undertaken using different spectroscopic as well as quantitative methods. A brief discussion of the characterization method along with its experimental aspects is given in the following sections.

2.3.1. X-Ray Diffraction Analysis

X-ray powder diffraction (XRD) is a rapid analytical technique primarily used for phase identification of a crystalline material and can provide information on unit cell dimensions [3]. The powder diffraction method is thus ideally suited for characterization and identification of polycrystalline phases. The analyzed material is finely ground, homogenized, and average bulk composition is determined [4]. About 95% of all solid materials can be described as crystalline. When X-rays interact with a crystalline substance (Phase), one gets a diffraction pattern [5].

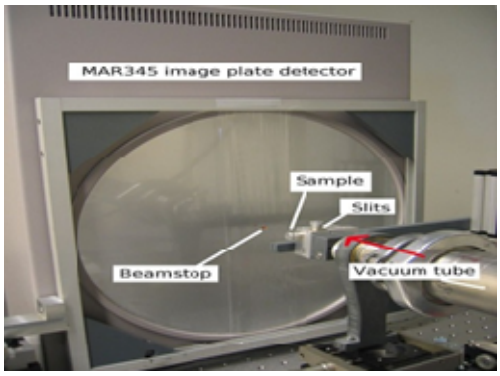

X-Ray Diffractometer

In 1919 A.W.Hull gave a paper titled, "A New Method of Chemical Analysis". Here he pointed out that "….every crystalline substance gives a pattern; the same substance always gives the same pattern; and in a mixture of substances each produces its pattern independently of the others [6]. The X-ray diffraction pattern of a pure substance is, therefore, like a fingerprint of the substance [5]. X-ray diffraction is based on constructive interference of monochromatic X-rays and a crystalline sample. These X-rays are generated by a cathode ray tube, filtered to produce monochromatic radiation, collimated to concentrate, and directed towards the sample. The interaction of the incident rays with the sample produces constructive interference (and a diffracted ray) when conditions satisfy Bragg's Law ($n\lambda=2d$ sin θ). This law relates the wavelength of electromagnetic radiation to the diffraction angle and the lattice spacing in a crystalline sample [7]. An electron in an alternating electromagnetic field will oscillate with the same frequency as the field. When an X-ray beam hits an atom, the electrons around the atom start to oscillate with the same frequency as the incoming beam. In almost all directions we will have destructive interference, that is, the combining waves are out of phase and there is solid sample [8]. However the atoms in a crystal are arranged in a regular pattern, and in a very few directions we will have constructive interference. The waves will be in phase and there will be well defined X-ray beams leaving the sample at various directions. Hence, a diffracted beam may be described as a beam composed of a large number of scattered rays mutually reinforcing one another.

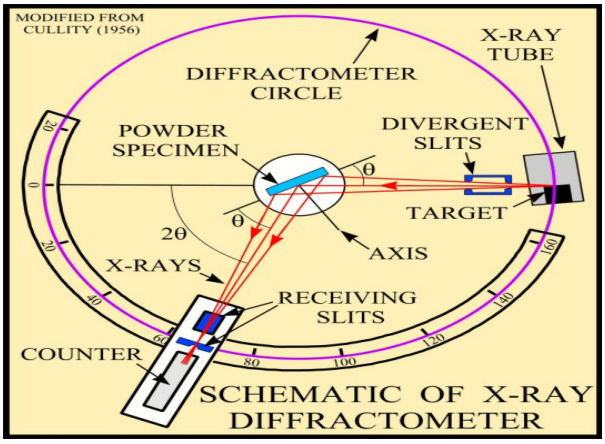

Fig.2.1. Schematic of X-Ray Diffractometer

Only crystallites having reflecting planes (h, k, l) parallel to the specimen surface will contribute to the reflected intensities. These diffracted X-rays are then detected, processed and counted. By scanning the sample through a range of 2θ angles, all possible diffraction directions of the lattice should be attained due to the random orientation of the powdered material. Conversion of the diffraction peaks to d-spacings allows identification of the mineral because each mineral has a set of unique d-spacings. Typically, this is achieved by comparison of d-spacings with standard reference patterns.

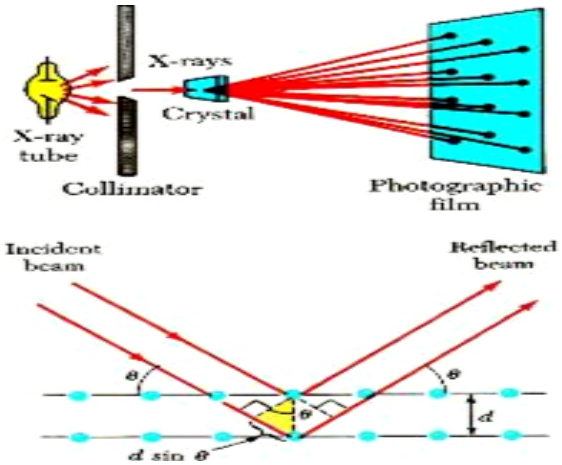

Fig.2.2. Schematic diagram of XRD process

Applications

The most common use of powder (polycrystalline) diffraction is chemical analysis. This can include phase identification (search/match), investigation of high/low temperature phases, solid solutions and determinations of unit cell parameters of new materials. X-ray powder diffraction is most widely used for the identification of unknown crystalline materials (e.g. minerals, inorganic compounds). Determination of unknown solids is critical to studies in geology, environmental science, material science, engineering and biology. Other applications include: characterization of crystalline materials, identification of fine-grained minerals such as clays and mixed layer clays that are difficult to determine optically, determination of unit cell dimensions, measurement of sample purity etc. Some of the strengths and limitations of XRD technique are listed below [9].

Strengths	Limitations
1. Powerful and rapid (< 20 min) technique for identification of an unknown mineral.	1. Homogeneous and single phase material is best for identification of an unknown sample.
2. In most cases, it provides an unambiguous mineral determination.	2. Must have access to a standard reference file of inorganic compounds (d-spacings, *hkl*'s).
3. Minimal sample preparation is required.	3. Requires tenths of a gram of material which must be ground into a powder.
4. XRD units are widely available.	4. For mixed materials, detection limit is ~ 2% of sample.
5. Data interpretation is relatively straight forward.	5. For unit cell determinations, indexing of patterns for non-isometric crystal systems is complicated.
	6. Peak overlay may occur and worsens for high angle 'reflections'.

For mesoporous materials reflections are observed in X-ray powder patterns at low 2θ angles (0.5□2θ□10º). These reflexes are due to the long range order induced by the very regular arrangement of the pores. Generally the d-spacing of the mesopores are rather big so the X-ray diffraction at low angles are observed.

XRD patterns were recorded in Bruker AXS D8 Advance X-Ray Diffractometer using Ni filtered CuKα radiation (λ=1.5406 A°) in the range 5-70° at a scan rate 2^0/ min. Low angle XRD measurements of the samples were taken on a Panalytical Xpert PRO MPD model with Ni filtered Cu K α radiation (λ= 1.5406 Aº) within the 2θ range 0.1-5º at a speed of 0.25º/min. at room temperature.

2.3.2. UV-Visible Diffuse Reflectance Spectroscopy

Optical properties of un-supported or powdered nanostructures are frequently determined through UV-Vis absorption spectroscopy of their dispersed solutions in liquid media. Though the peak position of the absorption band of semiconductor nanostructures could be defined well from such measurements, precise determination of their band gap energies (*Eg*) is difficult. However, using the Kubelka-Munk treatment on the diffuse reflectance spectra of such powdered semiconductor nanostructures, it is possible to extract their *Eg* unambiguously. Effects of light scattering in the absorption spectra of powder samples dispersed in liquid media can be avoided using DRS [10]. Spectroscopic investigations of

UV-Vis. Diffuse reflectance

solutions, gas phase and individual crystals usually take place in transmission, but it is very difficult to obtain transparent films of powders and solids (e.g., heterogeneous catalysts), making transmission experiments almost impossible. Alternatively, diffuse reflected light can be collected and this technique has been named diffuse reflectance spectroscopy (DRS) [11]. One of the advantages of DRS is that the obtained information is directly chemical in nature since outer shell electrons of the transition metal ions are probed. This provides information about the oxidation state and coordination environment of transition metal ions in catalytic solids. DRS is quantitative and can be used under in-situ conditions. The main disadvantage of the technique is that DRS spectra are complex, and usually encompass several broad and overlapping bands [12].When electromagnetic radiation in the UV/Visible wavelength range interacts with a sample, four results are possible: the radiation is absorbed, transmitted, reflected or scattered. When equipped with the proper accessories, UV/Vis. instruments can measure the reflected and scattered energy from a sample. Reflected radiation can be either specular or diffuse. An integrating sphere, when used in combination with the Lambda 35 spectrometer, is a valuable tool for collecting and measuring specular and/or diffuse reflectance [13]. The interaction of light of the UV-Vis-NIR region with catalytic solids is considered to be a complex process due to absorption and scattering phenomena.

These phenomena are largely overcome by the application of techniques such as DRS spectroscopy. DRS is based on the reflection of light by a powdered sample, and the dimensions of the individual particles in such powdered samples are comparable to the wavelength; i.e., 0.2-3μm. This makes it impossible to distinguish the phenomena of reflection, refraction and

diffraction; the light is scattered. Diffuse reflected light from a non-absorbing medium involves photons, which are scattered in all directions [14]. Excellent reference materials are totally reflecting over an as-wide-as-possible wavelength range. All reference materials (MgO, $BaSO_4$, Spectralon®, etc.) have reflectance losses at wavelengths below 250 nm. This leads to artefacts, which implies that recording spectra below 250 nm is not really reliable [15, 16]. In addition, reference materials must be stable toward water and other chemical compounds. Absorbance measurements as well as onset absorption were taken in Spectrophotometer UV-Vis. Double beam UVD-3500, labomed, Inc.

2.3.3. FT-IR Spectroscopy

During the past years, the technique of infrared Fourier Transform Spectroscopy has become more and more important as an instrument for obtaining high quality IR spectra in analytical research and process control. There are two reasons for this development, viz. the capability of Infrared Fourier Transform Spectrometers of producing routine spectra in shorter times and of better quality than those from conventional grating systems and the extension of the possibilities of performing measurements which would be impossible with grating systems. Superior sensitivity and resolution, rapid sample measurement, absolute wavelength accuracy, versatile spectra processing, and total automation of complex analysis are fundamental reasons why one is turning to Fourier Transform Infrared (FT-IR).

Infrared Spectroscopy gives information on the vibrational and rotational modes of motion of a molecule and hence an important technique for identification and characterization of a substance. The infrared spectrum originates from the vibrational motion of the molecule. The vibrational frequencies are a kind of fingerprint of the compounds. This property is used

for characterization of organic, inorganic and biological compounds [17,18]. The band intensities are proportional to the concentration of the compound and hence qualitative estimations are possible. Generally organic compounds and many inorganic compounds give useful results. Hence FTIR is an important technique for identification and characterization of a substance.

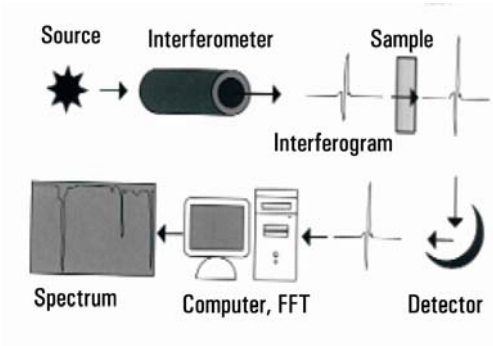

Fig.2.3. Working Principle of FT-IR Spectrometer

FT-IR Spectrometer

Applications:

Fourier Transform Infrared Spectroscopy is exceptionally suitable for obtaining spectra in energy limited situations (small quantities of samples, trace impurities in mixtures, weakly absorbing samples etc.) and conditions under which conventional dispersive instruments fail to produce the desired spectra.

The use of FT-IR in research, analytical and quality control laboratories has brought new and extended capabilities to all users.

Physical Properties: Thickness, Crystallinity, Polymerisation, Vulcanisation, Phase change, hydrogen bonding.

Kinetics of Reactions: Degradation studies, Photochemistry. Time Resolved Spectroscopy.

Theoretical: Molecular orientation. Molecular Interactions, Pure rotation.

Low Energy: ATR. Highly scattering, strongly absorbing. Typical application includes Chemistry & Chemical Engineering, Polymer & Rubber Industries, Forensic Labs, Pharmaceutical Labs Food Industries, Agriculture, Petroleum Industries and Nanotechnology.

The Infrared induced vibrations of the samples were recorded using *Thermo NICOLET 380 FTIR* Spectrometer by means of KBr pellet procedure. Spectra were taken in the transmission mode under atmospheric pressure and room temperature. The changes in the absorption bands were investigated in the 400-4000 cm^{-1} range. The resolution and acquisition applied were 4 cm^{-1} and 60 scans respectively.

2.3.4. Transmission Electron Microscopy

Transmission Electron Microscope

It is a microscopic technique whereby a beam of electrons is transmitted through an ultra thin specimen and interacts as it passes through the sample. An image is formed from the electrons transmitted from the specimen are magnified and focused by an objective lens and appears on an imaging screen [19]. TEM images are formed using transmitted electrons (instead of the visible light) which can produce magnification details up to 1,000,000x with resolution better than 10 A°. The images can be resolved

over a fluorescent screen or a photographic film. Furthermore the analysis of the X-ray produced by the interaction between the accelerated electrons with the sample allows determining the elemental composition of the sample with high spatial resolution [20]. In TEM the crystalline sample interacts with electron beam by diffraction rather than by absorption. The intensity of diffraction depends upon the orientation of the planes of atoms in a crystal relative to the electron beam; at certain angles the electron beam is strongly diffracted from the axis of the incoming beam, while at other angles the beam is largely transmitted. Therefore a highly contrasted image can be formed by blocking electrons deflected away from the optical axis of the microscope by placing the aperture to allow only unscattered electrons through it.

This produces a variation in electron intensity that reveals information on the crystal structure [19]. The specimens must be prepared as a thin foil so that electron beam can penetrate. In the case of materials that are in the form of powders or nanotubes, which are electron transparent, the specimens were prepared by deposition of the diluted sample on to the support grids [19].

Applications

It is used both in material science and biological science. It also finds application in the field of Nanotechnology, Ceramics, Pharmaceuticals and Semiconductors etc.

Morphology of all samples was observed on a PHILIPS, CM200 Transmission Electron Microscope, Operating voltages: 20-200kv Resolution: 2.4 A^{o}.

2.3.5. Raman Spectroscopy

FT-Raman Spectrometer

Raman Spectroscopy is a spectroscopic technique used to study vibrational, rotational and other low frequency modes in a system. Raman spectroscopy results from inelastic scattering (Raman scattering) of radiation from molecules. The difference in frequencies of the incident and scattered light corresponds to the vibrational and rotational energies of the molecule. It is the change in the polarisability of the molecule that is responsible for the transitions. Symmetry selection rules predict that for centro-symmetric molecules, the Raman active vibrations will be IR inactive and vice versa (mutual exclusion principle) [21]. The laser light interacts with phonons or other excitations in the system resulting in the energy of the laser photons shifted up or down and the shift in energy gives information about the vibrational modes in the system [22].

When light impinges on a molecule it interacts with electron cloud of the bonds and the incident photon excites one of the electrons in to a virtual state. For the spontaneous Raman effect the molecule will be excited from the ground state to a virtual energy state and relax in to a vibrational excited state which generates stokes Raman scattering. If the molecule was already in an elevated vibrational excited state, it is then called antistokes Raman scattering. The amount of deformation of electron cloud or the polarisability change will determine the Raman scattering intensity whereas Raman shift is equal to the vibrational level that is involved [23].

Applications

It is widely used in chemistry since vibrational information is very specific for chemical bonds in molecules. It provides a fingerprint by which molecules can be identified in the range of 500-2000 cm^{-1}. Raman gas analysers are used in medicine for real time monitoring of anaesthetic and respiratory gas mixtures during surgery. The polarisation of Raman scattered light with respect to the crystal and the polarisation of laser light can be used to find the orientation of the crystal [19, 22].

Raman spectra were recorded on Horiba Jobin Yvon Lab Ram HR system at a spatial resolution of 2 mm in a backscattering configuration. The 514.5 nm line of Argon ion laser was used for excitation.

2.3.6. Thermo Gravimetric Analysis (TGA)

Thermogravimetric analysis (TGA) is the most widely used thermal method. It is a technique in which the mass of a substance is monitored as a function of temperature or time as the sample specimens is subjected to a controlled temperature programme in a controlled atmosphere. It is based on the measurement of mass loss of material as a function of temperature. In thermogravimetry a continuous graph of mass change against temperature is obtained when a substance is heated at a uniform rate or kept at constant temperature. A plot of mass change versus temperature (T) is referred to as the thermogravimetric

Thermogravimetric Analyser

curve (TG curve). For the TG curve, we generally plot mass (*m*) decreasing downwards on the *y* axis (ordinate), and temperature (*T*) increasing to the right on the x axis (abscissa). Sometime we may plot time (*t*) in place of T [24]. TG curve helps in revealing the extent of purity of analytical samples and in determining the mode of their transformations within specified range of temperature. A TGA consists of a sample pan that is supported by a precision balance. The pan resides in a furnace and is heated or cooled during the experiment. The mass of the sample is monitored during the experiment. A sample purge gas controls the sample environment. This gas may be inert or a reactive gas that flows over the sample and exits through an exhaust. In most cases, TGA analysis is performed in an oxidative atmosphere (air or oxygen and inert gas mixtures) with a linear temperature ramp. The maximum temperature is selected so that the specimen weight is stable at the end of the experiment, implying that all chemical reactions are completed (i.e., all of the carbon is burnt off leaving behind metal oxides). This approach provides two important numerical pieces of information: ash content (residual mass, M_{res}) and oxidation temperature (T_o). Thermogravimetric analysis (TGA) is an analytical technique used to determine a material's thermal stability and its fraction of volatile components by monitoring the weight change that occurs as a specimen is heated. The measurement is normally carried out in air or in an inert atmosphere, such as Helium or Argon, and the weight is recorded as a function of increasing temperature. Sometimes, the measurement is performed in a lean oxygen atmosphere (1 to 5% O_2 in N_2 or He) to slow down oxidation. In addition to weight changes, some instruments also record the temperature difference between the specimen and one or more reference pans (differential thermal analysis, or DTA). Measurements are used primarily to determine the composition of materials and to predict their thermal stability at temperatures

up to 1000°C.The technique can characterize materials that exhibit weight loss or gain due to decomposition, oxidation, or dehydration.

Applications

TGA can be used to understand the chemistry of decomposition of a particular compound. TGA also provides information about the temperature range over which a particular sample appears to be stable or unstable. We have also interpreted TG curves qualitatively. Beside these there are many other applications of thermogravimetric analysis. Some are listed below [25].

i) Purity and thermal stability.
ii) Solid state reactions.
iii) Decomposition of inorganic and organic compounds.
iv) Determining composition of the mixture.
v) Corrosion of metals in various atmospheres.
vi) Pyrolysis of coal, petroleum and wood.
vii) Roasting and calcinations of minerals.
viii) Reaction kinetics studies.
ix) Evaluation of gravimetric precipitates.
x) Oxidative and reductive stability.
xi) Determining moisture, volatile and ash contents.
xii) Desolvation, sublimation, vaporizations, sorption, desorption, chemisorptions.

TG/DTA analysis was done on a *Perkin Elmer Pyris Diamond* thermogravimetric/differential thermal analyzer instrument under nitrogen atmosphere at a heating rate of 5-10°/min from room temperature to 1000°C with samples mounted on analyser.

2.3.7. X-ray photoelectron spectroscopy

X-ray Photoelectron Spectroscopy –XPS (also known as ESCA-Electron Spectroscopy for Chemical Analysis) is a non-destructive technique which provides chemical analysis of the outermost 5-10 nm of any vacuum compatible solid. The sample is illuminated with monochromatic X-rays which have sufficient photon energy to cause the photoemission of the core level electrons whose binding energies are characteristic of the elements present. The position and intensity of the peaks provide both chemical (e.g. oxidation state) and quantitative (> ~0.1 atom %) information for all elements except hydrogen. Underlying layers can be examined by the use of XPS in conjunction with argon-ion bombardment providing elemental depth information due to the destructive nature of the ion bombardment [26].

X-Ray Photoelectron Spectrometer

X-ray Photoelectron Spectroscopy (XPS) is one of a number of surface analytical techniques that bombards the sample with photons, electrons or ions in order to excite the emission of photons, electrons or ions. It is also known as electron spectroscopy for chemical analysis (ESCA). A semi-quantitative technique for determining composition based on the photoelectric effect. XPS measures the elemental composition, empirical formula, chemical state and electronic state of the elements that exist within a material. XPS is based on the principle that X-rays hitting atoms generate photoelectrons. It is a typical example of a surface-sensitive technique. Only electrons that are generated in

the top few atomic layers are detected. In this way quantitative information can be obtained about the elemental composition of the surface of all kinds of solid material (insulators, conductors, polymers). An important strength of XPS is that it provides both elemental and chemical information XPS spectra are obtained by irradiating a material with a beam of X-rays while simultaneously measuring the kinetic energy and number of electrons that escape from the top 1 to 10 nm of the material being analyzed. XPS requires ultra-high vacuum (UHV) conditions. Bombarding a sample in vacuum with X-rays gives rise to the emission of electrons. If monochromatic X-rays are used with a photon energy hν, the kinetic energy of the emitted electrons K_e is given by:

$$K_e = h\nu - B_e - \square$$

where B_e is the binding energy of the atomic orbital from which the electron originates and φ is the work function. The work function is the minimum amount of energy an individual electron needs to escape from the surface. Each element produces unique set of electrons with specific energies. By measuring the number of these electrons as a function of kinetic (or binding) energy, an XPS spectrum is obtained. All elements can be detected, except H and He because the diameter of these orbitals is so small, to reduce the catch probability to almost zero. The sample analysis is conducted in a vacuum chamber, under the best vacuum conditions achievable, typically ~10^{-10} torr. This facilitates the transmission of the photoelectrons to the analyzer but more importantly minimizes the re-contamination rate of a freshly cleaned sample. This is crucial because XPS is very surface-sensitive, with a typical "sampling depth" of only a few nanometers.

Application

- Characterization of thin layers (< 10 nm)
- Characterization of thick layers by sputtering
- Contamination
- Cause of bad adherence
- Chemical information

XPS measurement was done using SPECS XPS system with150W achromatic Al Kα X-ray source at 1486.6 eV energy. The survey scans were obtained at 70eV pass energy and composition was obtained from survey scan. Core level spectra of C1s and S 2p were obtained at 25 eV pass energy and Ti 2p and O1s core levels at 40eV pass energies. C1s, S 2p and Ti 2p core levels were deconvoluted with Gaussian-Lorenztian to get component peaks.

2.3.8. Scanning Electron Microscopy (SEM)

The scanning electron microscope (SEM) enables the investigation of specimens with a resolution down to the nanometer scale. It is a type of electron microscope that images a sample by scanning it with a beam of electrons in a raster scan pattern. Here an electron beam is generated by an electron cathode and the electromagnetic lenses of the column and finally swept across the surface of a sample. The path of the beam describes a raster which is correlated to a raster of gray level pixels on a screen. As a consequence the magnification is simply computed by the ratio of the image width of the output medium divided by the field width of the scanned area.

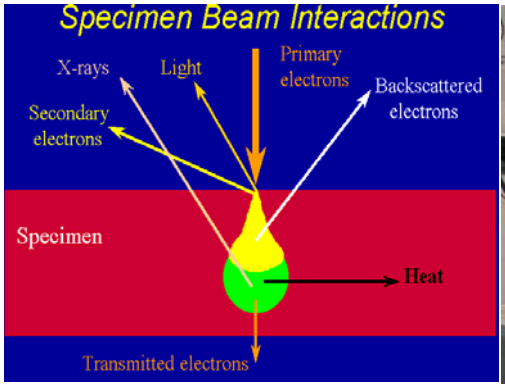

Fig.2.5. Principle of SEM Imaging Scanning Electron Microscope

The electrons interact with the atoms that make up the sample producing signals that contains information about the sample's surface topography, composition, and other properties such as conductivity. The main signals which are generated by the interaction of the primary electrons (PE) of the electron beam and the specimen´s bulk are secondary electrons (SE) and backscattered electrons (BSE**)** and furthermore X rays. Accelerated electrons in SEM carry significant amounts of kinetic energy, and this energy is dissipated as a variety of signals produced by electron-sample interactions when the incident electrons are decelerated in the solid sample. These signals include secondary electrons (that produce SEM images), backscattered electrons (BSE), diffracted backscattered electrons (EBSD that are used to determine crystal structures and orientations of minerals), photon characteristic X-rays that are used for elemental analysis and continuum X-rays), visible light (cathodoluminescence--CL), and heat. Secondary electrons and backscattered electrons are commonly used for imaging samples: secondary electrons are most valuable for showing morphology and topography on samples and backscattered electrons are most valuable for illustrating contrasts in composition in multiphase samples (i.e. for rapid phase discrimination[28].

SEM gives high resolution surface morphological images, and also has the analytical capabilities such as detecting the presence of elements down to boron (B) on any solid conducting materials through the energy dispersive X-ray spectrometry (EDX) providing information about crystallanity from the few nanometer depth of the material surface via electron back scattered detection (BSD) system attached with microscope and advanced technological PBS (WDS) for elemental analysis. Liquid samples and solid samples which are magnetic/ferrite cannot be measured.

In the conventional scanning electron microscope, which operates in high vacuum, the specimen has to be electrically conductive or has to be coated with a conductive layer (e.g. Carbon, Gold etc.).

Applications

The SEM is routinely used to generate high-resolution images of shapes of objects and to show spatial variations in chemical compositions: (1) acquiring elemental maps or spot chemical analyses using EDS,(2) discrimination of phases based on mean atomic number (commonly related to relative density) using BSE, and (3) compositional maps based on differences in trace element "activitors" (typically transition metal and Rare Earth elements) using cathodoluminescence (CL). The SEM is also widely used to identify phases based on qualitative chemical analysis and/or crystalline structure [28].

The main features and benefits of the SEM are:-

- Image magnification and resolution
- Magnification range X 15 - X 200,000
- Resolution 2 nm

- Accelerating voltage 1 - 30 keV
- Secondary and backscattered electron imaging
- Stereo imaging and stereo height measurement
- EDX analysis of known or unknown materials
- Automatic particle counting and characterisation
- Qualitative and quantitative analysis for all elements from carbon upwards
- Quantitative analysis of bulk materials and features ≥ 2 μm
- Qualitative analysis of features ≥ 0.2 μm
- Detection limits typically 0.1 - 100 wt% for most elements
- Multi-element X-ray mapping and line scans
- Multi-layer, multi-element thin film analysis-Thickness and composition
- Particle / Phase analysis - Detection, analysis, morphology and size
- Image Analysis
- Automatic particle counting and characterization[29]

The scanning electron micrographs of the samples were taken using *JEOL Model JSM-6390LV* scanning electron microscope with a resolution of 1.38 eV. The powdered samples were dusted on a double sided carbon tape, placed on a metal stub and was coated with a layer of gold to minimize charge effects.

2.3.9. Energy Dispersive X-ray Spectrometry (EDX)

Energy dispersive X-ray analysis is a technique to analyze near surface elements and estimate their proportion at different position, thus giving an overall mapping of the sample. EDS makes use of the X-ray spectrum emitted

by a solid sample bombarded with a focused beam of electrons to obtain a localized chemical analysis. All elements from atomic number 4 (Be) to 92 (U) can be detected in principle, though not all instruments are equipped for 'light' elements (Z < 10). Energy Dispersive Spectroscopy (EDS) allows one to identify particular elements and their relative proportions (Atomic % for example).

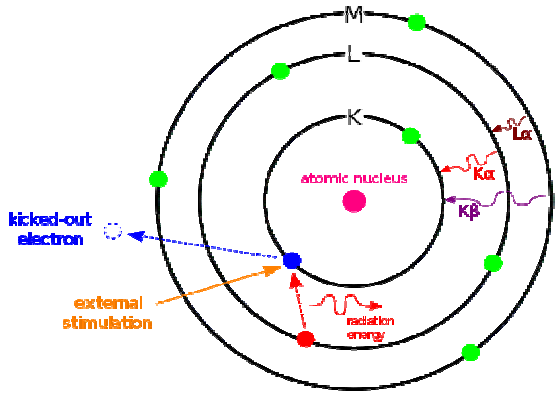

Fig.2.6. Basic phenomenon of EDAX analysis of an atom

The electron beam excites the atoms in the sample that subsequently produce X-rays to discharge the excess energy. The energy of the X-rays is characteristic of the atoms that produced them, forming peaks in the spectrum. The EDS- X-ray detector measures the relative abundance of emitted X-rays versus their energy. The detector is typically lithium-drifted silicon, solid-state device. When an incident X-ray strikes the detector, it creates a charge pulse that is proportional to the energy of the X-ray. The charge pulse is converted to a voltage pulse (which remains proportional to the X-ray energy) by a charge-sensitive preamplifier. The signal is then sent to a multichannel analyzer where the pulses are sorted by voltage. The energy, as determined from the voltage measurement, for each incident X-ray is sent to a computer for display and

further data evaluation. The spectrum of X-ray energy versus counts is evaluated to determine the elemental composition of the sampled volume. Many elements will have overlapping peaks (e.g., Ti K_β and V K_α, Mn K_β and Fe K_α). The accuracy of the spectrum can also be affected by the nature of the sample.

Typical Applications

- Foreign material analysis
- Corrosion evaluation
- Coating composition analysis
- Rapid material alloy identification
- Small component material analysis
- Phase identification and distribution

Compositional information about the sample was analysed by EDX using JEOL model JED-2300.

2.3.10. N_2 adsorption –desorption Isotherm

BET-Surface Area Analyser

In heterogeneous catalysis, the reaction occurs at the surface. To predict the catalyst properties, surface area determination is very important. Brunauer-Emmett-Teller method is the widely used procedure for the determination of the surface area of solid materials and involves the use of BET equation. This method is based on the physical adsorption of gases on solid surfaces which leads to multilayer adsorption. The BET equation can be represented as

$P/V\ (P_0-P) = (1/V_m.C) + ((C-1)/V_m.C)\ P/P_0$

V - Volume of gas adsorbed at equilibrium pressure P

P_0 - Standard vapour pressure of the adsorbate at liquid nitrogen temperature

C - Isothermal constant.

By plotting $P/V\ (P_0-P)$ Vs P/P_0 and determining V_m from slope of the resultant straight line in the partial pressure range of 0.05 to 0.35, the specific surface area can be calculated using the relation

$A = V_M N_0 A_M / Wx22414$

N_0 - Avogadro number

A_M - the molecular cross sectional area of the adsorbate (0.162 nm^2 for N_2)

W - Weight of the sample (g)

The method is based on the adsorption of N_2 at liquid N_2 temperature.

Several computational procedures are available for derivation of pore size distribution of mesoporous samples from physisorption isotherms. Most popular among them is the Barrett-Joyner-Halenda (BJH) model. First, the volumes desorbed from the sample at different partial pressures are converted to liquid volumes (multiplying by 0.00156).The next step is to use Kelvin equation to calculate the value of the volume of the liquid in the capillary. The Kelvin equation shows that the smaller the pore radius, the lower the vapour pressure, P, in the pore

$$P/P_o = \exp(-2\upsilon\gamma/r_k RT)$$

Pore volume is a property that has been utilized extensively in characterizing a molecular sieve material due to its ability to adsorb selected

molecules. It is always determined using several probe molecules such as n-hexane, water, nitrogen etc. The probe molecules of various sizes also have been used to gain information on the size of the pore openings, using gravimetric adsorption methods.

Advantage with nitrogen as adsorbate lies in that the value of C, on almost all surfaces is sufficiently small to prevent localized absorption and at the same time large enough to prevent the adsorption layer from behaving as a two dimensional gas. Here we determine the volume of N_2 gas adsorbed by a known weight of sample at liquid N_2 temperature. Since the area occupied by single adsorbed molecular nitrogen can be estimated, the total surface area can be calculated by multiplying the area of one molecule by the number of molecules required for forming the monolayer. Adsorption varies directly with pressure and inversely with temperature. Here the temperature is held constant and the amount of nitrogen adsorbed at liquid nitrogen temperature is measured at different relative pressures. Linearity of the plot is limited to relative pressures in the range 0.1 to 0.3.

In the present investigation simultaneous determination of surface area, pore size distribution and total pore volume of the samples were achieved in a *Micromeritics Tristar 3000* surface area and porosity analyser. Prior to the analysis the samples were degassed at 90°C for half an hour and then at 250°C for overnight.

2.3.11. Cyclic Voltametry

The common characteristic of all voltammetric techniques is that they involve the application of a potential (E) to an electrode and the monitoring of the resulting current (i) flowing through the electrochemical cell. In many

cases the applied potential is varied or the current is monitored over a period of time(t). Thus, all voltammetric techniques can be described as some function of E, i, and t. They are considered active techniques (as opposed to passive techniques such as potentiometry because the applied potential forces a change in the concentration of an electroactive species at the electrode surface by electrochemically reducing or oxidizing it. Cyclic voltammetry is the most widely used technique for acquiring qualitative information about electrochemical reactions. Cyclic voltammetry (CV) has become an important and widely used electro analytical technique in many areas of chemistry. It offers a rapid location of redox potentials of the electroactive species. It is rarely used for quantitative determinations, but it is widely used for the study of redox processes, for understanding reaction intermediates, and for obtaining stability of reaction products. This technique is based on varying the applied potential at a working electrode in both forward and reverse directions (at some scan rate) while monitoring the current. For example, the initial scan could be in the negative direction to the switching potential. At that point the scan would be reversed and run in the positive direction. Depending on the analysis, one full cycle, a partial cycle, or a series of cycles can be performed. A three-electrode arrangement is used. The method uses a reference electrode, working electrode, and counter electrode which in combination are sometimes referred to as a three-electrode setup. Electrolyte is usually added to the test solution to ensure sufficient conductivity. The combination of the solvent, electrolyte and specific working

Electrochemical Analyser

electrode material determines the range of the potential. Common materials for working electrodes include glassy carbon, platinum, and gold. These electrodes are generally encased in a rod of inert insulator with a disk exposed at one end. The main virtue of voltammetric techniques is their good accuracy, excellent precision (<1%), sensitivity, and wide dynamic range. In cyclic voltammetry, the electrode potential ramps linearly versus time. This ramping is known as the experiment's scan rate (V/s). The potential is applied between the reference electrode and the working electrode and the current is measured between the working electrode and the counter electrode. This data are then plotted as current (*i*) vs. potential (*E*).

General Uses

- Quantitative determination of organic and inorganic compounds in aqueous and nonaqueous solutions.
- Measurement of kinetic rates and constants
- Determination of adsorption processes on surfaces
- Determination of electron transfer and reaction mechanisms
- Determination of thermodynamic properties of solvated species
- Fundamental studies of oxidation and reduction processes in various media
- Determination of complexation and coordination values

Common Applications

- Quantitative determination of pharmaceutical compounds
- Determination of metal ion concentrations in water to sub–parts-per-billion levels

- Determination of redox potentials
- Detection of eluted analytes in high-performance liquid chromatography (HPLC) and flow injection analysis
- Determination of number of electrons in redox reactions
- Kinetic studies of reactions

Limitations

- Substance must be oxidizable or reducible in the range were the solvent and electrode are electrochemically inert.
- Provides very little or no information on species identity.
- Sample must be dissolved
- Accuracy varies with technique from 1 to 10%.
- Detection limit varies with technique from parts per thousand to parts per trillion.

Electrochemical measurements were made on BAS Epsilon Electrochemical analyzer (Bioanalytical system USA) interfaced to a PC.

2.3.12. Photoluminescence Spectroscopy

Photoluminescence (PL) spectroscopy is a contactless, non-destructive method to probe the electronic structure of materials. The energy levels in a semiconductor quantum well structure are investigated using the technique of photoluminescence (PL). If a light particle (photon) has energy

Spectrofluorometer

greater than the band gap energy, then it can be absorbed and thereby raise an electron from the valence band up to the conduction band across the forbidden energy gap. In this process of photoexcitation, the electron generally has excess energy which it loses before coming to rest at the lowest energy in the conduction band. At this point the electron eventually falls back down to the valence band. As it falls down, the energy it loses is converted back into a luminescent photon which is emitted from the material. Thus the energy of the emitted photon is a direct measure of the band gap energy, Eg. The process of photon excitation followed by photon emission is called photoluminescence. The period between absorption and emission is typically extremely short, in the order of 10 nanoseconds. Under special circumstances, however, this period can be extended into minutes or hours.

The intensity and spectral content of the emitted photoluminescence is a direct measure of various important material properties, including:

1) **Band gap Determination.** The spectral distribution of PL from a semiconductor can be analyzed to non-destructively determine the electronic band gap. This provides a means to quantify the elemental composition of compound semiconductor and is vitally important material parameter influencing solar cell device efficiency.

2) **Impurity Levels and Defect Detection:** The PL spectrum at low sample temperatures often reveals spectral peaks associated with impurities contained within the host material. The high sensitivity of this technique provides the potential to identify extremely low concentrations of intentional and unintentional impurities that can strongly affect material quality and device performance.

3) **Recombination Mechanisms:** The quantity of PL emitted from a material is directly related to the relative amount of radiative and nonradiative recombination rates. Nonradiative rates are typically associated with impurities and thus, this technique can qualitatively monitor changes in material quality as a function of growth and processing conditions

4) **Material Quality:** In general, nonradiative processes are associated with localized defect levels, whose presence is detrimental to material quality and subsequent device performance. Thus, material quality can be measured by quantifying the amount of radiative recombination.

Photoluminescence measurements were carried using Jobin Yvon Fluoromax-3 spectrometer equipped with 150W Xe lamp.

2.3.13. Electron spin resonance spectroscopy (ESR)

ESR is sometimes also referred to as EPR (electron paramagnetic resonance) or EMR (electron magnetic resonance). Electron spin resonance (ESR) or electron paramagnetic resonance spectroscopy (EPR) is a sophisticated spectroscopic technique that detects free radicals or inorganic complexes in chemical and biological systems. Generally, these radicals are unstable, but when they are first reacted with spin-trapping reagents, they can be trapped and stabilized. On the other hand, with use of a spin-labelling reagent, the molecules without radicals can also be measured with ESR/EPR. EPR detects unpaired electrons of materials contained in a homogeneous magnetic

EPR Spectrometer

field using microwave radiation to establish a resonance condition that can be detected by suitable microwave detectors. It is often called electron spin resonance (ESR) since many systems with unpaired electrons are free radicals. EPR is a technique used in chemistry and physics, in materials science (e.g. to characterize polymers, magnetic and conducting materials, crystalline defects, etc.) and increasingly in biology and medicine. EPR can also be used for magnetic resonance imaging where it has the special advantage of only detecting unpaired electrons contained, usually, in a specific spin-labelled drug. It uses magnetic fields corresponding to a microwave frequency range between 1GHz and 500GHz to study paramagnetic materials and molecules. ESR can be used to obtain structural information of molecules together with details about their electron density distributions. In principle, EPR spectra can be generated by either varying the photon frequency incident on a sample while holding the magnetic field constant or doing the reverse. In practice, it is usually the frequency that is kept fixed. A collection of paramagnetic centers, such as free radicals, is exposed to microwaves at a fixed frequency. By increasing an external magnetic field, the gap between the $m_s = +1/2$ and $m_s = -1/2$ energy states is widened until it matches the energy of the microwaves. At this point the unpaired electrons can move between their two spin states. Since there typically are more electrons in the lower state, due to the Maxwell-Boltzmann distribution, there is a net absorption of energy, and it is this absorption that is monitored and converted into a spectrum. Since the source of an EPR spectrum is a change in an electron's spin state, it might be thought that all EPR spectra for a single electron spin would consist of one line. However, the interaction of an unpaired electron, by way of its magnetic moment, with nearby nuclear spins, results in additional allowed energy states and, in turn, multi-lined spectra. In

such cases, the spacing between the EPR spectral lines indicates the degree of interaction between the unpaired electron and the perturbing nuclei.

Applications

EPR spectroscopy is used in various branches of science, such as biology, chemistry and physics, for the detection and identification of free radicals and paramagnetic centers such as F centers.

EPR measurements were made on a VARIAN, USA E-112 ESR Spectrometer with X-band microwave frequency (9.5 GHz) with sensitivity of $5 \times 10^{10} \Delta H$ spins.

2.3.14. Conductivity Studies

The electrical conductivity was measured at room temperature using a standard Four Point Probe technique. The probes were placed on the surface of the pellet. The thickness of the pellets was measured using a micrometer. The calculation of conductivity is as stated below,

$$\sigma = I \ln 2 / V \pi t$$

where σ =conductivity, I=current in Ampere, V= voltage in Volts and t = thickness of the pellet in cm.

Conductivity measurements are taken in Keithley 2400 Source meter, 2001 Multimeter, a 4-point probe set up.

2.4. Application studies

2.4.1. Photocatalysis

The photocatalytic experiments were carried out in an Oriel Arc lamp designed to produce uniform illumination. The diameter of the collimated beam is around 1 inch (2.54 cm) and the work plane is 2.6 inches (6.65cm)

from the lower end of the beam tuning assembly. The uniform illuminator contains a fan cooled lamp housing that provides a stable and temperature controlled environment for the lamp. The light source of the photoreactor system used is a 150 W Xe ozone free lamp with an average life of 1500 hrs. The filter used for the study is 420-630 nm dichoric mirrors (cold mirror) with an irradiance of 96 mW/cm^2 in order to get visible light irradiation.

The photocatalytic degradation of some water pollutants such as dyes, pharmaceutical residues, endocrine disruptors, phenolic compounds such as phenol and nitrophenol were performed under visible light irradiation. The percentage degradation of dyes and 4-nitrophenol were studied using the equation, $((C_0\text{-}C)/C_0)*100$, where C_0 and C represent the initial and final concentration of the samples. Degradation of the endocrine disruptor Bisphenol-A, the antibiotic Sulfamethoxazole and phenol were analysed using HPLC (Dionex Ultimate 3000) with photodiode array UV detector and a 5µm Thermo Hypersil ODS-2 C-18 reverse phase column (150*4.6mm).The degradation products were analysed using LC-MS.

The antibacterial studies were also performed under visible light irradiation. The bacteria selected for the present study was salmonella typhi, the Typhoid causing bacteria. The antibacterial activity was measured using colony counting method.

2.4.2. Thermal diffusivity Measurement

The thermal diffusivity measurements of the polyaniline modified samples were performed using thermal lens spectroscopy. The excitation source is a continuous wave (cw), 532 nm diode pumped solid state laser, (DPSS) with a maximum power of 150 mW. A 2mW He–Ne used as the probe

is arranged to be collinear with the pump, using a dichroic beam splitter. The thermal lens signal was collected using an optical fiber, positioned at the center of the probe beam spot and connected to a photodetector–DSO system. A filter for 532 nm was used before the detector to remove the residual pump.

2.4.3. Nonlinear optical studies

The 3rd order nonlinearity of the polyaniline modified samples was analysed using Z-scan technique. A Q-switched Nd: YAG laser (Spectra Physics LAB-1760, 532 nm, 7 ns, 10 Hz) is used as the light source. The Z-scan system is calibrated using CS_2 as a standard. The transmitted beam energy, reference beam energy and their ratio are measured simultaneously by an energy ratio meter (Rj7620, Laser Probe Corp.) having two identical pyroelectric detector heads (Rjp735). The effect of fluctuations of laser power is eliminated by dividing the transmitted power by the power obtained at the reference detector; both being measured using identical photo detectors.

2.4.4. Light amplification in dye doped nanocomposites

The Lasing studies of the same systems were also performed and in the experimental setup, the laser dye containing aqueous dispersion of polyaniline samples were placed in cuvettes length of 3cm, and width of 0.5 cm. The pumping source of random lasing is a frequency doubled Q-switched Nd: YAG laser (Spectra Physics, 532 nm, 10 Hz). A set of calibrated neutral density filters was used for varying the pump energy. The pump power was measured by using 'COHERENT Labmater Power meter' and it is varied from 14 to 170 mW. The laser emission was recorded using a collecting fiber coupled to a monochromator-CCD system (Spectra Pro) with a resolution of 0.03 nm. A high-speed photodetector and an oscilloscope (Tektronix) were used to measure the temporal intensity profile of the emitted laser pulse.

References

[1]. R. A. Landisc, In Analytical Chemistry: Key to Progress in National Problems, W.W. Meinke, J.K. Yaylor (Eds.), NBS Special Publ. 351, NBS, Washington (1972)19.

[2]. K. Lal, In Advances in Crystallography and Crystal Growth, Krishan Lal (Ed.), Indian National Science Academy, New Delhi 1991:125.

[3]. A. Maqsood and K Iqbal, Materials Characterization by Non-Destructive Methods J Pak Mater Soc. 2010; 4(1).

[4]. B.D. Cullity, S.R. Stock, Elements of X-ray diffraction, 3rd Ed. Upper Saddle River, N.J. Pearson/Prentice Hall, ISBN 0-13-178818-3 2001.

[5]. R. Sharma, D.P. Bisen, U. Shukla, B.G. Sharma, X-ray diffraction: a powerful method of characterizing nanomaterials, Recent Research in Science and Technology 4(8) (2012) 77.

[6]. http://blog.nus.edu.sg/kyawthetlatt/2014/02/03/material-characterizationx-raydiffraction xrd.

[7]. http://serc.carleton.edu/research_ education/geochemsheets/ techniques/XRD.html.

[8]. http://www.vscht.cz/clab/RTG/dokumenty/thermo/xrd/Introduction%20to%20powder%20diffraction.pdf.

[9]. B. L Dutrow, Louisiana State University, C. M. Clark, Eastern Michigan University, X-ray Powder Diffraction (XRD) http://serc.carleton.edu/research education/geochemsheets/techniques/XRD.html.

[10]. A. Escobedo Morales, E. S´anchez Mora, and U. Pal ,REVISTA MEXICANA DE F´ISICA S 53 (5) (2007) 18.

[11]. B. M. Weckhuysen, R. A. Schoonheydt, Catal. Today, 49, (1999) 441.

[12]. In-situ Spectroscopy of Catalysts, Edited by B. M. Weckhuysen, Utrecht University, The Netherlands, Copyright © 2000-2014 American Scientific Publishers.

[13]. http: people.bath.ac.uk / gp304 /uv/4474668PRDDiffuseReflectanceTransmittance.pdf.

[14]. B. M. Weckhuysen, In-situ Spectroscopy of Catalysts, Copyright © 2004 by American Scientific Publishers Edited by B. M. Weckhuysen.

[15]. R. Ahmad, J. Melsheimer, F. C. Jentoft, R. Schlogl, J. Catal., 218, (2003) 365.

[16]. J. Melsheimer, M. Thiede, R. Ahmad, G. Tzolova-Muller, F. C. Jentoft, Phys. Chem. Chem. Phys. 5 (2003) 4366.

[17]. R. D. Waldron, Phy. Rev. 99 (1955) 1727.

[18]. J. T. Hafner, Z. Fur.Krist. 115 (1961) 331.

[19]. M. Joshi, A. Battacharya, S. W. Ali, Indian journal of fibre and Textile Research, 33 (2008) 304.

[20]. http://www.rsic.iitb.ac.in/Tem.html.

[21]. http://saif.iitm.ac.in/facilityinstrument.html.

[22]. http://en.wikipedia.org/wiki/Raman_spectroscopy.

[23]. Electrical Conductive Adhesives with Nanotechnologies By Yi (Grace) Li, Daniel Lu, C.P. Wong; Springer New York Dordrecht Heidelberg London.

[24]. http://anibal.gyte.edu.tr/hebe/AblDrive/77281304/w/Storage/987_2010_2_210_77281304/ Downloads/lecture-21.pdf

[25]. http://www.tahg.org/research/singh_navpreet_tools%20in%20nanotechnology_Nanotech%20TP%20Final.pdf.

[26]. http://www.uq.edu.au/nanoworld/index.html?page=160330&pid=159437.

[27]. http://portal.tugraz.at/portal/page/portal/felmi/research/Scanning%20Electron%20Microscopy/Principles%20of%20SEM.

[28]. http:serc.carleton.edu/research_education/geochemsheets/techniques/SEM.html.

[29]. http://www.lpdlabservices.co.uk/analytical_techniques/sem/sem_instrument.php.

Chapter 3

PHYSICO –CHEMICAL CHARACTERIZATION

Contents

Characterization is an inevitable part of material research. Determination of physico-chemical properties of the prepared materials using suitable characterization techniques is very crucial to find its exact field of application. This chapter presents a comprehensive study of the physico-chemical properties of various TiO_2-conducting polymer hybrid nanocomposites. Various types of spectroscopy, diffraction and imaging techniques were used to achieve the goal of determining and understanding quantitative structure/composition/activity and selectivity relationships.

3.1. Introduction

Synthesis of a compound with desired properties depends on its method of preparation and characterization. These are functionalised by various qualitative, quantitative, sensitive and specific techniques. Quantitative determination of composition and structure on the atomic scale is one of the major advantage of characterization techniques.

3.2. Physico-chemical characterizations

3.2.1. X-ray diffraction analysis

X-ray diffraction is regularly used to identify the different phases in a polycrystalline sample. Two of its most important advantages for analysis of hybrid materials are that it is fast and nondestructive. When the positions and intensities of the diffraction pattern are taken into account the pattern is unique for a single substance. The X-ray pattern is like a fingerprint and mixtures of different crystallographic phases can be easily distinguished by comparison with reference data. X-ray diffractions of the TiO_2, PANI and PANI/TiO_2 composites are presented in Fig.3.1. Pure TiO_2 shows peaks around $2\theta = 25.4^{\circ}$, 37.9°, 48.1°, 54.2°, 55.1°, 62.8°, 69.1°, 70.3° and 75.4°, which correspond to the (101), (004), (200), (105), (211), (204), (116), (220) and (215) reflections of the anatase TiO_2, respectively (JCPDS 21-1272). In the pattern of PANI, the Bragg diffraction peaks of 2θ = 9.4, 14.0, 15.7, 16.9, 26.5 and 27.4 can be found. It indicated that the pure PANI was in partial orthorhombic structure [1]. The other two broad peaks centered at $2\theta = 20.8$ and 25.4° are ascribed to the periodicity parallel and perpendicular to the polymer chain and indicated that the pure PANI was in semi-crystalline phase [2]. In the pattern of PANI-TiO_2 composite, the peaks of 2θ = 9.4, 14.0, 15.7, 16.9 and 27.4° of PANI disappeared and the peak at 20.8° of PANI became weaker.

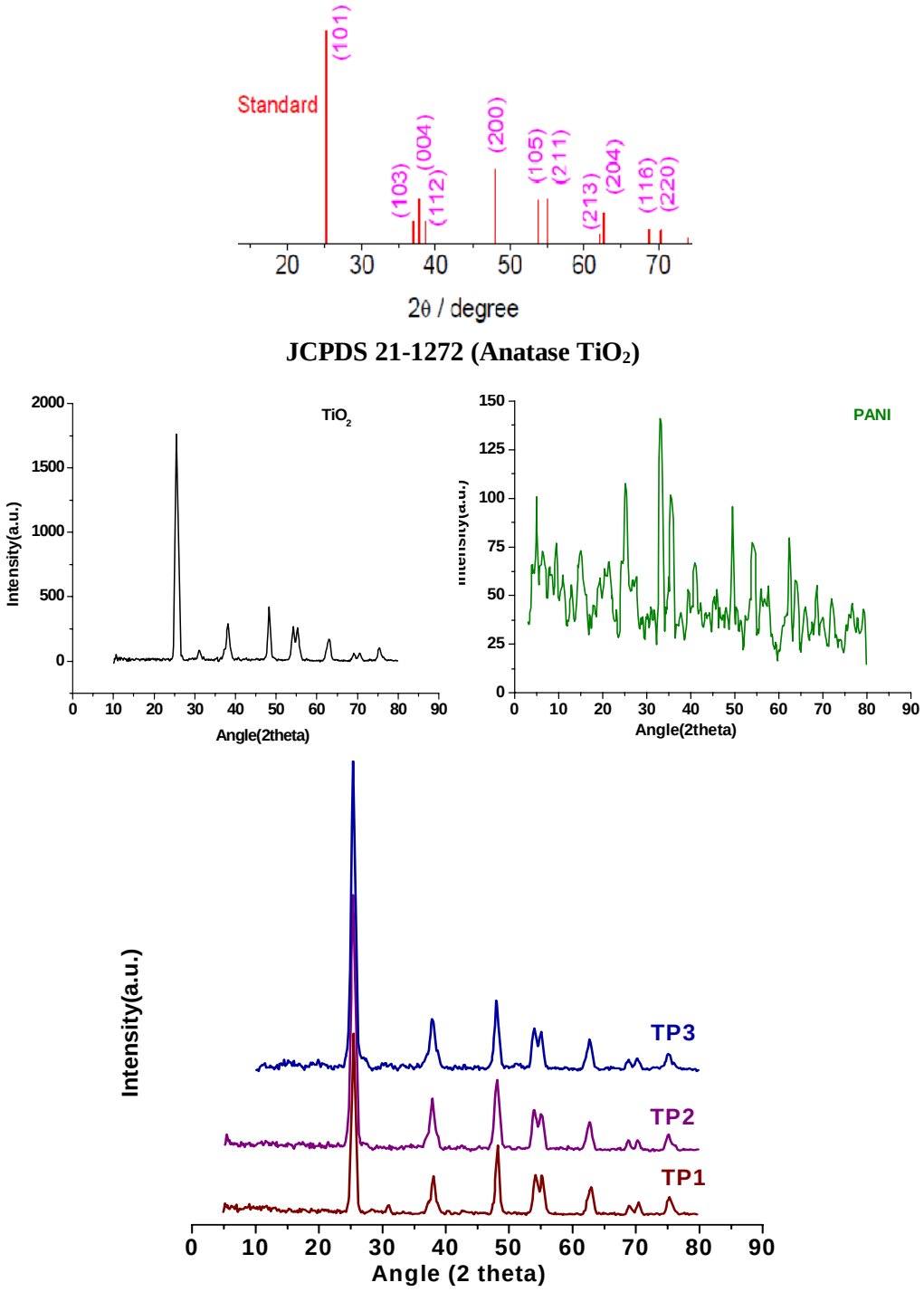

Fig. 3.1. X-ray diffraction pattern of the TiO_2, PANI and PANI/TiO_2 composites

The result suggests that the addition of nanocrystalline TiO_2 hampers the crystallization of the polyaniline molecular chain. This is because when the deposited polyaniline is adsorbed onto the surface of the nano TiO_2 particle, due to the restrictive effect of the surface of TiO_2 nanoparticles and the interaction of PANI and TiO_2 nanoparticles, the molecular chain of adsorbed polyaniline is tethered, and the degree of crystallinity decreases. The diffraction pattern of the nanocomposites is the same as TiO_2 nanoparticles. This result means that PANI deposited on the surface of TiO_2 nanoparticles has no influence on crystallization performance, of TiO_2 nanoparticles [3-5].

Fig.3.2. shows the XRD pattern of TiO_2-Polypyrrole hybrid nanocomposites. Well-defined sharp peaks are observed in the spectra of TiO_2-Polypyrrole hybrid composites, where the peaks at 2θ= 25.28º, 37.8º, 48.04º, 55º and 62.75º match with those of the anatase titania card (JCPDS 21-1272), confirming the crystallinity of TiO_2 phase [6].

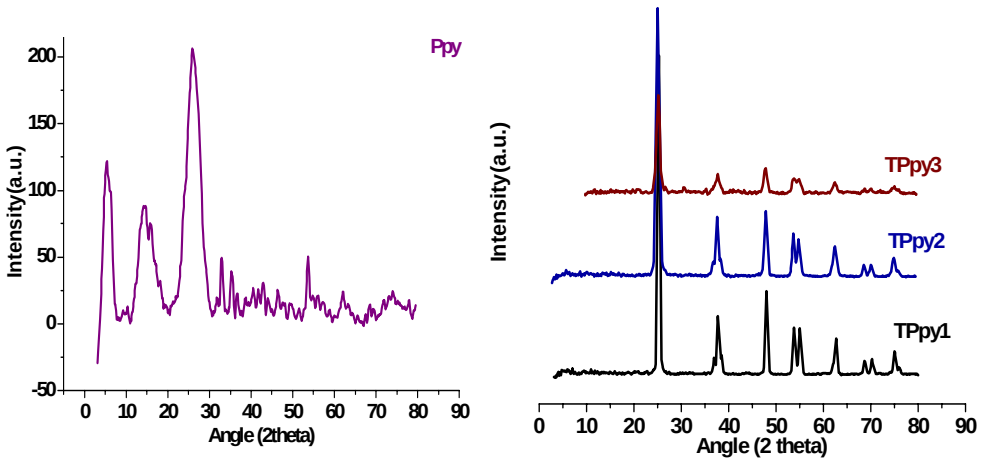

Fig.3.2. X-ray diffraction pattern of the polypyrrole/TiO_2 composites

The modification of TiO_2 by polypyrrole does not change the crystallization performance of neat TiO_2 [7-8].

From the Fig.3.3.which shows the XRD pattern of polythiophene/TiO_2 nanocomposite, it is clear that, the main peaks of the polythiophene/TiO_2 composite are similar to those of pure anatase TiO_2 particles which indicate that the crystalline structure of TiO_2 can be maintained by coating polythiophene conducting polymer because the polythiophene was polymerized after forming the nano-TiO_2 particles [9].

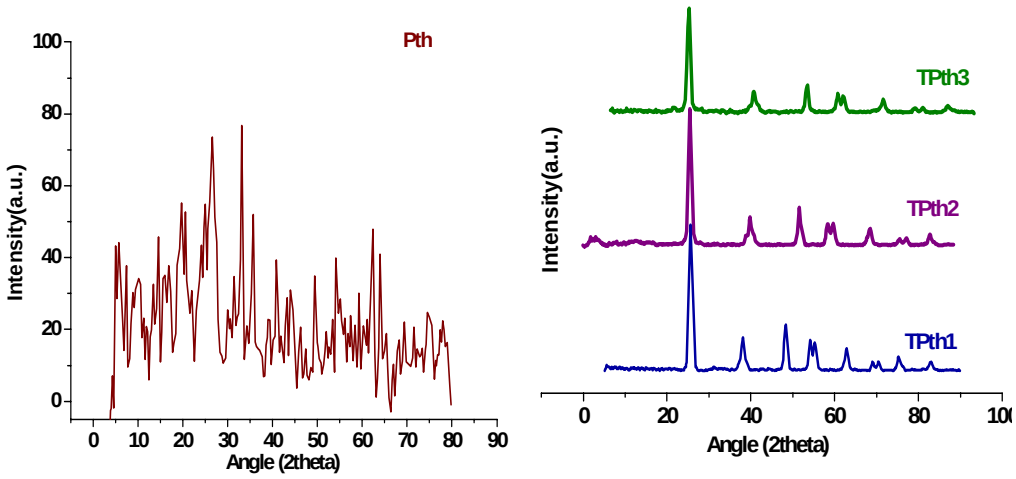

Fig.3.3. X-ray diffraction pattern of the polythiophene/TiO_2 composites

3.2.2. Low angle X-ray diffraction

Low angle XRD pattern of TiO_2 and the hybrid nanocomposites are shown in Fig. 3.4. A broad diffraction peak centred at 2θ of 0.878° in the XRD pattern of TiO_2 suggests the formation of mesostructured textures. The absence of other distinguishable peaks indicates that mesoporous TiO_2 is not well ordered [10].In the case of TiO_2 –polyaniline nanocomposites also a peak at 2θ approximately equal to 0.873° occur with slight lowering of intensity. These results suggest that mesotexture is not much affected due to the incorporation of polyaniline. But in the polypyrrole and polythiophene composites no diffraction

peaks are observed. This may be because of the destruction of the mesostructure by the incorporation of the polymer chain.

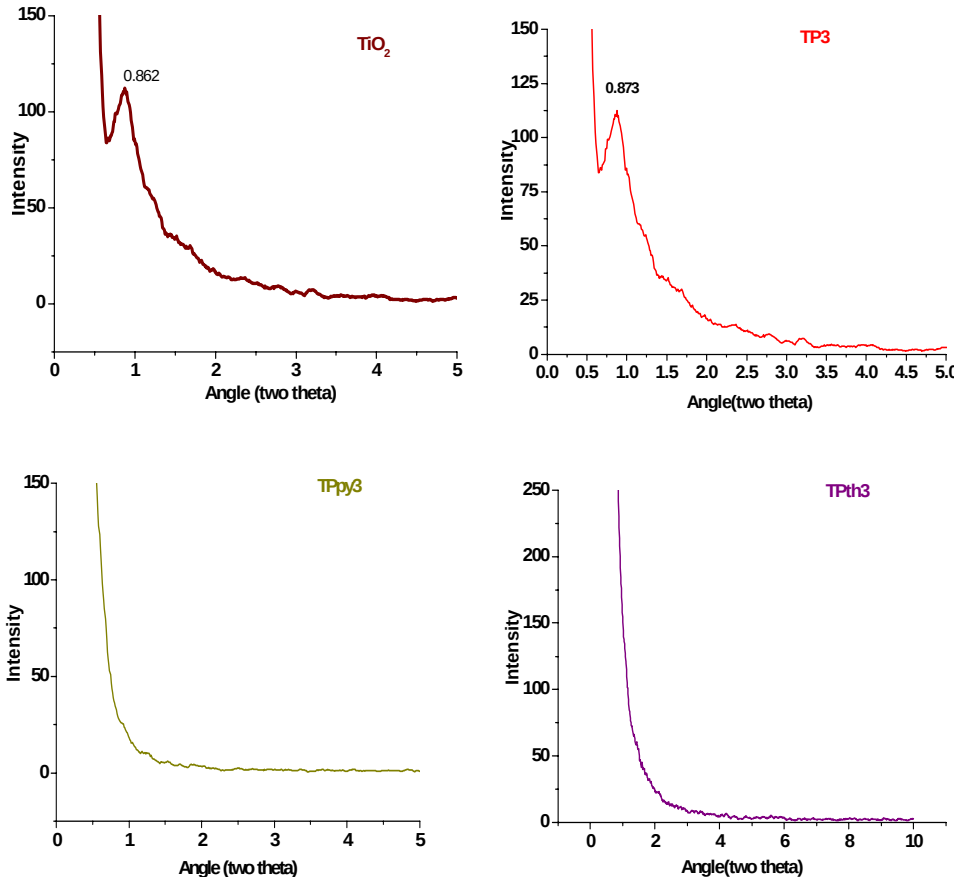

Fig.3.4. Low angle XRD pattern of TiO_2 and the hybrid nanocomposites

The line broadening can be a measure of the average size of the crystallites by using the Scherrer formula [11]

$$D_v = K \lambda / \beta \cos\theta$$

where; D_v is the average particle size, λ is wavelength of the radiation and β is the FWHM(full width at half maximum) of the reflection peak that has the

same maximum intensity in the diffraction pattern (integral breadth of the peak located at angle M).K is the Scherrer constant. The Scherrer constant (K) in the formula accounts for the shape of the particle and is generally taken to have the value of 0.9 [12]. The size obtained from the Scherrer formula yields the apparent or average particle size for a material. Powders of materials are generally aggregates of smaller particles, and thus consist of a distribution of particle size. The crystallite size calculated is tabulated in Table 3.1.

Table 3.1. Crystallite size of the prepared samples

Sample	Crystallite size(nm)
TiO_2	15.1
TP1	13.4
TP2	11.7
TP3	12.3
TPpy1	23.7
TPpy2	14.9
TPpy3	10.6
TPth1	13.2
TPth2	14.6
TPth3	13.3

3.2.3. UV-Visible Diffuse Reflectance Spectroscopy

UV-Visible (UV–Vis.) spectroscopy has been proven to be an effective optical characterization technique to understand the electronic structure of semiconductors. Measurement of diffuse reflectance with a UV-Visible spectrophotometer is a standard technique in the determination of the absorption properties of materials. Determination of the band gap from the

measurement of the diffuse reflectance of a powder sample is a standard technique [13, 14]. The powder sample has to be sufficiently thick that all incident light is absorbed or scattered before reaching the back surface of the sample; typically a thickness of 1–3mm is required. Kubelka–Munk model is the basis for measurements of the band gap of thick powder samples [15].

The band gap energy (Eg) of TiO_2 is about 3.2 eV, corresponding to a threshold wavelength of 387 nm. The weak degradation of organic molecules in pure TiO_2 is due to the poor light absorption under visible irradiation. PANI has a narrower band gap, showing strong absorption in the range from visible to near infrared light [16]. The TiO_2/PANI composites not only can strongly absorb the UV light but also can absorb the visible and near-IR light. The result indicates that PANI is capable of sensitizing TiO_2 efficiently, and the resulting composite photocatalyst can be activated by absorbing both the ultraviolet and visible light (190 - 800 nm) to give a maximum visible light harvesting and is a promising photocatalytic material for the efficient use of light, especially sunlight [17]. It is obvious that the composite has higher response over the whole range of UV–Vis spectrum. The electrons in π-orbital of PANI are excited to π*- orbital by visible light and can readily inject into the CB of TiO_2 because the energy level of them matched well for the charge transfer. Thus the charge separation can be enhanced, and then electrons in TiO_2 (CB) will react with water and oxygen to produce reactive oxygen species (ROS), which initiate the chain reaction for degradation [18].

Three distinctive peaks of polyaniline appear at about 336, 451 and 924 nm, which are attributed to the π–π*, polaron- π* and π- polaron transition [19, 20] respectively. From Fig.3.5, it can be noted that the characteristic peaks

of nano TiO_2 and polyaniline (EB) all appear in polyaniline/nano TiO_2 composite [21]. A broad peak in the range 500–750 nm, indicating the presence of the PANI on the surface of TiO_2 nanoparticles. Similar behaviour was observed by Wang and Min [17] and Min etal [22]. Min etal not only depends on their UV/Vis-diffuse spectral results but also measured the ESR spectra for the free TiO_2, PANI, and PANI/TiO_2composite. They concluded the existence of PANI on the surface of TiO_2 [23]. In PANI/TiO_2 composites, the peak at 385 nm red-shifts to 427 nm and the peak at 638 nm disappears, displaced by a broad and strong absorption band with a long tail characterization (called ''free-carrier-tail'') by Alan etal [24] in the near IR region. This tail is indicative of charge carriers' delocalization in the polaron band favoured by an extended chain conformation of the polyaniline [25]. This result reveals that in composites, the PANI has a more expanded coil molecular conformation [26], and there is an interaction between PANI molecular chains and TiO_2 nanoparticles [27]. In pure PANI, the strong interaction of chains caused π-conjugated defects, and always leads to ''compact coil'' conformation. While in PANI/TiO_2 composites, the TiO_2 not only eliminate the interaction of different PANI chains, but also limit the contraction of the chains. Therefore, the interaction between the adjacent isolated polarons become stronger and the polaron band become more dispersed in energy. As a result the ''free-carrier tail'' appears and the localized polaron band disappears. Also, the observed enhancement of the PANI photoresponse in composites can be attributed to the increased efficiency of charge photogeneration due to a photoinduced charge transfer from the photoinduced PANI to the TiO_2 [28,29]. The result indicates that polyaniline is capable of sensitizing TiO_2 efficiently and resulting nanocomposite photocatalyst can be activated by absorbing both the ultraviolet and visible light (λ = 190–800 nm) to give a maximum visible light harvesting,

and is a promising photoelectric conversion and photocatalytic material for the efficient use of light, especially sunlight [22].

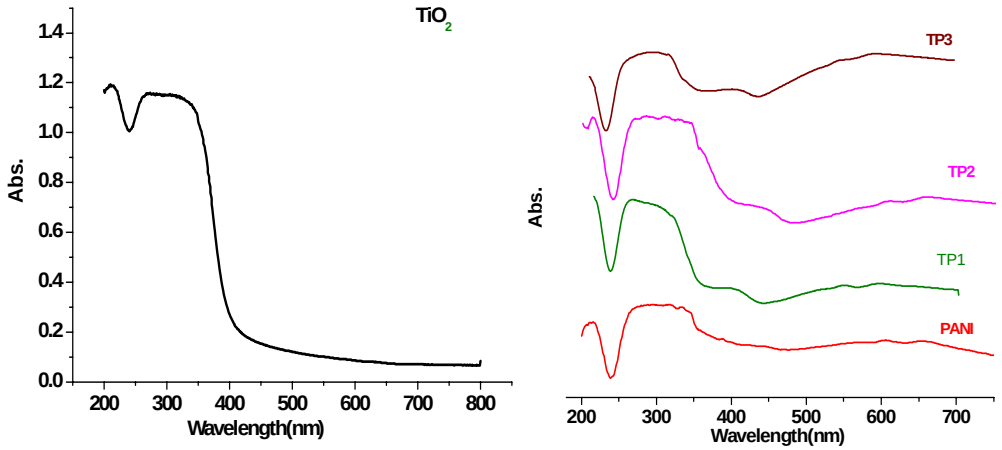

Fig. 3.5. Absorption spectra of TiO_2, polyaniline and the polyaniline modified TiO_2 systems

Fig.3.5. shows the absorption spectra of TiO_2, polyaniline and the modified systems. The absorption edge of TiO_2 is in the UV region while that of polyaniline is in the visible region. On nanocomposite formation the absorption edge of TiO_2 shifted towards visible region.

The optical band gaps of pure anatase and conducting polymer modified TiO_2 systems were determined using a Tauc plot of the modified Kubelka-Munk (KM) function with a linear extrapolation. Fig. 3.6. shows the Optical band gap (Tauc plot) of TiO_2, PANI and PANI modified TiO_2 samples.

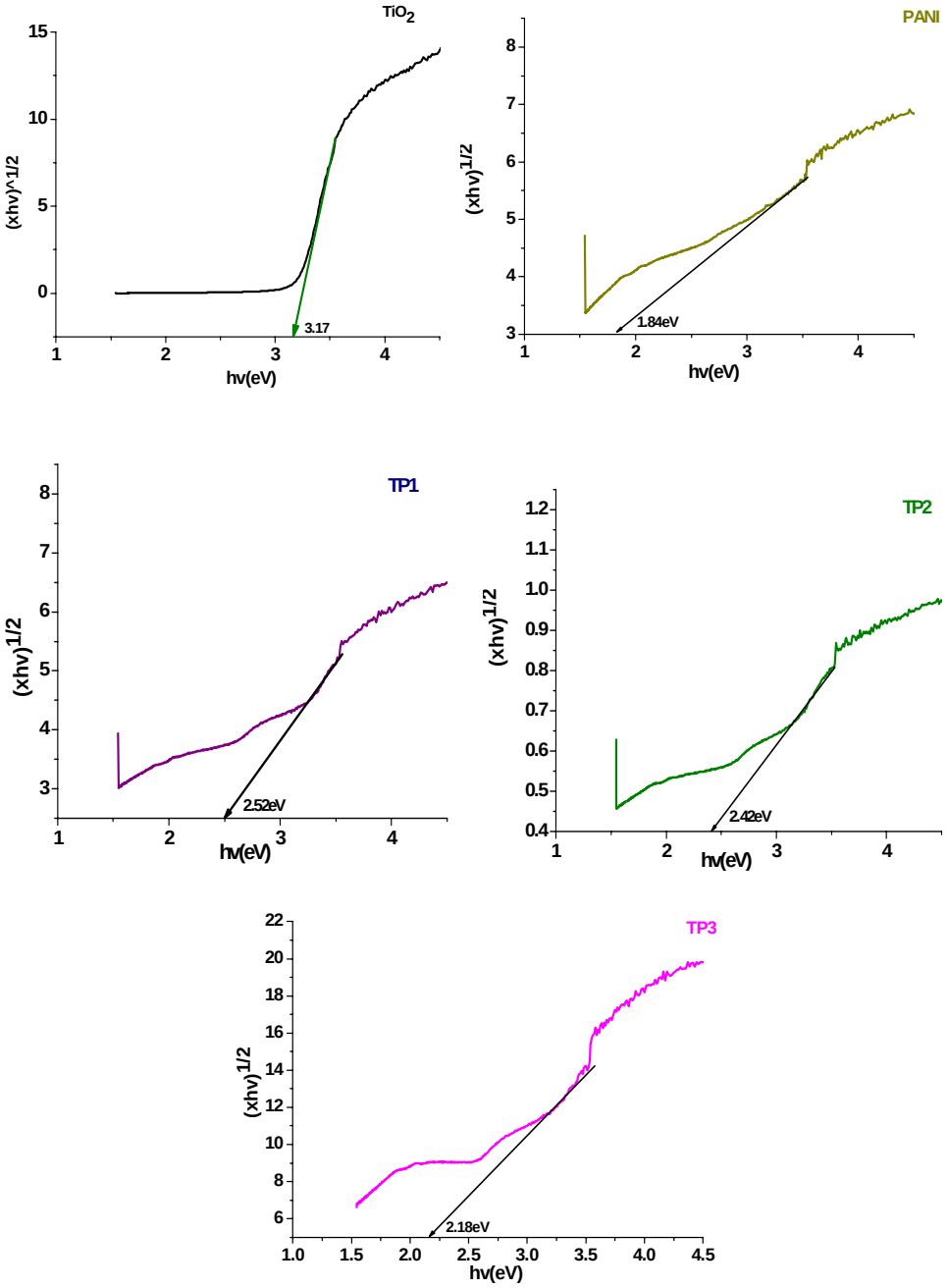

Fig. 3.6. Optical band gap (Tauc plot) of TiO_2, PANI and PANI modified TiO_2 samples

Fig. 3.7 shows the absorption Spectra and Optical band gap (Tauc plot) of Ppy and Ppy modified TiO_2 samples.

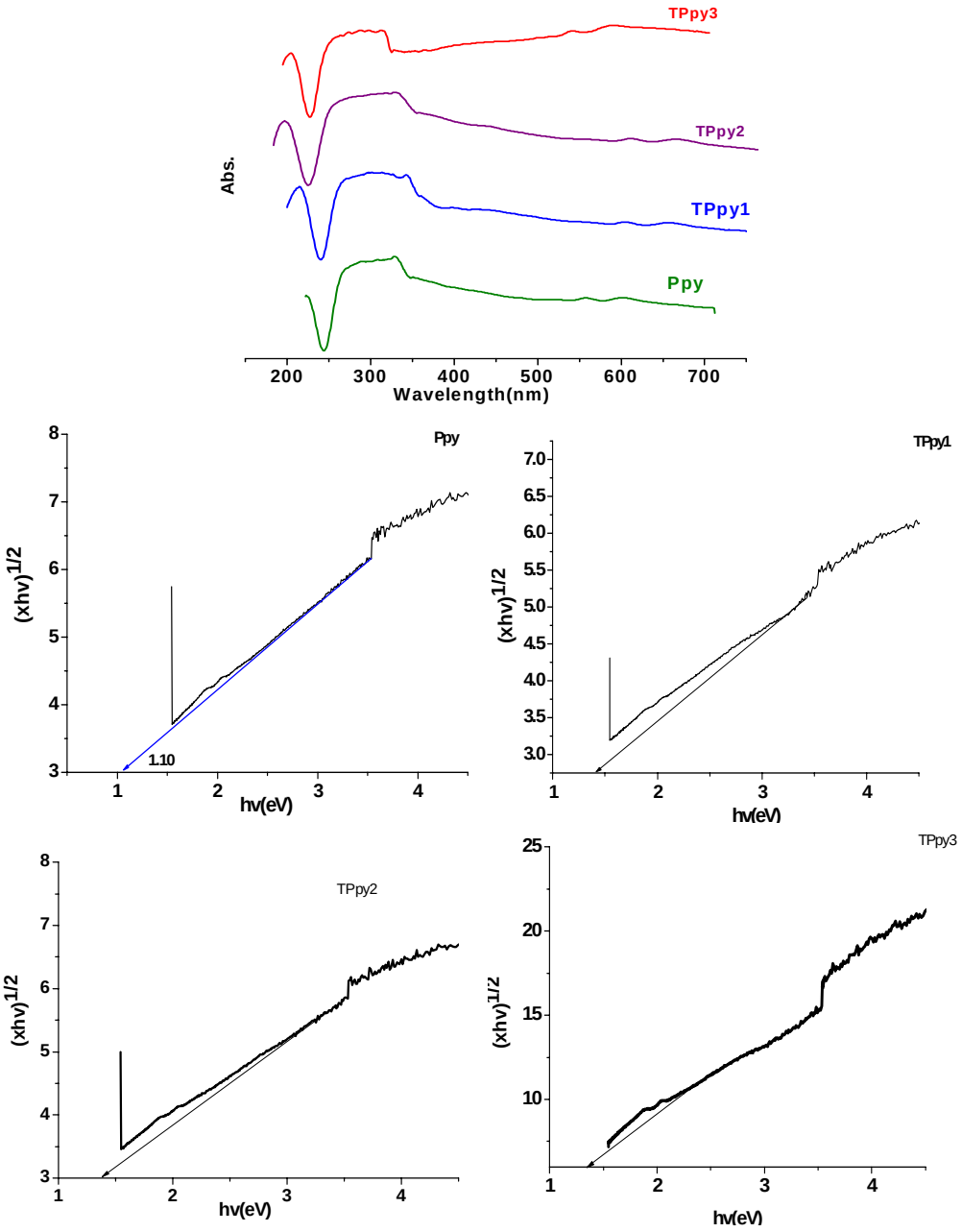

Fig.3.7. Absorption spectra and optical band gap (Tauc plot) of Ppy, and Ppy modified TiO_2 samples

From Fig.3.7. it is clear that the absorption edge of the TiO_2/Ppy composite is shifted to longer wavelengths compared with the neat TiO_2. A well defined band in the visible region which is attributed to the Ppy absorption and indicates that these composites could be useful in harvesting energy for optoelectronic applications, such as in photovoltaic devices [30].

The TiO_2/Polythiophene hybrid nanocomposites can absorb both UV light and visible light moreover, there are two absorption bands from 200 to 400 nm and from 400 to 700 nm, respectively. The band from 200 to 400 nm can be assigned to the characteristic absorption of TiO_2 in the TPth composite in the UV light region. The second band is attributed to the electron transition from the valence bond to the antibonding polaron state (π-π*type) of polythiophene. With an increase of polythiophene content, the absorbency for TPth composites increases in the visible light region. Compared with the spectrum of TiO_2, the presence of polythiophene significantly changes the spectrum of TiO_2 in the visible light [31]. Figure 3.8 shows the absorption spectra and optical band gap (Tauc plot) of Pth, and Pth modified TiO_2 samples.

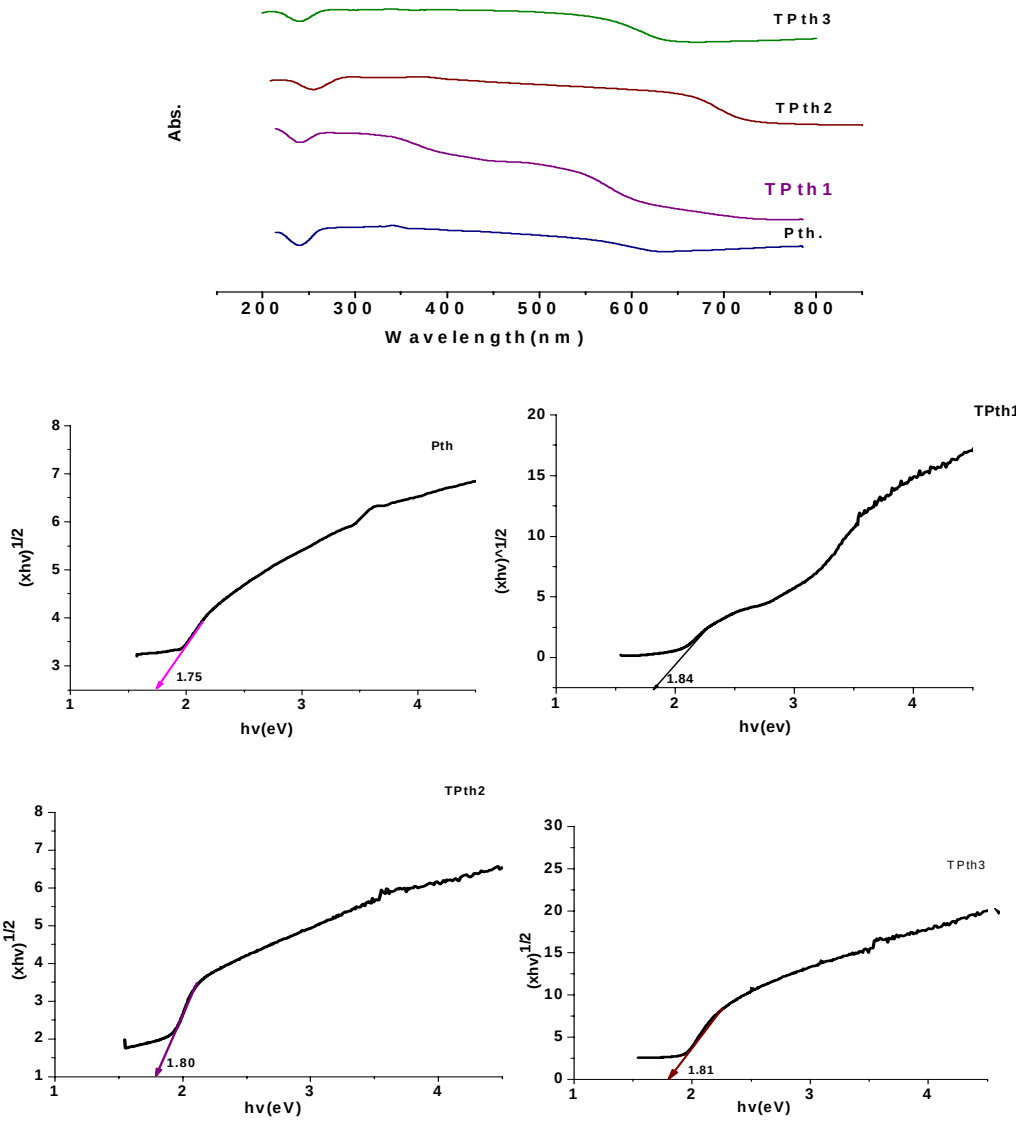

Fig. 3.8. Absorption spectra and optical band gap (Tauc plot) of Pth, and Pth modified TiO_2 samples

3.2.4. FT-IR Spectroscopy

Infrared spectroscopy is an essential and crucial characterization technique to elucidate the structure of matter at the molecular scale. Figure 3.9.

shows the FT-IR spectra of TiO_2, polyaniline and polyaniline modified TiO_2 nanocomposites. Pure TiO_2 shows peaks around 456, 1623, 3441 cm^{-1} which may be attributed to the Ti-O-Ti stretching, O-H bending, and O-H stretching vibrations respectively. The spectra of PANI mainly included the characteristic absorption bands as following: the band at 3450cm^{-1} was attributable to N–H stretching mode, 1554cm^{-1} (C-C stretching mode for the quinonoid unit), 1479cm^{-1} (C-C stretching mode for benzenoid unit), 1298$cm^{-1}$and 1242cm^{-1} correspond to N–H bending and asymmetric C–N stretching modes of the benzenoid ring and 1122cm^{-1} (a plane bending vibration of C–H). The peak around 1134$cm^{-1}$was associated with vibrational modes of N=Q=N (Q refers to the quinonoid-type rings), indicating that PANI is formed in the composites [32]. For the spectrum of PANI/TiO_2, the characteristic peaks of PANI at 1554cm^{-1}, 1479cm^{-1}, 1298cm^{-1}, 1242cm^{-1} and 1122cm^{-1} also appeared which proved the existence of PANI in PANI / TiO_2 nanocomposites [33].

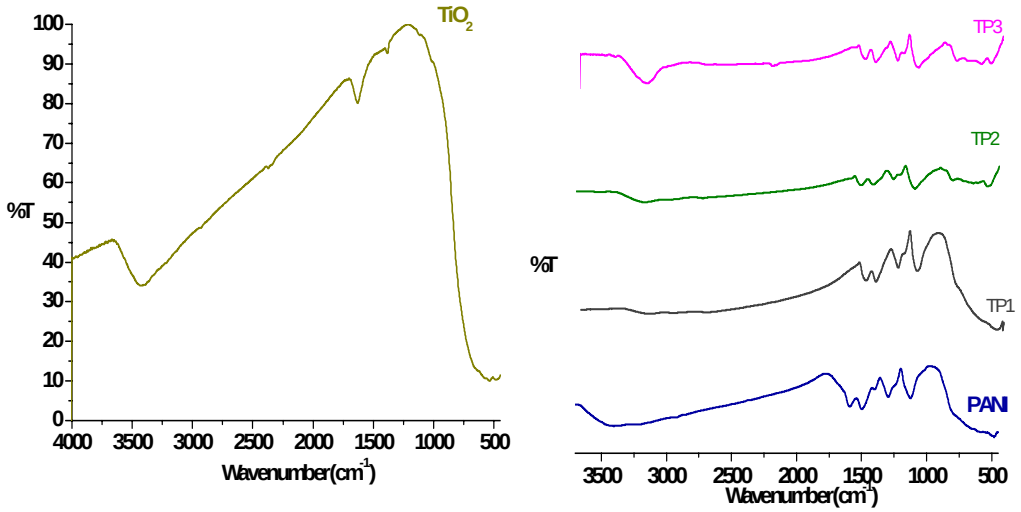

Fig.3.9. FT-IR Spectra of TiO_2, polyaniline and polyaniline modified TiO_2 nanocomposites

Molecular structure of different nanocomposites of Ppy/TiO_2 was characterized by FTIR. The typical signature of Ppy is verified from peaks at 1050, 1185, 1300, 1477, 1551, and 3442 cm^{-1} which characterize the response of N–H bands, doping state of conducting chains, C–N stretching, C=N stretching, C=C stretching, and N–H stretching, respectively [34]. In pure Ppy the peaks at 2917 and 2854 cm^{-1} are associated with five membered ring C–H stretching .The stretching and bending motion of N–H in Ppy appear at 3361 and 1645cm^{-1}, respectively. The peaks at 1249 and 1086cm^{-1} are due to C–N stretching and C–H deformation vibrations of Ppy. Additionally, the peaks at 991 and 853cm^{-1} related to the in-plane and out-of-plane vibration modes of N–H and C–H [35].

Ppy/TiO_2 nanocomposites showed a peak around 1350–1280cm^{-1} is due to N–C stretching mode and a peak at 1550 cm^{-1} is attributed to the C=C stretching mode of Ppy in the composite. The bands near 1623 and 3400 cm^{-1} were assigned to O-H bending and the O–H stretching vibrations respectively [36]. Figure 3.10. shows the FT-IR Spectra of Ppy and Ppy modified TiO_2 nanocomposites

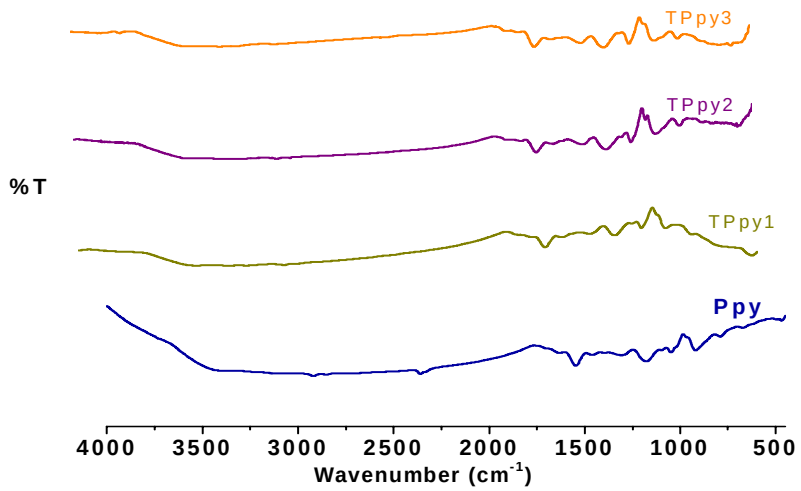

Fig. 3.10. FT-IR Spectra of Ppy and Ppy modified TiO_2 nanocomposites

Fig.3.11 shows the FT-IR spectrum of polythiophene and polythiophene modified TiO_2 nanocomposites. The IR spectrum indicates a broad band between 3500 and 3000 cm^{-1}, indicating the presence of -OH groups on the surface of titania. Molecularly adsorbed water in the dried titania nanopowders is found with two peaks at around 3411 cm^{-1} and around 1627 cm^{-1}, characteristic of stretching and bending vibrations of water molecules. In the FT-IR spectra of polythiophene, in the stretching vibration region, the peak of 1,644 cm^{-1} can be attributed to the C=C characteristic vibration. In the fingerprint region of polythiophene, the IR absorption peaks at 795 cm^{-1} is ascribed to the C–H out of-plane stretching vibration of the 2,5-substituted thiophene rings, which confirms the polymerization of thiophene monomer. The absorption peak at 697 cm^{-1} is assigned to the C–S bending mode, which indicates the presence of thiophene monomer.

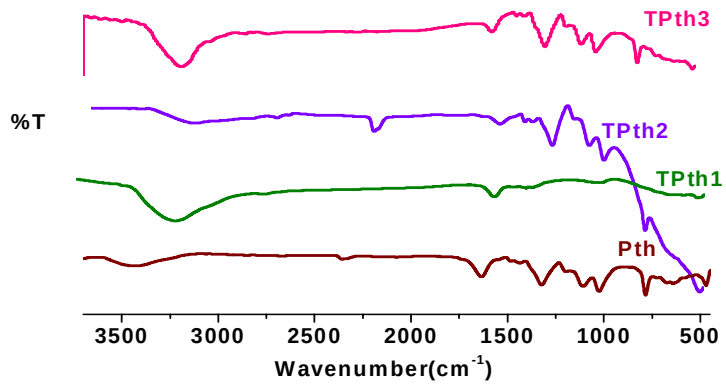

Fig. 3.11. FT-IR Spectra of polythiophene and polythiophene modified TiO_2 nanocomposites

Fig.3.11. reveals that the characteristic absorption bands of polythiophene and the maximum peak of TiO_2 (571 cm^{-1}) occur in the composite, which illustrates that polythiophene, is incorporated with TiO_2

successfully. We can assign the 1450 cm^{-1} band to symmetric C=C stretching, and the 1488 cm^{-1} band to C-H stretching of the thiophene ring, and the 1156 and 1215 cm^{-1} band to C-H bending. Peak of Ti-O-Ti stretching appeared in the range 400~600 cm^{-1}. Peak of C-H out of plane stretching vibration appeared in the 788 cm^{-1} [37], while bands 997 and 695 $cm^{-1}$are indicative of the C-S stretching in the thiophene ring [38].

A strong interaction exists between the interface of polythiophene and nano TiO_2, which causes the shifts of bands. FT-IR measurements show that polythiophene and TiO_2 particles are not simply blended or mixed up, but a strong interaction exists at the interface of nano-TiO_2 and polythiophene [9].

3.2.5. Photoluminescence spectra

Photoluminescence (PL) emission spectra were used to investigate the efficiency of charge carrier trapping, immigration and transfer and the fate of electron-hole pairs in semiconductor particles. As shown in **Fig.3.12**, three peaks around 434, 463 nm are observed for the bare TiO_2. Generally, the peak at 434 nm can be attributed to self-trapped excitation localized in the TiO_6 octahedron, and the peak at 465 nm to oxygen vacancies. The bare TiO_2 sample showed the highest PL emission intensity, indicating that electrons and holes were more easily recombined. However, the PL emission intensity decreased greatly in the case of conducting polymer hybridised TiO_2 photocatalysts. So it indicated that the conducting polymer-TiO_2 nanocomposites have lower recombination of electrons and holes. Furthermore, it can be deduced that the photo-produced electrons of the excited conducting polymer-TiO_2 molecules may transfer more easily and effectively to the conduction band (CB) of the TiO_2 which reasonably leads to a higher photocatalytic activity since the photodegradation reactions are evoked by these charge carriers [39].

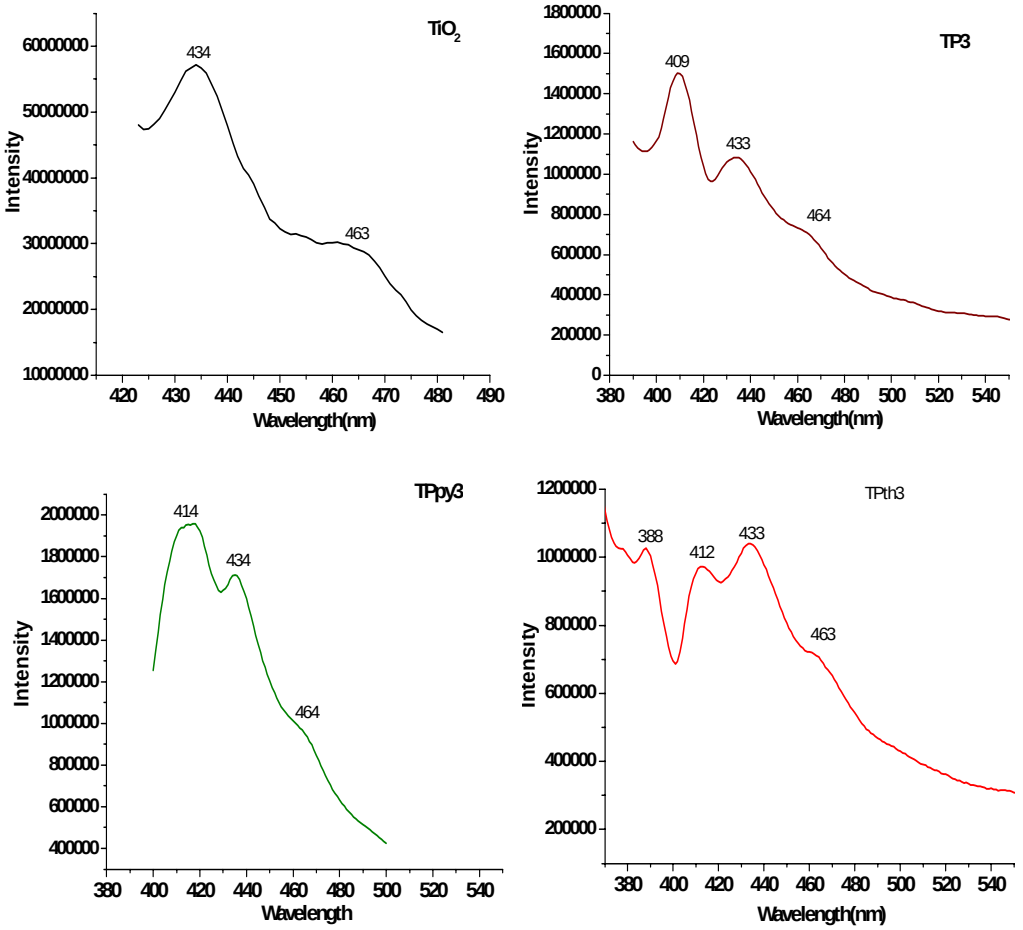

Fig.3.12. Photoluminescence Spectra of TiO_2 and conducting polymer modified TiO_2 nanocomposite systems

3.2.6. Raman Spectra

In the Raman spectrum of the anatase TiO_2 the following modes can be assigned: ~144 (Eg), 197 (Eg), 399 (B1g), 513 (A1g), 519 (B1g) and 639 cm^{-1} (Eg). Raman spectra recorded for the TiO_2/PANI nanocomposites show the vibration modes characterizing of PANI emeraldine salt and anatase TiO_2. From the Raman assignment of the PANI vibration modes, the band in the 1,490 cm^{-1} region is due to the C-N stretching vibration from benzenoid (B) ring while the band near 1,580 cm^{-1} is related to the C=N stretching from

quinoid (Q) structure, the 1,140 cm^{-1} band is assigned to a vibration mode of the B-NH^{+}= Q structure [40]. **Fig. 3.13(a)** shows Raman spectra of TiO_2 and polyaniline modified TiO_2 nanocomposite.

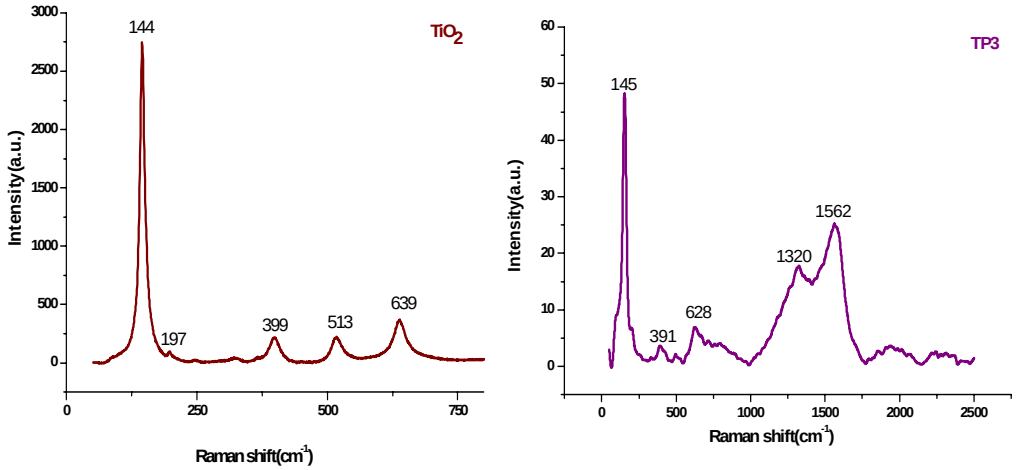

Fig.3.13 (a). Raman spectra of TiO_2 and polyaniline modified TiO_2 nanocomposite

In the Raman spectra of PANI/TiO_2 composite the peak at 1562cm^{-1} could be attributed to the C–C stretching vibration of the benzenoid, the peak at 1510cm^{-1} corresponding to the N–H stretching mode, the peak at 1394 cm^{-1} could be assigned to the C–C stretching vibration of the quinonoid rings, the peakat1320cm^{-1} was related to the C–N^{+} stretching mode, and the peak at 1167cm^{-1} was attributed to the C–H bending vibration of the benzenoid [41,42]. Compared with the spectrum of pristine PANI, the peaks of PANI/TiO_2 all shifted to lower wave numbers for about 2–9 cm^{-1}. The red shift of the bands indicated that the conjugated system of PANI was weakened, and an intensive interaction between PANI and TiO_2 occurred [43, 44].

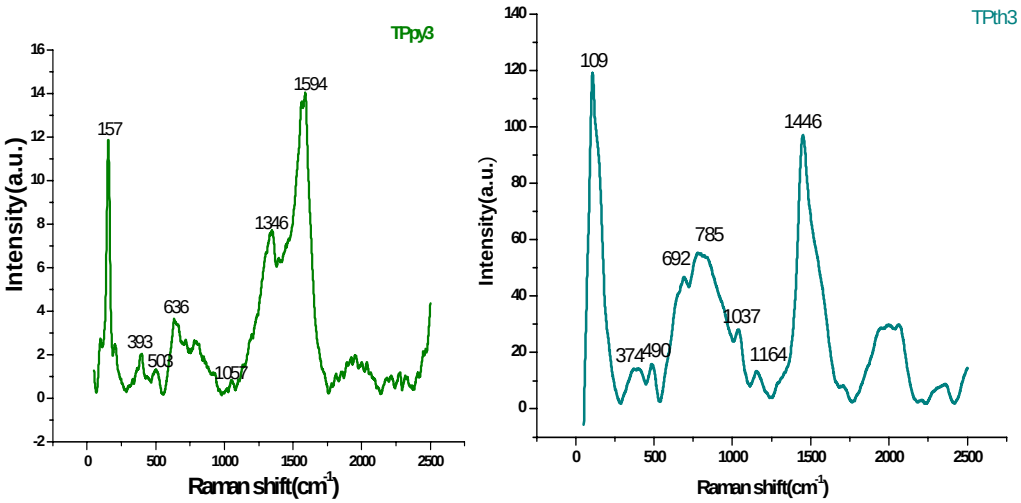

Fig. 3.13(b). Raman spectra of polypyrrole (TPpy3) and polythiophene (TPth3) modified TiO_2 nanocomposite

Fig. 3.13(b) shows the Raman spectra of polypyrrole (TPpy3) and polythiophene (TPth3) modified TiO_2 nanocomposite. Peaks at 1346 and 1594 cm^{-1} in TiO_2-Polypyrrole composites (oxidized form of polypyrrole) along with TiO_2 vibrations could be attributed to the C-N stretching and C=C stretching of the polymer chain respectively. The peak at 1057 cm^{-1} is assigned to C-H deformation [45, 46].

In the case of Raman spectra of the Pth/TiO_2 composite, in oxidized state, peak at 1420 cm^{-1} has been attributed to the quinoid units (radical cations). On the other hand, in reduced state this peak disappeared and a new peak at 1455 cm^{-1} has arisen, which is attributed to the $C_\alpha = C_\beta$ ring stretching of the neutral Pth. This gave clear evidence that the reduction of the polymer from its oxidized form (positively charged polymer chain) to its reduced form (neutral chain) proceeded via the extraction in methanol. TiO_2-polythiophene composites show peaks at 1452, 1158, 1069,789 cm^{-1} corresponding to C=C

stretching, C-C stretching, C-H bending and C-S-C deformation respectively, which is an indication of successive polymer incorporation into TiO_2.

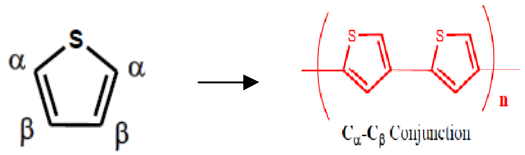

The bipolaron absorption, proposed to be at 1400 cm^{-1} in the oxidized state was not observed while a peak at 1420 cm^{-1} was found. It corresponds with the Cα= C_β ring stretching of the quinoid units in the oxidized Pth chain, it shows that the oxidized Pth presents mainly in radical cation [47].

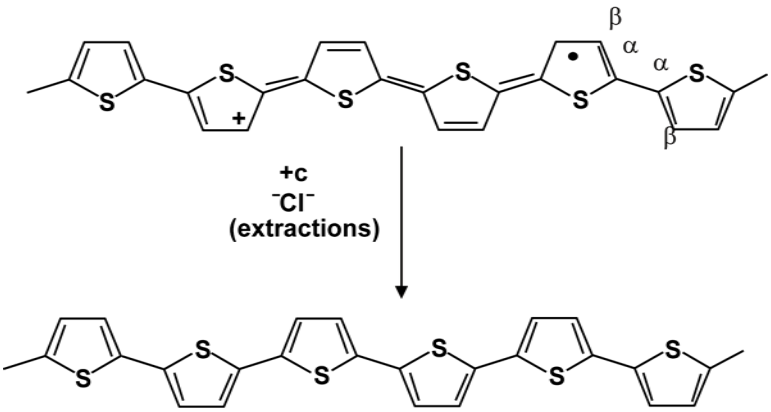

3.2.7. Scanning Electron Microscopy (SEM)

Scanning electron microscopy (SEM) produces high resolution images of a sample surface. SEM images have a characteristic 3-D appearance and are therefore useful for judging the surface structure of the sample. Regarding the morphology, Fig.3.14. shows the selected SEM images of the prepared catalysts. In SEM pictures spherical aggregates of small sub particles are observed. Particle shape is spherical, but the particles are coagulated each

other, and thus, the size of a single particle could not be calculated accurately. The particles were clustered together due to the electrostatic effect of very fine particles. This is a very common phenomenon in the case of nanoparticles [48].

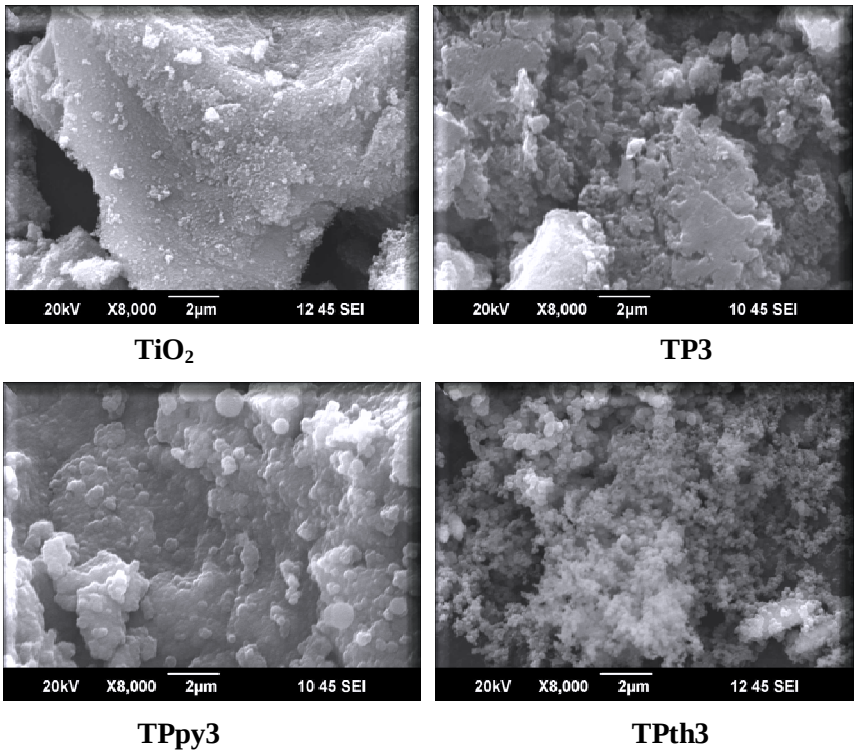

Fig. 3.14. SEM images of TiO_2 and the conducting polymer modified TiO_2 nanocomposites

3.2.8. Energy Dispersive X-ray analysis

The energy dispersive X-ray analysis gives both qualitative and quantitative information about elemental composition of the materials. Fig.3.15. shows the EDX pattern of the prepared systems. The elemental composition of the prepared systems were determined using EDX analysis and the results are tabulated in Table 2. The EDX data show the surface composition of the modified systems. From the table it is clear that there is

successive incorporation of conducting polymer with the TiO_2. In the case of polyaniline and polythiophene modified systems, at very low concentration of the polymer, the elements N and S could not be detected. This may be because the amount of such elements present in the composite may be low compared to the detection limit. The chemical compositions of the prepared samples were obtained from JEOL Model JED -2300, energy dispersive X-ray analyzer used in conjunction with SEM.

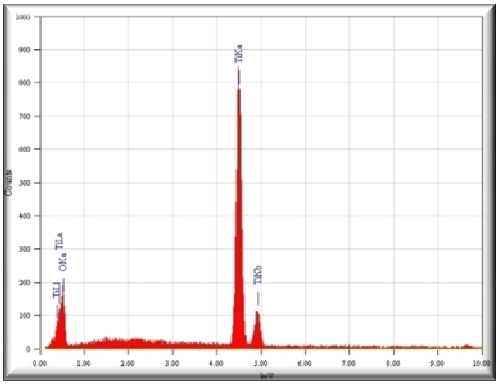

TiO_2

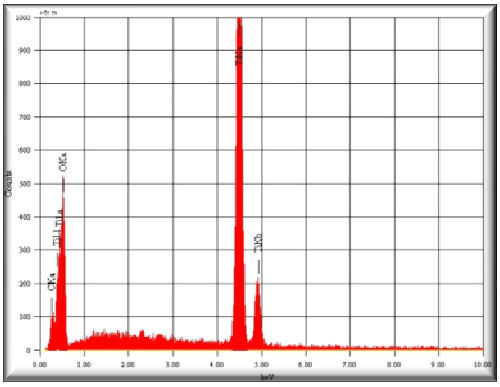

TP1

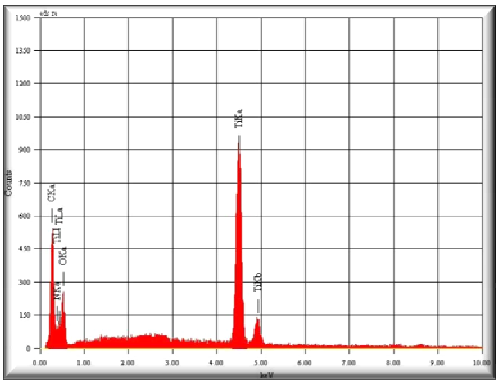

TP2

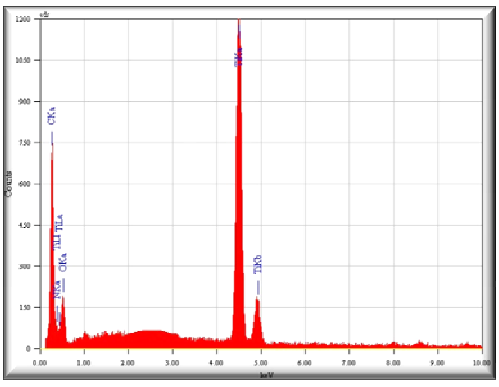

TP3

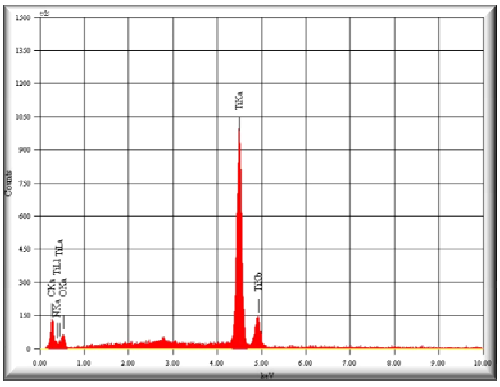

TPpy1

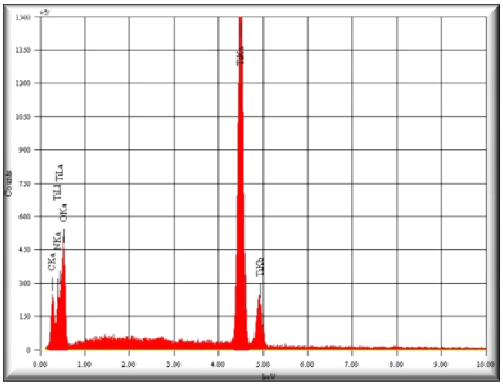

TPpy2

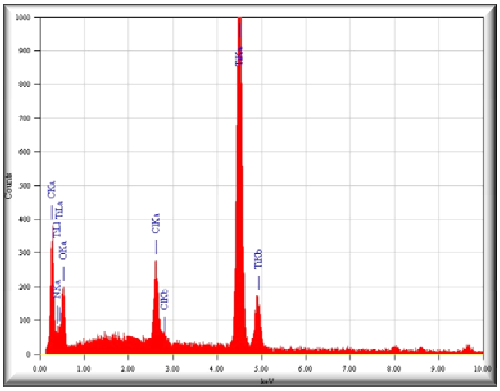

TPpy3

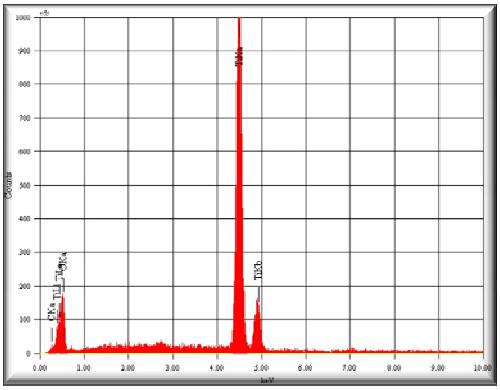

TPth1

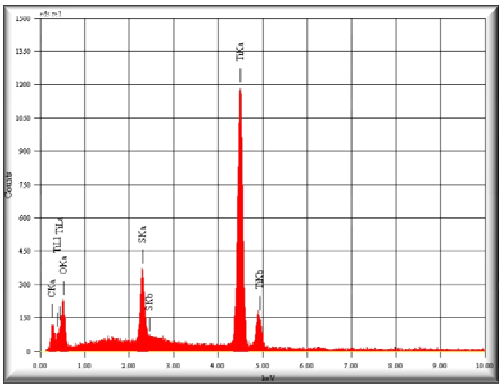

TPth2

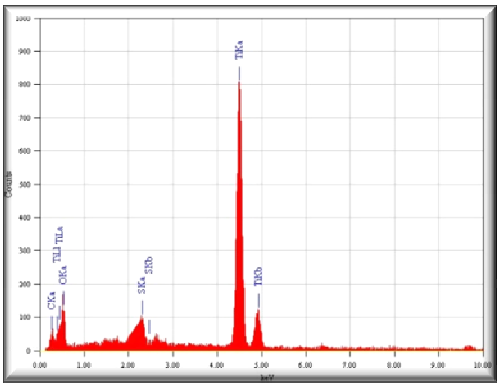

TPth3

Fig.3.15. EDX spectra of TiO_2 and the conducting polymer modified TiO_2 nanocomposites

Table 3.2. The elemental composition of the prepared systems (using EDX analysis)

Sample	Mass%				
	Ti	O	C	N	S
TiO_2	92.35	7.65	-	-	-
TP1	84.28	10.71	5.01	-	-
TP2	55.13	5.72	38.07	1.08	-
TP3	55.78	3.07	38.81	2.33	-
TPpy1	77.28	9.88	12.55	0.28	-
TPpy2	85.04	1.97	12.65	0.34	-
TPpy3	65.74	4.41	21.21	1.38,7.26(Cl)	-
TPth1	92.85	6.43	0.72	-	-
TPth2	86.58	6.2	4.84	-	2.39
TPth3	75.14	5.44	8.02	-	11.4

3.2.9. Thermogravimetric Analysis

The thermogravimetric analysis is a well established technique for evaluating the thermal stability of the materials. It provides a quantitative measurement of any weight changes associated with thermally induced transitions. The rate of these thermally induced processes is often a function of the molecular structure in TGA. Thermogravimetric analysis (TGA) studies give an idea about the weight changes of samples in relation to changes in temperature. TGA is commonly employed with respect to hybrid materials and nanocomposites to investigate the thermal stability (degradation temperatures), the amount of inorganic component, which usually stays until the end of the measurement due to its high thermal resistance, and the level of absorbed moisture or organic volatiles in these materials.

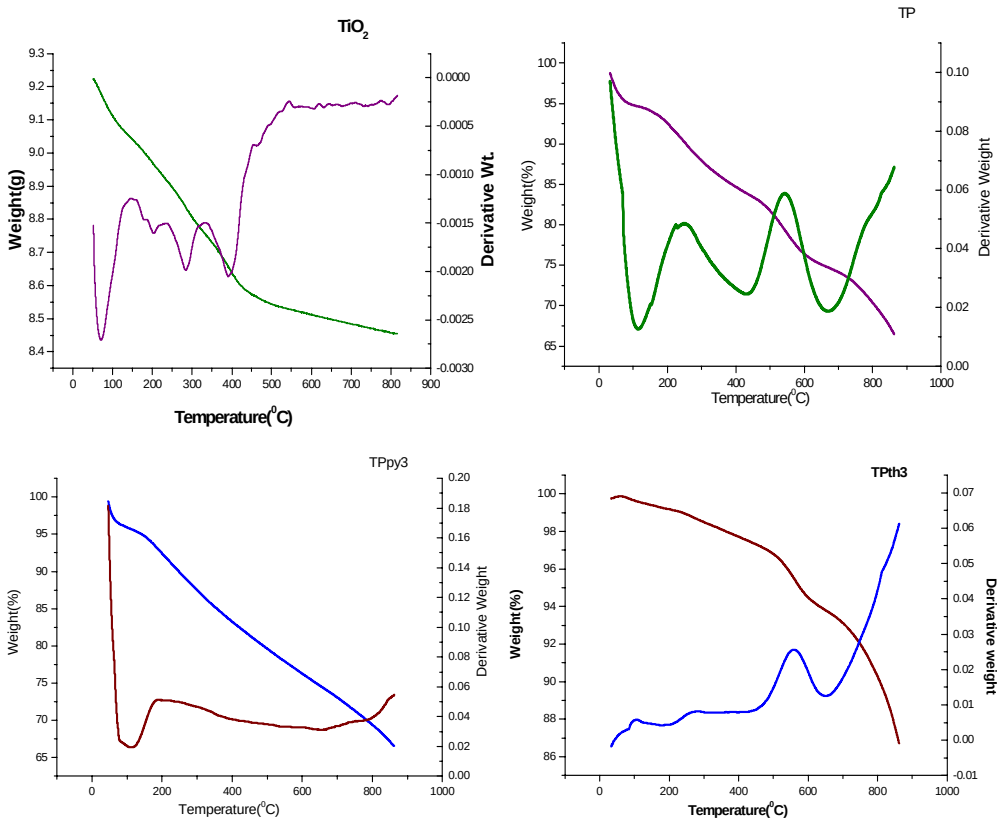

Fig.3.16. TG-DTG curves of the prepared nanocomposite systems

The TG-DTG curves of pure TiO_2 and polyaniline/TiO_2 nanocomposites with various weight percentages are shown in **Fig. 3.16.** In the case of TiO_2 the weight loss around 100^0 C is due to the elimination of water and a major weight loss around 100-250^0C may be due to the volatilization of water of hydrations and at 300-400^0C is due to the combustion of organic species such as P123 and CH_3COOH **[**49] . In the case of polyaniline composite, 3 major weight losses are observed; the one around 100^0C is due to the elimination of water and the second one corresponds to the loss of dopant HCl and the final weight loss at high temperature around 400^0C is due to the breakage of polymer backbone **[**50].

In case of TiO_2 - polypyrrole composite, the weight loss at temperatures lower than 150^0C is due to the evaporation of moisture. In the range of 200–800^0C, there is an obvious weight loss attributed to the decomposition of polypyrrole moiety of the nanocomposites. The TiO_2–polythiophene (Pth/TiO_2) composites show a small amount of weight decrease in the range of 30–200^0C which is attributed to the water evaporation. In the range of 200–800^0C, there is an obvious weight loss which is attributed to the decomposition of polythiophene adsorbed on the surface of TiO_2 particles. There are two stages of mass decrease in the range of 35–800^0C. The temperature of polymer decomposition in the Pth/TiO_2 composite is 650^0C.

3.2.10. Transmission Electron Microscopy

The surface morphology and structural properties of the prepared nanocomposite systems are illustrated by TEM techniques. In transmission electron microscopy (TEM) images are produced by focusing a beam of electrons onto a very thin specimen which is partially transmitted by those electrons and carries information about the inner structure of the specimen. The image is recorded by hitting a fluorescent screen, photographic plate, or light sensitive sensor such as a CCD camera. The latter has the advantage that the image may be displayed in real time on a monitor or computer.

Fig.3.17. shows the TEM images of pure TiO_2 and conducting polymer modified TiO_2 nanocomposite systems. Micrographs showed that the sample is in polycrystalline form and is constituted by small crystallites. Irregular shaped structures are seen from the micrographs which may due to the agglomeration of particles during hydrothermal synthesis. Selected area electron diffraction (SAED) pattern of the sample shows concentric rings that are essentially continuous, implying that the samples consisted of many small crystallites.

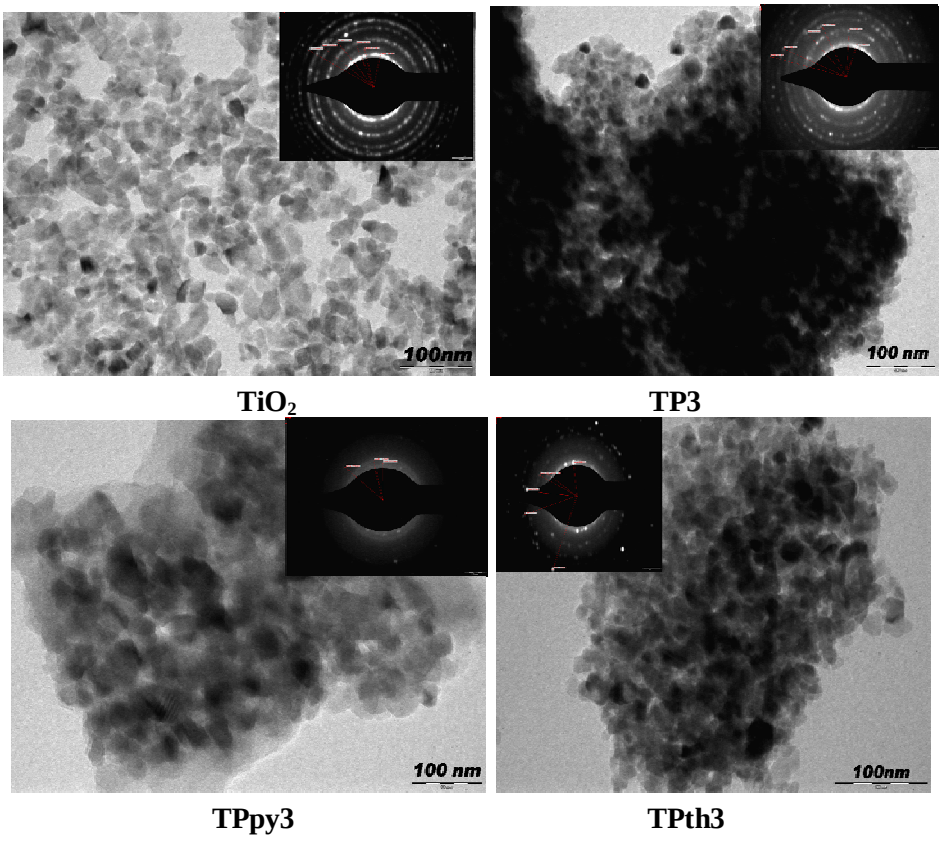

Fig.3.17. TEM images of TiO_2 and the prepared nanocomposites

3.2.11. X-Ray Photoelectron spectroscopy

X-ray photoelectron spectroscopy (XPS) is a surface sensitive analytical tool used to examine the chemical compositions and electronic state of the surface of a sample. It is also used for the study of the electronic structure of condensed matter and is moreover a widely used technique for quantitative surface analysis. Here spin orbit splitting and peak area ratios are the two factors responsible for determining elemental composition. Peak ratio and spin orbit splitting of an element that is present in different compounds are the same.

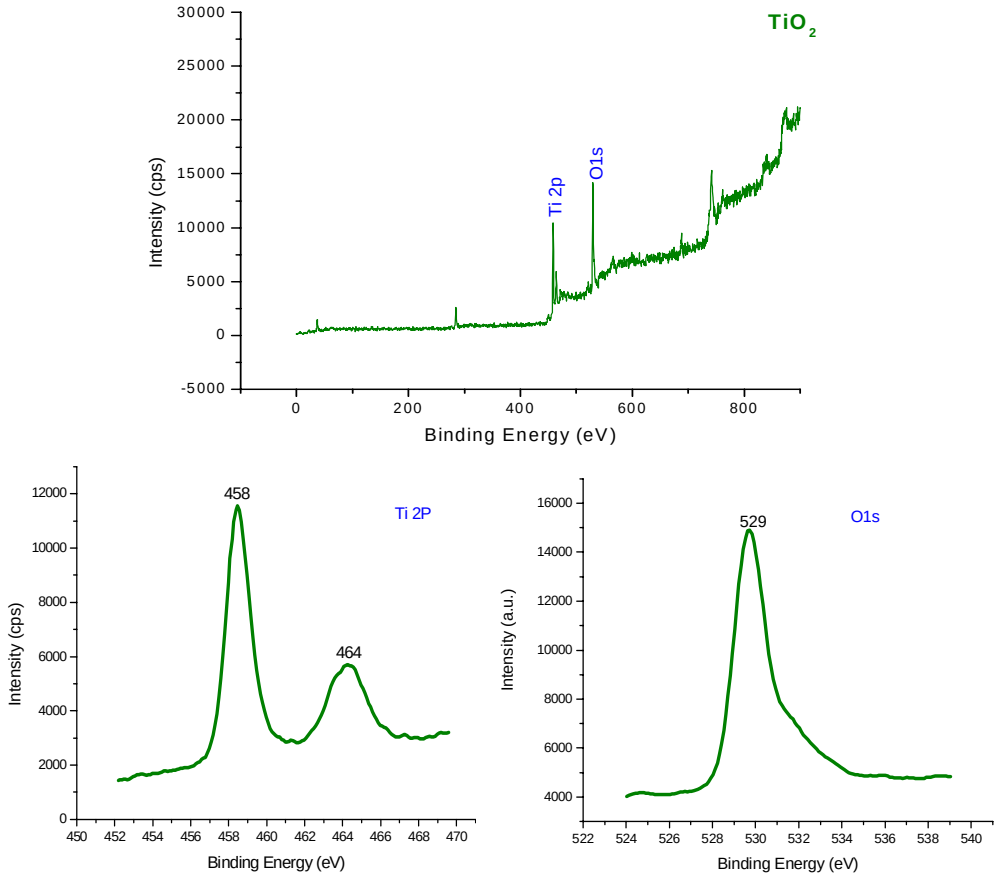

Fig.3.18 (a). XPS Spectra of TiO_2

Fig.3.18 (a) shows the survey scan and core level spectra of TiO_2. The peaks appear at 458 and 464 eV are assigned to the Ti $2p_{3/2}$ and Ti $2p_{1/2}$ states of pure TiO_2.These doublet peaks are due to the spin-orbit splitting of Ti 2p.The above value indicates that titanium exists as Ti^{4+} with stable Ti-O bond in the prepared system. Meanwhile, the lower BE peak of anatase observed at 529.84 eV for O (1s) can be attributed to the typical oxide of Ti-O.

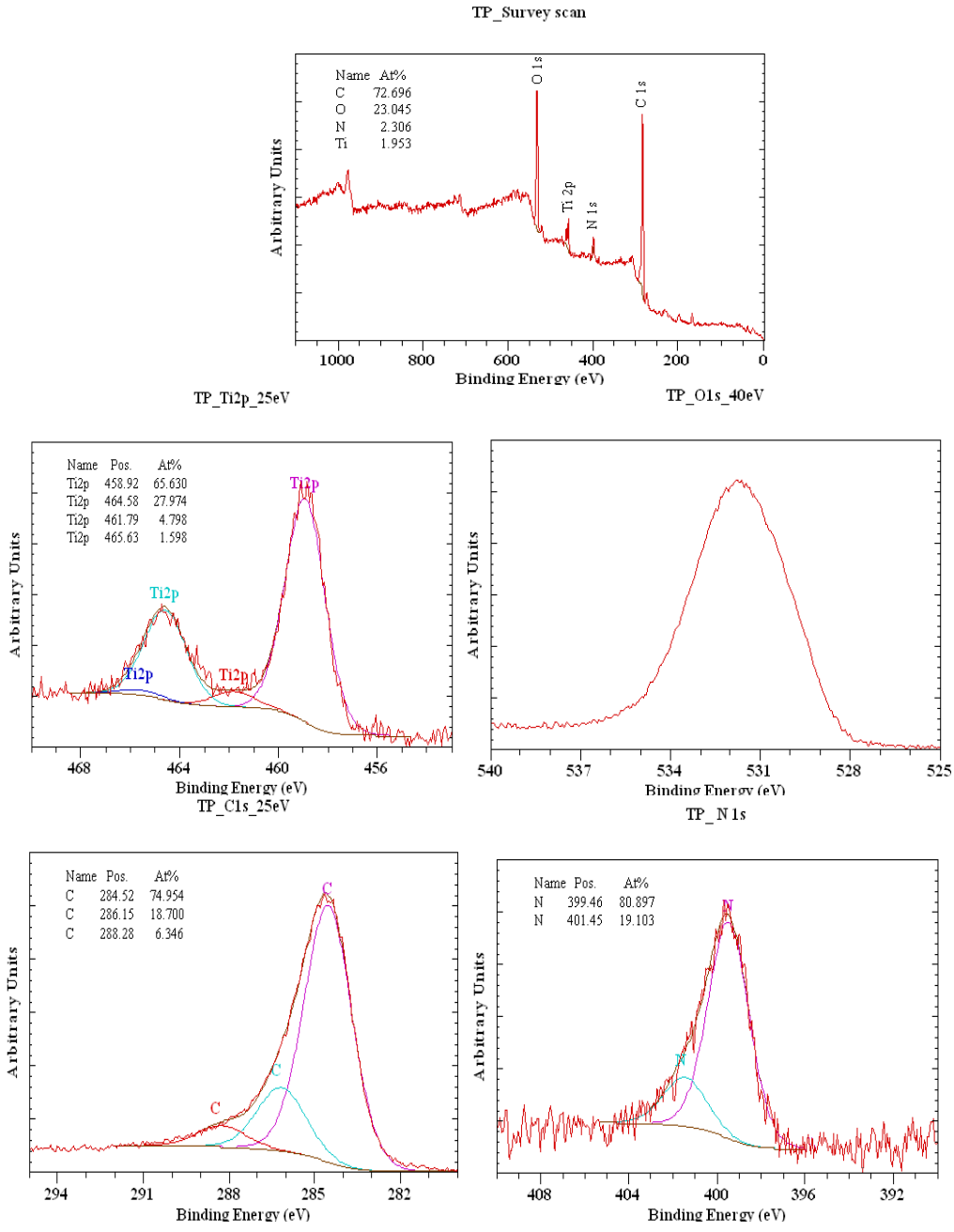

Fig.3.18 (b): XPS spectra of polyaniline modified TiO_2 system (TP)

Fig.3.18 (b) shows the XPS spectra of polyaniline modified TiO_2 system (TP). In the X-ray photoelectron spectrum of PANI modified TiO_2, the elements of C, O, Ti and N can be detected and their binding energies are 284.8, 529.8, 458.5, 400.3 eV, respectively. In the case of C1s and O1s core levels, the results imply that three peaks are observed at binding energies of 284.8, 286.3, 288.6 eV for C1s and one peak at 529.8 eV is observed for O1s. The signal of O1s at 529.8 eV confirms the Ti–O bond in the TiO_2 [51]. The peak (284.8 eV) of C1s indicates the presence of 1C and the peak (286.3 eV) is attributed to 2C in the structure of PANI. A small quantity of C atoms whose binding energy is 288.6 eV suggests the presence of C–O–Ti bond [51, 52]. The binding energy peak of N1s at 399.2 eV can be assigned to the benzenoid aniline (–NH–) structure. The binding energy (401 eV) of N1s in the nanocomposite, which is higher than that of PANI, also indicates that there is a strong interaction (eg. Hydrogen bonding) between TiO_2 and PANI.

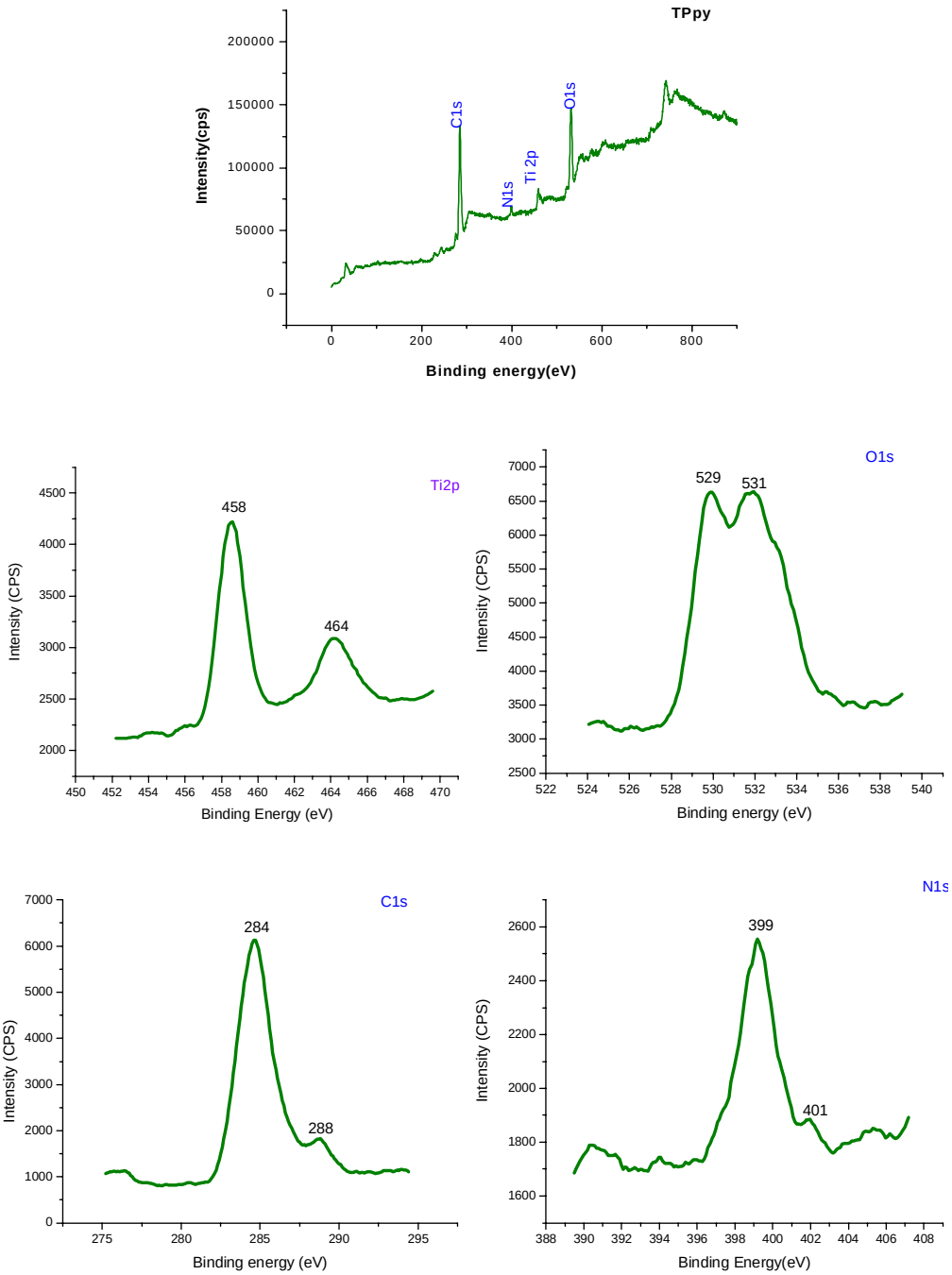

Fig.3.18(c). XPS spectra of polypyrrole modified TiO_2 system (TPpy)

Fig.3.18(c) shows the survey scan and core level spectra of TiO_2 – Polypyrrole composites. According to the XPS survey spectrum of PPy–TiO_2 the sample contains O, C, N and Ti. Binding energies for C 1s, O 1s, N 1s and Ti 2p are at 284.8, 531, 399.44, and 458.5eV; respectively. The stronger peak at 399.4 eV can be assigned to neutral -N- whereas the higher binding energy peak at 401.4 eV is assigned to the oxidized $-N^+-$ moieties. The signal of O1s peak at 531.9 eV is attributed to the presence of O–H bond. These peaks are observed for C 1s. The peak at binding energies of 284.87 eV indicates the presence of C in alpha position of polypyrrole, and the peak of 286.66 eV indicates the presence of C in beta position of polypyrrole. The peak 288.75 eV indicates the presence of C–O bond. The binding energy of Ti 2*p* in Ppy/TiO_2 can be deconvoluted into two peaks centered at 458.92 eV and 464.52 eV. These two peaks are assigned to Ti 2*p*3/2 and Ti 2*p*1/2. [53].

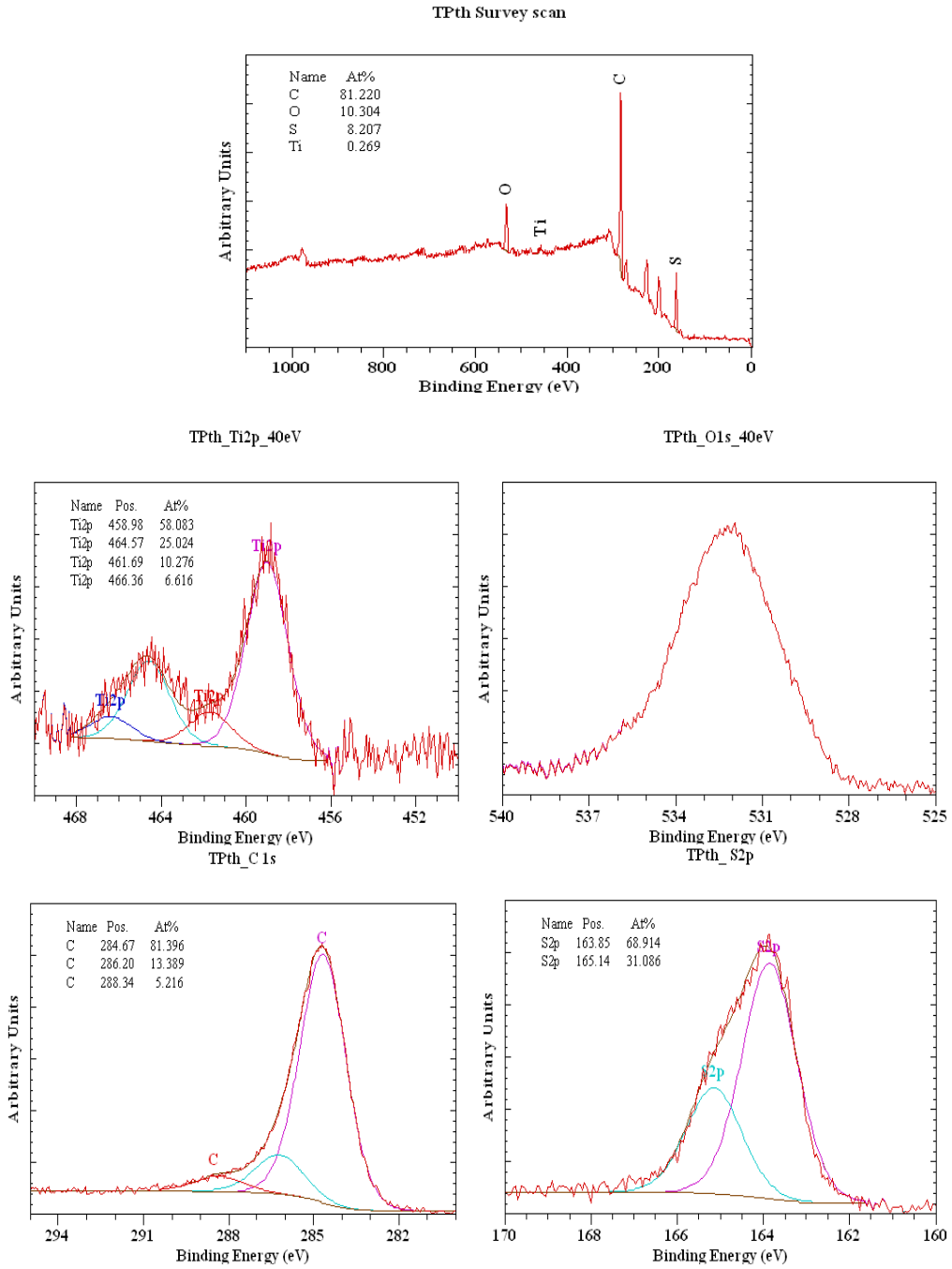

Fig.3.18 (d). XPS spectra of polythiophene modified TiO_2 system (TPth)

XPS results for Pth/TiO_2 composites in terms of C 1s, S 2p, Ti 2p and O 1s core levels and survey scan are shown in Fig.3.18 (d). The S 2*p* core level from Pth displays a peak at 164 eV, typical for thiophene sulphur [54]. The binding energy of Ti 2*p* in Pth/TiO_2 can be deconvoluted into two peaks centered at 458.92 eV and 464.52 eV. These two peaks are assigned to Ti 2*p*3/2 and Ti 2*p*1/2. A small shift to the lower value of the Ti 2*p* binding energy (458.9 eV) of Pth/TiO_2 is apparent compared to the naked TiO_2 (459.5 eV[28]. This also reflects the strong interaction between the S sites of the polymer backbone and the TiO_2 nanoparticles, in which electron transfer from polythiophene to titania takes place [55].

3.2.12. N_2 adsorption desorption Isotherm

As an approach to identify the surface area, pore size and the extent of porosity, a nitrogen adsorption-desorption isotherm was recorded. The surface area and porosity of mesoporous titania and the hybrid nanocomposites were investigated *via* nitrogen adsorption and desorption isotherm. **Fig. 3.19** shows the nitrogen adsorption-desorption isotherm of the as-prepared samples. It shows a classic type IV-like isotherm shape with H1 hysteresis loop, indicating the presence of mesoporous material according to the IUPAC classification [56]**.** The inset gives the pore size distribution plot determined by BJH (Barret-Joyner-Halenda) method from the desorption branch of the isotherm, which shows that the titania have obvious nanoporous structures with an average pore diameter *ca*. 4.3nm. The BET surface area and specific pore volume of the sample is about 56 m^2/g and 2.49 cm^3/g, respectively.

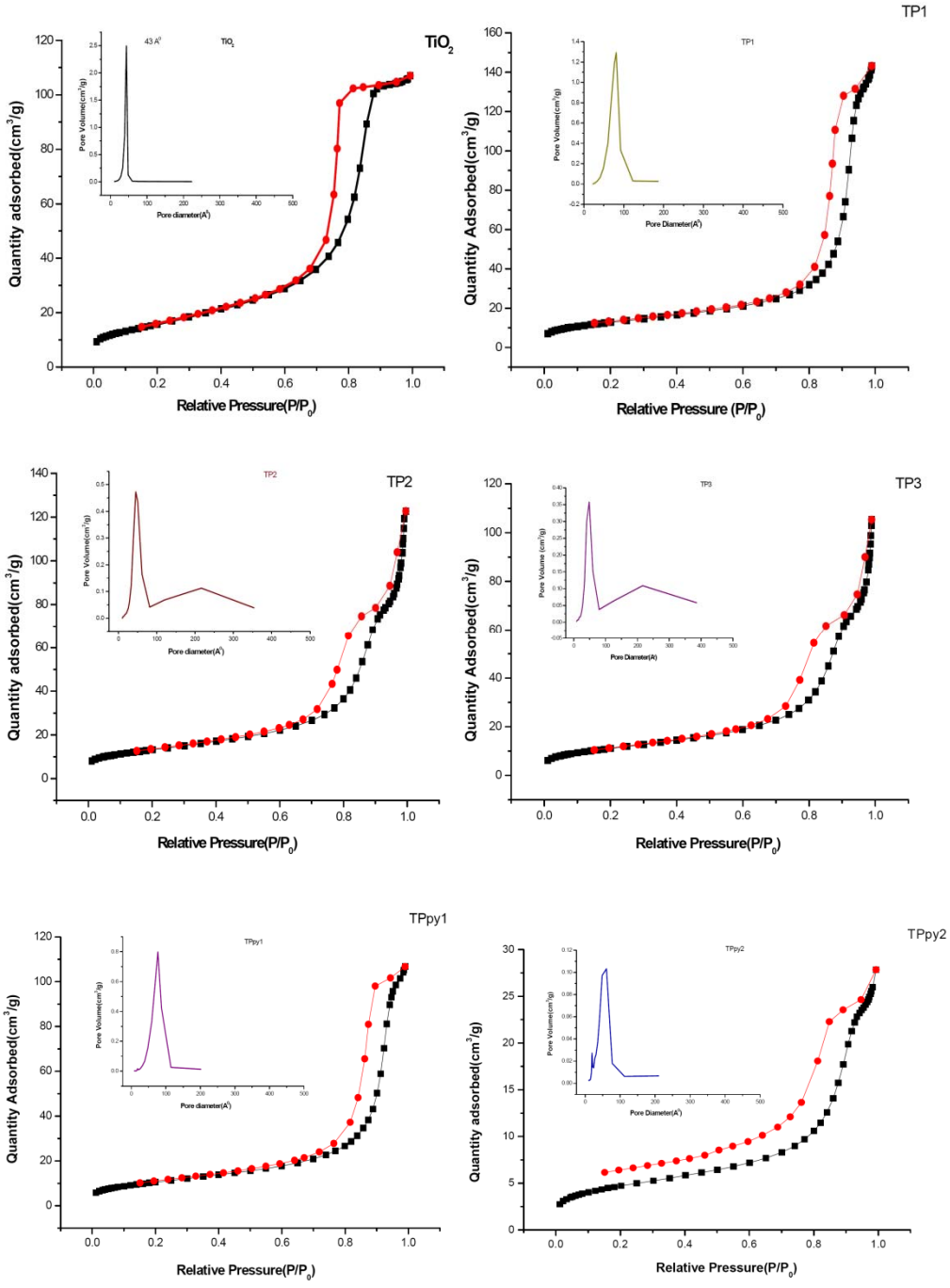
TiO2
Quantity adsorbed(cm3/g)
Relative Pressure(P/P0)
Pore Volume(cm3/g)
Pore diameter(A)
TP1
Quantity Adsorbed(cm3/g)
Relative Pressure (P/P0)
Pore Diameter(A)
TP2
Quantity adsorbed(cm3/g)
Relative Pressure(P/P0)
Pore diameter(A)
TP3
Quantity Adsorbed(cm3/g)
Relative Pressure(P/P0)
Pore Diameter(A)
TPpy1
Quantity Adsorbed(cm3/g)
Relative Pressure(P/P0)
Pore diameter(A)
TPpy2
Quantity adsorbed(cm3/g)
Relative Pressure(P/P0)
Pore Diameter(A)

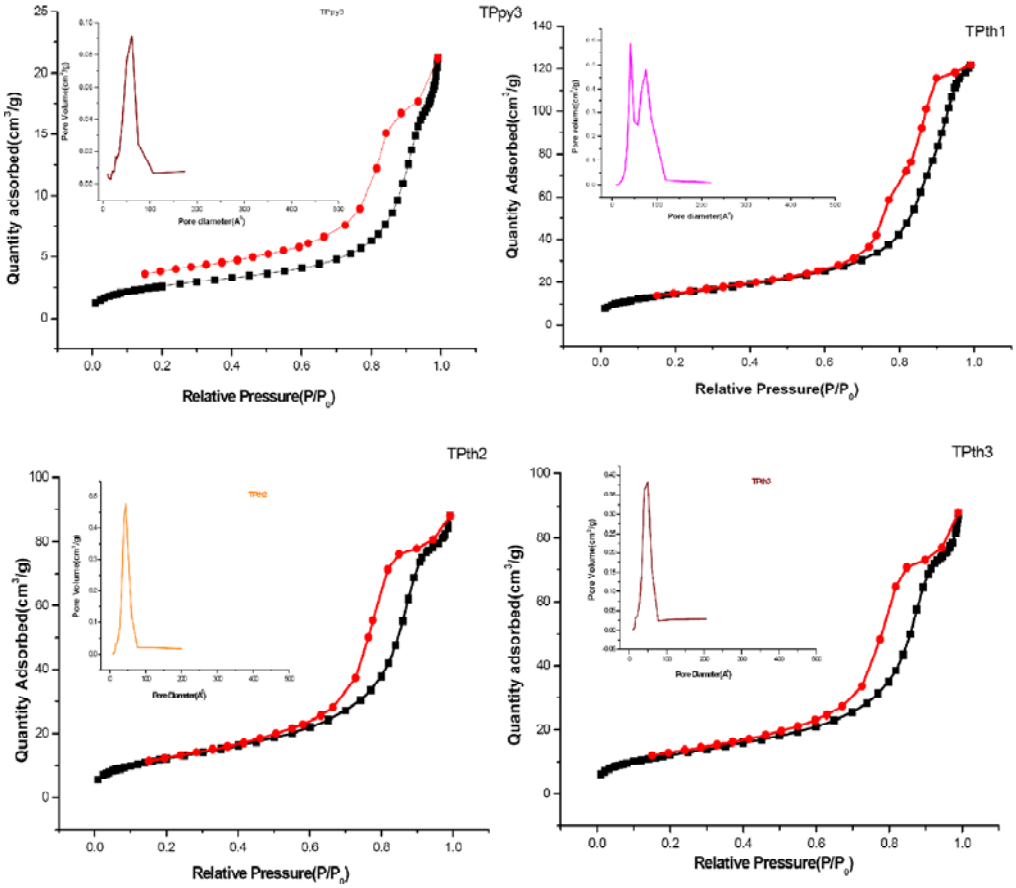

Fig.3.19. N_2 adsorption- desorption isotherms of TiO_2 and the conducting polymer modified nanocomposites

As we incorporate conducting polymer in to the titania the surface area and pore volume decreases and the pore diameter increases. The change in pore diameter is drastic when we incorporate lower amount of the polymer and the change is not so large as the amount of polymer in the composite increases. This may be due to the fact that at lower monomer concentration the rate of diffusion of monomer in to the pore channels of titania is comparable to that of the rate of polymerisation. So there is a chance of polymer formation inside the pore channels. This results in a pore volume decrease and may cause the expansion of the pores which results in an increase in pore diameter. But as the

concentration or amount of monomer increases the rate of polymerisation is high compared to the rate of diffusion. So the polymerisation occurs at the surface before the monomer diffuses in to the pore channels. This may cause pore blockage which results in a decrease of surface area and pore volume but the change in pore diameter is not so prominent. In the case of TPth1 sample (TiO_2 with low amount of polythiophene) we got a bimodal pore size distribution with a large and comparable pore diameter to that of bare mesoporous TiO_2.The exact reason for this behaviour is not clear.

The main textural properties of different samples are listed in the Table 3.3. including BET surface area (S_{BET}), total pore volume (Vp) and pore diameter (D_{BJH}) from N_2 adsorption –desorption measurements.

Table 3.3 Textural properties of the prepared nanocomposites

Sample	**Surface Area(m^2/g)**	**Pore volume(cm^3/g)**	**Pore diameter(A^o)**
TiO_2	56.87	2.49	43.6
PANI	35.68	-	-
Ppy	26.10	-	-
Pth	19.75	-	-
TP1	45.14	1.29	81.4
TP2	46.04	0.47	45.6
TP3	39.32	0.35	49.0
TPpy1	37.64	0.79	77.8
TPpy2	16.14	0.10	55.2
TPpy3	9.24	0.09	61.0
TPth1	52.19	0.59,0.47	40.9,75.9
TPth2	44.18	0.47	44
TPth3	43.38	0.37	45

3.2.13. Cyclic Voltammetry

Electrochemical measurements were made on BAS Epsilon Electrochemical analyzer (Bioanalytical system USA) interfaced to a PC. Cyclic voltammograms (polarographic mode) of the samples were measured using a three electrode system. The 3 electrode system consists of an Ag/AgCl electrode as the reference, Pt wire as auxiliary and carbon paste electrode in 0.1M HCl as working electrode. Scan range -1 to +1 V and scan rate is 100 mv/s. Fig.3.20 shows the cyclic voltammograms of the prepared systems.

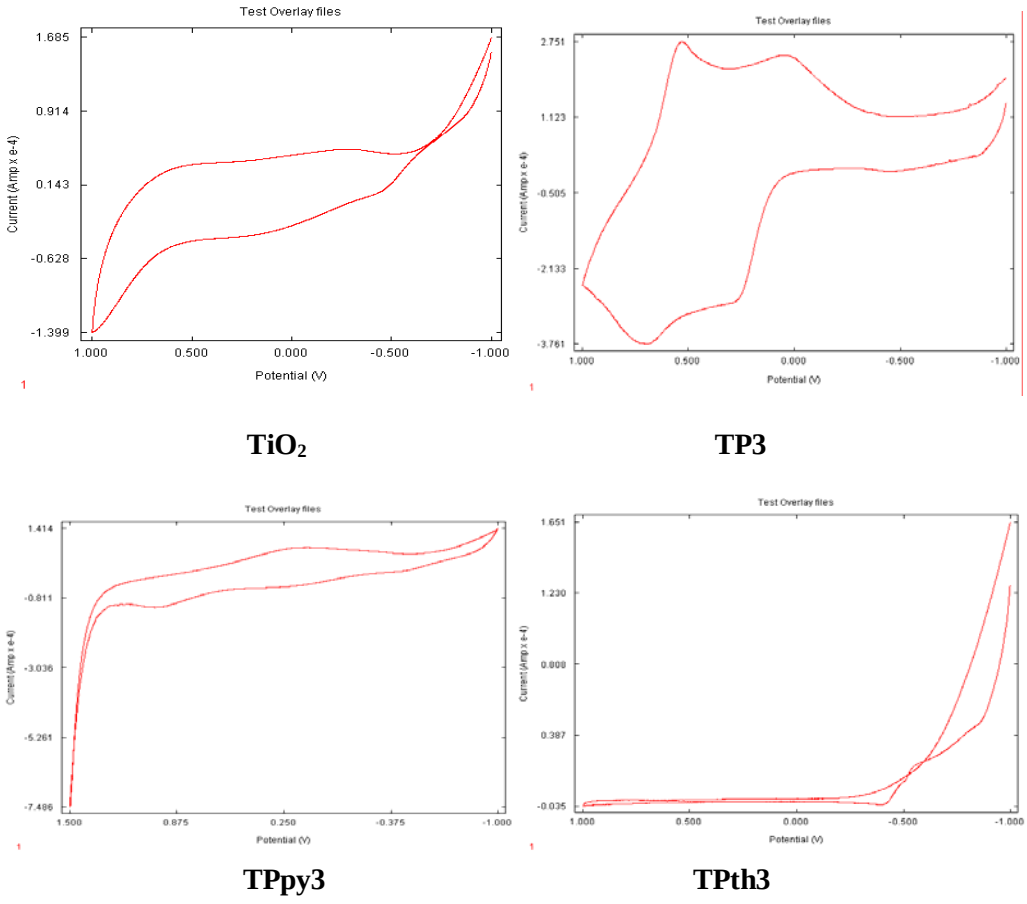

TiO_2 **TP3**

TPpy3 **TPth3**

Fig. 3.20. Cyclic voltammograms of the prepared systems.

Pure TiO_2 shows no oxidation or reduction peaks but polyaniline incorporated TiO_2 composites show two sets of redox couples. The first oxidation wave peak in the CV (at ESCE = 250-300mV), which was assigned to the leucoemeraldine to emeraldine transition, and the oxidation wave at around ESCE= 695 mV was due to the transition from the emeraldine to the pernigraniline state **[**57**].** In the case of TiO_2-Polypyrrole composites only one set of oxidation – reduction peak was obtained. In case of TiO_2-Polythiophene composites the CV shows only one oxidation peak and no reduction peak was observed.

3.2.14. Electron paramagnetic Resonance spectra (EPR)

EPR measurements were made on a E-112 ESR Spectrometer (VARIAN, USA) with specification X-band microwave frequency (9.5 GHz) with sensitivity of 5 x 10^{10} Δ H spins. Pure TiO_2 is EPR inactive. Figure 3.21. shows EPR spectra of prepared systems. In the case of polymer incorporated TiO_2 samples an ESR signal is obtained with different g values. The difference in g value may be due to the difference in electronic environment created due to the incorporation of polymer. In case of TiO_2-conducting polymer composites, the spectrum shows a signal having 'g'value approximately equal to 2.004. Such a sharp symmetrical ESR signal, of which g value is close to that of free electron is typical in organic radicals or polaron species formed in conducting polymers. [58-60].

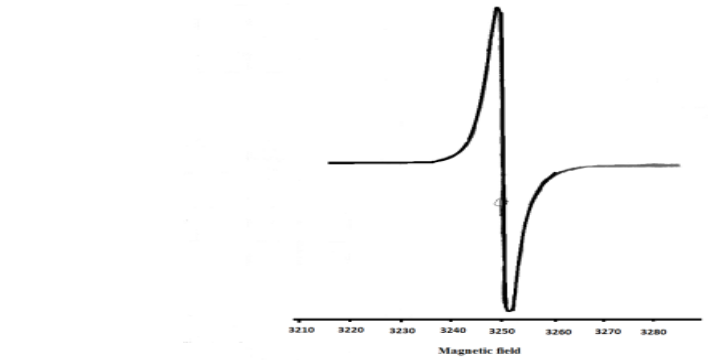

TP3 g value=2.003

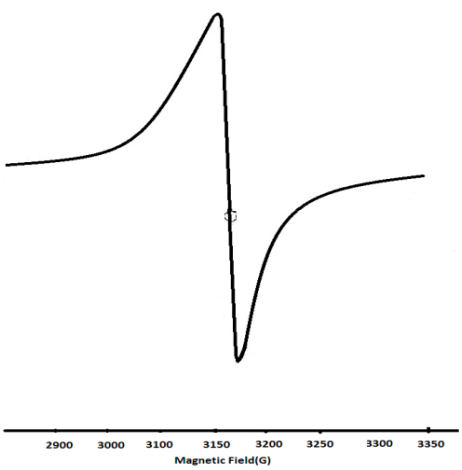

TPpy3 g value=2.004

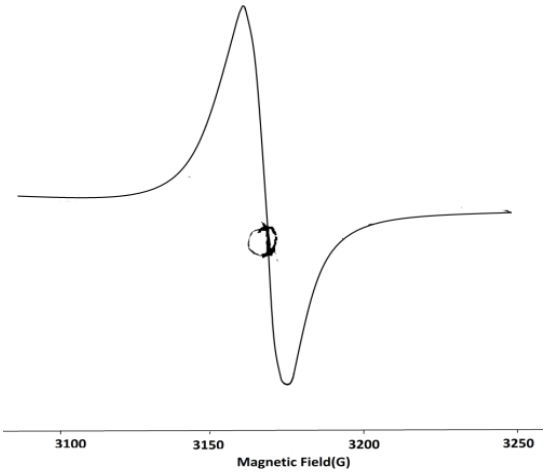

TPth3 g value=2.002

Fig. 3.21. EPR spectra of prepared systems

3.2.15. Conductivity Measurements:

Conductivity measurements of the samples are done using both 2- probe and 4-probe setup.

Sample	Conductivity*10^{-2} (S/cm)
Polyaniline	**1.06**
Polypyrrole	**1.24**
Polythiophene	**0.1240**

Table 3.4.Conductivity values of Various prepared systems

Catalyst	Conductivity*10^{-2}(S/cm)
TiO_2	0.0002(T)
TP1	0.9640
TP2	115.45
TP3	17.46
TPpy1	$2.99*10^{-7}$
TPpy2	0.6070
TPpy3	0.0373
TPth1	0.0007(T)
TPth2	0.0005(T)
TPth3	0.2191

The conductivity values of various samples obtained are shown in the above Table 3.4.A representative I-V plot of the samples are shown in Fig. 3.22.

The conductivities of PANI/TiO_2 composite with different amounts of PANI were measured by a standard four probe method. The results show that in the studied content range of PANI, the conductivity of nanocomposites does not show a regular trend. Pure PANI shows a conductivity value of $1.06*10^{-2}$ S/cm. On composite formation with TiO_2 the conductivity first shows an increase then as the polymer content increases the conductivity decreases. That means there is an optimum value of polymer content for conductivity increase. With further increase in PANI content, the conductivity of PANI/TiO_2 composite decreases. This could be explained by the fact that on the one hand, TiO_2 nanoparticles hinder the carrier transport between different conjugated chains of PANI, and on the other hand the existence of interaction between PANI and TiO_2 nanoparticles will lead to

the reduction of the conjugated lengths in the PANI chains. Same observation can be seen in the case with TiO_2/polypyrrole composites. In the case of polythiophene composites, for the first two compositions the conductivity is extremely small and it can be measured using the two point probe method. But in the case of composite with higher polymer content the conductivity is high compared to pure polythiophene. Reason for this behaviour cannot be explained.

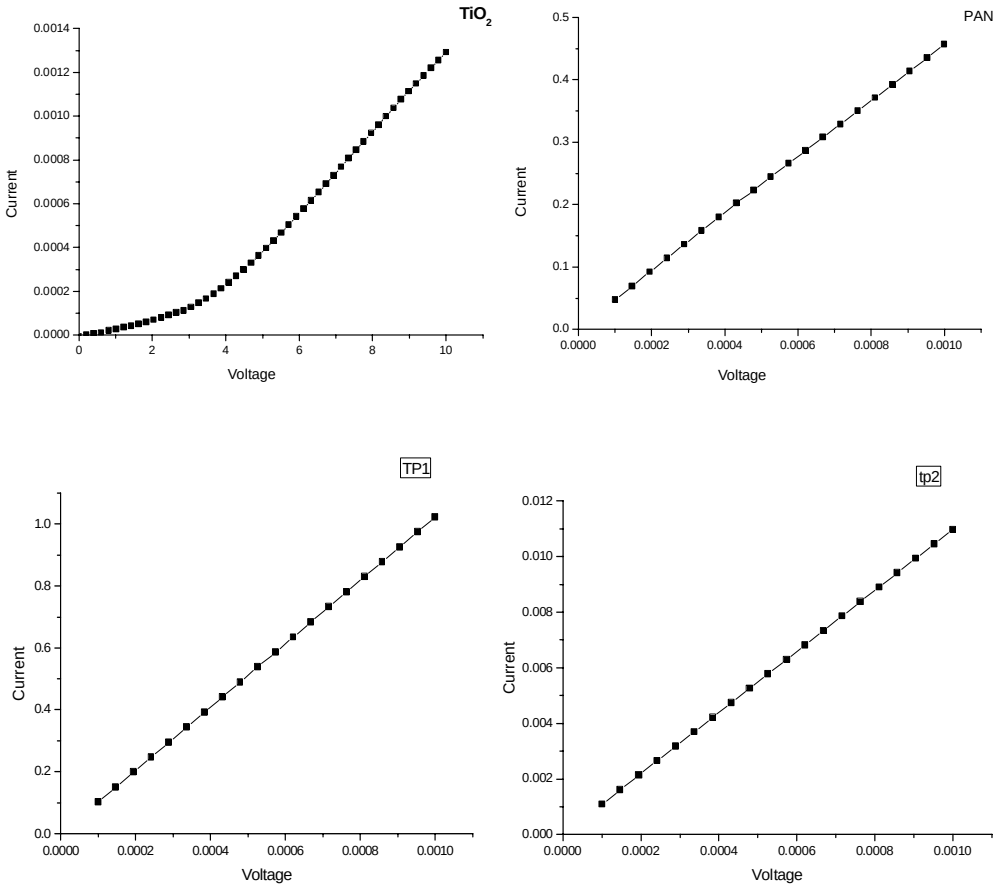

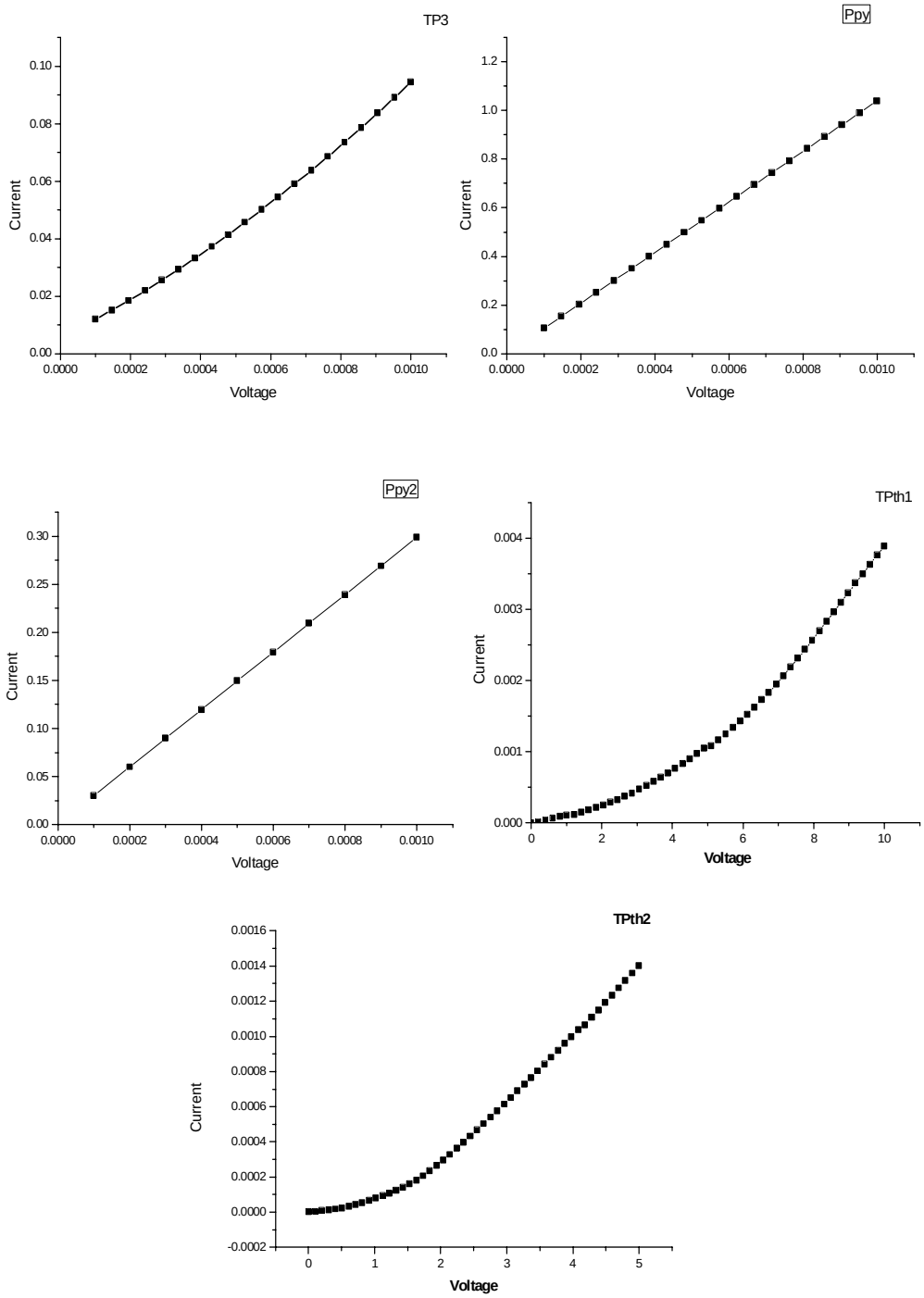

Fig. 3.22. I-V plots of the samples

References

[1]. H.S. Xia, Q. Wang, J Nanopart Res 3(2001)399.

[2]. J.P. Pouget, M.E. Jozefowicz, A.J. Epstein, X. Tang, A.G. MacDiarmid, Macromolecules 24(1991) 779.

[3]. S. Min, F.Wang, Y. Han, J Mater Sci 42 (2007)9966.

[4]. H.S. Xia, Q.Wang, Chem Mater 14(2002) 2158.

[5]. L. Zhang, P. Liu, Z. Su, Polymer Degradation and Stability 91 (2006) 2213.

[6]. M.C. Arenas, L. F. Rodrigu. Rangel, O. Martinez-Alvarez, C. Martinez-Alonso, V.M. Castano, Ultrasonics Sonochemistry 20 (2013) 777.

[7]. D.Wang, Y.Wang, X. Li, Q. Luo, J.An, J. Yue, Catalysis Communications 9 (2008) 1162.

[8]. X. Lu, H.Mao , W. Zhang, Nanotechnology 18 (2007) 025604.

[9]. S. H. Xu, S. Y. Li, Y. X. Wei, L. Zhang, F. Xu, Reac Kinet Mech Cat 101 (2010)237.

[10]. K. Hou, B. Tian, F. Li, Z. Bian, D. Zhaob, C.Huang, J.Mater. Chem. 15(2005) 2414.

[11]. A. R. West, Solid State Chemistry and Its Applications, Wiley, New York,1974.

[12]. H. Jensen, J. H. Pedersen, J. E. Jorgensen, J. Skov Pedersen, K.D Joensen, S.B. Iversen, E.G. Sogaard, J. of Experiemental Nanoscience 1(2006)355.

[13]. B. Karvaly, I. Hevesi, Z. Naturforsch. 26a (1971) 245.

[14]. W.W. Wendlandt, H.G. Hecht, Reflectance Spectroscopy, Wiley Interscience, New York, 1966.

[15]. A.B. Murphy, Solar Energy Materials & Solar Cells 91 (2007) 1326.

[16]. J. Wang, X.Y. Ni, Solid State Commun. 146 (2008) 239.

[17]. F.Wang, S. X. Min, Chinese Chemical Letters 18 (2007) 1273.

[18]. L.Gu, J. Wang, R.Qi, X. Wang, P. Xu, X. Han, Journal of Molecular Catalysis A: Chemical 357 (2012) 19.

[19]. S.G.Pawar, S.L.Patil, A.T.Mane, B.T.Raut, V.B.Patil, Archives of Applied Science Research 1 (2009)109.

[20]. N. Gospodinova, L. Terlemezyan, Prog. Polym. Sci. 23(1998)1443

[21]. S. G. Pawar, S. L. Patil, M. A. Chougule, B. T. Raut, D. M. Jundale , V. B. Patil, Archives of Applied Science Research 2 (2010) 194.

[22]. S. Min, F. Wang, Y. Han, J. Mater. Sci. 42 (2007) 9966.

[23]. M.A. Salem, A. F. Al-Ghonemiy, A. B. Zaki, Applied Catalysis B: Environmental 91 (2009) 59.

[24]. G.M. Alan, J.E. Arthur, Synth Met 69(1995)85.

[25]. S.J. Su, N. Kuramoto, Synth Met 114(2000)147.

[26]. Q.Wu, Z. Xue, Z. Qi, F. Wang, Polymer 41(2000)2029.

[27]. H.S. Xia, Q. Wang, Chem Mater 14(2002)2158.

[28]. S. Luzzati, M.Basso, M.Catellani, C.J. Brabec, D.Gebeyehu, N.S. Sariciftci, Thin Solid Films 52 (2002) 403.

[29]. G.K.R. Senadeera, T. Kitamura, Y.Wada, S .Yanagida, J Photochem Photobiol A: Chem 61 (2004)164.

[30]. M.C. Arenas , L. F. Rodríguez-Núnez, D.Rangel , O. Martínez-Álvarez, C. Martínez-Alonso, V.M. Castaño, Ultrasonics Sonochemistry 20 (2013) 777.

[31]. Y. Zhu, Y.Dan, Solar Energy Materials & Solar Cells 94 (2010) 1658.

[32]. Q. Li, C. Zhang, J. Li, Applied Surface Science 257 (2010) 944.

[33]. G. Liao, S. Chen, X. Quan, Y. Zhang, H. Zhao, Applied Catalysis B: Environmental 102 (2011) 126.

[34]. A. H. P. de Oliveira, H. P. de Oliveira, Polym. Bull. 70(2013)579.

[35]. N.V.Hieu, N. Q. Dung, P. D. Tam, T. Trung, N. D. Chien, Sensors and Actuators B 140 (2009) 500.

[36]. M.E. Nicho, H. Hu, Solar Energy Materials & Solar Cells 63 (2000) 423.

[37]. J. Roncali, Chem Rev 92 (1992) 711.

[38]. M. G. Han, S. H. Foulger, Adv. Mater. 16(2004)231.

[39]. W.Ma, J.Li, J. Liu, M.Feng, Chin. J. Chem., 31(2013) 230.

[40]. D.N. Huyen, N. T.Tung, N. D. Thien, L.H. Thanh, Sensors 11(2011) 1924.

[41]. X. Li, W. Chen, C. Bian, J. He, N. Xu, G. Xue, Appl. Surf. Sci. 217 (2003) 16.

[42]. L. Zhang, M. Wan, J. Phys. Chem. B 107 (2003) 6748.

[43]. H. Zhang, R. Zong, J. Zhao, Y. Zhu, Environ. Sci. Technol. 42 (2008) 3803.

[44]. Y.Wang, J. Xu, W. Zong, Y. Zhu, Journal of Solid State Chemistry 184 (2011) 1433.

[45]. Y. Furukawa, S. Tazawa, Y. Fujii, I. Harada, Synth. Met. 24(1988)329.

[46]. S. J. Vigmond, V. Ghaemmaghami, M.Thompson, Can. J. Chem. 73(1995) 1711.

[47]. Q.T. Vu, M. Pavlik, N. Hebestreit, U. Rammelt, W.Plieth, J. Pfleger, Reactive & Functional Polymers 65 (2005) 69.

[48]. C.G.Granqvist, R.A.Buhraman, J.Appl.Phys. 47(1996)2200.

[49]. J. Liu, T.An, G. Li, N. Bao, G. Sheng, J. Fu, Microporous and Mesoporous Materials 124 (2009) 197.

[50]. C.S. Danielle ,S.M. Michelle, A.H, Ivo,J.G.Z.Aldo, Chem Mater 15(2003) 4658.

[51]. X. Li, D.Wang, G. Cheng, Q.Luo, J.An, Y. Wang, Applied Catalysis B: Environmental 81 (2008) 267.

[52]. B.T. Su, X.H. Liu, X.X. Peng, T. Xiao, Z.X. Su, Mater. Sci. Eng. A 349 (2003) 59.

[53]. D.Wang, Y.Wang, Xu.Li, Q.Luo, J.An, J.Yue, Catalysis Communications 9 (2008) 1162.

[54]. R. B. Ambade, S.B. Ambade, N. K. Shrestha, Y.C. Nah, S.H. Han, W. Lee, S.H. Lee, Chem. Commun. 49**(**2013) 2308.

[55]. X.U. Shoubin, J.Long, Y.Haigang, S. Yuanqing, D.Yi, Chinese Journal of Catalysis 32(2011) 536.

[56]. K. S. W.Sing, Pure Appl. Chem. 54(1982) 2201.

[57]. C.Bian, Y.Yu, G. Xue, Journal of Applied Polymer Science (2006) DOI 10.1002/app25636.

[58]. A. Matsumnoto, T.Kitajima, K. Tsutsumi, Langmuir 15(1999)7626.

[59]. T. H Chao, H. A. Erf, J. Cat. 100(1986) 492.

[60]. G. Larsen, G. L. Haller, M. Marquez, J. Phys. Chem. 96(1992) 414.

Chapter 4

PHOTOCATALYSIS

Contents

Photocatalysis potentially can provide solutions for many of the environmental challenges facing the modern world because it provides a simple way to use light to induce chemical transformations. Pollution control, either in aqueous solutions or air, is very likely the most studied application of photocatalysis, although commercial uses relate mainly to self-cleaning surfaces. Currently, TiO_2 is by far the most widely used photocatalyst because it comprises the best balance of properties among the known or assayed semiconductors. However, it still presents some disadvantages such as limited activity and reduced sensitivity to sunlight. Therefore, in the last few years significant effort has been devoted to the search for new materials that may overcome the limitations of TiO_2. TiO_2, have also been tested for the most relevant photocatalytic applications: water splitting, detoxification and disinfection, and organic synthesis.

4A- PHOTOCATALYTIC DEGRADATION OF DYES

4A.1. Introduction

Synthetic dyes are major part of our life as they are found in various products ranging from clothes to leather accessories to furniture. An unfortunate side effect of their widespread use is the fact that up to 12% of these dyes are wasted during the dyeing process, and that approximately 20% of this wastage enters the environment (mostly in water supply). Organic dyes came up as one of the many new chemicals which could be used in many industrial activities. Due to the extensive use of these dyes in industries, they have become an integral part of industrial effluent. In fact, of the 450, 000 ton of organic dyes annually produced worldwide, more than 11% is lost in effluents during manufacture and application processes. Most of these dyes are toxic and potentially carcinogenic in nature and their removal from the industrial effluents is a major environmental problem [1]. Dyes are the major industrial pollutants and water contaminants. The control of water pollution has become an important environmental issue in recent years. Although release of dyes into the environment constitutes only a small proportion of water pollution, dyes are visible in small quantities due to their brilliance. Dyes have been identified as problematic compounds in textile wastewaters as they are water soluble and cannot be easily removed by conventional aerobic biological wastewater treatment systems. Anaerobic systems could reduce the colour intensity more satisfactorily than the aerobic processes [2]. Many synthetic dyes in industrial wastewaters are resistant to degradation in conventional biological treatment process [3]. India's dye industry produce every type of dyes and pigments. Production of dyestuff and pigments in India is close to 80,000 tonnes. India is the second largest exporter of

dyestuffs and intermediates among the developing countries, next only to China. The Indian textile industries now predominantly use synthetic organic dyes like direct dyes, processing dyes, reactive dyes etc. A large variety of dyes and chemicals used in an attempt to make more attractive popular shades of fabrics for a competitive market render them very complex [4] in several aspects causing environmental issues. During the last decade, environmental issues associated with dye stuff production and application have grown significantly and are indisputably among the major driving forces affecting the textile dye industry today [5]. The textile and food industries use organic dyes which represent an important source of environmental contamination. Most of dyes are toxic on aquatic creatures and have carcinogenic effects on humans [6, 7]. Different techniques such as adsorption, oxidation, reduction, electrochemical and membrane filtration are applied to remove these pollutants from the industrial effluents. Oxidation processes are widely used both in industrial preparations and in environmental treatments [8, 9]. An alternative and conventional method called the advanced oxidation processes (AOPs) based on the insitu generation of reactive OH radical is applied. This radical species can quickly and nonselectively oxidize broad range of organic pollutants [10, 11]. Most of AOPs comprise of the combination of UV-light with H_2O_2, TiO_2, and O_3 [12]. Triphenylmethane dyes are used extensively in textile, printing, food, and cosmetic industries [13]. The wastewater drained from these industries may cause a dramatic source of aesthetic pollution and may exert long-term adverse effects on the aquatic environment [14, 15]. They can persist for a long period in the aquatic environment because of their resistance to chemical and bacterial attacks [16-18].

4A.2. Degradation of Rhodamine B

Rhodamine is a family of related chemical compounds, fluorone dyes. Examples are Rhodamine 6G and Rhodamine B. They are used as a dye and as a dye laser gain medium. They are often used as a tracer dye within water to determine the rate, direction of flow and transport. Rhodamine dyes fluoresce and can thus be detected easily and inexpensively with instruments called fluorometers. They are used extensively in biotechnology applications such as fluorescence microscopy, flow cytometry, fluorescence correlation spectroscopy and ELISA. These are generally toxic, and are soluble in water, methanol and ethanol. Rhodamine B is used in biology as a staining fluorescent dye, sometimes in combination with auramine O, as the auramine-rhodamine stain to demonstrate acid-fast organisms, notably *Mycobacterium*.

Rhodamine B is tunable around 610 nm when used as a laser dye [19]. Its luminescence quantum yield is 0.65 in basic ethanol [20],0.49 in ethanol [21-23]1.0, and 0.68 in 94% ethanol. The fluorescence yield is temperature dependent [24]. Rhodamine B is being tested for use as a biomarker in oral rabies vaccines for wildlife, such as raccoons, to identify animals that have eaten a vaccine bait. The rhodamine is incorporated into the animal's whiskers and teeth [25]. It is also often mixed with herbicides to show where they have been used. Rhodamine B (RhB) is a common dye in the triphenyl methane family, which contains four *N*-ethyl groups at either side of the xanthene ring (structure given below).

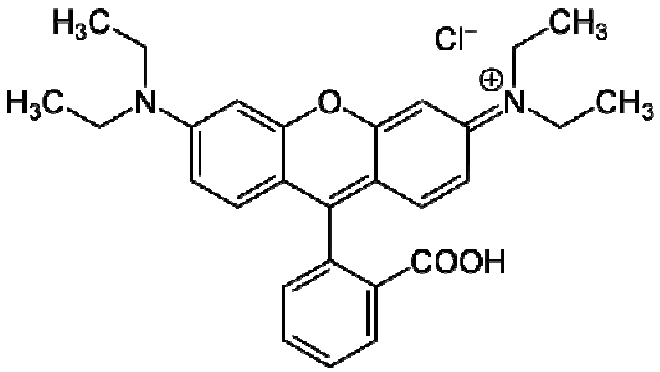

Rhodamine B

4A.2.1. Effect of catalyst amount

Several studies have indicated that the photocatalytic rate initially increases with catalyst loading and then decreases at high catalyst amount values because of light scattering and screening effects. The tendency towards agglomeration (particle-particle interaction) also increases at high solid concentration, resulting in a reduction in surface area available for light absorption and hence a drop in photocatalytic degradation rate. Fig.4A.1. shows the effect of catalyst dosage on % degradation of Rhodamine B. A further increase in catalyst loading beyond the optimum will result in non-uniform light intensity distribution, so that the reaction rate would indeed be lower with increased catalyst dosage. At high concentration, the degradation rate was observed to have levelled off. An increase in the amount of catalyst provides an increased number of active sites for adsorption; however, the simultaneous increase in solution opacity causes a decrease in the penetration of the photon flux. As a result of decreased effective light intensity, the photo generation of electrons and positive holes would be reduced and then the rate of photocatalytic degradation is also reduced. This suggests that the amount of photocatalyst to be used should maintain a balance between these two

opposing effects, the aggregation of free catalyst particles and the screening effect resulting from the excessive opacity of the solution. In contrast to accelerating the rate of reaction resulting from the addition of excess catalyst, it can possibly cause a negative effect by reducing the light transmittivity due to the formation of an opaque solution. At high catalyst loading, the reported low degradation rate is attributed to the deactivation of activated molecules through collision with ground state titania molecules. In order to ensure uniform light intensity in the photocatalytic reactor, optimum catalyst loading must be determined [26].

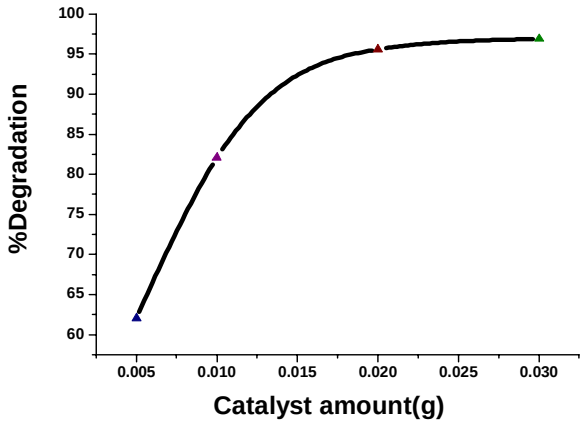

Fig.4A.1.Effect of catalyst dosage on % degradation

4A.2.2.Effect of Time

The required duration for the complete photocatalytic reaction was also observed. The reaction irradiation time was varied from 0-60 min under the visible light source by loading of 0.20 g/L catalyst into 10 ml of 10^{-4}M the dye solution. Before irradiation the reaction mixture was magnetically stirred for 30 minutes under dark to achieve adsorption desorption equilibrium between the catalytic surface and the pollutant. A dichoric mirror of 420-630 nm with

irradiance intensity of 96.8 mW/cm^2 is used as the visible light source. Results represented that dye removal efficiency increases with time as shown in Fig.4a.2. From the figure it is clear that as time increases the degradation rate also increases and a maximum degradation of 95% was obtained within time duration of 60 minutes. So the optimum time for degradation was selected as 60 minutes.

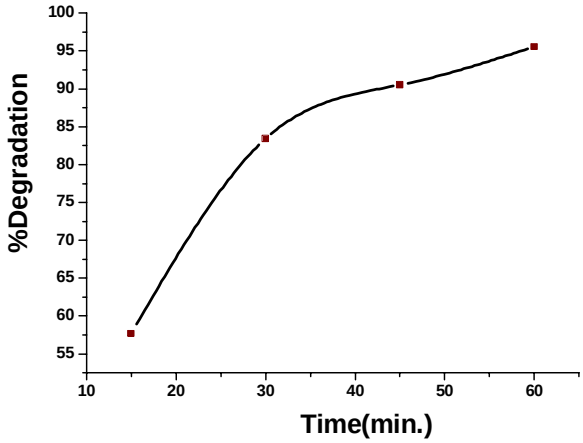

Fig.4A.2.Effect of time on % degradation

4A.2.3. Effect of light source

Light intensity plays an important role in degradation rate. The effect of visible light intensity on the degradation of rhodamine B is shown in Fig.4A.3. For this purpose two different lamp systems were used. A 150 W Xe lamp with a light irradiation intensity of 96.8 mW/cm^2 and a 100W Xe lamp with a light irradiation intensity of 64.7 mW/cm^2 are used as the visible light source. From the figure it is clear that as the lamp power increases the % degradation also increases.

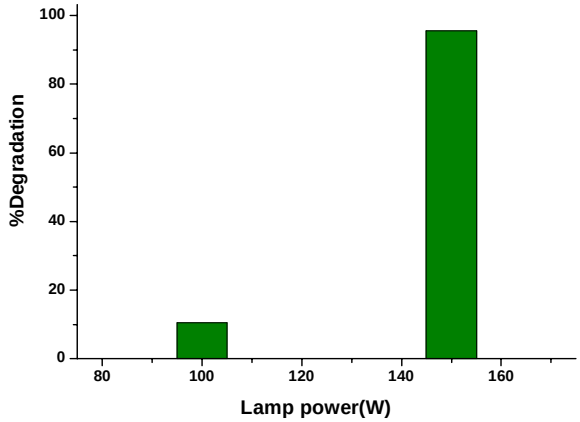

Fig.4A.3.Effect of light source on % degradation

4A.2.4. Effect of dye concentration

The effect of dye concentration on its photodegradation rate was investigated over the range of 10^{-3} to 10^{-4} M using the optimum catalyst dose of 0.02g. The effect of concentration on the removal of Rhodamine B dye solution is shown in Fig.4A.4.It is noted that the percentage removal of dye decreases as the concentration of dye increases. For a fixed time period, say 60 minutes, the % degradation is very low at high concentration and it increases as the concentration decreases. This can be explained in terms of the saturation of the limited number of accessible active sites on the photocatalyst surface and/or deactivation of the active sites of the catalyst. Several studies have reported that high organic substrate loadings induce the formation of intermediates that could be adsorbed onto the catalyst surface and deactivate the active sites [26, 27]. Moreover, the significant absorption of light by the substrate at high concentrations might decrease the level of the light reaching the photocatalyst and thus its efficiency by reduction of the amount of $OH^-$and O^{-}_2 free radical produced [28].

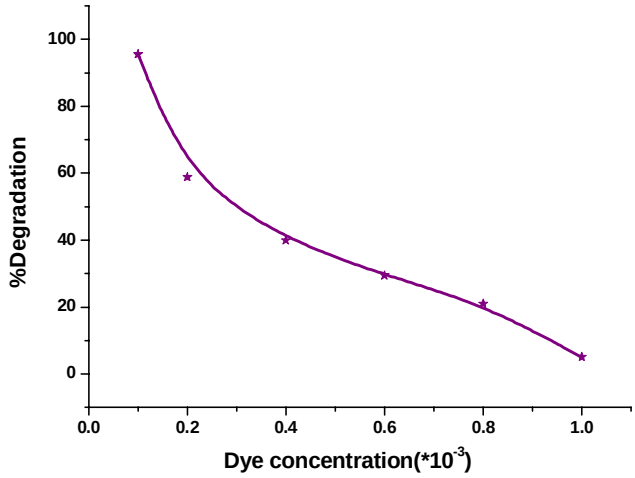

Fig.4A.4.Effect of dye concentration on % degradation

4A.2.5.Effect of various catalysts

The photocatalytic activity for TiO_2 and various TiO_2-conducting polymer nanocomposite catalysts are presented in Fig.4A.5. From the figure it is clear that all the prepared catalysts shows superior activity compared to pure TiO_2 under visible light irradiation. It is observed that as the amount of conducting polymer in the composite increases the photocatalytic activity decreases. Polyaniline and polythiophene blended nanocomposites show more activity compared to the polypyrrole blended ones. This may be because of the extremely small surface area of polypyrrole nanocomposite compared to that of the polyaniline and polythiophene blended ones. Basically, the photocatalytic activity depends on the surface and structural properties of the catalyst such as crystal composition, surface area, particle size distribution, porosity, band gap and surface hydroxyl density. Particle size is a primary importance in heterogeneous catalysis, because it is directly related to the efficiency of a catalyst through the definition of its surface area.

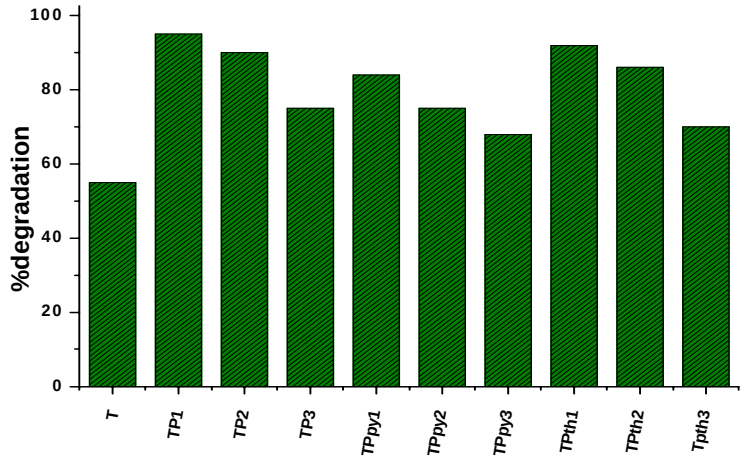

Fig.4A.5.Effect of various catalysts on % degradation

The increase in the particle size decreases the net available surface area of the catalyst, which in turn decreases the number of available active sites for the reaction [29].

4A.2.6. Kinetics of degradation

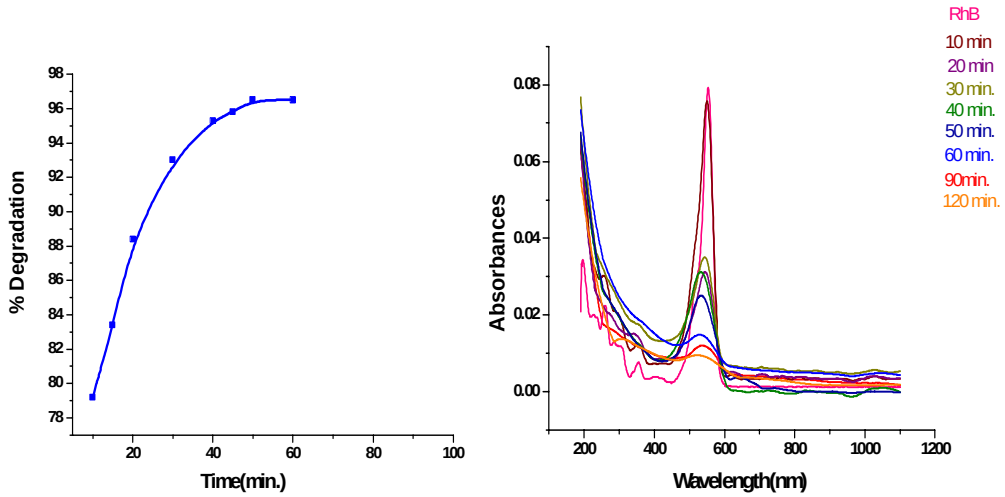

Fig.4A.6. Variation of RhB degradation with time

Fig.4A.6. shows the variation of RhB degradation with time. The kinetic plots for RhB degradation with PANI/TiO_2 nanocomposite photocatalysts under visible light illumination are shown by pseudo-first order reaction [30-34]. This model is described by the equation $-\ln (C_t/C_0) = k_{app}t$, where k_{app} is the apparent rate constant, C_0 the initial concentration of RhB and C_t the concentration of RhB at various contact times, t. Half life of RhB photodegradation was calculated using the equation $t_{1/2} = \ln 2/k = 0{\cdot}6931/k_{app}$, which was derived from the above equation by replacing C_t with $C_0/2$ [35, 36].

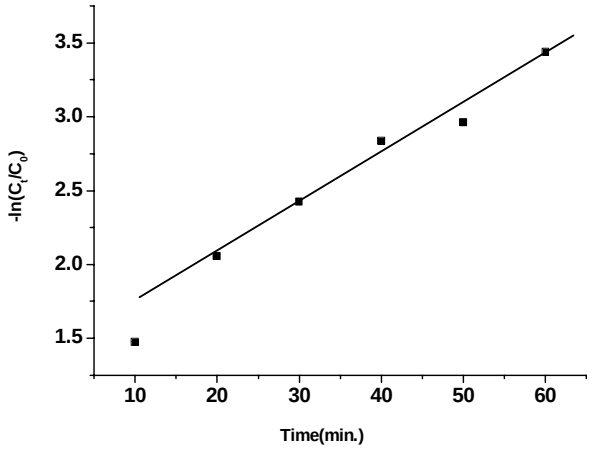

Fig.4A.7. Kinetic plots for linear fitting of data obtained from pseudo-first-order reaction model

Fig. 4A.7. shows the kinetic plots for linear fitting of data obtained from pseudo-first-order reaction model for Rhodamine B degradation under visible light irradiation using PANI/TiO_2 as photocatalyst.

4A.3. Degradation of Malachite Green

Malachite green (MG) is an extensively used biocide in the aquaculture industry world-wide. It is highly effective against important protozoal and

fungal infections [37-39]. Basically, it works as an ectoparasiticide. It has also been used to control skin flukes and gill flukes. Aquaculture industries have been using malachite green extensively as a topical treatment by bath or flush methods without paying any attention to the fact that topically applied therapeutants might also be absorbed systemically and produce significant internal effects. On the other hand, it is also used as a food colouring agent, food additive, a medical disinfectant and anthelminthicas as well as a dye in silk, wool, jute, leather, cotton, paper and acrylic industries [40]. However, malachite green has now become a highly controversial compound due to the risks it poses to the consumers of treated fish [41] including its effects on the immune system, reproductive system and its genotoxic and carcinogenic properties [42-44]. There is concern about the fate of MG and its reduced form, leucomalachite green in aquatic and terrestrial ecosystems since they occur as contaminants [45, 46] and are potential human health hazards.

Malachite green is an organic compound that is used as a dyestuff and has emerged as a controversial agent in aquaculture. Malachite green is classified in the dyestuff industry as a triarylmethane dye.

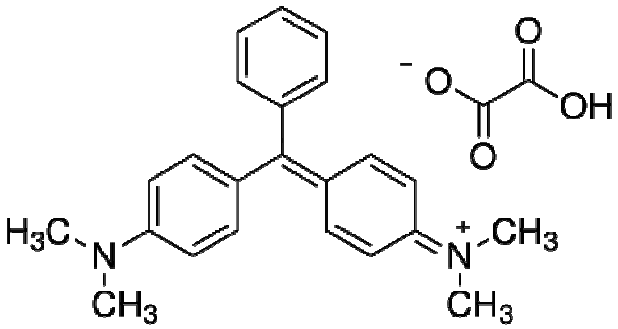

Malachite green Oxalate

Malachite green is a basic dye. Basic dyes are salts of the coloured organic bases containing amino and imino groups and also combined with a colourless acid, such as hydrochloric or sulfuric. They are brilliant and most fluorescent among all synthetic dyes. Basic dyes are cationic which has positive electrical charge and are used for anionic fabrics which are negative-charge-bearing, such as wool, silk, nylon, and acrylics where bright dying is the prime consideration. Malachite green does not contain the mineral malachite; the name comes from the similarity of color. This chemical dye is primarily designed to be used as a dye for silk, leather, and paper. Malachite green in dilute solution is widely used medicinally as a local antiseptic. It is effective against parasites, fungal infections and gram-positive bacteria. In combination with formalin as a synergist, malachite green is a common antiseptic agent against the fungus Saprolegnia, a typical water mold that kills fish eggs and young fry. But the use has been banned in many countries due to its suspect of carcinogenicity. Malachite green is used as a biological stain as a counter stain against fuchsine which stains gram-positive and gram-negative bacteria reddish colors and safranin which stains nuclei red. Malachite green stain background to the surrounding tissue blue-green. Malachite green is used as a pH indicator between pH 0.2 (green) -1.8 (blue-green). Malachite green**,** also called aniline green, benzaldehyde green, or china green. Malachite green is effective against fungi and gram-positive bacteria. In the fish-breeding industry it has been used to control the fungus *Saprolegnia*. Malachite green also is used as a direct dye for silk, wool, jute, and leather and to dye cotton that has been mordanted with tannin. Prepared from benzaldehyde and dimethylaniline, the dye occurs as lustrous green crystals soluble in water and in alcohol.

Malachite green (MG), also called basic green 4 or victoria green B having IUPAC name 4-[(4-dimethylaminophenyl)-phenyl-methyl]-N, N-dimethyl aniline, is a green crystal powder with a metallic lustre, highly soluble in water and ethanol with blue green solutions. It is a highly toxic chemical primarily used as a dye.

4A.3.1.Effect of catalyst amount

To study the effect of catalyst dose on the degradation of compound, catalyst dose was varied from 0.01 to 0.07g during the photocatalytic treatment process. Fig.4A.8. shows the effect of catalyst dosage on % degradation. It is observed that the rate of photocatalytic process increased with the increase in concentration of the catalyst up to 0.05g. The addition of excess of catalyst above 0.05g did not significantly enhance the degradation. The reason for this is clustering of catalyst particles at higher concentrations and thus causing a decrease in the number of active sites on its free surface.

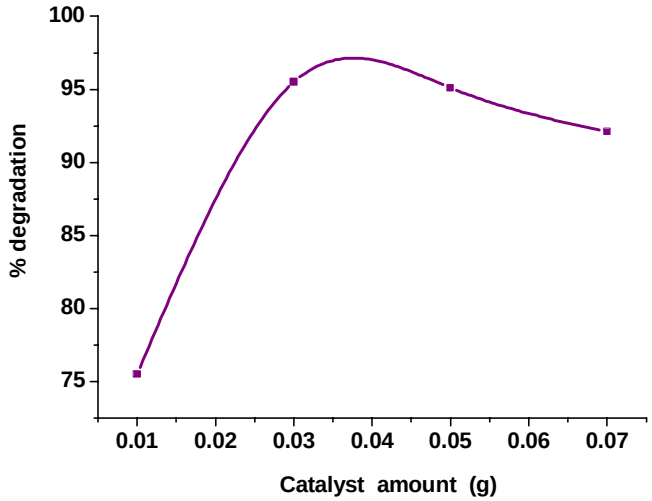

Fig.4A.8.Effect of catalyst dosage on % degradation

Above a certain level, the compound molecules available are not sufficient for the adsorption by the increased number of catalyst particles. Hence the increased catalyst amount is not involved in the catalytic activity and the rate does not increase with an increase in the amount of catalyst beyond a certain limit [47]. Other reasons may be an increase in the opacity and light scattering by the particles. Fig.4A.8. depicts that the maximum degradation was achieved with 0.05 g of photocatalyst.

4A.3.2.Effect of Reaction time:

To elucidate the influence of irradiation time on degradation rate, photocatalysis was performed by treating aqueous solution of p-nitrophenol of concentration 10^{-4} M and photocatalytic dose of 0.05g for 1h. Fig.4A.9. shows the effect of time on % degradation. Initial degradation rate is higher which may be due to more contact between photocatalyst surface and p-nitrophenol. Later on the degradation rate is slower which may be due to the less availability of surface active sites on photocatalyst surface.

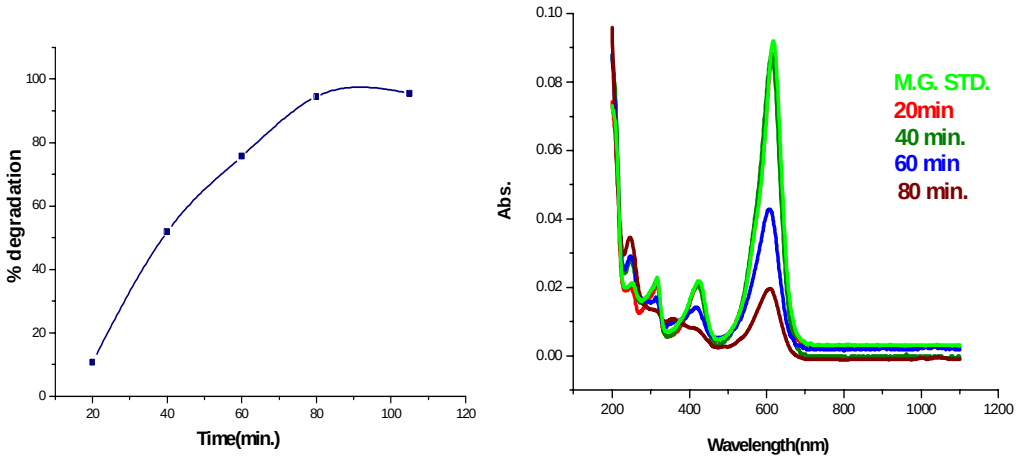

Fig.4A.9.Effect of time on % degradation

So the optimum time at which a maximum degradation of malachite green was obtained is 1 hour with a catalyst loading of 0.05g.

4A.3.3.Effect of various catalysts

The photocatalytic degradation of malachite green was carried out over all the conducting polymer modified TiO_2 nanocomposites under the optimised conditions. The results are given below in Fig.4A.10.

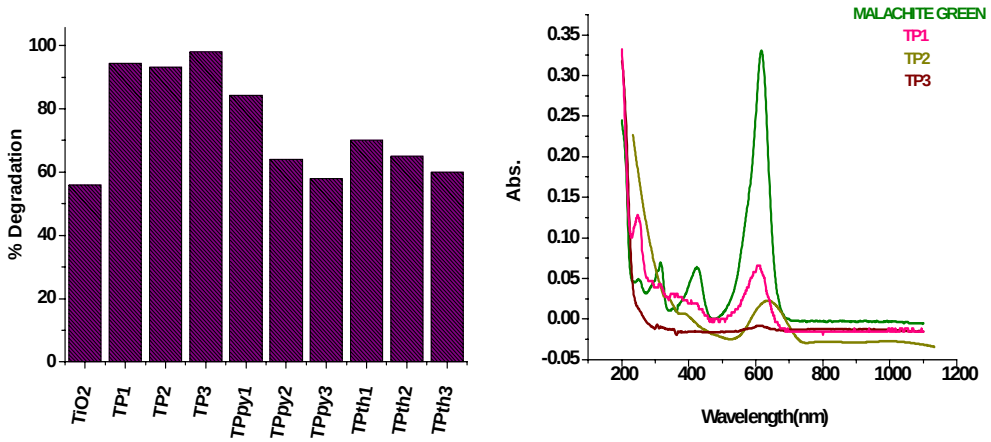

Fig.4A.10.Effect of various catalysts on % degradation

From the figure it is clear that the prepared systems shows superior activity compared to TiO_2 under visible light irradiation towards the degradation of Malachite green. The polyaniline modified TiO_2 nanocomposites show relatively higher activity. Photodegradation of MG can be expressed by the following reaction mechanism:

$$TiO_2 \xrightarrow{h\upsilon} h^+ + e^-$$

$$h^+ + e^- \xrightarrow{h\upsilon} \text{heat}$$

$$MG^+ + H^+ + 2e^- \xrightarrow{K_1} MGH^-(leuco)$$

$$MGH^-(leuco) \longrightarrow NH_4 + CO_2$$

The PANI-TiO_2 nanocomposite absorbs radiation of energy corresponding to its band gap and generates electron-hole pair. The electron and hole may recombine nonradiatively to release the energy absorbed in the form of heat. The cationic dye MG^+ combines with two electrons and a proton to give its reduced form MGH^-.This step is the rate determining step for the photocatalytic degradation of malachite green. The leuco form of the dye ultimately degrades to final products containing CO_2 and NH_4.

4A.3. 4. Kinetics of degradation

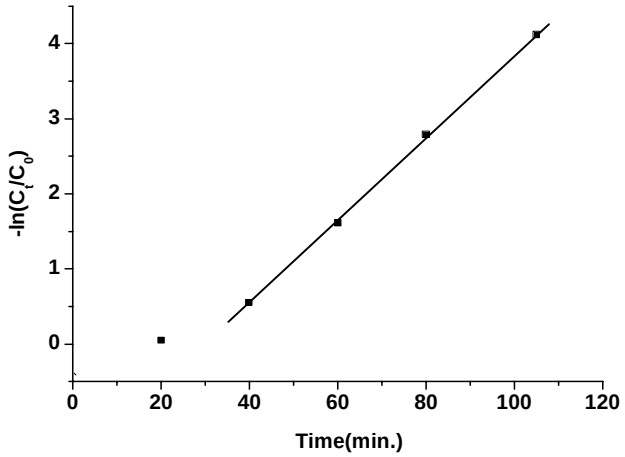

Fig.4A.11. Kinetic plots for linear fitting of data obtained from pseudo-first-order reaction model

Fig.4A.11. shows the kinetic plots for linear fitting of data obtained from pseudo-first-order reaction model. It is found that the degradation of MG accords with pseudo-first order kinetics by linear transforms, $-\ln (C_0/C_t) = kt$, where C_0 is the initial concentration of MG, C_t is the concentration of MG at time t, and k is kinetic constant.

4A.4. Mechanism of Dye degradation

For photocatalytic behaviour under visible-light irradiation, the introduction of PANI to TiO_2 nanoparticles obviously enhanced the photoactivity. The band

gap energy (Eg) of TiO_2 is about 3.2 eV, corresponding to a threshold wavelength of 387 nm. The weak degradation of organic molecules in pure TiO_2 is due to the poor light absorption under visible irradiation. PANI has a narrower band gap, showing strong absorption in the range from visible to near infrared light [48]. Hence, it may function as an effective sensitizer toTiO_2 photocatalysts. It is obvious that the composite has higher response over the whole range of UV–Vis spectrum. Based on the well-established energy band theory of PANI/TiO_2 composites, the photocatalytic mechanism under visible light irradiation is described as follows. Fig.4A.12.shows the mechanism of photocatalytic degradation of dyes using TiO_2 –PANI composite.

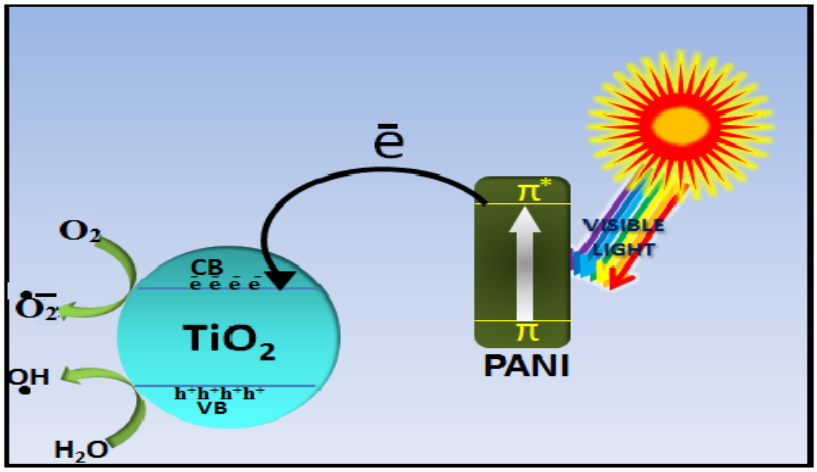

Fig.4A.12. Mechanism of photocatalytic degradation of dyes using TiO_2 –PANI composite

It is well known that the overall photocatalytic activity of photocatalyst is mainly governed by three properties: light harvest efficiency, separation efficiency of photogenerated charges and the interfacial reaction process. The high separation efficiency of photogenerated charges could be achieved by the heterojunction built between TiO_2 and PANI. The highest occupied molecular

orbital and the lowest unoccupied molecular orbital of PANI were 0.8V and −1.9V vs. NHE, respectively [49]. The valence band and conduction band of TiO_2 was 3.0V and −0.2V vs. NHE, respectively [50, 51]. The energy levels of PANI have been known as well matched for wide band gap semiconductor TiO_2. Both PANI and TiO_2 nanoparticles absorb photons at their interface under irradiation. Since the CB of TiO_2 and lowest unoccupied molecular orbital (LUMO) of PANI are well matched for the charge transfer, the electrons generated by PANI $\pi \rightarrow \pi^*$ transition under visible light illumination can be injected into the CB of TiO_2 and the electrons in the VB of TiO_2 are delivered to PANI layer [52]. Enhancement of charge separation in the PANI/TiO_2 nanocomposite is achieved, because PANI is an efficient electron donor and good hole transporter. These features of PANI lead to the effective separation of photogenerated electron–holes at the interface of PANI and TiO_2 in the nanocomposite [53-54]. The improvement of PANI/TiO_2 photocatalytic activity under UV light illumination is negligible compared to pristine TiO_2 nanoparticles while; photocatalytic activity of the same composition of PANI/TiO_2 under visible light irradiation is considerably higher than pristine TiO_2 nanoparticles.

4A.5.Conclusions

Addition of conducting polymer/TiO_2 composite to the dye solution in the presence of visible light led to the degradation of dyes. The results showed that the conducting polymer-hybridized TiO_2 possessed higher catalytic activity compared with pure TiO_2 under visible light irradiation due to the sensitizing effect of conducting polymer. Out of the three different polymer modified systems the polyaniline modified systems showed superior activity compared to the other two systems. Furthermore, it has good sedimentation ability. Therefore, it can be expected as a promising material for large-scale environmental applications.

References

[1]. M.A. Rauf, S. S. Ashraf, Chemical Engineering Journal 151 (2009) 10.

[2]. T. Panswad, W. Luangdilok, Wat. Res. 34 (2000) 4177

[3]. L. Young, J.Yu, Wat. Res. 31 (1997)1187.

[4]. S. Rajagopalan, Water pollution problem in textile industry and control. In: R.K.Trivedy (Ed.), Pollution management in industries. Environmental Pollution, Karad, India (1990)21.

[5]. C.P. Sajan, B. Basavalingu, S. Ananda, K. Byrappa, Journal of Geological Society of India 77 (2011)82.

[6]. G. Liu, X. Li, J. Zhao, H. Hidaka, N. Serpone, Environ. Sci. Technol 34 (2000) 3982.

[7]. G.L. Baughman, E.J. Weber, Environ. Sci. Technol. 28 (1994) 267.

[8]. J. Qin, Q. Zhang, K.T. Chuang, Appl. Catal. B: Environ 29 (2001) 115.

[9]. T. Fujitani, J. Nakamura, Appl. Catal. A: Gen 191 (2000) 111.

[10]. W.S. Kuo, P.H. Ho, Chemosphere 45 (2001) 77.

[11]. O. Legrini, E. Oliveros, A.M. Braun, Chem. Rev. 93 (1993) 671.

[12]. W.H. Glaze, J.W. Kang, D.H. Chapin, Ozone Sci. Eng 9 (1987) 335.

[13]. K. N. Vinod, T.Puttaswamy, K. N. N. Gowda, J. Mol. Catal. A:Chem., 298 (2009) 60.

[14]. L.Ayed, K.Chaieb, A.Cheref, A.Bakhrouf, World J. Microbiol. Biotechnol., 25(2009) 705.

[15]. L. Waldau, Kem. Tidskr., 91(1979) 20.

[16]. Z. He, C.Sun, S.Yang, Y. Ding, H. He, Z. Wang, J. Hazard.Mater. 162(2009) 1477.

[17]. L.Li, W. K.Dai, P.Yu, J. Zhao, Y. B. Qu, J. Chem. Technol. Biotechnol. 84(2009) 399.

[18]. K. Yu, S. Yang, H. He, C.Sun, C. Gu, Y. Ju, J. Phys. Chem. A. 113(2009) 10024.

[19]. http://en.wikipedia.org/wiki/RhodamineB

[20]. R.Kubin, Journal of Luminescence 27 (1983)455.

[21]. K.G. Casey, G. Kelly, Quitevis, L. Edward The Journal of Physical Chemistry 92 1988) 6590.

[22]. R. E. Kellogg, R.G. Bennett, The Journal of Chemical Physics 41 (1964)3042.

[23]. M. Snare, Journal of Photochemistry 18 (1982) 335.

[24]. T.Karstens, K. Kobs, The Journal of Physical Chemistry 84 (1980) 1871.

[25]. D.Slate, A. P. Timothy, K. M. Nelson, R. B. Chipman, D. Dennis, J. D. Blanton, M. Niezgoda, C.E.Rupprecht, "Oral Rabies Vaccination in North America: Opportunities, Complexities, and Challenges". In Bethony, Jeffrey M. PLoS Neglected Tropical Diseases 3 (2009). (12): 549. doi:10.1371/ journal.pntd.0000549.PMC 2791170. PMID 20027214

[26]. S. Ahmed, M.G. Rasul, W.N.Martens R. Brown, M.A.Hashib, Desalination 261 (2010) 3

[27]. R. Jain, M. Shrivastava, J. Hazard. Mater. 152 (2008) 216.

[28]. K.M. Parida, S.S. Dash, D.P. Das, J. Colloid Interface Sci. 298 (2006) 787.

[29]. L.Das, M.Dutta, J. Kumar Basu, International Journal of Environmental Sciences 4(2013)415.

[30]. X. Li, D. Wang, G. Cheng, Q. Luo, J. An, Y. Wang, Appl.Catal. B 81(2008) 267.

[31]. X. Li, D. Wang, Q. Luo, J. An, Y. Wang, G.Cheng, J. Chem. Technol. Biotechnol. 83 (2008)1558.

[32]. D. P. Wang, H. C. Zeng, Chem. Mater. 21 (2009) 4811.

[33]. F .Wang, S. Min, Y. Han, L. Feng, Superlattices Microstruct. 48(2010) 170.

[34]. G. Liao, S.Chen, X. Quan, H. Chen, Y. Zhang, Environ. Sci.Technol. 44 (2010)3481.

[35]. D.Dong, P.Li, X. Li, Q.Zhao, Y.Zhang, C.Jia, P.Li, J.Hazard. Mater. 174 (2010) 859.

[36]. A.O.S. Behboudi, A.A. Entezami, Bull. Mater. Sci., 35, (2012) 801, Indian Academy of Sciences.

[37]. G.L.Hoffman, F.P. Meyer, Parasites of Freshwater Fishes. TFH Publications, Neptune, New Jersey (1974).

[38]. D.J.Alderman, J. Fish Dis. 8(1985)289.

[39]. R.A. Schnick, Prog. Fish Cult. 50(1988) 190.

[40]. S.J. Culp, F.A.Beland, J. Am. Coll. Toxicol. 15(1996) 219.

[41]. D.J.Alderman, R.S.Clifton-Hadley, J. Fish Dis. 16 (1993)297.

[42]. C. Fernandes, V.S.Lalitha, V.K.Rao, Carcinogenesis 12(1991) 839.

[43]. K.V.K Rao, Toxicol. Lett. 81 (1995)107.

[44]. C.Gouranchat, Malachite green in fish culture (state of the art and perspectives), Bibliographic studies, Ecole Natl.Veterinaire ENVT, Nantes, France(2000) 142.

[45]. S. Burchmore, M.Wilkinson, Proposed environmental quality standards for malachite green in water (DWE 9026) Department of the Environment, report no. 3167/2. Water Research Center, Marlow, Buckinghamshire, UK (1993).

[46]. C.R Nelson, R.A.Hites, Environ. Sci. Technol. 14(1980) 147.

[47]. A.P.Toor, A.Verma, V.Singh, C.K.Jotshi, P.K.Bajpai, Indian Journal of Chemical Technology, 12(2005)75.

[48]. J. Wang, X.Y. Ni, Solid State Commun. 146 (2008) 239.

[49]. G.K.R. Senadeera, T. Kitamura, Y. Wada, S. Yanagida, J. Photochem. Photobiol. B164 (2004) 61.

[50]. M.A. Fox, M.T. Dulay, Chem. Rev. 93 (1993) 341.

[51]. M.R. Hoffmann, S.T. Martin, W. Choi, D.W. Bahnemann, Chem. Rev. 95 (1995) 69.

[52]. F. Wang , S. X. Min, Chin. Chem. Lett. 18 (2007)1273.

[53]. H. Zhang, R. Zong, J. Zhao, Y. Zhu, Environ. Sci. Technol.42 (2008) 3803.

[54]. F. Wang, S. Min, Y. Han, L. Feng, Superlattices Microstruct.48(2010)170.

4B-PHOTOCATALYTIC DEGRADATION OF 4- NITROPHENOL

4B.1.Introduction

The pollution of drinking water reservoirs and aquatic environment by chemicals is a dramatic problem of these last years. Nitroaromatic compounds are recognized as environmentally hazardous. Phenolic hydrocarbons including nitrophenols are widely used in pharmaceutical, petrochemical, and other chemical manufacturing processes. Because of their harmful effects, wastewaters containing phenolic compounds must be treated before being discharged into receiving water bodies. The methods to treat wastewaters containing phenolic compounds can be classified into biological methods, physical methods, and chemical methods [1]. Nitrophenols are some of the most refractory substances present in industrial wastewaters because of their high stability and solubility in water [2]. They are considered to be priority toxic pollutants by the United States Environmental Protection Agency (U.S.EPA) [3]. 4-nitrophenol is toxic as are the other phenol derivatives. Owing to high toxicity and carcinogenic character, 4-nitrophenol is characterized as environmentally hazardous material. It is one of the 114 organic compounds listed by EPA. It can poison the central nervous system, damage liver and kidney, irritate eye and skin and disorder humans and animal's blood. Its maximum allowed concentration in water is 20 ppb. Even if in very low concentrations, it causes chronic poisoning. Polynitrophenols (PNP), a hazardous waste and priority toxic pollutant is used to manufacture drugs, fungicides, insecticides, and dyes. 4-NP can be released into soil as a result of hydrolysis of several organophosphates pesticides such as parathion and methyl parathion. Investigations on animals suggest that PNP may cause a blood disorder. It is difficult to purify PNP-contaminated wastewater due to its

stability to chemical and biological degradation [4]. There is evidence that 4-nitrophenol is one of the secondary pollutants formed in tropospheric transformation of monoaromatic chemicals with NOx and ozone. Purification of wastewater contaminated with 4-nitrophenol is very difficult. The presence of nitro substituent is known to render benzenoid compounds more resistant to microbial degradation. 4-Nitrophenol is very photostable, a phenomenon believed to be due to the charge transfer (CT) character of its triplet state. In aqueous aerated solutions, 4-nitrophenol is very reluctant to undergo photochemical transformations [5]. Nitrophenols are involved in the synthesis of many products and appear in the degradation of pesticides like parathion [6] and nitrofen [7]. Controlled incineration of 4-nitrophenol is suggested as a removal method [8]. The reaction rates of the biological methods are usually slow; thus huge reactor volumes or spaces are usually required. The physical methods only transform the pollutants into other forms; thus new waste disposal problems are generated. The reaction rates of the chemical methods are relatively high and total mineralization is possible if the reaction conditions and reactor is adequately designed. Incineration of large quantities of this pollutant requires scrubbers to control the emission of NOx. It has been recently reported [9] that 4-nitrophenol undergoes anaerobic biodegradation but a long period of incubation is required for the nitro group reduction. The process probably involves formation of such carcinogenic substances as nitroso compounds and hydroxylamines which are common intermediates of the reduction of the molecules containing nitro group(s). In aqueous aerated solutions, 4-nitrophenol is also very reluctant to undergo photochemical transformations. Nakagawa and Crosby reported [7] that 4-nitrophenol was one of the products of photodecomposition of the herbicide nitrofen in aqueous suspension under sunlight or simulated sunlight. While nitrophen

disappeared rapidly in the first week, subsequent degradation became very slow. Hydroquinone, 4-nitrocatechol and non volatile, dark polymers were photoproducts of the decomposition of 4-nitrophenol. Nakagawa and Crosby suggested [7] that aquatic photodegradation of this pollutant might represent a photo nucleophilic displacement of the nitro group. Results of the investigations carried out by Ishag and Moseley [10] confirmed the suggestion [7] that the effect of UV light on dilute aqueous solutions of 4-nitrophenol is largely nitrite displacement by OH' nucleophile with the formation of HNO_2 in the initial stage. Direct photolysis of 4-nitrophenol is so slow that it cannot be considered as a practical means for its destruction. Among the many chemical methods, the advanced oxidation process (AOP) using the hydroxyl radical ($OH^{\bullet}$) has been recognized as a promising technology to treat wastewaters containing refractory organic compounds. The quest for an efficient and inexpensive method for the removal of 4- nitrophenol from wastewaters, led to attention being given to the photocatalytic degradation using TiO_2 based photocatalysts. The photocatalytic degradation rate of the different nitrophenols depends on various parameters, such as temperature [11], pH [11, 12], and initial concentration of the pollutant [13]. Since it has a significant water solubility, 1.6 g/100 ml, it is often present in wastewater discharges from such facilities. It may also be found in ground water wells and surface waters where it has to be removed in order to achieve drinking water quality [14]. Photocatalytic treatment is an effective oxidation process for the treatment of toxic and bio-resistant pollutants at a low energy cost [15]. Priya etal [16] compared the photocatalytic degradation of nitrophenols using combustion synthesised nano-TiO_2 and Degussa P-25. The photodegradation kinetics is first order. The photocatalytic degradation rates were considerably higher in combustion synthesized TiO_2 compared to that of P-25. For both catalysts, the

degradation rate was shown to follow the order 4-Nitrophenol> 2-Nitrophenol> 3-Nitrophenol> 2, 4-Ditrophenol. The position of substitution is reported to affect the rate of degradation. Lacheb etal [17] reported that in comparison to PC-500, P-25 was more efficient for the degradation of phenols and poly nitrophenols (4-NP, 2, 4-DNP, 2, 4, 6-TNP) in the presence of either artificial or solar light. The degradation followed first order kinetics. The photocatalytic degradations of the tested compounds were shown to be in the following order: 2, 4, 6-TNP>2, 4-DNP>4-NP>Phenol. However, for PC 500 supported on Ahlstrom paper 1048, the order is the opposite - Phenol>4-NP>2, 4-DNP>2, 4, 6-TNP. The difference in poly nitrophenols disappearance rates was related to the variation in adsorption behaviour. For both supported Degussa P25 and Millennium PC-500 photocatalysts, the maximum quantities of adsorbed phenolic compounds increase in the order: Phenol <4-NP<DNP<TNP. Huang etal studied the degradation of 4-nitrophenol using a coupled Photocatalytic–Biological Aerated Filter Process. N-TiO_2/γ-Al_2O_3 granules were used as photocatalyst, Degradation efficiency of 4-NP using BAF process after a short-duration photocatalytic pretreatment (PC) were studied in detail. It was found that PC of 4-NP for 2.5 h, during which period about 20%–50% chemical oxygen demand removal occurred. It could be coupled to second-stage biological treatment for achieving enhanced biodegradation of 4-NP [18]. Qourzal et al showed that photooxidation of 4-nitrophenol in aqueous TiO_2 '700°C' suspensions follows a pseudo-first-order kinetics. The apparent rate constant depends on the initial 4-nitrophenol concentration. Their investigations clearly demonstrate the importance of choosing the optimum degradation parameters to obtain high degradation rates, which is essential for any practical application of photocatalytic oxidation processes [**19**]. Rahimi etal studied the photocatalytic degradation of

4-Nitrophenol using N, S co-doped TiO_2 nanoparticles synthesized by two different routes under visible light irradiation. Their results indicated that morphology parameter is more important in photocatalytic degradation [20]. Li etal investigated the photocatalytic activity of thienyl-porphyrins-TiO_2 for Degradation of 4-nitrophenol. According to them the prepared catalyst systems exhibited much higher photoactivity than bare TiO_2 not only under UV light but also under visible light irradiation [21].

This chapter deals with the study of photocatalytic degradation of 4-nitrophenol using conducting polymer modified TiO_2 nanocomposite systems. The aim of the present work is: (i) to determine the optimum treatment conditions on photo disappearance of 4-nitrophenol in the presence of TiO_2-conducting polymer hybrid nanocomposites under visible light irradiation. The excellent degradation properties indicated that this technology had potential application in the treatment to industrial wastewater containing nitrophenol pollutants.

4B.2.Optimization of Reaction Parameters:

4B.2.1.Effect of Catalyst Amount

Studies were carried out to find the optimum catalyst dosage for the degradation of nitrophenol under visible light irradiation. For this the catalyst amount was varied between 0.005 to 0.05g. Fig.4B.1 shows the variation in % degradation with the amount of catalyst. From the graph it is evident that at first the % degradation increases with the increase in amount of catalyst and beyond a certain limit the % degradation decreases. It may be due to light scattering effect and reduction in light penetration through the effluent due to the obstruction of large number of solid particles.

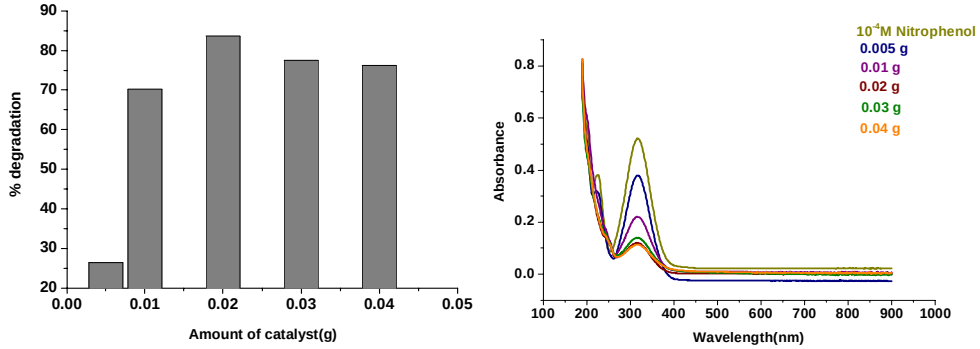

Fig.4B.1 Effect of catalyst dosage on % degradation

So the optimum catalyst loading for maximum degradation efficiency was selected as 0.02g and further experiments are carried using this optimum amount of catalyst.

4B.2.2.Effect of Time

Fig. 4B.2 shows the photocatalytic degradation profiles of 4-NP with time. An appropriate reaction time is the main assurance for a perfect reaction. Here the photocatalytic activity systematically increased with reaction time. A maximum of 83% was obtained within 60 minutes. Further increase in time shows no noticeable change in conversion. So the optimum time for maximum degradation is set as 60 minutes.

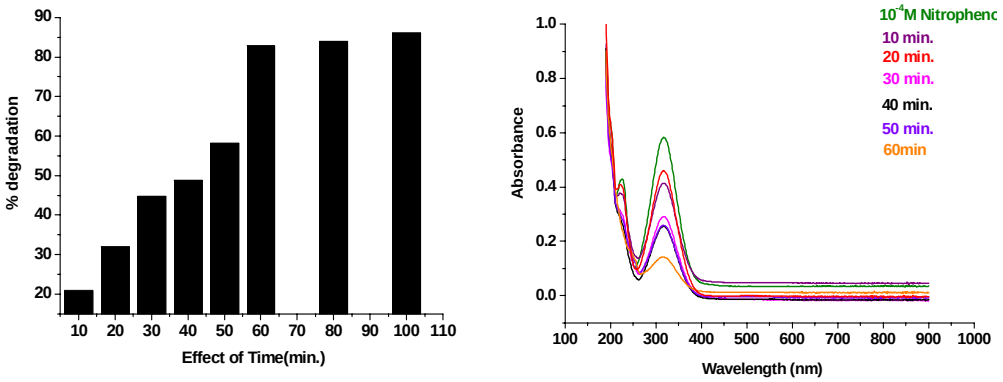

Fig. 4B.2. Effect of time on % degradation

4B.2.3.Effect of pH

The pH value is an important parameter in photodegradation that takes place on the surface of photocatalyst. The point of zero charge (pzc) for TiO_2 is at pH values between 5.6 and 6.4 [22]. Hence, at more acidic pH values, the catalyst surface is positively charged, while at pH values above 5.6, it is negatively charged.

$$TiOH + H^+ \rightleftharpoons TiOH_2^+ \qquad pH < pH\ pzc$$

$$TiOH + OH^- \rightleftharpoons TiO^- + H_2O \qquad pH > pH\ pzc$$

Therefore, pH value will have significant effect on the adsorption-desorption properties at the catalyst's surface. The pH changes can thus influence the adsorption of pollutant molecules onto the TiO_2 surface, an important step for the photooxidation to occur. The effect of pH on the photocatalytic degradation efficiency of AOP, according to some literatures is one of the major factors influencing the rate of degradation of some organic compounds. The degree of photocatalytic degradation of 4-NP was found to be affected by a change in pH. The effect of initial pH on the photocatalytic degradation of 4-NP is presented in Fig. 4B.3 with the optimum amount of catalyst. A maximum degradation was obtained at pH 6. The effect of the solution pH on the degradation rate can be explained mainly by adsorption of compound on TiO_2 surface. TiO_2 shows an amphoteric character so that either a positive or a negative charge can be developed on its surface. The point of zero charge of the used TiO_2 (Degussa P-25) is widely reported at pH≈6.5 [6, 25]. The TiO_2 surface is negatively or positively charged above and below this value according to the following equations:

$$-TiOH \leftrightarrow TiO^- + H^+$$

$$-TiOH + H^+ \leftrightarrow TiOH_2^+$$

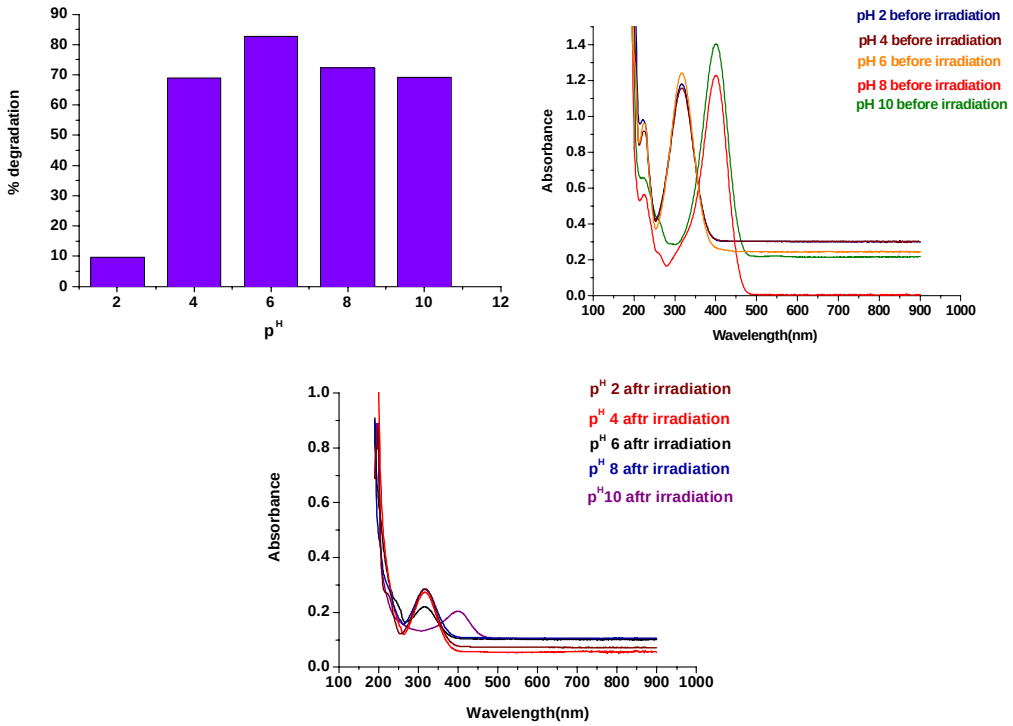

Fig. 4B.3. Effect of Initial pH of 4-Nitrophenol solution on % degradation

Hence, employing TiO_2 as photocatalyst the degradation of compound in the aqueous suspensions was studied in the pH range between 2 and 10. It is interesting to note that the degradation rate of phenol was better at pH 6. In our study the degradation rate was maximum at pH 6 but decreased after 6.0 and continues to decrease in alkaline conditions. Thus the pH 6.0 was selected as optimum pH [23]. Too low OH^- concentration in strong acidic medium is unfavourable to the formation of hydroxyl radicals [24] and subsequently reduces the degradation rate of 4-NP. The hydroxyl radicals are produced from the reaction between the photogenerated holes and OH^-.

4B.2.4.Effect of various catalysts

Fig.4B.4 shows the effect of conducting polymer in the photocatalytic degradation of 4-Nitrophenol under visible light irradiation. It was observed that the polyaniline systems shows superior activity compared to the other two. It is also evident from the figure that as the amount of polymer content in the nanocomposites increases the degradation efficiency decreases. This may be because of the fact that, the surface area decreases as the amount of polymer in the composite decreases.

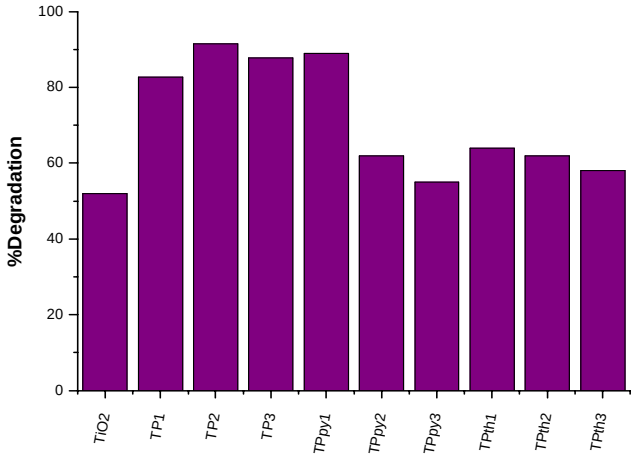

Fig.4B.4. Effect conducting polymer in the % degradation of 4-Nitrophenol

4B.2.5. Reusability studies

One of the major objectives guiding the development of solid heterogeneous catalysts includes easy separation of final products from the reaction mixture and efficient catalyst recovery. Fig.4B.5 shows the reusability result of the catalyst. It was observed that the prepared catalyst can retain comparable activity up to 4^{th} cycle.

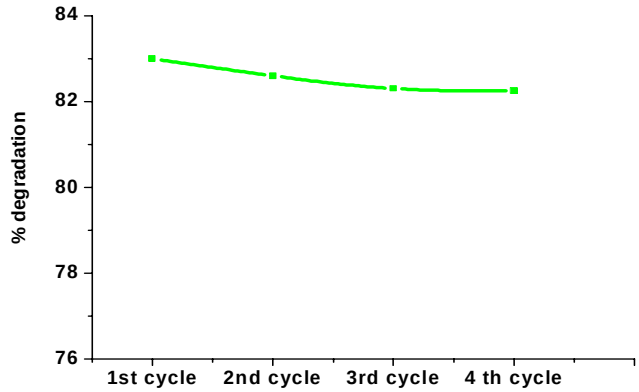

4B.3.Conclusions

The photocatalytic degradation reaction of 4-nitrophenol, is tested to compare the efficiencies of different conducting polymer modified TiO_2 and pure TiO_2 photocatalysts.

References

[1]. M.W. Chang, T.S.Chen, J.M. Chern, Ind. Eng. Chem. Res. 47 (2008) 8533.

[2]. D. Paola, V. Augugliaro, L. Palmisano, G. Pantaleo, E. Savinov, Journal of Photochemistry and Photobiology A: Chemistry 155 (2003) 207.

[3]. U.S. Environmental Protection Agency (1980) Ambient Water Quality Criteria for Nitrophenols, Washington, DC.

[4]. L.Yang, S.Luo, Y.Li, Y.Xiao, Q.Kang, Q.Cai, Environ. Sci. Technol. 44 (2010) 7641.

[5]. E. L. Kochany, Environmental Technology 12 (1991) 87.

[6]. P. Meallier, J. Nury, B. Pouyet, J. Bastide, Chemosphere 12 (1977) 815.

[7]. M. Nakagawa, D.G. Crosby, J. Agric. Food Chem. 22 (1974) 849.

[8]. M. Sittig, Ed., Handbook of Toxic and Hazardous Chemicals and Carcinogens 2nd ed. , NP Noyes Publications, Park Ridge, New Jersey, USA, (1985)664.

[9]. O. A. O'Connor, L. Y. Young, Environ. Toxicol. Chem. 8 (1989) 853.

[10]. M. O. Ishag, P.G.N. Moseley, *Tetrahedron* 33 (1977) 3141.

[11]. D. Chen, A. K. Ray, *Water Research* 32 (1998) 3223.

[12]. V. Augugliaro, M. J. L´opez-Mu˜nos, L. Palmisano,J. Soria, Applied Catalysis A 101 (1993)7.

[13]. V. Augugliaro, L. Palmisano, M. Schiavello, et al., "*Applied Catalysis*, 69 (1991) 323.

[14]. N. San, A. Hatipoğlu, G. Koçtürk, Z. Çınar, Journal of Photochemistry and Photobiology A: Chemistry 146 (2002) 189.

[15]. M.Ksibi, A.Zemzemi, R. Boukchina, J. Photochem. Photobiol., 159 (2003) 61.

[16]. M.H.Priya, G Madras,. Journal of Photochemistry and Photobiology A: Chemistry 178 (2006) 1.

[17]. H.Lachhe, A. Houas, J.M. Herrmann, International Journal of Photoenergy Article ID 497895 Doi: 1155/2008/497895

[18]. D.Huang, F.Zhang, Z.Tu, Q.Yang, S.Quan, L. Liu. Environmental Engineering Science 28 (2011) 677.

[19]. S. Qourzal, N. Barka, M. Belmouden, A. Abaamrane, S.Alahiane, M. Elouardi, A. Assabbane ,Y. A. Chou, Fresenius Environmental Bulletin Volume 21 (2012) No 7a.

[20]. R. Rahimi, S.S. Moghaddam, M. Rabbani, J Sol-Gel Sci Technol 64 (2012) 17.

[21]. W. Ma, J. Li, J. Liu, and M.Feng, *Chin. J. Chem.*, 31 (2013) 230.

[22]. N.Guettaï, A.H.Amar, Desalination 185 (2005) 427.

[23]. A.Verma, H. Kaur, D. Dixit, Archieves of Environmental Protection 39 (2013)17.

[24]. D. W.Chen, A. K. Ray, Water Res. 32 (1998) 3223.

4 C - PHOTOCATALYTIC DEGRADATION OF PHENOL

4C.1. Introduction

Nowadays significant contamination of surface water and ground water with various organic compounds coming from both industry and agriculture is observed. These contaminants are resistant to biological degradation, and they are not susceptible to removal in conventional water treatment processes such as coagulation, flocculation, and filtration [1]. In the recent past, problems involving water contamination have called the attention to the necessity of removing toxic organic compounds from industrial aqueous effluents. The purification of waste water by heterogeneous photocatalysis is one of the most rapidly growing areas of interest to both research workers and water purification plants. Mainly because of their high stability, high toxicity and carcinogenic character, they have caused considerable damage and threat to the ecosystem in water bodies and human health [2, 3]. As the toxicity of phenolic compounds is an important problem, their concentration unfortunately inhibits or even eliminates micro-organisms in biological wastewater treatment plant. Therefore, the presence of phenols strongly reduces the biodegradation of the other components [4]. Phenol, listed in both the non-conventional and the priority list, can be classified as a dissolved pollutant where it is homogeneously dispersed in the liquid. According to the State of Ohio EPA, phenol is also a high priority PBT chemical. PBT chemicals, refer to persistent, bio-accumulative and toxic chemicals, non biodegradable, are not easily metabolized and may be hazardous to both human and the environment (State of Ohio EPA (Environmental Protection Agency (EPA) 2002). Phenol is a recalcitrant species in conventional wastewater treatment processes [5] as it continues to form toxic solutions. Therefore phenol and its

derivatives can act as useful model contaminants for photocatalytic degradation research. The widespread occurrence of phenols in waste water and associated environmental hazards has heightened concern over public health [6]. Phenols and their derivatives are well known for their bio-recalcitrant and acute toxicity. Phenols are being introduced continuously into the aquatic environment through various anthropogenic inputs. Exposure to these compounds can cause liver damage, haemolytic anaemia, paralysis and severe damage to the internal organs in human body. Phenols and their derivatives are well-known hazardous substances due to bio recalcitrant and acute toxicity for biota [7]. Many of them are very toxic, showing adverse effects on animal and plants. Photocatalysis has been proven to be a plausible technique to decontaminate phenolic waste-water as complete mineralization has been successfully achieved under a variety of conditions [8]. Due to toxicity of phenols and their derivatives, their disposal in water bodies causes severe problem [9]. Phenol is a major environment contaminant from various industries such as coke, pesticides, insecticides, fungicides, *paper mill* and dyes due to high toxicity on the skin, eyes and mucous membrane in humans. Industrial wastewater containing phenols are conventionally treated by $FeSO_4$ and H_2O_2 to oxidize phenol to CO_2 and H_2O. $FeSO_4$ is converted to $Fe_2\ (SO_4)_3$ and H_2O_2 is decomposed and then the reactants could not be recycled. Sources of phenol include the discharges of chemical process industries such as petrochemical & pharmaceutical, coal gasification, polymeric resin production, coking plants, paper mill, herbicides and fungicides production [10]. Phenol is an important by-product in different industrial sectors such as textile, leather, rubber industry, fiber glass manufacturing and paint manufacturing [12].

Phenol and their degradation products in the environment are major aquatic pollutants. When phenol containing water is chlorinated, toxic polychlorinated phenols can be formed; hence, such effluent requires proper treatment before being discharged into the environment. Since they are stable and soluble in water, their removal to reach safety levels in the range 0.1–1.0 mg/L is not easy [11].

Many authors [13-15] have studied the heterogeneous photocatalytic decomposition of phenol over TiO_2 powder. With the above information in hand, we decided to undertake a study aiming to clarify different aspects of the mechanisms of direct visible light photodegradation and of TiO_2 photocatalytic degradation of phenol in aqueous solution, to give a better understanding of AOPs. So, the focus of our investigation is to study the effect of hybridisation of TiO_2 with conducting polymers such as polyaniline, polypyrrole and polythiophene, thereby to enhance the photocatalytic degradation rate of phenol on illuminated TiO_2 powder under visible light.

In this respect reviewing the technical literature, one can notice that many compounds are reported as intermediate species of phenol degradation on TiO_2 photocatalysts including hydroquinone, catechol, 1, 4-benzoquinone, and resorcinol. These species are identified as potential hydroxylated intermediate compounds. Additionally, several carboxylic acids have been detected as intermediates, with the main ones being fumaric acid, maleic acid, oxalic acid, lactic acid, and formic acid [16].

4C.2. Influence of reaction parameters

For a typical reaction, 10 ml of 10^{-4} M aqueous phenolic solution was used. A high pressure xenon short arc lamp was served as the visible light

source; a glass filter was added to allow visible light (> 400 nm) to pass through. The illumination intensity was 96 mW/cm^2. Before illumination, the suspensions were stirred for 30 min. in the dark in order to reach adsorption–desorption equilibrium between the photocatalyst and phenolic solution and the irradiation was performed for about one hour. Phenol was quantified using a Shimadzu series high-performance liquid chromatograph system coupled with a photodetector. Phenol and aromatic intermediates were quantified using a HPLC with a C18 column (ODS Hypersil, Thermo scientific) 4.6 mm × 150 mm, 5 μm) operating at a constant temperature of 30°C. The eluent consisted of phosphate buffer: methanol: THF in the ratio 90:5:5 with a flow rate of 1 mL min^{-1}. Detection of aromatic compounds was performed using GC-MS analysis.

4C.2.1. Effect of catalyst amount:

Experiments were carried out with various amounts of catalyst powders (0.03-0.1g) at constant [phenol] ($1.0*10^{-4}$) mol.dm^{-3}. Fig.4C.1. shows the effect of catalyst amount on % degradation.

The rate increases initially with an increase in the catalyst amount and reaches a maximum and then gets decreased. This is due to the fact that with increasing catalyst amount, absorption of light by photocatalyst particles also increases. Hence, the rate of degradation of phenol also increases. After a certain limit, there is a decrease in rate observed. This is due to the scattering of light by the catalyst particles, which is responsible for the reduction in the rate. Although the number of active sites in solution will increase with catalyst loading, a point appears to be reached where light penetration is compromised because of excessive particle concentration. The trade off between these two opposing phenomena results in an optimum catalyst loading for the photocatalytic reaction [17].

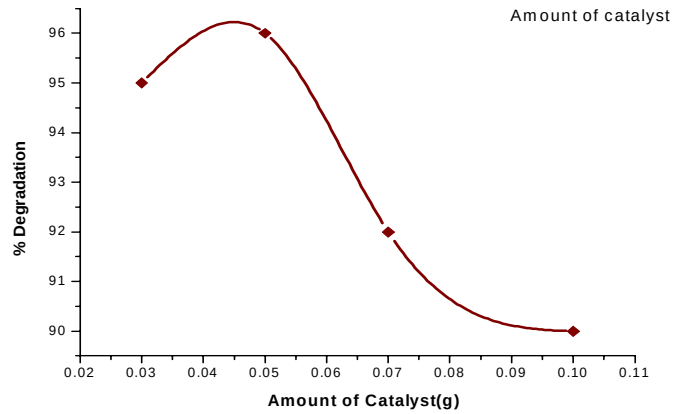

Fig.4C.1.Effect of Catalyst amount on % degradation

So the optimised amount of catalyst was found to be 0.05g.Further studies were carried out using this optimised amount.

4C.2.2. Effect of Time:

Fig.4C.2. shows the effect of time on % degradation. The degradation study was carried out continuously for 2 hour over the prepared catalyst systems in order to study the effect of time on the reaction. It is clear from the graph that the rate of phenol degradation increases with time.

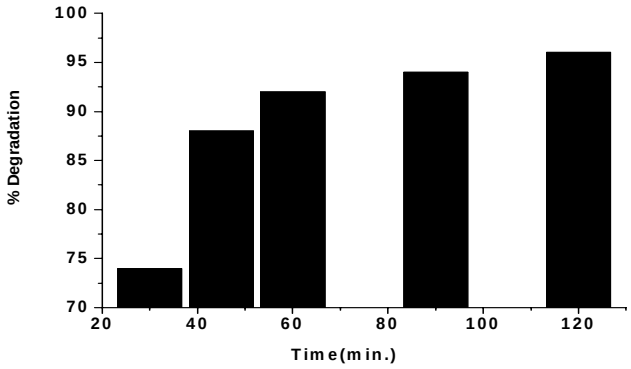

Fig.4C.2. Effect of time on % degradation

A maximum degradation of 96% is obtained after 2 hour. So optimized time for degradation was selected as 2 hour and further studies were carried out within this time period.

4C.2.3. Effect of Different conducting polymer on the degradation

Fig.4C.3. shows the effect of different conducting polymer on the photocatalytic degradation of phenol. The degradation studies were performed using higher amount of polymer contents in the nanocomposite systems. It was observed that both polyaniline and polypyrrole modified TiO_2 shows more or less comparable activity and a degradation of 91% was obtained after 2 hours of irradiation. But the polythiophene modified samples show a degradation of 60%.

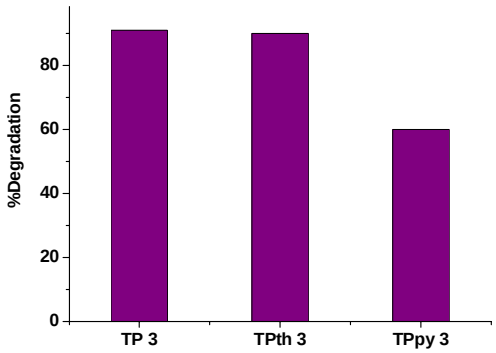

Fig.4C.3. Effect of Different conducting polymer on the degradation

4C.2.4.Effect of Different catalyst:

In order to study the effect various conducting polymers and their composition in the nanocomposite, on the photocatalytic degradation of phenol, experiment was performed with optimized parameters. Fig.4C.4. shows the effect of different catalyst on % degradation. All the polymer modified TiO_2 nanocomposites shows superior activity compared to pure

TiO_2. Out of the three systems polyaniline and polythiophene modified TiO_2 nanocomposite systems are found to be better compared to polypyrrole modified systems.

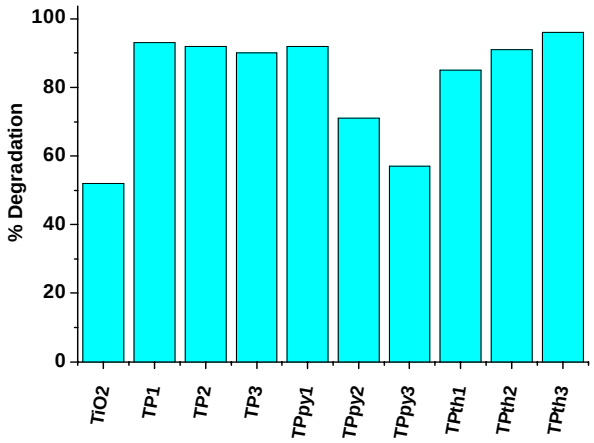

Fig.4C.4. Effect of different catalyst on % degradation

Also it is evident from the above graph that as the amount of polymer in the nanocomposite systems increases the activity decreases. A drastic decrease in activity was seen in the case of polypyrrole modified systems. One of the reasons for the decrease in activity may be the decrease in surface area with increase in polymer content. The decrease in surface area is prominent in the case of polypyrrole modified systems.

4C.2.5. Aromatic intermediates of phenol degradation

Phenol has an electron rich aromatic ring which is susceptible to both electrophillic aromatic substitution and to oxidation reactions. Phenol oxidation is believed to produce several aromatic intermediates such as quinones (benzoquinone) [17], hydroxylated phenols, notably catechol (benzene-1,2-diol), hydroxyquinone (1,4-Dihydroxybenzene) [18] and resorcinol (benzene-1,3-diol); and some acyclic compounds including oxalic acid, formic

acid, maleic acid, glyoxalic acid and fumaric acid. Alapi and Dombi [19] reported obtaining 1, 2-dihydroxybenzene and 1, 4-dihydroxybenzene during UV and UV/VUV photolysis of phenol. Sobczyński et al [20] identified resorcinol in solution during photocatalysis of phenol in non-quantifiable amounts.

Hydroquinone, *p*-benzoquinone and catechol were detected and determined quantitatively as main reaction intermediates. Photocatalytic oxidation of organic compounds on illuminated TiO_2 proceeds via •OH attack on the substrate. Dihydroxy benzenes are the primary products of the process.

A possible pathway for the photocatalytic degradation of phenol is shown in Fig.4C.5.

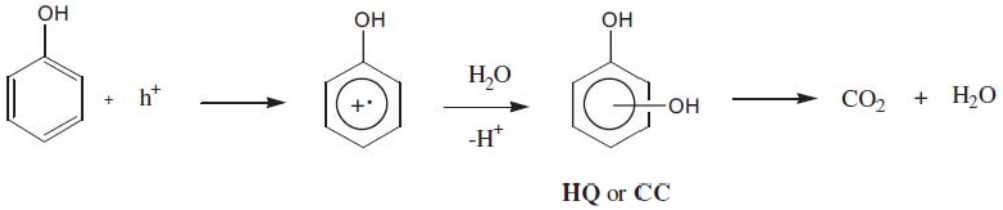

Fig. 4C.5. Possible pathway for the photocatalytic degradation of phenol

The atmospheric oxygen present in the solution can react with e^-_{CB} and prevent the recombination of electron–hole pairs [21-25].It is likely that H_2O_2 is formed from $O_2^{\cdot -}$ (and OH may be generated) [26]. Hydroxyl radical attacks phenol molecules to form the dihydroxy products—HQ and CC, which under prolonged irradiation, further degrade finally to CO_2 and H_2O.

4C.3. Conclusions

The present study establishes several basic features concerning the performance of photocatalytic degradation of phenol in the presence of conducting polymer/TiO_2 photocatalyst under visible light irradiation. The influence of fundamental parameters such as catalyst amount, time and effect of different conducting polymer etc is now established, which opens up the way for further development of these systems.

References

[1]. D. Bahnemann, Solar Energy 77 (2004) 445.

[2]. L. S. Andrade, E. A. Laurindo, Regina V. de Oliveira, R.C. Rocha-Filho, Q. B. Cass, *J. Braz. Chem. Soc.* 17 (2006) 369.

[3]. J.C Zhang, L.L Gao, W.L Cao, Chin J Inorg Chem 19 (2003)934.

[4]. N.A.Laoufi,D.Tassalit,F.Bentahar, Global NEST Journal 10(2008), 404.

[5]. M.Salaices, B.Serrano, H.de Lasa, Chem.Eng.Sci.59 (2004)3.

[6]. E.Eriksson, A.Baun, P.S. Mikkelsen, A. Ledin, Desalination 215 (2007) 187.

[7]. A.Arques, A.M. Amat, G. Ripoll, R.Vicente, Journal of Hazardous Materials 146 (2007)447.

[8]. V.Kruefu, H. Ninsonti, N. Wetchakun, B. Inceesungvorn, P. Pookmanee, S. Phanichphant, Engineering Journal 16 (2012)91 ISSN 0125-8281.

[9]. R. Kar, O.Gupta, K. Mandol, S. Bhattacharjee, J Chem Eng Process Technol 4 (2013) 1.

[10]. J.W. Pattersom, Ann Arbor Science Pub. Inc., Ann Arbor, MI, (1985)199.

[11]. V.M. Brown, D.H.M. Jordan, B.A. Tiller, Water Res. 1 (1967) 587.

[12]. T.S. Jamil, T. A. Gad-Allah, M. Y. Ghaly, Desalination and Water Treatment50 (2012) 264.

[13]. T.R.N. Kutty, S. Ahuja, Mater. Res.Bull. 30 (1995) 233.

[14]. S. Lathasree, A.N. Rao, B. Sivasankar, V. Sadasivam, K. Rengaraj, J.Mol. Catal. A: Chem. 223 (2004) 101.

[15]. D.W. Chen, A.K. Ray, Appl. Catal. B: Environ. 23 (1999) 143.

[16]. Ortiz-Gomez, B. Serrano-Rosales, H. de Lasa, Chem. Eng. Sci. 63(2008) 520.

[17]. K.B. Dhanalakshmi, S. Anandan, J. Madhavan, P. Maruthamuthu, Solar Energy Materials & Solar Cells 92 (2008) 457.

[18]. J. McMurry, Organic chemistry, 8th Ed. Brooks/Cole Publishing Company, California, USA (2012).

[19]. A. Sobczyński, Ł. Duczmal, W. Zmudziński, J of Mol. Catal A: Chemical, 213 (2004) 225.

[20]. I. Izumi, W.W. Dunn, K.O. Wilbourn, F.R.F. Fran, A.J. Bard,J. Phys. Chem. 84 (1980) 3207.

[21]. T. Alapi, A.Dombi, J. Photochem. Photobiol.A Chem. 188 (2006) 409.

[22]. M. Fujihira, Y. Satoh, T. Osa, Bull. Chem. Soc. Japan 55 (1982) 666.

[23]. I. Izumi, F.F. Fan, A.J. Bard, J. Phys. Chem. 85 (1981) 218.

[24]. R.W. Mathews, J. Chem. Soc. Faraday Trans. I 80 (1984) 457.

[25]. J.M. Herrmann, P. Pichat, J. Chem. Soc. Faraday Trans. 176 (1980)1138.

[26]. G.Munuera, V. Rives-Arnau, A. Saucedo, J. Phys. Chem. 75 (1979) 736

4 D- PHOTOCATALYTIC DEGRADATION OF SULFAMETHOXAZOLE

4D.1. Introduction

The presence of drugs in the aquatic media has emerged in the last decade as a new environmental risk and thus its adverse potential effects have become of increasing concern [1]. The entry of drugs into the aquatic environment can involve serious risks for the human being, since these substances are by nature biologically active, and they have a limited biodegradability. Drugs can reach wastewaters by many routes: via industrial effluents (i.e. drugs industries residues and effluents from hospitals) and via domestic effluents (faeces may contain both these compounds and their metabolites) [2, 3].

In recent years, pharmaceutical residues in the environment have become a subject of growing concern, and are regarded as "emerging" contaminants [4, 5]. Human and veterinary drugs are absorbed by the organism after consumption and are subject to metabolic reactions, for example hydroxylation, cleavage, or glucuronation. Because of their physicochemical properties (high water solubility and often poor degradability), pharmaceuticals can pass through all natural filtration steps and enter ground and surface water, and drinking water [4,6,7] .

Frequent occurrences of trace xenobiotic organic contaminants such as pharmaceuticals, pesticides, and personal care products in sewage effluent and the aquatic environment have raised concerns about their potential impact on the environment and public health. Pharmaceutical compounds are designed to produce a biological effect in human beings or animals and their possible side-effects on aquatic ecosystems is still not clear [8].

Sulfonamides were the first antibacterial agents successfully applied in human infectious diseases. They may be prescribed to treat urinary tract infections, ear infections, bronchitis, bacterial meningitis, certain eye infections, Pneumocystiscarinii pneumonia, traveller's diarrhea, and a number of other kinds of infection [9]. They are the antimicrobial agents widely used in food producing animals as growth promoters as well as for therapeutic and prophylactic purposes [10 -15].

Among the pharmaceuticals found in hospitals, antibiotics form an important group, both in human and veterinary medicine, and sulfamethoxazole (SMX) and trimethoprim (TMP) are antimicrobials that are used in great deal [16,17]. SMX is a broad-spectrum sulfonamide, belonging to the group of the first systemic antibacterial drugs used by humans [18].

Sulfamethoxazole (SMX) is a synthetic antimicrobial frequently used in human medicine to treat bronchitis and urinary tract infections and also in veterinary medicine, for prevention and treatment of infections, as well as growth promoter [19]. Trimethoprim (TMP) is mainly used in the prophylaxis and treatment of urinary tract infections, as well as for prevention and treatment of respiratory or gastro-intestinal tract infections in cattle, swine and poultry [20].

The combination SMX–TMP represented an important breakthrough in the development of antimicrobial pharmaceuticals, since it is clinically effective, and is recommended for the treatment of infections [16, 21] and, also, widely used in preventive veterinary medicine

Sulfamethoxazole

Sulfamethoxazole (abbreviated *SMZ* or *SMX*) is a sulfonamide bacteriostatic antibiotic. It is most often used as part of a synergistic combination with trimethoprim in a 5:1 ratio in co-trimoxazole (abbreviated SMZ-TMP and SMX-TMP, or TMP-SMZ and TMP-SMX), also known under trade names such as Bactrim, Septrin, or Septra; in Eastern Europe it is marketed as Biseptol. Its primary activity is against susceptible forms of *Streptococcus*, *Staphylococcus aureus* (including MRSA), *Escherichia coli*, *Haemophilus influenzae*, and oral anaerobes. In addition it can be used as an alternative to amoxicillin-based antibiotics to treat sinusitis. It can also be used to treat toxoplasmosis and it is the drug of choice for *Pneumocystis pneumonia*, which affects primarily patients with HIV. Other names include: sulfamethylisoxazol, sulfisomezole, MS 53, RO 4 2130, and sulfamethazole [22].

Sulfamethoxazole is 4-amino-N-(5-methyl-3-isoxazolyl) benzene sulfonamide. It is an almost white, odorless, tasteless compound with a molecular weight of 253.28, and the molecular formula $C_{10}H_{11}N_3O_3S$. The structural formula is:

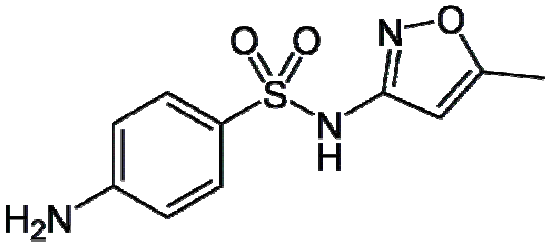

Sulfamethoxazole

Sulfamethoxazole is an anti- bacterial sulfonamide. It prevents the formation of dihydrofolic acid, a compound that bacteria must be able to make

in order to survive. Although it was once a very useful antibiotic, it is almost obsolete as a single agent today due to the development of bacterial resistance to its effects. Sulfamethoxazole was approved by the FDA in 1961. According to the FDA database, all brand and generic formulations of sulfamethoxazole have been discontinued. Sulfamethoxazole is used for the treatment of malaria(in combination with quinine sulfate and pyrimethamine), conjunctivitis (inflammation of the conjunctiva of the eye) due to chlamydia, toxoplasmosis (in combination with pyrimethamine), and urinary tract infections (UTI). Sulfamethoxazole may cause dizziness, headache, lethargy, diarrhea, anorexia, nausea, vomiting, and rash. Sulfamethoxazole should be stopped at the first appearance of a skin rash since the rash may become severe. Serious rashes include Stevens-Johnson syndrome (aching joints and muscles; redness, blistering, and peeling of the skin); toxic epidermal necrolysis (difficulty in swallowing; peeling, redness, loosening, and blistering of the skin). Sulfamethoxazole therapy also can cause extensive sunburn, following exposure to sunlight. Patients receiving sulfamethoxazole should avoid excessive exposure to sunlight and should wear sunscreen. Other rare side effects include liver damage, low white blood cell count, low platelet count (thrombocytopenia), and anaemia. Sulfamethoxazole may form crystals in the urine which may damage the kidney and cause bleeding into the urine. It is important to drink additional liquids during sulfonamide therapy to prevent these side effects. [23].

The present study was undertaken to evaluate the photocatalytic activity of conducting polymer modified TiO_2 based nanocomposites. The photocatalytic activity of the sample was evaluated by performing the degradation of sulfamethoxazole (SMX). Photocatalytic activity of the prepared systems was

scanned using Oriel Uniform illuminator (Newport Model 66901). For a typical reaction, 10 ml of 10^{-4} M aqueous SMX solution was used. A high pressure xenon short arc lamp was served as the visible light source; a glass filter was added to allow visible light (> 400 nm) to pass through. The illumination intensity was 96 mW/cm^2. Before illumination, the suspensions were stirred for 30 min. in the dark in order to reach adsorption–desorption equilibrium between the photocatalyst and SMX solution and the irradiation was performed for about one hour. Sulfamethoxazole was quantified using an Ultimate 3000 series high-performance liquid chromatograph system (HPLC, Ultimate 3000) coupled with a photodiode array detector (at 260 nm). After irradiation samples were analyzed via HPLC equipped with a C18 analytical column (ODS Hypersil, Thermo scientific) 4.6 mm × 150 mm, 5 μm) operating at a constant temperature of 30°C. The eluent consisted of 40:60 (v/v) of water/acetonitrile with a flow rate of 0.5 mL min^{-1} and the products formed were analysed by Waters LC-MS system.

4D.2. Influence of reaction parameters

The effect of reaction parameters such as amount of catalyst, time, lamp power, effect of various conducting polymers and their different compositions on the photocatalytic degradation of Sulfamethoxazole is investigated. The degradation product identification was done using LC-MS.

4D.2.1. Effect of Catalyst Amount

The effect of catalyst amount on the photocatalytic degradation of sulfamethoxazole was scanned by varying the amount of catalyst keeping the amount of reactant constant.

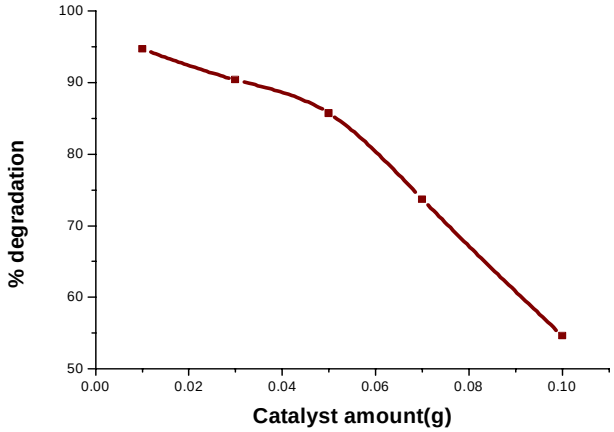

Fig.4D.1. Effect of catalyst amount against Sulfamethoxazole degradation

Fig.4D.1. shows effect of catalyst amount against sulfamethoxazole degradation. Several studies have indicated that the photocatalytic rate initially increases with catalyst loading and then decreases at high values because of light scattering and screening effects. The tendency toward agglomeration (particle–particle interaction) also increases at high solids concentration, resulting in a reduction in surface area available for light absorption and hence a drop in photocatalytic degradation rate. Although the number of active sites in solution will increase with catalyst loading, a point appears to be reached where light penetration is compromised because of excessive particle concentration. The trade off between these two opposing phenomena results in an optimum catalyst loading for the photocatalytic reaction [24]. A further increase in catalyst loading beyond the optimum will result in non-uniform light intensity distribution, so that the reaction rate would indeed be lower with increased catalyst dosage. It was found that at lower catalyst amounts the % of degradation is high and as the amount of catalyst increases the degradation decreases. A slight decrease in activity is observed with an increase in the amount of PANI-TiO_2 nanocomposite, which is a general characteristic of

heterogeneous photocatalysts [25, 26]. As the concentration of the photocatalyst increases for a given concentration of the SMX solution, PANI-TiO_2 nanocomposite photocatalyst particles come closer in the SMX solution and agglomerate, thereby reducing the surface active sites of photocatalyst in contact with SMX solution available for photocatalytic reaction. Also at higher dosages the vacant sites are consumed by the intermediate species formed during the reaction which retard further degradation of the substrate. As a result the % degradation is decreased. Moreover, the particle-particle interaction becomes significant as the amount of particles in solution increases, which reduce the active site density for the surface excited holes and electrons [27]. The maximum activity was obtained at a catalyst loading of 1g/L. So this catalyst amount is set as optimum for further studies.

4D.2.2.Effect of Time

Fig. 4D.2. shows the photocatalytic degradation profiles versus reaction time. From the figure it is evident that as time increases the % degradation also increases. The % degradation shows a sharp rise at the initial stages and then it becomes almost steady after one hour irradiation.

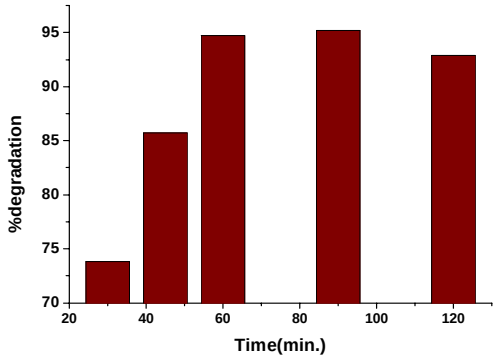

Fig.4D.2. Effect of time against sulfamethoxazole degradation

4D.2.3.Effect of Lamp Power:

In this section we evaluated the effect of light intensity for the degradation of sulfamethoxazole. Here studies involve the usage of 10 ml of 10^{-4} M aqueous solution of sulfamethoxazole with a visible light irradiation of one hour. A 100W Xe lamp with irradiation intensity of 64.7mW/cm^2 and a 150 W Xe lamp with irradiation intensity of 96.8mW/cm^2 are used as the visible light source. Fig.4D.3.shows the effect of lamp power on sulfamethoxazole degradation. From the graph it is clear that the prepared catalyst shows maximum degradation when the lamp power is 150 W.

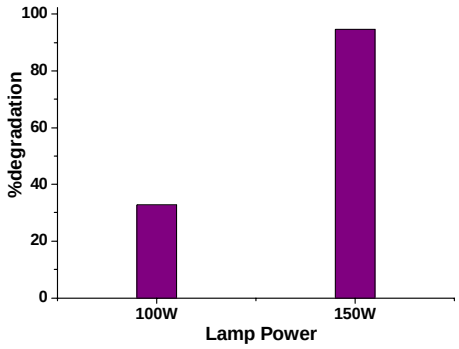

Fig.4D.3. Effect of lamp power against Sulfamethoxazole degradation

When lamp power increases, its light intensity also increases which enhances the production of more photoexcited species on catalyst surface. As the number of photoexcited species increases it causes degradation of more pollutants adsorbed on the catalytic material and enhances the activity.

4D.2.4.Effect of Various Catalysts

To compare the photocatalytic performance of the nanocomposite systems, the degradation reaction was carried out using the prepared systems under optimized conditions. Results show that the prepared systems are

good photocatalysts for the degradation of sulfamethoxazole under visible light irradiation. Fig.4D.4.shows the effect of different catalyst against Sulfamethoxazole degradation.

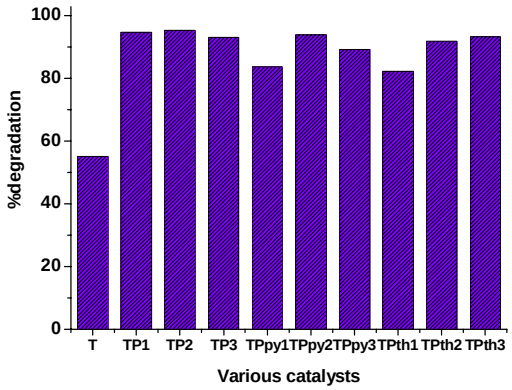

Fig.4D.4. Effect of different catalyst against sulfamethoxazole degradation

In order to elucidate the products formed after irradiation and to predict a plausible reaction pathway, mass spectroscopic study was realized. LCMS analysis was used for the identification of products. The products identified were sulphanilic acid, 3-amino-5-methylisoxazole, hydroxy-5-methyl isoxazole and acetic acid. Sulphanilic acid and 3-amino-5-methylisoxazole was observed only after 60 minutes but the hydroxyl methyl isoxazole were observed after 30 minutes of irradiation. The OH radical mediated pathway leads to the production of 3-amino-5-methylisoxazole and sulphanilic acid. Fig.4D.5. depicts the proposed pathway for the degradation.

The attack of hydroxyl radical to the isoxazole ring of sulfamethoxazole followed by subsequent cleavage leads to the formation of hydroxy methyl isoxazole (a molecular ion having m/z=99 (ES+) was observed). Both sulphanilic acid and 3-amino-5-methylisoxazole were observed in the ES- mode, having m/z ratio equal to 172 and 97 respectively [28-30]. We can also observe an

m/z= 61(ES+) which may be due to the formation of acetic acid, which is formed by the further degradation of the intermediate species. Trace amounts of other compounds were also detected but cannot be identified.

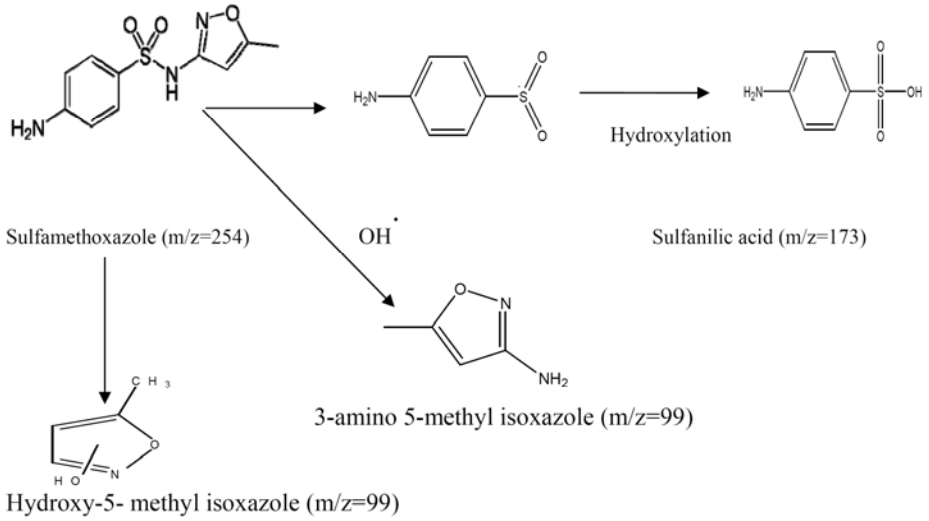

Fig.4D.5. Proposed pathway for the photocatalytic degradation of sulfamethoxazole

4D.3. Conclusions

The sulfamethoxazole is prone to undergo photolysis degradation, by means of direct absorption of radiation with wavelength below 310 nm. When working without any optical filter and without TiO_2, the sulfamethoxazole degradation can reach 80% but the mineralization is much lower. The amount of TiO_2 has influence on the reaction rate, since the degradation rate is improved when the amount of catalyst is increased. The optimum catalyst concentration in the studied set up is found to be 0.01g.The percentage degradation was analyzed using HPLC technique and the product identification was carried out using LC-MS. Various parameters such as effect of catalyst amount, effect of time and effect of different catalysts were monitored for the degradation of sulfamethoxazole.

References

[1]. F.M. Christensen, Regul. Toxicol. Pharm. 28 (1998) 212.

[2]. T. Heberer, Toxicol. Lett. 131 (2002) 5.

[3]. M.L. Richardson, J.M. Bowron, J. Pharm. Pharmacol. 37 (1985) 1.

[4]. H.J. Stan, T. Heberer, Analysis Magazine, 25(1997) 20.

[5]. M. Petrovic, M.D. Henrando, S. Diaz-Cruz, D. Barcelo, J Chromatogr A 1067 (2005) 1.

[6]. M. Carballa, F. Omil, J.M. Lema, M. Llompart, C. Garcia-Jares, I. Rodriguez, M. Gomez, T. Ternes, Water Res. 38 (2004) 2918.

[7]. M. Huber, S. Korhonen, T. Ternes, U. Gunten, Water Res 39 (2005) 3607.

[8]. O. Gonz´alez, C. Sans,a S. Esplugasa and S. Malato, Photochem. Photobiol. Sci., 8 (2009) 1032.

[9]. M. Jesu´ s Garcı´a-Gala´n, M. Silvia Dı´az-Cruz, Damia` Barcelo, Trends in Analytical Chemistry 27 (2008).

[10]. L. Verzegnassi, M. C. Savoy-Perroud, R.H. Stadler, Journal of Chromatography A 977 (2002) 77.

[11]. Feed Additives with Synergic Effect for Growth Promotion, Jpn. Kokai Tokkyo Koho. Patent no. JP 60227641, 1985.

[12]. R. Hirsch, T.A. Ternes, K. Haberer, A. Mehlich, F. Bal- Jpn. Kokai Tokkyo Koho. Patent no. JP 60227641, 1985.

[13]. K. Lawanz, L. Kratz, J. Chromatogr. A 815 (1998) 213.

[14]. N.T. Crosby, Determination of Veterinary Residues in Food, Ellis Horwood, Chichester (1991) 97.

[15]. N.A. Botsoglou, D.J. Fletouris, Drug Residues in Foods, Marcel Dekker, New York (2001) 85.

[16]. J. Y. Pailler, A. Krein, L. Pfister, L. Hoffmann, C. Guignard, Sci. Total Environ. 407 (2009) 4736.

[17]. S. Babic, D. Asperger, D. Mutavdzi, Talanta 70 (2006) 732.

[18]. S. M. Dı´az-Cruz, D. Barcelo´, Trends Anal. Chem. 24 (7) (2005) 645.

[19]. A. Nieto, F. Borrull, R.M. Marce, E.J. Pocurull, Chromatogr. A 1174 (1–2) (2007) 12.

[20]. F.C.C.R. De Paula, A.C. de Pietro, Q.B.J. Cass, Chromatogr. A 1189 (2008) 221.

[21]. H. Amini, A. Ahmadiani, J. Pharm. Biomed. Anal. 43 (2007) 1146.

[22]. en.wikipedia.org/wiki/sulfamethoxazole.

[23]. www.medicinenet.com

[24]. A.A. Adesina, Catalysis Surveys from Asia 8 (4) (2004) 265.

[25]. C.C. Chen, C.S. Lu, Y.C. Chung and J.L. Jan, *J. Hazardous Materials* 141 (2007)520.

[26]. M. Saquib and M. Muneer, *Dyes Pigment* 56 (2003) 37.

[27]. K.M. Rajesh, Studies on photo catalysis by nano titania modified with non-metals, Ph.D Thesis, CUSAT (2011) 80.

[28]. L. Hu, P. Flanders, P. Miller, T.J. Strathmmann, Water Res. 41 (2007) 2612.

[29]. A.G. Trovo, R. Nogueira, A. Aguera, C. Sirtori, A. Fernandez- Alba, Chemosphere 77 (2009) 1292.

[30]. M.W. Lam, S.A. Mabury, Aquat. Sci. 67 (2005) 177.

4 E-PHOTOCATALYTIC DEGRADATION OF BISPHENOL -A

4E.1. Introduction

The research of endocrine disrupters in the environment has received increasing attention in recent years. An important class of emerging environmental contaminants is endocrine disrupting compounds (EDCs) [1]. Several types of environmental pollutants referred to as endocrine disruptors (EDs) have been suggested to be associated with abnormal sexual development and abnormal feminizing responses of animals in a number of reports. EDs exhibit biological behaviour that is similar to that of natural and synthetic estrogens with steroid structures and their metabolites [2]. Endocrine disrupting chemicals (EDCs) have attracted great concern nowadays because they mimic hormonal activity and interfere with the functions of endocrine systems [3]. Several adverse effects such as spontaneous abortion, neutron-behavioral disorder, and skewed sex rations within the offspring of the exposed communities, intersex, impaired immune function, and varieties of cancer are induced by EDCs [4]. High hydrophobicity of EDCs results in their great accumulation in activated sludge during bio-transformation or biodegradation, thereby significantly decreasing the treatment efficiency. EDCs pose increasing threat to human health, aquatic organisms and micro-organisms, livestock, and wildlife. It has been found that EDCs mimic or interfere with the action of animal endogenous hormones by acting as oestrogen antagonists, binding to the oestrogen receptor, altering the synthesis and metabolism of natural hormones, modifying hormone receptor levels or eliminating a normal biological response. Because of its wide usage and its endocrine disrupting effects, BPA has been regarded as a representative material among endocrine disruptors and causes reproductive damage to

aquatic organisms. Endocrine-disrupting chemicals have spread over the environment, leading to the deterioration of the generative function of some living species on the earth, among which bisphenol A (BPA) receives great concern because of the strong estrogenic activity [5].

Endocrine disruptors such as bisphenols, alkyl phenols, and phthalates are pollutants that have raised great concern because of their high resistance to traditional wastewater treatments and their potential health effects [6]. Bisphenol A, 2,2-bis(4-hydroxyphenyl)propane, (BPA), a suspected endocrine disrupting compound (EDC), is widely adopted in the production of epoxy resins and polycarbonate plastics, which are used in various food and drink packaging applications, baby bottles and dental sealants [7]. It was reported that BPA could be released from polycarbonate flasks during autoclaving and lacquer coating in food cans , and it is well known that BPA causes not only strong estrogenic endocrine disrupting effect [8] but also various disease including carcinogenesis [9,10]. BPA has an acute toxicity in the range of about 1–10 mg l^{-1} for a number of freshwater and marine species [11]. Complete mineralization of bisphenol A is therefore a primary environmental issue.

Bisphenol A (BPA) is an alkylphenolic compound with the chemical formula $(CH_3)_2C(C_6H_4OH)_2$ belonging to the group of diphenylmethane derivatives and bisphenols.

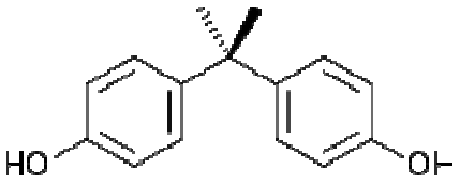

It has been reported that BPA can cause reproductive toxicity and to affect cellular development in rats and mice and is generally regarded as a serious contributor to water pollution. It has also been used as a reaction inhibitor, antioxidant, and flame retardant. It is non-biodegradable, highly resistant to chemical degradation, and presents a health risk to both humans and animals. Consequently, because of the wide range of applications of BPA, exposure to which is a serious concern and a health hazard, researchers must develop effective remediation procedures for destroying BPA in contaminated effluent [12]. BPA exhibits very good physical and chemical properties such as excellent transparency, high mechanical strength, and good thermal stability [13]. This compound is catalogued like an endocrine disruptor that causes several diseases and syndromes. This is distributed as a result of its multiple use, to its low degradability, to that it can be transported by air, ground and water, to its bioaccumulation in the trophic chain because is accumulated in the fat of the organisms and, to that are transmitted to the descendants through the mother during the gestation.

BPA creates environmental contamination by releasing into the aquatic sources from industrial discharges, landfill leachate, and water streams containing plastic debris [14]. Charcoal adsorption process was constrained by adsorbent saturation, reclamation, and formation of secondary pollution [15]. For the byproducts absorbed at UV 254nm, it is hard to totally decompose BPA at low ozone dosage through ozone oxidation [16]. Degradation by biological methods suffered from a long reaction time [17].Thus, the development of methods to remove BPA is needed urgently.

Many countries throughout the world have large production capacities for BPA, especially Germany, the Netherlands, the United States, and Japan.

BPA has exhibited estrogenic activity and alters metabolic kinetics, induces DNA damages, and results in chromosomal aberrations. According to the American standards the maximum allowable limit of BPA concentration in the natural water is 0.1 mg/L [18]. Rosenfeldt and Linden [19] studied the degradability of BPA by direct photolysis using low- and medium-pressure mercury UV lamps, finding 5% and 10–25% degradations, respectively. Moreover, the exposure of the same samples to UV/H_2O_2 eliminated more than 90% BPA, independently of the UV source. Katsumata etal [20] found that the destruction of BPA was maximal at pH=3.5–4.0 with an H_2O_2: Fe(II) ratio of ten under UV (λ=300 nm) irradiation, under which conditions 50% mineralization occurred in 24 h. The degradation of BPA by the Fenton process was much more rapid in the presence of ultrasound than in its absence [21]. In previous studies, TiO_2 was the most commonly used catalyst in the treatment of wastewater because of its non-toxicity, reasonable cost, high availability, photochemical stability and relatively high photocatalytic activity [22-27]. Coleman etal [28] found that adding silver or platinum did not affect photocatalytic degradation or mineralization by UV/TiO_2 for any of the EDCs at concentrations present in water. At a high concentration of BPA, a significant increase in the reaction rate was observed over Pt/TiO_2. However, the reaction rate of BPA was reduced over Ag/TiO_2.

4E.2. Effect of reaction parameters on photocatalytic degradation of Bisphenol -A

A 10 ml of 10^{-4} M solution of Bisphenol A in water is used for the degradation. A definite amount of catalyst is added and the sample is stirred under dark for about half an hour to achieve adsorption-desorption equilibrium. Then the sample is irradiated under visible light for about one hour. After that the reaction mixture is analysed by HPLC with a UV detector

(Agilent Technologies). The HPLC chromatograms of BPA solution before and after irradiation are shown in Fig.4E.1.

The UV detector was set to a wavelength of 278 nm. Separations were performed using a ODS Hypersil C18 reverse phase column. The mobile phase was Milli Q-water and CH_3CN (40:60 v/v) at a flow rate of 0.5 mL/min. The injection volume was 20 μL. The products formed were analysed by Waters LC-MS system.

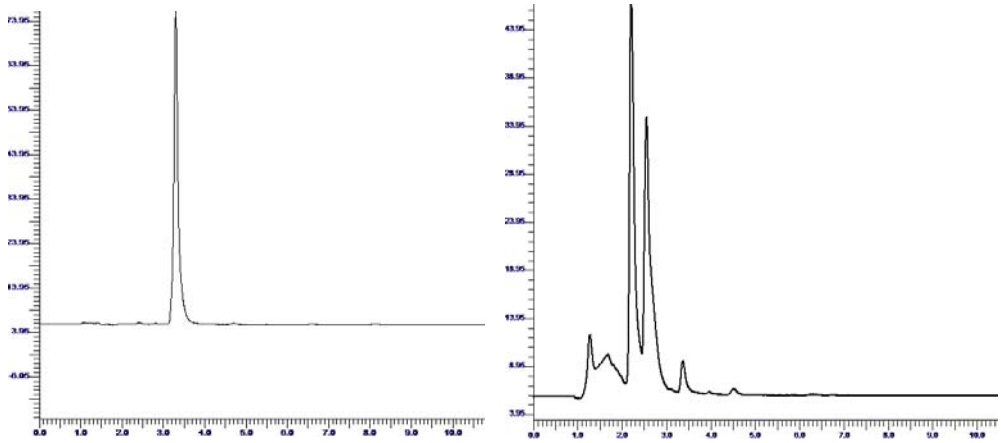

(a) **(b)**

Fig.4E.1. HPLC chromatograms of BPA (a) Before irradiation
(b) After irradiation

4E.2.1. Effect of Catalyst Amount

The effect of catalyst amount on the degradation of Bisphenol-A was evaluated by performing the reaction using various amount of catalyst. The catalyst amount was varied from 0.01 to 0.1g. Before irradiation the suspension was stirred about 30 minutes, in order to attain adsorption desorption equilibrium and then the time of irradiation was limited to 60 minutes. A

dichoric mirror of 420-630 nm was used as the source for visible light. The percentage degradation was analysed using HPLC technique. A maximum degradation of 96% was obtained with 0.05g catalyst. Fig.4E.2. shows the effect of amount of catalyst on % degradation.

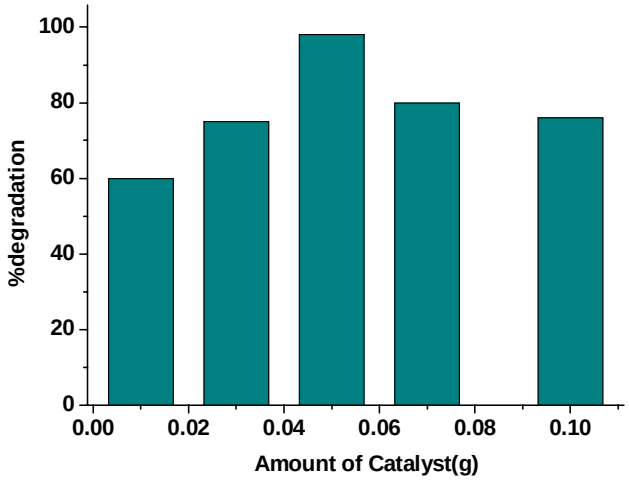

Fig.4E.2. Effect of amount of catalyst on % degradation

From the graph it is clear that as the amount of catalyst increases the % degradation also increases but the increase is limited by an optimum catalyst amount. The optimum catalyst amount was found to be 0.05g. Beyond an optimum amount the catalyst has a negative influence. As the amount of catalyst increases the number of active site for reaction increases which improves the photocatalytic efficiency through the formation of activated photo excited species. Increasing of catalyst amount beyond optimum value increases solution opacity, leading to a decrease in the penetration of photon flux, thereby reducing the photocatalytic degradation.

4E.2.2.Effect of time

To study the effect of time on photocatalytic degradation of bisphenol-A, the reaction was performed using the optimum amount of catalyst 0.05g. Fig.4E.3. shows the effect of time on % degradation. It is evident from the graph that as time increases the percentage degradation increases and a maximum of 95% is obtained with an irradiation time of 60 minutes. Further increase of time does not have much effect on the photocatalytic activity. Increase of irradiation time on the catalyst surface enhances the generation of photo excited species which facilitates the generation of reactive oxygen species that are responsible for the degradation of adsorbed substrates.

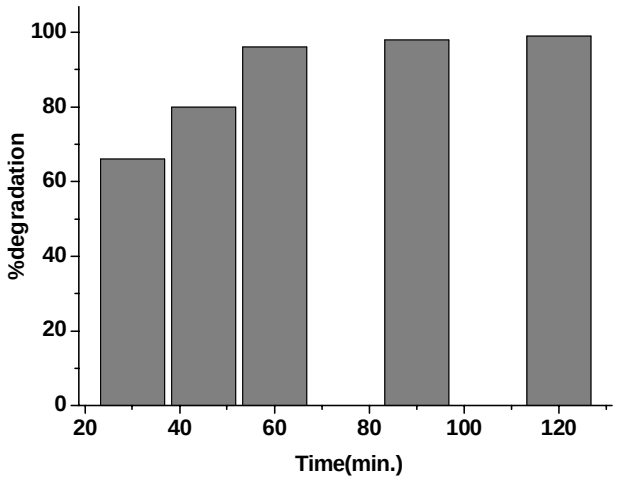

Fig.4E.3. Effect of time on % degradation

4E.2.3. Effect of Different Catalysts

Here we evaluated the degradation of bisphenol-A using various conducting polymer sensitized TiO_2 under visible light irradiation. Fig.4E.4. shows the effect of different catalyst on % degradation. All the modified catalysts are superior in activity compared to TiO_2 under visible light irradiation.

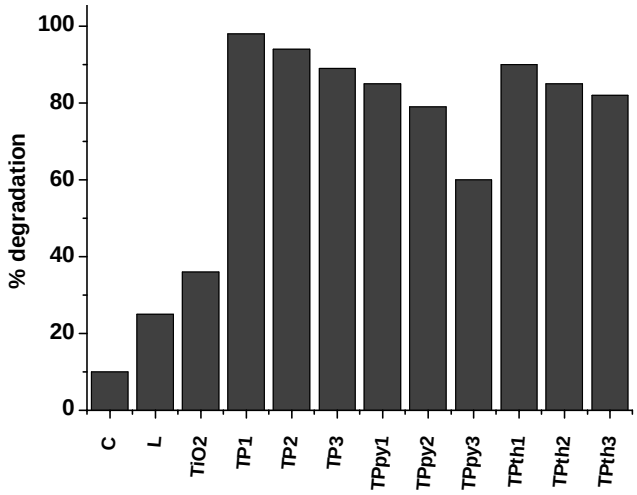

Fig.4E.4.Effect of different catalyst on % degradation

Out of the 3 types of conducting polymer modified systems the polyaniline modified systems show comparatively good activity. When the conducting polymer/TiO_2 composites were subjected to visible light irradiation with energy equal to or greater than the band gap of TiO_2, both TiO_2 and the polymer absorb the photons at their interface, and then charge separation occurs at the interface. Since the conduction band of TiO_2 and the LUMO level of the polymer are well matched for the charge transfer, the electrons which are promoted from a π–π^* absorption band of the outside polymer film upon natural light, are easily injected into the conduction band of inner TiO_2 nanoparticles; whereas electrons in the valence band of TiO_2 are transferred into the polymer and left holes, which can yield hydroxyl and superoxide radicals on the surface of TiO_2, leading to the higher activity. In competition with charge transfer is intrinsic and interfacial electrons and holes recombination. The electron transfer process is more efficient because of the intrinsically π-conjugated structure of conducting polymer and the preadsorption of conducting polymer on the surface of TiO_2 [29, 30]. When the content of conducting polymer is lower than optimum

value conducting polymer not only exhibit its noticeable effect on transfer charge but also decrease the visible light intensity that the composite can absorb. With increasing the content of conducting polymer, it gradually exhibits its contribution on charger transfer, and the adsorption capacities of composites was enhanced, conducting polymer/TiO_2 composites exhibit the highest activity. With a further increase in conducting polymer content, the decrease in activity of conducting polymer TiO_2 composites is considered to be related to the increased absorbing and scattering of photons by a large amount of conducting polymer adsorbed on the surface of TiO_2, even the high adsorption capacity cannot offset the influence of the decrease in light intensity [31]. From the graph it is evident that as the polymer content in the composite increases the activity is found to decrease. This may be because of the blockage of the active TiO_2 surface by the polymer. The decrease in activity can also be explained on the basis of the decrease in surface area with increase in polymer content in the composite systems. The surface area decrease is prominent in the case of polypyrrole modified TiO_2 systems compared to polyaniline and polythiophene modified systems.

4E.2.4. Identification of Intermediate species of BPA degradation

Conducting polymer with π-conjugated structure has high electron mobility, which can facilitate the separation of the electron–hole pairs generated under visible light irradiation; a certain content of conducting polymer can improve the photocatalytic activities of conducting polymer /TiO_2 composites. Fig.4E.5. shows the mechanism of photocatalytic degradation of Bisphenol A by polyaniline sensitized nanoTiO_2 .The mechanism of the reaction can be explained as follows; upon visible light irradiation the electrons of the π-orbital are excited to the π*-orbital. The energy levels of the π*- orbital of polyaniline and the conduction band of TiO_2 are closer; the excited electrons are injected into the

conduction band of TiO_2.These electrons combine with the surface adsorbed molecular oxygen to produce super oxide anion radical. This superoxide anion radical interacts with bisphenol-A causing its destruction. The intermediate product identification was carried out using LC-MS. All the products formed were not identified. Some of the products identified were *p*-isopropenyl phenol, 4, 4'-(ethane-1, 1-diyl) diphenol (Bisphenol E) and fumaric acid.

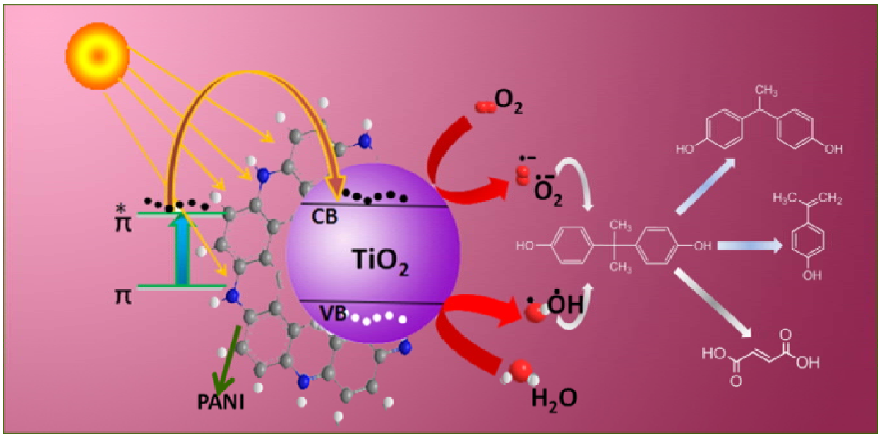

Fig.4E.5. Mechanism of photocatalytic degradation of Bisphenol A by polyaniline sensitized nanoTiO_2

4E.3.Conclusions

Conducting polymers are found to be very good sensitizers to tune the photocatalytic activity of TiO_2 towards visible region. Prepared conducting polymer/TiO_2 nanocomposites are proved to be efficient visible light photocatalyst for the degradation of the endocrine disruptor Bisphenol A. The degradation products were identified using LCMS. The products identified were *p*-isopropenyl phenol, 4, 4'-(ethane-1, 1-diyl) diphenol (Bisphenol E) and fumaric acid.

References

[1]. M. Auriol, Y. Filali-Meknassi, R.D. Tyagi, C.D. Adams, R.Y. Surampalli, Process Biochemistry 41 (2006) 525.

[2]. Y. Ohko, I.Ando, C.Niwa, T. Tatsuma, T.Yamamura, T.Nakashima, Y. Kubota, A. Fujishima, Environ. Sci. Technol. 35(2001) 2365.

[3]. W.V. Welshons, K.A. Thayer, B.M. Judy, J.A. Taylor, E.M. Curran, F.S. vom Saal, Environ. Health Perspect. 111 (2003) 994.

[4]. R. McKinlay, J.A. Plant, J.N.B. Bell, N. Voulvoulis, Environ. Int. 34 (2008) 168.

[5]. I.Gültekin, N. H. Ince, Journal of Environmental Management 85(2007)816.

[6]. A. Colombo, G. Cappelletti, S. Ardizzone, I. Biraghi, C. L. Bianchi, D. Meroni, C.Pirola, F. Spadavecchia, Environ Chem Lett. 10(2012)55.

[7]. C.A. Staples, P.B. Dorn, G.M. Klecka, S.T. O'Block, L.R. Harris, Chemosphere 36 (1998) 2149.

[8]. J.A. Brotons, M.F. Olea-serrano, M. Villalobs, Environ. Health Persp. 103 (1995) 608.

[9]. J. Ashby, R.W. Tennant, Mutat. Res. 204 (1) (1988) 17.

[10]. S. Suarez, R.A. Sueiro, J. Garrido, Mutat. Res. 470 (2) (2000) 221.

[11]. H.C. Alexander, D.C. Dill, L.A. Simth, Environ. Toxicol.Chem. 7 (1998) 119.

[12]. C.Y. Kuo Desalination 256 (2010) 37.

[13]. J. Qu, Q. Cong, C. Luo, X. Yuan, RSC Adv. 3(2013) 961.

[14]. M.Furhacker, H.Weber, S.Scharf, Chemosphere 41(2000)751.

[15]. W.Zhang, L.Zou, L.Wang, Applied Catalysis A: General 371(2009)1.

[16]. B.Xu, N.Y.Gao, R.Mui, H.Wang, H. H. Wu, Frontiers of Environmental Science & Engineering in China 1(2007)294.

[17]. X. L.Wang, G. D. Wu, J. P. Li, W.Wei, Y. H. Sun, Journal of Molecular Catalysis. A: Chemical 27(2007)86.

[18]. R. Thiruvenkatachari, T.O.Kwon, I. Shik Moon, Separation Science and Technology 40: (2005)2871.

[19]. E.J. Rosenfeldt, K.C. Linden, Environmental Science and Technology 38 (2004) 5476–5483

[20]. H. Katsumata, S. Kawabe, S. Kaneco, T. Suzuki, K. Ohta, Journal of Photochemistry and Photobiology A 162 (2004) 297.

[21]. I. Ioan, S. Wilson, E. Lundanes, A. Neculai, Journal of Hazardous Materials 142 (2007) 559.

[22]. N. Watanabe, S. Horikoshi, H. Kawabe, Y. Sugie, J. Zhao, H. Hidaka, Chemosphere 52 (2003) 851.

[23]. K. Chiang, T.M. Lim, L. Tsen, C.C. Lee, Applied Catalysis A 261 (2004) 225.

[24]. T.Kanki, S.Hamasaki, N.Sano, A. Toyoda, K. Hirano, Chemical Engineering Journal 108 (2005) 155.

[25]. H.M. Coleman, K. Chiang, R. Amal, Chemical Engineering Journal 113 (2005)65.

[26]. N.Venkatachalam, M.Palanichamy, B.Arabindoo, V.Murugesan, Catalysis Communications 8 (2007) 1088.

[27]. R. Wang, D. Ren, S. Xia, Y. Zhang, J. Zhao, Journal of Hazardous Materials 109(2009) 926.

[28]. H.M. Coleman, K. Chiang, R. Amal, Chemical Engineering Journal 113 (2005) 65.

[29]. A.L.Linsebigler, G.Lu, J.T.Yates Jr., Chem.Rev.95 (1995)735.

[30]. F. Wang, S.X. Min, Chinese Chemical Letters 18 (2007) 1273.

[31]. Y. Zhu, Y. Dan, Solar Energy Materials & Solar Cells 94 (2010) 1658.

4 F- ANTIBACTERIAL STUDIES

Since the microbicidal ability of TiO_2 nanoparticles depends on their photoresponse and photocatalytic reactivity, all of the issues pertinent to the improvement of photocatalysis will aid with the killing of bacteria, viruses, and fungi. Again, the creation of nanocomposites to circumvent the partial photocatalytic reactivity of the TiO_2 due to charge recombination, and to increase the photoresponse of TiO_2, would permit nanocomposites to be used for sterilization with sunlight, in a most energy - effective way. Currently, TiO_2 nanocomposites are used in multiple antimicrobial, antifungal, and waste decontamination applications, and can also be used to sterilize medical devices such as catheters and dental implants. TiO_2 nanocomposites have also been tested for sterilization of food packaging and food preparation surfaces, to prevent the bacterial contamination of food. However, perhaps the most often used application of TiO_2 nanocomposites in this area has been for the purification of drinking water and decontamination of waste water. In this chapter we have attempted to study the antibacterial activity of conducting polymer modified TiO_2 nanocomposites.

4F.1. Introduction

The widespread use of antibiotics and the emergence of more resistant and virulent strains of microorganisms have caused an urgent need to develop alternative sterilization technologies. Photocatalytic effect of titanium dioxide (TiO_2) is a conceptually feasible technology since this material is easy and inexpensive to produce in industrial scale [1]. One of the interesting applications of TiO_2 photocatalysis is the bactericidal activity. In general, antibacterial reagents inactivate cell viability, but pyrogenic and toxic ingredients such as endotoxins remain even after the bacteria have been killed. Endotoxin is the cell wall constituent of bacteria which consists of a sugar chain expressed as O-antigen and a complex lipid called lipid A. This endotoxin is toxic and causes critical problems in medical facilities and in factories manufacturing pharmaceuticals and medical devices [2].

Worldwide, typhoid fever affects roughly 17 million people annually, causing nearly 600,000 deaths. The causative agent, *Salmonella enterica typhi* (referred to as *Salmonella typhi* from now on), is an obligate parasite that has no known natural reservoir outside of humans. Originally isolated in 1880 by Karl J. Erberth, *S. typhi* is a multi-organ pathogen that inhabits the lymphatic tissues of the small intestine, liver, spleen, and blood stream of infected humans. This gram-negative enteric bacillus belongs to the family *Enterobacteriaceae*. It is a motile, facultative anaerobe that is susceptible to various antibiotics. Currently, 107 strains of this organism have been isolated; many containing varying metabolic characteristics, levels of virulence, and multi-drug resistance genes that complicate treatment in areas where resistance is prevalent. Infection of *S. typhi* leads to the development of typhoid, or enteric fever. This disease is characterized by the sudden onset of a sustained and systemic fever, severe headache, nausea, and loss of appetite. Other symptoms include constipation or diarrhea, enlargement of the spleen, possible development of meningitis, and/or general malaise. The encounter of humans to *S. typhi* is made via faecal-oral route from infected individuals to healthy ones. Poor hygiene of patients shedding the organism can lead to secondary infection, as well as consumption of shell fish from polluted bodies of water. The most common source of infection, however, is drinking water tainted by urine and faeces of infected individuals.

Salmonella is a genus of rod-shaped, gram-negative, non-spore-forming, predominantly motile enterobacteria with diameters around 0.7 to 1.5 µm, lengths from 2 to 5 µm, and flagella which grade in all directions (i.e. peritrichous).

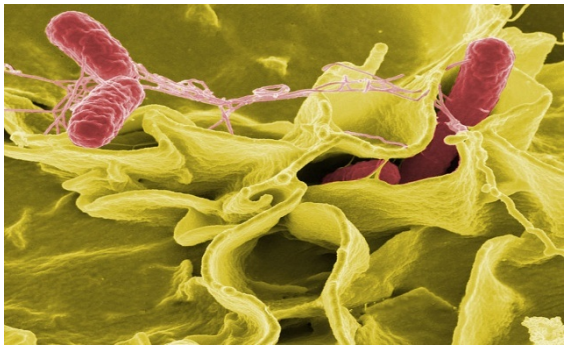

Fig. 4F.1. Rod shaped Salmonella Typhi

Traditional chemical-based disinfectants, such as alcohols, aldehydes, iodine, phenols, and chlorine, have been used for centuries in environmental cleaning. Although these disinfectants are highly efficient against pathogenic microbes, they also have problems. These disinfectants are usually volatile, and their byproducts can be toxic and carcinogenic to humans. As the widespread use of antibiotics and the emergence of more resistant and virulent strains of microorganisms became great clinical challenges [3-8], the establishment and development of novel antibacterial strategies is, therefore, significant in the control of human pathogens and prevention of infectious diseases. From this point of view, photocatalyst based antibacterial agents are conceptually feasible alternative approaches.

The photocatalytic reaction of TiO_2 has been used to inactivate a wide spectrum of microorganisms [9-13]. The first work on the microbicidal effect of TiO_2 photocatalyst was carried out with Escherichia coli in water [14]. These authors reported that E. coli was killed by contact with a TiO_2 photocatalyst upon illumination with light. Hydroxyl radicals (•OH) and reactive oxygen species (ROS) generated on the illuminated TiO_2 surface play a role in inactivating microorganisms by oxidizing the polyunsaturated

phospholipid component of the cell membrane of microbes [9,15- 19]. OH radicals are approximately one thousand or possibly ten thousand times more effective for E. coli inactivation than common disinfectants such as chlorine, ozone and chlorine dioxide [19]. Bactericidal and fungicidal effects of TiO_2 on E. coli, Salmonella choleraesuis, Vibrio parahaemolyticus, Listeria monocytogenes, Pseudomonas aeruginosa, Stayphylococcus aureus, Diaporthe actinidiae and Penicillium expansum have been reported [9, 13,14, 16,20-26].

4F.2. Procedure for Antibacterial study

A fixed amount of the photocatalyst was added to 9 ml of 0.9% saline solution in a reagent bottle and then sterilized by autoclaving at 120^0C and 15 lbs pressure for 30 minutes. It is then mixed with 1ml of the bacteria cell suspension after cooling. The reaction mixture was stirred with a magnetic stirrer to prevent the settling of the photocatalyst. It is then irradiated with visible light obtained from a 150W ozone free Xe lamp with a dichoric mirror of 420-630nm.A bacterial suspension without photocatalyst was irradiated and kept as control and reaction mixture without visible light irradiation was used as dark control. After irradiation, 1ml of the sample was spread on a petridish containing nutrient agar and incubated for 48 hrs at 37^0C and then it was taken for counting. The antibacterial efficiency increases as the number of colonies decreases.

4F.3.Effect of amount of Catalyst

Fig. 4F.2. shows the effect of catalyst dosage on antibacterial activity. In order to study the effect of the amount of photocatalyst on antibacterial activity, experiments were repeated with different amount of catalyst ranging from 0.02 to 0.1g per 10ml for a period of one hour. It was observed that as

the amount of catalyst increases the number of bacterial colony decreases which means that the antibacterial activity increases. The increase of activity with increase of catalyst dosage is attributed to the increase in catalyst surface area, increase of light absorption and consequently the creation of a higher number of active species. From the graph it is clear that maximum antibacterial activity observed for a catalyst amount of 0.1g. So the optimum catalyst amount selected for further experimental studies is 0.1g.

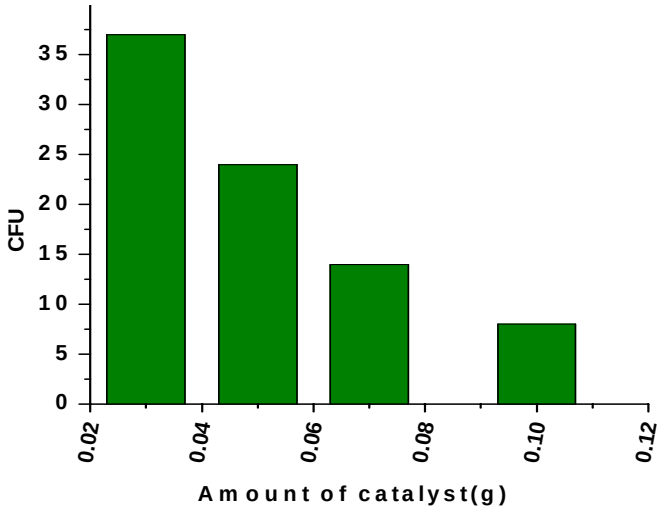

Fig. 4F.2. Antibacterial activity against amount of catalyst
Irradiation time 60 minutes

4F.4.Effect of Time

The influence of time on antibacterial activity is studied using optimum photocatalyst amount. The experiments were carried out at different time intervals. It was observed that as time increases from 15 minutes to one hr the number of bacterial colonies formed decrease, that is the antibacterial efficiency, increases. A maximum antibacterial efficiency of 95% is observed within a time period of 60 minutes. So the optimum time selected for further

studies is 60 minutes. Fig.4F.3. show the effect of irradiation time on antibacterial activity.

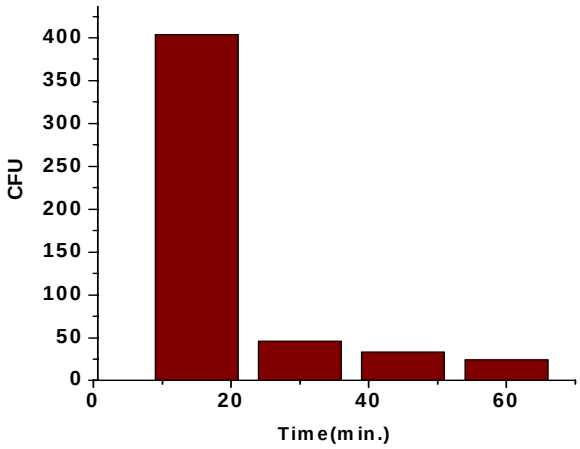

Fig. 4F.3. Antibacterial activity against irradiation time
Amount of catalyst 0.1g

4F.5.Effect of Light source

In this section we evaluated the effect of light intensity for the antibacterial activity. For this purpose we used two different lamp systems of – a 150 W Xe lamp with light irradiation intensity of 96.8mW/cm^2 and a 100W Xe lamp with light irradiation intensity of 64.7mW/cm^2 respectively. Fig. 4F.4 shows the antibacterial efficiency under visible light irradiation with different lamp power. Results show that the antibacterial activity increases as the lamp power increases. When the lamp power increases, its light intensity also increases which enhances the production of more excited species on catalyst surface. As the number of photoexcited species increases the antibacterial activity also increases.

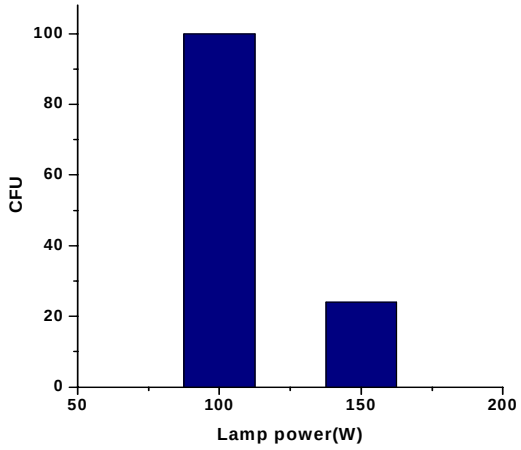

Fig.4F.4 Antibacterial activity against lamp power
Amount of catalyst 0.1g and irradiation time 60 minutes

4F.6. Effect of Various Catalysts:

Fig. 4F.5. shows the effect of various conducting polymers and their different composition with TiO_2, on the antibacterial activity. Studies were performed using the optimum amount of catalyst for a period of one hour light irradiation.

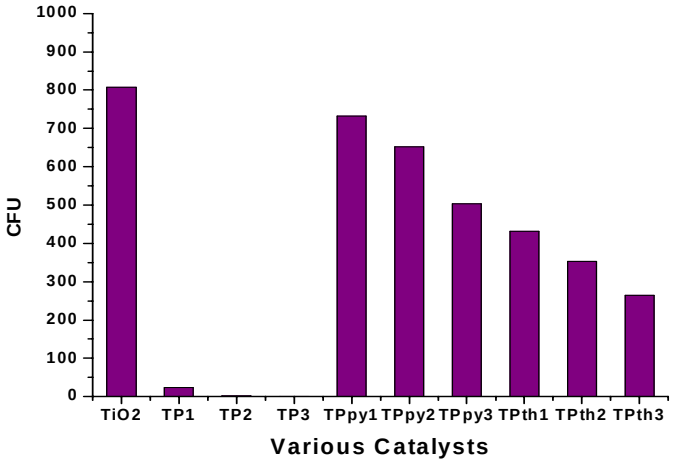

Fig.4F.5. Antibacterial activity against various photocatalysts

Amount of catalyst 0.1g, irradiation time 60 minutes, lamp power 150W

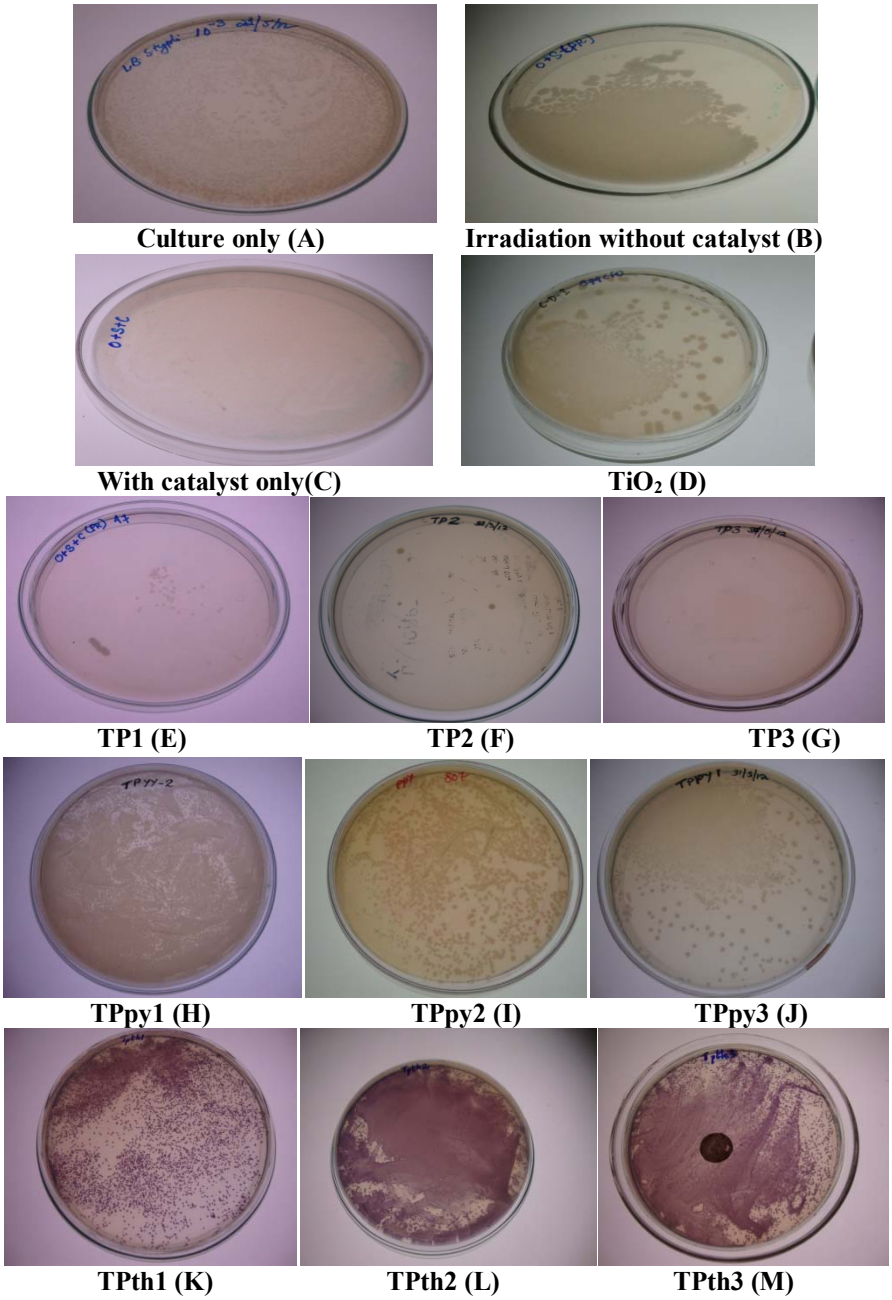

Fig.4F.6. Formation of bacterial colonies under different conditions(A)Pure Culture only(B)After One hr irradiation without catalyst(C)One hr stirring with catalyst & without irradiation; after one hr irradiation in presence of (D)TiO_2 (E)TP1 (F)TP2 (G)TP3 (H)TPpy1(I) TPpy2 (J)TPpy3 (K)TPth1 (L)TPth2 (M)TPth3.

From the graph it was evident that compared to polypyrrole and polythiophene modified TiO_2 systems the polyaniline modified systems show good antibacterial activity. The poor activity of polypyrrole systems may be due to the very low surface area. Although the surface area decreases as the polymer content in the nanocomposite increases, it was observed that composites with a higher polymer content show comparatively good activity compared to those with a lesser polymer content. The reason for this behaviour cannot be explained. Fig.4F.6. shows the formation of bacterial colonies under different conditions.

4F.7. Mechanism of Antibacterial activity

The mechanism of antibacterial activity of conducting polymer blended TiO_2 is as follows. When irradiated with visible light, the π electrons of polymer get excited to π^* level. The excited electrons are then injected to the conduction band of TiO_2. The excited electrons then react with surface adsorbed oxygen to produce superoxide anion, which then react with the cell wall of the bacteria.

Salmonella typhi is a gram negative bacteria. The gram negative bacteria have only a thin layer of peptidoglycan and a more complex cell wall with two cell membranes, an outer membrane, and a plasma membrane. The addition of the outer membrane of the gram-negative bacteria cells influences the permeability of many molecules. Under certain conditions, the gram-negative bacteria are more resistant to many chemical agents than gram-positive cells [28]. The photocatalytic process of anatase TiO_2 particles includes chemical steps that produce highly reactive species such as hydroxyl radical, hydrogen peroxide, and superoxides that, in principle, can cause fatal damage to microorganisms [23]. Among these reactive oxygen species, the hydroxyl

radicals are highly reactive and therefore short-lived. The superoxide ions are relatively longer lived. Due to their negative charge they cannot penetrate the cell membrane. They must contact directly the outer surface of bacteria unless the TiO_2 particle has penetrated the cell. Hydrogen peroxide is less harmful compared to hydroxyl radicals and superoxide ions, but it can enter the cell [29]. However, among these reactive oxygen species, which species are directly involved in the damage of bacterial cells or which species contribute more to the oxidative reactions with organic compounds is still subject to investigation.

The bacterial cell wall contains lipopolysaccharide and peptidoglycan. The damage of peptidoglycan will change the morphology of the bacteria. Without the protection of peptidoglycan and phospholipid layer the leakage of interior substances would occur that ultimately causes the destruction of the bacteria.

4F.8.Conclusions

Traditional antibacterial photocatalysts are primarily induced by ultraviolet light to elicit antibacterial reactive oxygen species. New generation visible light responsive photocatalysts were discovered, offering greater opportunity to use photocatalysts as disinfectants in our living environment.

References

[1]. C.L. Cheng, D.S.Sun, W.C. Chu, Y.H. Tsen, H.C. Ho, J.B. Wang, P.H.Chung, J.H. Chen, P.J. Tsai, N.T. Lin, M.S.Yu, H.H. Chang, Journal of Biomedical Science 16(2009)7.

[2]. A.Fujishima, Photocatalytic and Self Cleaning functions of TiO_2 coatings, Department of Applied Chemistry, The University of Tokyo,7-3-1 Hongo, Bunkyo-ku, Tokyo 113-8656, Japan.

[3]. A.E. Aiello, E. Larson, Lancet Infect. Dis. 3 (2003) 501.

[4]. E.Y. Furuya, F.D. Lowy, Nat. Rev. Microbiol. 4 (2006) 36.

[5]. A.D. Russell, J. Hosp. Infect. 57 (2004) 97.

[6]. G. Taubes, Science 321 (2008) 356.

[7]. M.W. Wassenberg, G.A. de Wit, B.A. van Hout, M.J. Bonten, Quantifying cost effectiveness of controlling nosocomial spread of antibiotic-resistant bacteria: the case of MRSA, PLoS One 5 (2010) 11562.

[8]. C.A. Arias, B.E. Murray, N. Engl. J. Med. 360 (2009) 439.

[9]. T. Matsunaga, R. Tomoda, T. Nakajima, N. Nakamura, T. Komine, Applied Environmental Microbiology 54 (1988) 1330.

[10]. A. Fujishima, K. Hashimoto, T. Watanabe, TiO_2 Photocatalysis Fundamentals and Applications Best Knowledge Center (BKC), Tokyo Japan (1999)

[11]. B. Kim, D. Kim, D. Cho, S. Cho, Chemosphere 52 (2003) 277.

[12]. E.F. Duffy, F.Al. Touati, S.C. Kehoe, O.A. McLoughlin, L.W. Gill, W. Gernjak, I. Oller, M.I. Maldonado, S. Malato, J. Cassidy, R.H. Reed, K.G. McGuigan, Solar Energy 77 (2004)649.

[13]. C. Maneerat, Y. Hayata, International Journal of Food Microbiology 107 (2006) 99.

[14]. T. Matsunaga, R. Tomada, T. Nakajima, H. Wake, FEMS Microbiology Letters 29 (1985)211.

[15]. T. Saito, T. Iwase, T. Morioka, Journal of Photochemistry and Photobiology. B, Biology 14 (1992)369.

[16]. P.C. Maness, S. Smolinski, D.M. Blake, Z. Huang, E.J. Wolfrum, W.A. Jacoby, Applied Environmental Microbiology 65 (1999) 4094.

[17]. Z. Huang, P.C. Maness, D.M. Blake, E.J. Wolfrum, S.L. Smolinksi, W.A. Jacoby, Journal of Photochemistry and Photobiology. A, Chemistry 130 (2000) 163.

[18]. K.P. Kuhn, I.F. Chaberny, K. Massholder, M. Stickler, V.W. Benz, H.G. Sonntag, L. Erdinger, Chemosphere 53 (1) (2003) 71.

[19]. M. Cho, H. Chung, W. Choi, J. Yoon, Water Research 38 (2004) 1069.

[20]. C. Wei, W.Y. Lin, Z. Zaina, N.E. Williams, K. Zhu, A.P. Kruzic, R.L. Smith, K. Rajeshwar, Environmental Science & Technology 28 (1994) 934.

[21]. Y. Kikuchi, K. Sunada, T. Iyoda, K. Hashimoto, A. Fujishima, Journal of Photochemistry and Photobiology. A, Chemistry 106 (1997) 51.

[22]. Y.Horie, M. Taya, S. Tone, Journal of Chemical Engineering of Japan 31 (1998) 577.

[23]. K. Sunada, Y. Kikuchi, K. Hashimoto, A. Fujishima, Environmental Science & Technology 32 (1998) 726.

[24]. Y.S. Choi, B.W. Kim, Journal of Chemical Technology and Biotechnology 75 (2000) 1145.

[25]. J. Wist, J. Sanabria, C. Dierolf, W. Torres, C. Pulgarin, Journal of Photochemistry and Photobiology. A, Chemistry 147 (2002) 241.

[26]. B. Kim, D. Kim, D. Cho, S. Cho, Chemosphere 52 (2003) 277.

[27]. J.S. Hur, S.O. Oh, K.M. Lim, J.S. Jung, Y.J. Koh, Postharvest Biology and Technology 35 (2005) 109.

[28]. G.Tortora, R. B. Funke, L. C. Case, Microbiology; An Introduction; Addison-Wesley Longman, Inc.: New York 2001

[29]. M. D. Blake, P.Manesss, Z.Huang, J. E.Wolfrun, J. Huang, Sep. Purif. Methods 28 (1999) 1.

Chapter 5

EVALUATION OF THE THERMAL DIFFUSIVITY OF POLYANILINE -TiO_2 COMPOSITE USING LASER INDUCED THERMAL LENS TECHNIQUE

Contents

Photothermal spectrometric techniques such as thermal lens spectrometry (TLS) are characterized by high sensitivity, which enables measurement of absorption as low as 10^{-7}.The thermal lens technique is based on measurement of the temperature rise that is produced in an illuminated sample as a result of nonradiative relaxation of the energy absorbed from a laser. Because the technique is based on direct measurement of the absorbed optical energy, its sensitivity is higher than conventional absorption techniques. In this chapter the thermal diffusivity measurements of polyaniline modified TiO_2 samples were studied using laser induced thermal lens technique.

5.1. Introduction

The knowledge of the thermal conductivity and/or the thermal diffusivity is more and more required in many industrial fields. As a matter of fact, these are the most important parameters when heat transfer processes are involved. In the power generation industries, materials are selected primarily considering

their thermal properties [1-4]. In the automotive and aeronautical industries, CMC (ceramic matrix composite) materials for high performance brakes and heat shields are under development and manufacturers require, as essential information the thermal diffusivity [5].

Photothermal spectroscopy is a group of high sensitivity spectroscopy techniques used to measure optical absorption and thermal characteristics of a sample. The basis of photothermal spectroscopy is the change in thermal state of the sample resulting from the absorption of radiation. Light absorbed and not lost by emission results in heating. The heat raises temperature thereby influencing the thermodynamic properties of the sample or of a suitable material adjacent to it.

The thermal lens technique is based on measurement of the temperature rise that is produced in an illuminated sample as a result of nonradiative relaxation of the energy absorbed from a laser. Because the technique is based on direct measurement of the absorbed optical energy, its sensitivity is higher than conventional absorption techniques. However, advantages of the thermal lens technique are not only limited to its ultrasensitivity but also include other unique characteristics including small volume sample capability and dependency on thermo optical properties of solvents [6]. The availability of lasers makes it possible to observe and measure a variety of phenomena, which would not otherwise be feasible using other light sources. One such phenomenon is the photothermal effect [7]. In the case of the thermal lens which is a type of photothermal effect, a sample is excited by a laser beam, which has a symmetrical intensity distribution [6]. The nonradiative relaxation releases the absorbed energy in the form of heat. The heat generated is strongest at the center of the beam because the beam intensity is strongest at that point.

Consequently, a lens like optical element is formed in the sample owing to the temperature gradient between the center of the beam and the bulk material. The thermal lens effect is observable for laser beams in the power range of only microwatts in samples normally thought to be transparent, and is thus suitable for the low absorption measurement of nonfluorescent samples. Its sensitivity is relatively higher than that of the conventional transmission or reflection measurements because, in this technique, the absorbed energy is measured directly. The first measurement of the thermal lens effect was performed by Gordon etal in 1965 using a simple single-beam apparatus [7].

The unique characteristics of lasers, namely low-beam divergence, pure polarization, high spectral and spatial resolution, and its ability to be focussed to a diffraction-limited spot, have been fully exploited to use the thermal lens as a detection technique for micro fluidic devices. As a consequence of these developments, the thermal lens technique has been established as a highly sensitive technique for trace chemical characterization, including single molecule detection. In addition to its ultrasensitive and small-volume capabilities, the thermal lens technique has other features such as the thermal lens signal is dependent not only on sample concentration and excitation laser power but also on the position and thermo physical properties of the sample. These unique features have been exploited either to further increase its sensitivity or to use it for sensitive and accurate determination of thermal physical properties of a variety of substances including solids, liquids, and gases.

Polyaniline (PANI) is one of the typical conducting polymers of the first generation. Much of the work was focused on tailoring its electrical conductivity. Heat diffusion in this material remains practically unexplored. Its use in diverse fields such as molecular electronics and sensor technology

makes proper thermal design of the devices employing conducting polymers essential [8-14]. Poor thermal management of devices employing conducting polymers may lead to device failure. An estimate of heat diffusion in a material can be obtained from its thermal diffusivity value. It is the ratio of thermal conductivity to the thermal capacity per unit volume, given by $\alpha = k/\rho C$; where k, ρ and C are the respective values of thermal conductivity, density and specific heat capacity of the material.

5.2. Theory

Thermal lens spectrometry (TLS) is one of precise photo-thermal techniques based on temperature gradient which is caused by absorption of optical radiation and non-radiative relaxation of the excited molecules. Photothermal lens spectroscopy (PTS or TLS) measures the thermal blooming that occurs when a beam of light heats a transparent sample. It is typically applied for measuring minute quantities of substances in homogeneous gas and liquid solutions [15]. The thermal lens effect originates from nonradiative relaxation of excited species in a sample irradiated by a laser beam with a Gaussian intensity profile. So when sample absorb the beam with Gaussian distributed intensity the temperature distribution has radially dependence. During such radiation less relaxation processes, which include vibrational relaxation, intersystem crossing, and external conversion, the absorbed energy from the excitation light is converted to heat. As a result, the temperature of the irradiated sample changes and a refractive index gradient is formed in the sample, resulting in a change in the laser beam radius, and a related change in the intensity of the beam on its axis. This gradient of temperature can create a refractive index gradient which behaves similarly to a converging or diverging lens depending on whether the change rate of refractive index with respect to

temperature, is positive or negative [16,17]. This technique has very important properties such as "high sensitivity" that makes it appropriate for measuring the thermal diffusivity of samples rely on physical changes that arise in the sample. The magnitude of the thermal lens effect is proportional to the amount of heat generated in the irradiated sample, and is consequently dependent on the power P of the excitation light, absorbance A of the sample, as well as on the fluorescence efficiency of absorbing species, which decreases the thermal lens effect.

5.3. Thermal lens technique

In a simplified form, the essence of this technique is as follows. Irradiation of an absorbing medium by a laser beam with a Gaussian intensity distribution in the transverse cross section induces a temperature gradient in it due to non uniform heating. In turn, a change in temperature causes local changes in the refractive index of the medium, in correspondence with the laser beam intensity distribution. The occurrence of the refractive index gradient in the medium leads to the formation of an optical element, which acts as a scattering/collecting lens; this element was referred to as a thermal lens. Since the refractive index of most materials in the transparency range decreases with an increase in the temperature, the thermal lens is generally scattering; i.e., the transverse laser-beam size increases when the medium is heated. Fig.5.1.shows the thermal lens formation of a sample.

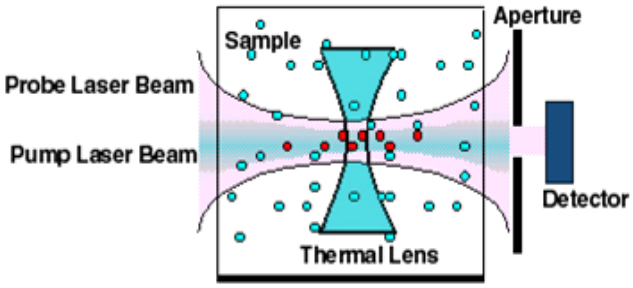

Fig.5.1. Thermal lens formation of a sample

Variations in the refractive index of the medium can be caused by changes in both the temperature *T* and density ρ of the medium

$$\Delta n = \left(\frac{\partial n}{\partial T}\right)_P \Delta T + \left(\frac{\partial n}{\partial \rho}\right)_T \Delta \rho .$$

The thermal lens technique can be implemented using both single- and double-beam measurement schemes. In the single-beam scheme radiation of one laser is simultaneously used for excitation (generation of a thermal lens) and probing. Being absorbed, laser radiation heats the sample, and the change in its intensity yields information about absorption in the medium. The measurement technique generally implies recording the temporal shape of photothermal signal from a photodetector with a diaphragm, located in the far-field zone [18].

The double-beam scheme is more universal. Here, a thermal lens induced by excitation (pump) radiation is recorded by measuring defocusing of an additional probe beam. Its main advantage is that it allows one to study the spectral dependence of the absorption of materials; this cannot be done within the single-beam scheme. One of configurations of the classical double-beam measurement scheme is shown in Fig.5.2.

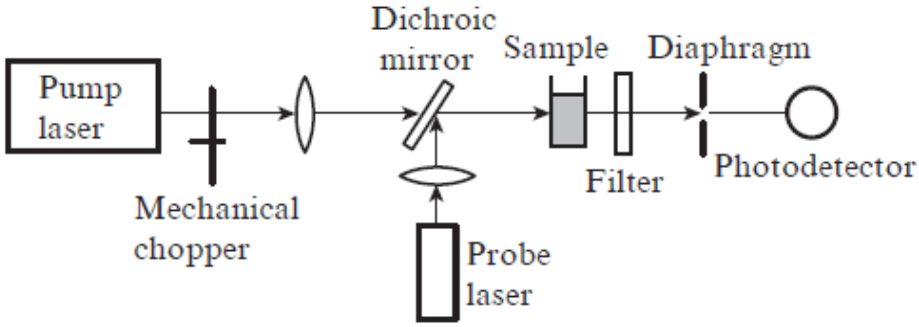

Fig. 5.2. Thermal lens technique (longitudinal version): double-beam measurement scheme; the pump and probe beams propagate coaxially

The double-beam scheme is implemented in either longitudinal (Fig. 5.2.) or transverse [19, 20] configurations; in the latter case, the excitation beam is focused into the sample perpendicularly to the probe beam. In most cases the longitudinal (collinear) version is used. In this case, applying, a dichroic mirror, one makes both beams propagate coaxially in the sample, due to which the maximum interaction length is provided. Here, the so-called mode-matched and mode-mismatched configurations are distinguished. In the former case the waists of both beams coincide in the measurement cell (sample), whereas in the latter version they are spatially separated (Fig. 5.3.).

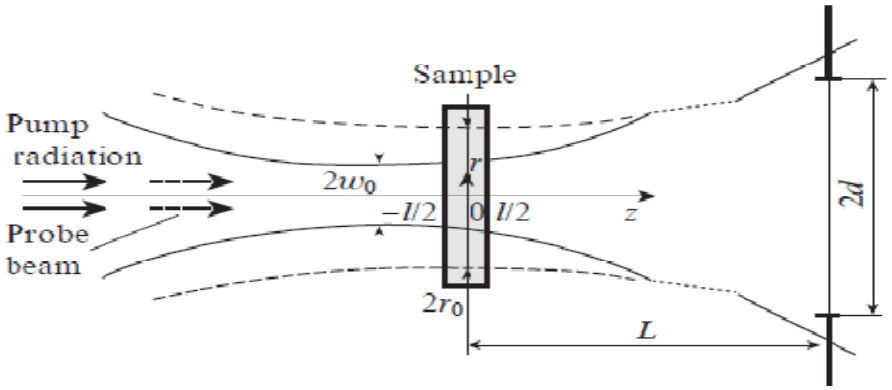

Fig. 5.3. Mode-mismatched configuration (measurement scheme with shifted waists [20].

Thermal diffusivity D of the sample can be calculated from the equation $t_c = \omega^2/4D$, where ω is the beam radius at the sample position (.225mm/2) and t_c, the time response to attain the steady state focal length. The time dependent probe beam intensity follows the expression, which used for fitting the data

$$I(t) = I_0 \Big/ \left[1 - \theta\left(1 + t_c/2t\right)^{-1} + \left(1/2\right)\theta^2\left(1 + t_c/2t\right)^{-2}\right]$$

5.4. Experiment

The excitation source is a continuous wave (cw), 532 nm diode pumped solid state laser, (DPSS) with a maximum power of 150 mW. The power at the sample is suitably adjusted using attenuators so that the probe beam spot is free from aberrations. A 2mW He–Ne laser used as the probe is arranged to be collinear with the pump, using a dichroic beam splitter. The two beams are focused into the sample cell such that the beam area at the sample plane is the same for both pump and probe resulting in a mode matched TL configuration. Sample was taken in cuvettes of 1 cm and 5 mm path lengths for various sets of measurements. A low frequency mechanical chopper and a shutter are used as required, either to quickly block the pump or to intensity modulate it, depending on the type of data recorded. For example if the aim is to optimize the TL experiment, it is desirable to use the chopper, and adjust the sample position, aperture position, etc. until the TL peak-to-peak signal is maximum. This also enables one to determine the thermal recovery of the sample. On the other hand, when a time dependent TL signal is required; one should replace the chopper with a shutter. The TL signal was collected using an optical fiber, positioned at the center of the probe beam spot and connected to a photodetector–

DSO system. A filter for 532 nm was used before the detector to remove the residual pump. Fig.5.4.shows the pulsed thermal lens experimental set-up.

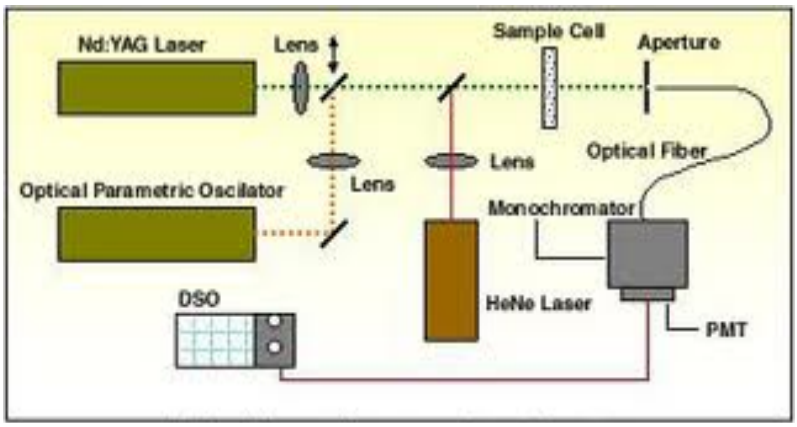

Fig. 5.4. Pulsed thermal lens experimental set-up

5.5. Thermal diffusivity studies

Pure TiO_2 does not show thermal lens effect due to lack of optical absorption. However pure polyaniline shows a thermal diffusivity of 0.0201cm^2/s. On blending with TiO_2, the thermal diffusivity of the composite is found to increase. As the amount of polyaniline content increases thermal diffusivity increases drastically. Table 5.1 shows the thermal diffusivity values.

Table 5.1.Thermal diffusivity values of PANI-TiO_2 composites for various fraction of PANI in the composites

Solution	θ	t_c (s)	D(10^{-3}) (cm^2/s)
PANI	-19.04	1.57	0.02
TP1	-9.46	0.79	0.04
TP2	-9.90	0.77	0.041
TP3	-5.46	0.34	0.09

The best interpretation for this phenomenon is that, absorption of exciting laser light by the conducting polymer generates oscillating electron which are called hot electron. These hot electrons rapidly transfer their energy to the TiO_2 particle through electron-phonon scattering. This thermal energy is finally get transferred to surrounding liquid by phonon scattering with particles as scattering centres [21]. Fig.5.6. & 5.7. show the TL decay and the normalized TL time evolution signal for sample dispersed in water.

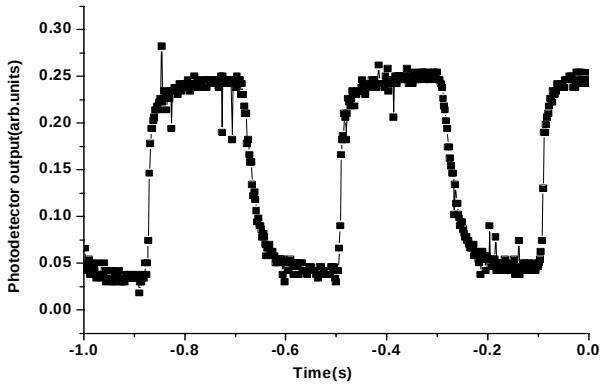

Fig.5.6. TL decay of representative sample

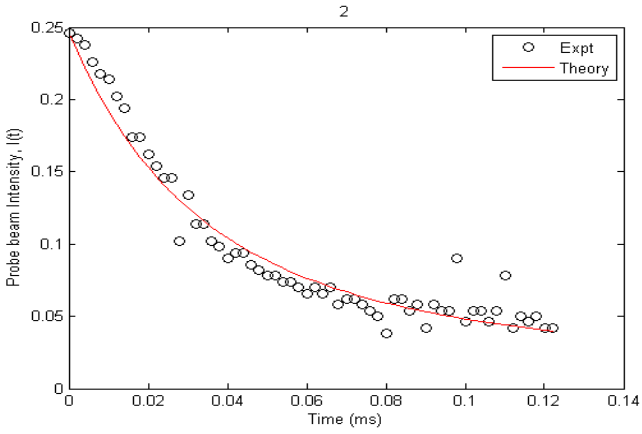

Fig.5.7.The normalized TL time evolution

Signal for sample dispersed in water. The circles are experimental data and solid lines are theoretical fit.

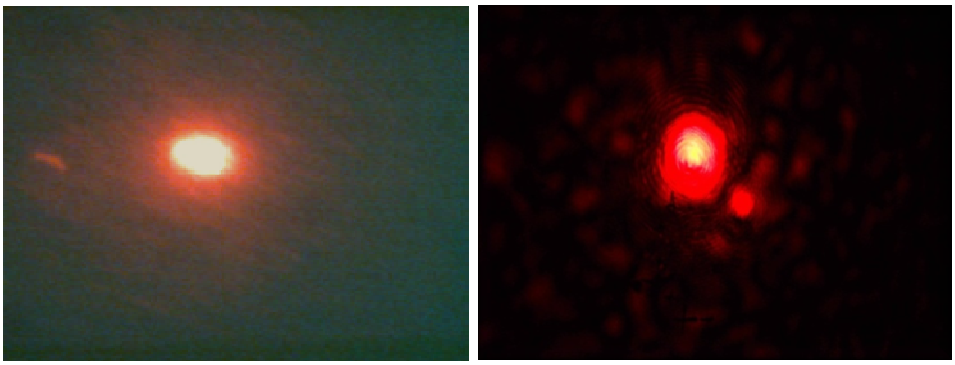

(a) **(b)**

Fig.5.8. Photograph showing (a) Probe beam without pump laser and (b) thermal blooming of the probe beam in presence of pump laser for the representative sample dispersed in water.

The fact that the PANI- TiO_2 composite has enhanced thermal diffusivity in comparison with PANI, can find practical uses as efficient coolants in various industrial applications.

5.6. Conclusions

Polyaniline is known to possess a conjugated structure and samples obtained by chemical synthesis do not show any cross linking or side reactions. The local order in such a sample will be relatively high. This can lead to reduced scattering of phonons in a chemically synthesized sample. By acid doping, a three-fold increase in the value of thermal diffusivity is observed. This increase can be related to the increase in carrier concentration upon doping. In the undoped state there is a phonon-assisted heat transport. In doped samples there is a carrier contribution to heat transport and a consequent higher diffusivity [22].Polyaniline blending modifies the thermal properties of TiO_2.There is an increase in thermal diffusivity with increase in amount of polyaniline content in the composites. This means that the composite material can be used as a good coolant material which will diffuse

heat from the medium at faster rate as polyaniline component increases in the composite material.

References

[1]. V.P. Swaminathan and N.S. Cheruvu, "Gas Turbine Hot-Section Materials and Coatings in Electric Utility Applications", in *Advanced Materials and Coatings for Combustion Turbines*, Edited by V.P. Swaminathan and N.S. Cheruvu. ASM International, 1994.

[2]. European Brite-Euram Project BRPR-CT97-0426 EFCC/UHTHE/B3.

[3]. European Brite-Euram Project BRPR-CT97-0426 EFCC/UHTHE/B4.

[4]. A. Donato, A. Ortona, C.A. Nannetti, S. Casadio, *SiC/SiC Fibre Ceramic Composite for Fusion Application: a new Manufacturing Process* Proc. 19th Symp.on Fusion technology (SOFT), Lisbon, (P) Sept. 1996.

[5]. TWI Bulletin Nov/Dec. 1996 Reprint 508/6/96.

[6]. Mladen Franko, Chieu D. Tran, Thermal Lens Spectroscopy, *Encyclopedia of Analytical Chemistry* R.A. Meyers (Ed.) Copyright 2010 John Wiley & Sons Ltd

[7]. J.P. Gordon, R.C.C. Leite, R.S. Moore, S.P.S. Porto,J.R. Whinnery, *J. Appl. Phys.* 36 (1965) 3.

[8]. K.Lee, S.Cho, S. H. Park, A. J. Heeger, C.W. Lee ,S.H. Lee, Nature 1 (2006) 65 .

[9]. F. Zhanga, P. A. Halversonb, B. Luntc, M. R. Linford, Synthetic Metals 156 (2006) 932.

[10]. H.K. Song, G. Tayhas , R. Palmore, Advanced Materials, 18 (2006) 1764.

[11]. K. Kaneto, M. Maxfield, D. P. Nairns, A. G. MacDiarmid and A. J.Heeger, J. Chem. Soc. Faraday Trans. 78 (1982) 3417.

[12]. S. Kuwabata, S. Ito, H. Yoneyama, J. Electrochem. Sci. Technol. 135 (1998) 1691.

[13]. J. W. Thackeray, H. S. White ,M. S. Wrighton, J. Phys. Chem. 89 (1985) 5133.

[14]. D. T. Hao, T. N. Suresh Kumar, R. S. Srinivasa, R.Lal, N. S. Punekar ,A. Contractor, Q. Anal. Chem. 64 (1992) 2645.

[15]. Wikipedia.

[16]. S. Bialkowski, Photothermal spectroscopy methods for chemical analysis, in: J.D. Winefordner (Ed.), Chemical Analysis. 134 (1996).

[17]. J. Shen, R.D. Lowe, R.D. Snook, Chem. Phys.165 (1998) 317.

[18]. A. Skvortsov, *Quantum Electronics* 43 (2013) 1.

[19]. V.P. Zharov, V.S. Letokhov Lazernaya optikooakusticheskaya spektroskopiya (Laser Photoacoustic Spectroscopy) (Moscow: Nauka, 1984).

[20]. A. Luk'yanov, M. Novikov, *Zh. Tekh. Fiz*. **70** (11) (2000) 99.

[21]. R. Zamiri, B.Z. Azmi, M.S. Husin, G. Zamiri, H. A. Ahangar, Z. Rizwan J Europ. Opt. Soc. Rap. Public. **7** (2012) 12022.

[22]. P. Z. Thomas, J. Honey Mary Kurien, T. M. A. Rasheed, International Journal of Polymeric Materials 57 (2008) 852.

.....ꕥ.....

Chapter 6

MODIFICATION OF OPTICAL LIMITING PROPERTIES OF POLYANILINE WITH NANO TiO_2

Contents

The potential applications of nonlinear optics in photonics and optoelectronics have got immense interest nowadays. The nonlinear optical response of π-conjugated polymers is currently a subject of considerable experimental and theoretical interest because of their potential use in all optical devices. Amongst the new classes of materials conjugated polymers are especially interesting because they combine the optical and electronic properties of semiconductors with the processing advantages and mechanical properties of polymers. The polyaniline (PANI) is a unique example since its electrical properties can be reversibly controlled both by changing the oxidation state of the main chain and by protonation of the imine nitrogen atoms. Besides, in addition to a wide range of desirable electrical, electrochemical and optical properties, PANI exhibits excellent environmental and thermal stability. This chapter deals with the study of third order nonlinear optical properties of polyaniline modified TiO_2 nanocomposite systems using Z-scan techniques.

6.1. Introduction

Nonlinear optics is the study of phenomena that occur as a consequence of the modification of the optical properties of a material system by the presence of light. Typically, only laser light is sufficiently intense to modify

the optical properties of a material system. The beginning of the field of nonlinear optics is often taken to be the discovery of second-harmonic generation by Franken *et al.* (1961), shortly after the demonstration of the first working laser by Maiman in 1960. Nonlinear optical phenomena are "nonlinear" in the sense that they occur when the response of a material system to an applied optical field depends in a nonlinear manner on the strength of the optical field. For example, second-harmonic generation occurs as a result of the part of the atomic response that scales quadratically with the strength of the applied optical field. Consequently, the intensity of the light generated at the second-harmonic frequency tends to increase as the square of the intensity of the applied laser light.

In order to describe more precisely what we mean by an optical nonlinearity, let us consider how the dipole moment per unit volume, or polarization $\tilde{P}(t)$, of a material system depends on the strength $\tilde{E}(t)$ of an applied optical field. In the case of light beam of low intensity, the induced polarization depends linearly on the electric field strength that can often be described by the relationship

$$\tilde{P}(t) = \epsilon_0 \chi^{(1)} \tilde{E}(t) \quad \text{..... (6.1)}$$

where the constant of proportionality $\chi^{(1)}$ is known as the linear optical susceptibility coefficient and ε_0 is the permittivity of free space. In the case of conventional low intensity light source available during the laser era, the equivalent electric field shift of the light wave is of the order 10^5-10^6 V/m which is very small in compared to the internal field in atoms or molecules which is of the order of 10^{10} V/m. So that the linear relationship between P and E is a good approximation. However with the advent of lasers, we can have equivalent

electric field as 10^{10}-10^{12} V/m, which is larger than the internal electric field. Hence induced polarization will be a function of E which can be expressed as a polynomial in E. Thus we have a new branch of optics called nonlinear optics, in which the optical response can often be described by generalizing Eq. (6.1) by expressing the polarization $\tilde{P}(t)$ as a power series in the field strength $\tilde{E}(t)$ as

$$\tilde{P}(t) = \epsilon_0[\chi^{(1)}\tilde{E}(t) + \chi^{(2)}\tilde{E}^2(t) + \chi^{(3)}\tilde{E}^3(t) + \cdots$$

$$= \tilde{P}^{(1)}(t) + \tilde{P}^{(2)}(t) + \tilde{P}^{(3)}(t) + \cdots \quad \text{..... (6.2)}$$

The quantities $\chi^{(2)}$ and $\chi^{(3)}$ are known as the second- and third-order nonlinear optical susceptibilities, respectively [1].

Study of the nonlinear optical (NLO) properties of materials and the design and fabrication of devices based on such nonlinear properties continue to be an exciting area of research in optoelectronics and photonics. Knowledge of the nonlinear optical properties such as nonlinear refraction, nonlinear absorption and rotational viscosity in dye-doped nematic liquid crystals (NLCs) is crucially important for photonic applications like liquid crystal display (LCD). Versatile optical methods have been developed for measuring the nonlinear refraction and nonlinear optical properties including third harmonic generation [2], degenerate four wave mixing [3], optical Kerr gate [4], nonlinear interferometry [5] ellipse rotation [6], phase distortion method [7]etc. There exists different types of experimental setup to measure the optical nonlinearities of materials of which the Z-scan technique [8] is a simple and highly sensitive single beam method that uses the principle of spatial beam distortion in the medium to measure both the sign and the magnitude of the third order optical nonlinearity.

Preparation of nonlinear optical materials have been explored extensively in respect of their various applications in all-optical switches, opto-electronic devices, 3-D optical memory devices, optical modulation, telecommunications, protection of human eyes and optical sensors against intense light etc., and applications in biological and medical sciences [9-14]. Continuous wave (CW) lasers ranging from mW to kW are widely used in many of the NLO based applications [15]. Wide range of materials including liquid crystals, porphyrins, dyes, semiconductor nanoparticles, thin films, phthalocyanines and crystals like KDP, $LiNbO_3$ are known to be optically nonlinear under CW laser illumination [16-24].

There is considerable interest in identifying materials with large and fast nonlinearities with fast optical response. This interest, that is driven primarily by the search for materials for all-optical switching and sensor protection applications, concerns both nonlinear optical absorption (NLA) and nonlinear refraction (NLR). Nonlinear optical materials have potential application in optical communications, optical storage, optical computing, optical switching, optical limiting, etc due to intensity dependant refractive index of the medium. We can arrive at the intensity dependant refractive index property as a consequence of third order optical nonlinearity as follows. We have the displacement field in EMF as

$$D = E_0\vec{E} + \vec{P}$$

$$\vec{P} = E_0\chi^{(1)}\vec{E} + E_0\chi^{(3)}\vec{E}^{(3)}$$

$$\vec{D} = E_0\vec{E} + E_0\chi^{(1)}\vec{E} + E_0\chi^{(3)}\vec{E}^{(3)} = \{E_0(1+\chi^{(1)}) + E_0\chi^{(3)}|E|^2\}E = E\vec{E}$$

$$\sqrt{E} = \text{n} = E_0(1+\chi^{(1)} + \chi^{(3)}|E|^2)^{1/2} = [E_0(1+\chi^{(1)})]^{1/2}\left[1 + \frac{\chi^{(3)}}{1+\chi^{(3)}}|E|^2\right]^{1/2}$$

$$= E_0(1+\chi^{(1)})^{1/2}\left[1+\frac{\chi^{(3)}|E|^2}{2(1+\chi^{(1)})}\right]$$

$$\left[E_0\left(1+\chi^{(1)}\right)^{1/2}+\frac{{E_0}^{1/2}\chi^{(3)}|E|^2}{2(1+\chi^{(1)})^{1/2}}\right]=n_0+\frac{E_0\chi^{(3)}|E|^2}{2n_0}\approx n_0+n_2I$$

$$Since|E|^2\sim I, then\ n=n(I)=n_0+n_2I$$

n_2 can be complex and can be positive or negative. The imaginary part of n_2 will describe the intensity dependant optical absorption which will increase or decrease with intensity of laser beam. This leads to two types of optical process like saturable absorption (n_2 □0, absorption→0 or I increase) and reversible saturable absorption (n_2 □0).

From a fundamental point of view, materials exhibiting nonlinear optical properties can be categorized depending on particular mechanism like SA or RSA [27]. Saturable absorption (SA), two photon absorption (TPA) and excited state absorption (ESA) are the most relevant types of nonlinear absorptive processes. Transitions involve one photon and two photons have different selection rules. TPA involves the simultaneous absorption of two photons to excite atoms or molecules. SA involves the saturation absorption, by populating the excited state of the material so that the material, which initially absorbed at that wavelength, becomes more transparent. ESA involves a sequential process in which a photon is initially absorbed and the molecule remains in an excited state of the material so that a second photon that arrives during that time is also absorbed to put the molecule into an even higher excited state [28-30].

Materials exhibiting saturable absorption: absorb the major fraction of the incident radiant power when the input fluence (total delivered energy per

unit area) is low, with the absorption diminishing as increasing the fluence. Physically, this occurs because the absorption cross-section for the ground state is greater than the absorption cross-section(s) to the excited state(s). The observed decrease in absorption with increasing fluence results simply from the depletion over time of the ground state population as an ever-increasing fraction of the excitation of molecules. The opposite situation, in which the absorption cross section(s) between the excited state(s) exceeds that of the ground state, gives rise to reverse saturable absorption (RSA), in which the absorption increases with input fluence. This enhancement of absorption reflects the increase in the population of the (more strongly absorbing) excited state(s) relative to that of the (less strongly absorbing) ground state. Both types of absorptive nonlinearity, saturable absorption as well as reverse saturable absorption, offer practical applications. For instance, saturable absorbers (the transmittance increases with the increase of optical intensity) are commonly used as passive Q-switches in pulsed lasers. Materials exhibiting RSA (their transmittances reduce with the increase of optical Intensity), on the other hand, could be exploited in two-photon microscopy and in optical limiting applications for devices which protects eye and sensitive devices, which require high transmission of low intensity radiation but high absorption at high input [31,32]. A full characterization of the nonlinear optical response of a material involves the measurement of both absorptive and refractive nonlinearities. These two quantities are typically measured with Z-scan techniques [25, 26]. In a Z-scan experiment, a sample of material is moved from one side of focus to the other along the propagation path (Z) of a tightly focused Gaussian beam and the apertured and unapertured transmittance of the sample is measured as a function of the sample's position relative to focus. From the apertured transmittance curve ("closed aperture Z scan"), one may

deduce the sign and magnitude of the nonlinear refractive index; one then uses the unapertured transmittance data ("open aperture Z-scan") to infer the strength of the nonlinear absorption.

Open aperture Z-scan is explored to evaluate SA or RSA properties of nonlinear medium to ascertain the usefulness of a material as an optical limiter. This will help us to understand the mechanism of the phenomena underlying the nonlinear absorption [26, 33].

Organic molecular structures represented by conjugated π-electron polymer chains play a key role in the realm of optoelectronics [34, 35]. They are of great importance since they possess high nonlinearity and ultra-fast response time. Among organic materials, π-conjugated polymers have received significant interest as third-order nonlinear optical materials for photonic switching devices, optoelectronic materials for light emitting diodes, solar cells, and xerographic photoreceptors [36-39]. The nonlinear optical response of π- conjugated polymers is currently a subject of considerable experimental and theoretical studies because of their potential use in most of the optical devices. Experimentally, polydiacetylenes are known to have very large third-order nonlinear susceptibilities $\chi^{(3)}$. The mechanism of the optical nonlinearity in these systems, however, remains unclear. Controversial, and sometimes contradictory, viewpoints regarding the importance of electron-phonon versus electron-electron' interactions exist. Numerical calculations of $\chi^{(3)}$ for finite systems are difficult to generalize to infinite systems. Moreover, identification of any possible dominant pathway contributing to $\chi^{(3)}$ is a formidable task from numerical calculations [40]. π-Conjugated polymers include polypyrrole, polyaniline, polythiophene, and other conjugated polymers. In conducting polymers conductivity is directly associated with the

presence of a conjugated backbone which enables electron delocalization. A conjugated backbone signifies a primary axis of carbon atoms interconnected by alternating single and double bonds. Among the conjugated polymers, polyaniline (PANI) has received special attention because it exhibits a controlled reversibility of its electrical conductivity [41]. The conjugated polymers can combine the optical and electronic properties of semiconductors with the processing advantages and mechanical properties of polymers [42].The most studied CP, polyaniline (PANI), is a unique example since its electrical properties can be reversibly controlled both by changing the oxidation state of the main chain and by protonation of the imine nitrogen atoms .Polyaniline (PANI) is an intrinsically conducting polymer located in the subgroup of ionic EAPs. It is a flexible polymer with characteristics that are similar to semiconductors. PANI is considered as one of the promising conducting polymer due to its (i) easy synthesis, (ii) comparatively stable in environment, (iii) good conductivity, (iv) variety of applications such as light emitting diodes, sensors, electro chromic devices, rechargeable batteries, corrosion resistant paints, etc. [43]. In addition to a wide range of desirable electrical, electrochemical, and optical properties, PANI also exhibits excellent environmental and thermal stability, being easily cast into films, gels, and fibers [44]. Disadvantages include low electrochemical strain, insolubility in most solvents and infusibility which makes it unsuitable for melting processes.

Nonlinear optical materials based on polymers are commercially important because of their potential optical limiting properties [45]. Optical limiters are extensively used as protective layers in sensors and also for eye protection devices like goggle when exposed to intense lasers [46]. Optical limiters are devices that strongly attenuate optical beams at high intensities

while exhibiting higher transmittance at low intensities. Such devices are useful for the protection of the human eye and optical sensors from intense laser beams [47-50]. The development of materials for optical limiting is based on various mechanisms such as thermal refractive beams spreading, two photon absorption (TPA) and excited state absorption (ESA). Polyaniline as a guest-host matrix has been found to be exhibiting nonlinear optical properties.

6.2. Theory

The nonlinear medium is scanned along the z axis in the back focal region of an external lens, and the far-field on-axis (i.e., closed aperture) transmittance and the whole (i.e., open aperture) transmittance are monitored as a function of the scan distance *z*. The open aperture Z-scan transmittance is insensitive to then on linear refraction and solely determines the nonlinear absorption, whilst the closed aperture Z-scan transmittance is coupled with both of the nonlinear effects. Actually, both the nonlinear refraction and the nonlinear absorption are often present simultaneously in nonlinear optical materials. Nonlinear absorption is inevitably present for resonant absorption wavelength ranges as well as for transparent regions owing to multi-photon absorption when the laser beam intensity is sufficiently high or because of other nonlinear processes. For simplicity, we only concentrate on two-photon absorption (TPA). Consider the fundamental Gaussian electric field (TEM00 mode) of travelling in the *z* direction as

$$E(r,z) = E_o \frac{\omega_o}{\omega(z)}\left[-\left(\frac{r^2}{\omega^2}+i\frac{kr^2}{2R}\right)\right]\exp\left[-i\varphi(z)\right] = E(0,z)\exp\left[-i\frac{kr^2}{2\tilde{q}}\right]$$

where E_0 is the amplitude of the electric field at the focus (i.e., z=0), $\omega(Z)=\omega_0\left(1+\widetilde{Z}^2\right)^{1/2}$ is the beam radius at, is the beam at z, w_0 waist radius at focus, $R(Z)=Z\left(1+1/\widetilde{Z}^2\right)$ is the radius of curvature of the wave front at z, is the dimensionless propagation distance, $Z_0=k\omega_0^2/2$ is the Rayleigh diffraction length of the beam, $k=2\pi/\lambda$ is the wave number and λ is the wavelength of laser beam. Here, $q\#$ denotes the complex beam parameter that contains all the information needed to specify its characteristics in the beam propagation and is defined by $1/\widetilde{q}=1/R-i\lambda/\pi\omega_{\bullet}^2$ [51]. There has been a great need for nonlinear optical materials that can be used with low-intensity lasers for applications such as the phase conjugation, image processing, and optical switching [52, 53]. The large nonlinear optical susceptibility resulting from the nonlinear response of organic molecules has attracted much attention. The study of nonlinear optical properties on an IR 140 dye [54], Methyl violet 2B dye [55] series Hydroxy Porphyrin [56] Bismuth-based glasses [57] and ultrafast optical nonlinearity in Polymethylmethacrylate-TiO_2 nanocomposites [58] has been recently reported.

Nonlinear optical phenomena can be due to electronic and non electronic processes. The former refers to those radiative interactions between the active electron and the optical-electrical field. Non electronic processes are nonradiative interactions such as temperature, density, cis-trans isomerism, phase transition, etc.

Experimental Technique:

The details of sample preparation are briefly described below

Pure TiO_2 was prepared by surfactant (P123) assisted hydrothermal technique using weak acidic medium followed by calcination at 500°C. TiO_2 -

Polyaniline composites were prepared by chemical oxidative polymerization of aniline over TiO_2 using ammonium peroxodisulfate as oxidizing agent using the same technique. Three different compositions of the nanocomposites were made by varying the molar ratio of titanium dioxide and aniline and they were named as TP1 (4:1), TP2 (2:1) and TP3 (1:1) respectively. Thin films of the samples are prepared by tape casting technique. Samples dispersed in polyvinyl alcohol are used for tape casting.

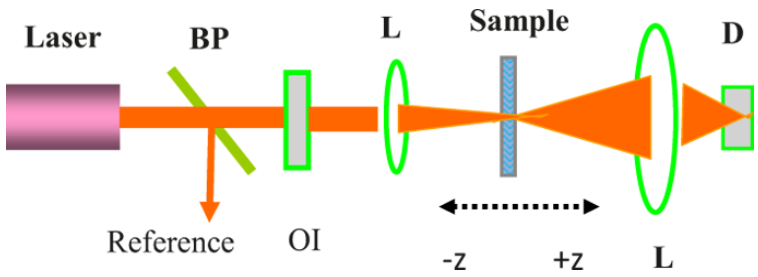

Fig.6.1.Schematic representations of Z scan technique

For nonlinear characterization, we have used the single beam z-scan technique with nanosecond laser pulses to measure nonlinear optical absorption and refraction properties of the TiO_2-Polyaniline nanocomposites. Fig.6.1.shows the Schematic representation of Z scan technique.

The experimental setup is as follows. A Q-switched Nd: YAG laser (Spectra Physics LAB-1760, 532 nm, 7 ns, 10 Hz) is used as the light source. The sample is moved in the direction of light propagation near the focal spot of the lens with the focal length 200 mm. The radius of the beam waist is calculated to be 43.3 lm. The Rayleigh length, z_0 is estimated to be 11 mm, which is much greater than the thickness of the sample, an essential prerequisite for z-scan experiment. The thickness of the films was measured

using screw gauge. The linear transmittance of the far field aperture S, defined as the ratio of the pulse energy passing the aperture to the total energy, is measured to be approximately 0.08. The z-scan system is calibrated using CS_2 as a standard. The transmitted beam energy, reference beam energy and their ratio are measured simultaneously by an energy ratio meter (Rj7620, Laser Probe Corp.) having two identical pyroelectric detector heads (Rjp735). The effect of fluctuations of laser power is eliminated by dividing the transmitted power by the power obtained at the reference detector; both being measured using identical photo detectors. The data are analyzed by using the procedure described by Sheik-Bahae et al [26].

6.3. Results and Discussion

Fig.6.2. shows the nonlinear absorption of PANI and TiO_2-PANI nanocomposites at a typical fluence of 300 MW/cm^2. The open aperture curve exhibits a normalized transmittance valley, indicating the presence of reverse saturable absorption in the colloids.

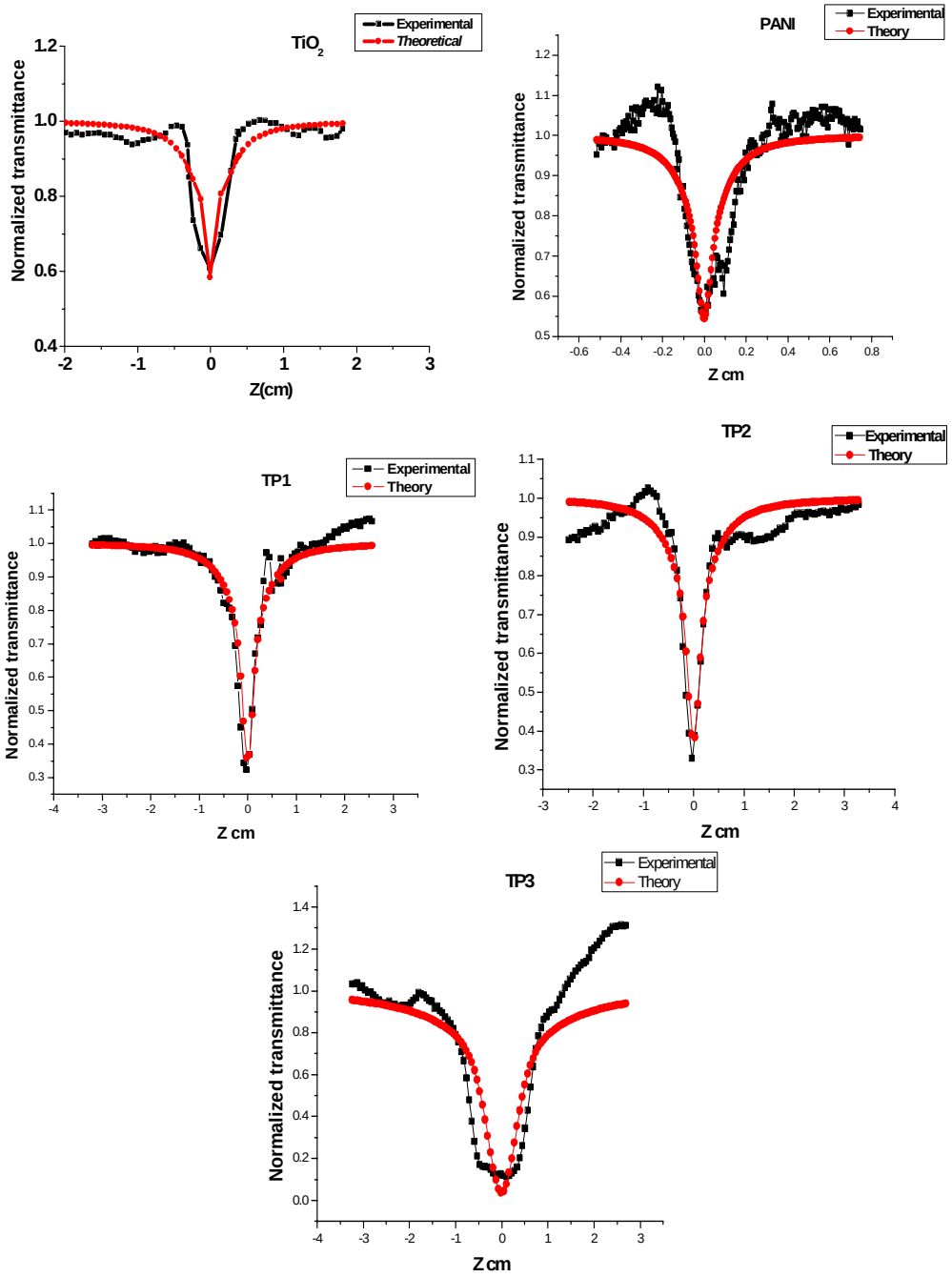

Fig.6.2. Open aperture Z scan traces of PANI and TiO_2-PANI nanocomposites at an intensity of 300 MW/cm^2 for an irradiation wavelength of 532 nm.

The observed optical nonlinearity is found to be of the third-order, as it fits theoretically to a two photon absorption process. The corresponding net transmission is given by

$$T(z) = \frac{1}{q_0\sqrt{\pi}} \int_{-\infty}^{\infty} \ln\left(1 + q_0 e^{-t^2}\right) dt, \text{ where } q_0(z, r, t) = \beta I_0(t) L_{eff.}$$

Here, $L_{eff} = 1 - \frac{e^{-\alpha l}}{\alpha}$ is the effective thickness with linear absorption coefficient a, nonlinear absorption coefficient β and I_0 is the irradiance at focus. The solid curves in **Fig. 6.2** are the theoretical fit to the experimental data. The obtained values of nonlinear absorption coefficient β at an intensity of 300 MW/cm^2 are shown in Table 6.1.

Table 6.1. Nonlinear optical absorption coefficient (β) and optical limiting threshold values of prepared samples

Sample	q	β(W/m)	Optical limiting threshold(GW/cm^2)
Polyaniline	1.42	$7.15*10^{-9}$	0.17
TiO_2	1.31	$6.60*10^{-9}$	0.15
TP1	1.59	$7.99*10^{-9}$	0.16
TP2	1.56	$7.85*10^{-9}$	0.14
TP3	1.78	$8.94*10^{-9}$	0.05

In the present case, the decrease in transmission with increase in the input intensity through the sample at the focus (z=0) indicates that the samples exhibits reverse saturation absorption (RSA). RSA also known as positive nonlinear absorption type of behaviour results due to any of the nonlinear mechanisms such as two-photon absorption (TPA), excited free carrier absorption (ESA), nonlinear scattering or with the combination of these

processes [59].It is clear from the figure that as the sample is translated towards focus, the transmittance decreases forming a well-defined dip at the focus (z = 0), indicating the occurrence of reverse saturable absorption process [60]. Reverse saturable absorption has been found to occur in centro-symmetric structural organic materials and especially in π-conjugated materials [59]. The origin of RSA is based on the two conditions, (i) the molecules present in ground state and excited states can absorb the incident photons of same wavelengths and (ii) the absorption of excited states must be larger than that of the ground states. Also from the fit, we can confirm that the basic mechanism involved in the nonlinear absorption of nanocomposites is TPA process because the photon energy of the 532 nm laser is within the range $Eg < 2h\upsilon < 2Eg$, where $h\upsilon = 2.33$ eV.

To examine the viability of PANI and TiO_2-PANI nanocomposites as optical limiters, the nonlinear transmission of the colloid is studied as a function of input fluence. The optical limiting property occurs mostly due to absorptive nonlinearity which corresponds to the imaginary part of third-order susceptibility [61]. From the value of fluence at focus, the fluence values at other positions could be calculated using the standard equations for Gaussian beam waist. Such plots represent a better comparison of the nonlinear absorption or transmission in these samples and are generated from z scan traces. Fig.6.3 illustrates the influence of PANI and TiO_2-PANI nanocomposites on the optical limiting response.

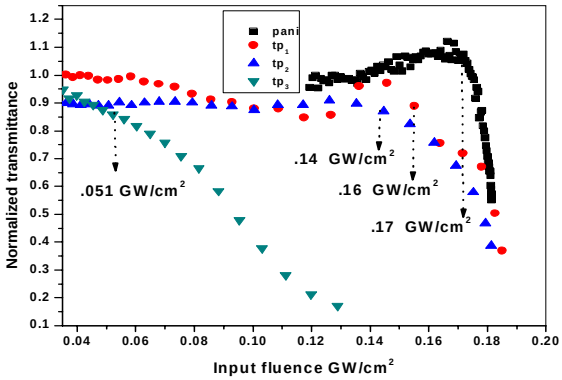

Fig.6.3. Optical limiting of TiO_2-Polyaniline nanocomposites with different polyaniline content

Polyaniline and its composite materials are generally used as a good optical limiting material due to their efficiency and highly conjugated framework. Pure polyaniline shows an optical limiting threshold of 0.17GW/cm^2.While on composite formation with TiO_2 the optical limiting threshold decreases to lower value. As the amount of polyaniline in the composite increases the optical limiting threshold decreases and reaches a minimum value of 0.05 GW/cm^2.

6.4. Conclusion

In summary, we have evaluated third-order nonlinear optical properties of Polyaniline and its nanocomposite with TiO_2 using z-scan technique. The polymer-TiO_2 samples exhibit strong optical power limiting with increase in concentration of the polymer in the nanocomposites. Also it was observed that the optical limiting threshold decreases with increase in polymer concentration in the composite and finally reaches a limiting value. Thus the investigated polymer-TiO_2 nanocomposites are promising candidates for optical limiting devices.

References

[1]. R. W. Boyd, Nonlinear Optics, 3rd edition.

[2]. P. C.deSouza, G. Nader, T. Catunda, M. Muramatsu & R. J. Horowicz, Opt. Comm. 177 (1999) 417.

[3]. H. B.Liao, R. F.Xiao, H.Wang, K. S. Wong & G. K. L. Wong, Appl. Phys. Lett. 72 (1998) 1817.

[4]. A. S. L.Gomes, L.Demenicis, , D. V.Petrov, C. B.de Araujo, C. P. de Melo & R.Souto-Maior Appl. Phys. Lett.69(1996) 2166.

[5]. A.Yavrian, T. V. Galstyan & M. Pich´e, IEEE J. Quantum Electron 35 (1999) 1430.

[6]. M. Lefkiry, X. N. Phu and G. Rivoire,Quantum Semiclass. Opt. 10 (1998) 283.

[7]. Y. Watanabe, M. Ohnishi & T. Tsuchiya, Appl. Phys. Lett. 66 (1995) 3431.

[8]. M. Sheik-Bahae, A. A. Said, T. H.Wei, D. J. Hagan & E. V. Stryland, IEEE J. Quantum Electron. 26 (1990) 760.

[9]. K.J. Ghaleh, S. Salmani, M.H. Majles Ara, Optics Communications 271 (2007) 551.

[10]. M.D. Zidan, A.W. Allaf, Z. Ajji, A. Allahham, Optics and Laser Technology 43 (2010) 531.

[11]. S.J. Mathews, S. C. Kumar, L. Giribabu, S. V. Rao, Optics Communications 280 (2007) 206.

[12]. F. Z. Henari, S. Cassidy, Optik 123 (2011) 711.

[13]. P.N. Prasad, D.J. Williams, Introduction to Nonlinear Optical Effects in Organic Molecules and Polymers Wiley, New York, 1991.

[14]. P. Poornesh, G. Umesh, P.K. Hegde, M.G. Manjunatha, K.B. Manjunatha, A.V. Adhikari, Applied Physics B 97 (2009) 117.

[15]. C. Gayathri, A. Ramalingam, Spectrochimica Acta Part A 69 (2008) 980.

[16]. S. Kaladevi, C. Vijayan, M.P. Kothiyal, Optics and Laser Technology 38 (2006) 512.

[17]. M. Rashidian, D. Dorranian, S.A. Darani, S. Saghafi, M. Ghoranneviss, Optik 120 (2009) 1000.

[18]. Z. Dehghani, S. Nazerdeylami, E. Saievar-Iranizad, M.H. Majles Ara, Journal of Physics and Chemistry of Solids 72 (2011) 1008.

[19].] P.G.L. Frobel, S.R. Suresh, S. Mayadevi, S. Sreeja, C. Mukherjee, C.I. Muneera, Materials Chemistry and Physics 129 (2011) 981.

[20]. G. Sree Kumar, B. Valsala Milka, C.I. Muneera, K. Sathiyamoorthy, C. Vijayan, Optical Materials 30 (2007) 311.

[21]. K. Sathiyamoorthy, C. Vijayan, M.P. Kothiyal, Optical Materials 31 (2008) 79.

[22]. N. Ramamurthy, S. Dhanuskodi, M.V. Manjusha, J. Philip, Optical Materials 33 (2011) 607.

[23]. B. Abbas, M. Alshikh Khalil, Acta Physica Polonica, A 117 (2010) 904.

[24]. K.K. Nagaraja, S. Pramodini, A. Santhoshkumar, H.S. Nagaraja, P. Poornesh, D. Kekuda, Optical Materials, http://dx.doi.org/ 10.1016/j.optmat.2012.09. 028, in press

[25]. M. Sheik-Bahae, A.A. Said, and E.W. Van Stryland, Opt. Lett. 14(1989) 955.

[26]. M. Sheik-Bahae, A.A. Said, T.H. Wei, D.J. Hagan, and E.W. Van Stryland, Journal of Quantum Electronics, JQE QE-26 (1990)760.

[27]. K.P.Unnikrishnan, PhD thesis, Cochin University of Science and Technology, 2003.

[28]. Donald L.Wise, Gary E. Wnek, Derbra J.Trantolo, Thomas M.Cooper, Joseph D. Gresser, Photonic Polymer Systems, Marcel Dekker, New York, 1998.

[29]. H.Yuhua, Y. Yizhong, D. Jingxin, S. Zhenrong, and Z. Heping, Appl. Phys. Lett 80(2002)4855.

[30]. S.N.R Swatton, K.R. Welford, S.J.Till, J.R.Sambells, Appl. Phys. Lett. 66 (1995) 1865.

[31]. P. A. Miles, Appl. Opt. 33 (1994) 6965.

[32]. T. Xia, D. J. Hagan, A. Dogariu, A. A. Said, and E. W. Van Stryland, Appl. Opt. 36 (1997) 4110.

[33]. W.Tai-Huei, H. Tzer-Hsiang, L. Huang-Der and L. Sheng-Hsien, Appl.Phys.Lett. 67 (1995) 2266.

[34]. R.R. Birge, ed., American Chemical Society 240 (1994).

[35]. R. O sterbacka, C. P. An, X. M. Jiang, and Z. V. Vardeny, Science 287 (2000) 839.

[36]. S.R. Marder, J.E. Sohn, G.D. Stucky (Eds.), Materials for Nonlinear Optics: Chemical Perspectives, American Chemical Society,(1991).

[37]. G. Gustafsson, Y. Cao, G.M. Treacy, F. Klavetter, N. Colaneri, A.J. Heeger, Nature 357 (1992) 477.

[38]. H. Antoniadisa, B.R. Hsieha, M.A. Abkowitza, S.A. Jenekhea, M. Stolkaa, Synthetic Metals 62 (1994) 265.

[39]. J.A. Osaheni, S.A. Jenekhe, J. Perlstein, Applied Physics Letters 64 (1994) 3112.

[40]. S. N. Dixit, G. Dandan, and S. Mazumdar, Physical Review B, 43 (1991).

[41]. M. R. Salaneck, I. Lundstrom, W. S. Huang, and A. G. Mac-Diarmid, Synth. Met. 13 (1986) 291.

[42]. G. S. Maciel, C. B. de Ara´ujo, R. R. B. Correia, and W.M. de Azevedo, Opt. Commun. 157 (1998) 187.

[43]. G. Neetika, D. Kumar, Indian Journal of Engineering and Materials Science 16 (2009) 403.

[44]. H. L. Wang, R. J. Romero, B. R. Mattes, Y. T. Zhu, and M. J.Winokur, J. Polym. Sci., Part B: Polym. Phys. 38 (2000) 194.

[45]. D. L.Wise, G.E.Wnek, D. J.Trantolo, T. M.Cooper, J. D. Gresser, Photonic Polymer Systems, Marcel Dekker, New York, 1998.

[46]. B. Yi Soon, J.W.Haus, M. Scalora, C.Sibilia, Optics Express 11 (2003) 2007.

[47]. R.Tong, H. X. Wu, B. Li 2005 Physica B. 366 192.

[48]. S. H. Guang, C. H. Gen, N. P. Paras, Opt. Lett. 20 (1995) 435.

[49]. C. L. Ji, K. W. Chuan , G. Faris, Phys. Rev. A. 76 (2007) 053804.

[50]. S. Sunita, M. Devendra, S. K. Ghoshal, Opt. Commun. 281 (2008) 2923.

[51]. Chapter 6, New Developments in Liquid Crystals, Gun Yeup Kim, and Chong Hoon Kwak, Yeungnam University, South Korea

[52]. M. A. Kramer, W. R. Tompkin, and R. W. Boyd, Phys.Rev. A 34 (1986) 2026.

[53]. F. E. Hernandez, A. O. Marcano, Y. Alvarado, Opt.Commun. 152 (1998) 77.

[54]. U. Tripathy, R. J. Rajesh, P. B. Bisht, and A. Subrahmanyam,Chem. Sci. 114 (2002) 557.

[55]. G. Vinitha and A. Ramalingam, Laser Phys. 18, 37(2008) 1176.

[56]. L. X. Wang, F. Pei, S. Peng, Proc. SPIE 6029 (2006) 370 .

[57]. H. Tomoharu, T.Nagashima, N. Sugimoto, Opt. Commun. 250 (2005) 411.

[58]. H. I. Elim, W. Ji, A. H. Yuwono, Appl. Phys. Lett .82 (2003)2691.

[59]. P.G.L. Frobel, S.R. Suresh, S. Mayadevi, S. Sreeja, C. Mukherjee, C.I. Muneera, Materials Chemistry and Physics 129 (2011) 981.

[60]. K.K. Nagaraja, S. Pramodini, A. Santhosh Kumar, H.S. Nagaraja, P. Poornesh, D. Kekuda, Optical Materials, http://dx.doi.org/ 10.1016/ j.optmat. 2012.09. 028, in press

[61]. F.M. Quereshi, S.J. Martin, X. Long, D.D.C. Bradley, F.Z. Heneri, W.J. Balu, E.C. Smith, C.H. Wang, A.K. Kar, H.L. Anderson, Chem. Phys. 231 (1998) 87.

.....ꕥ.....

Chapter 7

LIGHT AMPLIFICATION IN DYE DOPED NANOCOMPOSITES: TiO_2 - POLYANILINE COMPOSITE AS A POTENTIAL DYE LASER GAIN MEDIUM

Contents

The development of solid state dye lasers has paved the way for intense research in incorporating dye molecules into solid matrices with different host materials to get a gain medium of high optical quality and photostability. Random laser effects have been observed in a variety of organic and inorganic gain media including powders of solid-state luminescent and laser crystals,], liquid laser dyes with scatterers, polymeric films with and without intentionally introduced scatterers etc. Random lasers are very attractive for a variety of applications; low coherent random laser sources can be advantageous in holography, laser inertial confinement fusion (driver sources for mega joule lasers), transport of energy in fibers for medical applications etc.

7.1. Introduction

The research on lasing action in scattering gain media has attracted considerable attention in the past few decades due to its extraordinary properties, such as omni-directional emission and small dimension. When laser light propagates through a scattering medium containing dielectric micro or nano spheres, above a threshold concentration of scattering centres, light gets trapped inside the medium thereby stopping the forward propagation of light. This phenomenon is called Anderson localisation of light which was predicted by Sajeev John and experimentally confirmed by Storzer [1, 2]. The

light emitted from the random amplifying media exhibits similar optical characteristics of real laser light and have many potential applications using the Anderson localization with lasing action. The laser action has been observed in a great variety of disordered media including scattering materials combined with dye molecules, and the phenomena have been extensively studied by a number of researchers[3].Random laser effects have been observed in a variety of organic and inorganic gain media including powders of solid-state luminescent and laser crystals [4,5], liquid laser dyes with scatterers [6], polymeric films with and without intentionally introduced scatterers [7], ZnO scattering films and nanoclusters[8], dye-infiltrated opals [9], porous media infiltrated with liquid crystals with dyes [10] and many others.

The random laser was first predicted theoretically by Letokhovin 1968 **[**11**]** and was then observed experimentally by Lawandy **[**12**]** in dye solution and by Cao [13] in ZnO powder. Random lasers (RL) are unique sources of stimulated emission in which the feedback is provided by scattering in a gain medium **[**14,**].** Random laser is a system formed by elastic scatterers with random distribution, embedded in the optical gain medium [15, 16**].**The multiple scattering of light in the optical media replaces the traditional laser optical cavity. They are very attractive for a variety of applications; low power coherent random laser sources can be advantageous in holography, laser inertial confinement fusion, transport of energy in fibers for medical applications etc because of their extreme simplicity, low cost and robustness in operation. Random lasers are strongly scattering media that amplify light [17]. A random lasing is different from the conventional lasing since it does not require any cavity mirrors in its feedback mechanism **[**18**].** An example is the observation of a threshold for lasing action and frequency narrowing in

random lasers [17]. The feedback process in a random lasing is provided by optical scatterings in a disordered media. Evidently, the optical properties of random lasers are quite different from those of conventional lasers: the propagation of pump and fluorescence light is diffusive in a random laser. Since feedback is provided by multiple scattering, the random laser threshold is lowered by a stronger scattering, i.e., a shorter transport mean free path, because the feedback is more efficient. It has been shown that the threshold in random lasers is reduced dramatically when the photon transport mean free path approaches the stimulated emission wavelength [17**].**

At present, in the random laser experiments, a number of random laser emission phenomena of organic-inorganic disordered structure media are observed such as the spread nanoparticles laser dye, neodymium that doped with crystalline powder, ceramic, polymer, semiconductor nanoparticles, organic biological tissue, and liquid crystal **[**16, 19, 20**].** Each specific features and form of random media lead to the special feedback mechanism, so that it is difficult to use the same theory to describe all random laser phenomena.

The optical wave propagating through the laser cavity forms a standing wave between the two mirror facets of the laser. The distance L between the two mirrors determines the period of oscillation of this wave. This standing optical wave resonates only when the cavity length 'L' between the two mirrors is an integer number multiple of half wavelengths. Fig.7.1. shows the schematic representation of various longitudinal modes in a laser cavity. In other words, a node must exist at each end of the cavity. The only way this can take place is for 'L 'to be exactly a whole number multiple of half wavelengths λ/2. This means that $L = m(\lambda/2)$, where λ is the wavelength of light in the medium and is related to the wavelength of light in free space through the index of refraction n

by the relationship $\lambda = \lambda_o/n$. As a result, there can exist many longitudinal modes in the cavity of the laser system, each resonating at its distinct wavelength of $\lambda_m = 2L/m$. From this we can note that two adjacent longitudinal laser modes are separated by a wavelength of $\Delta\lambda = (\lambda_o)^2/2nL$.

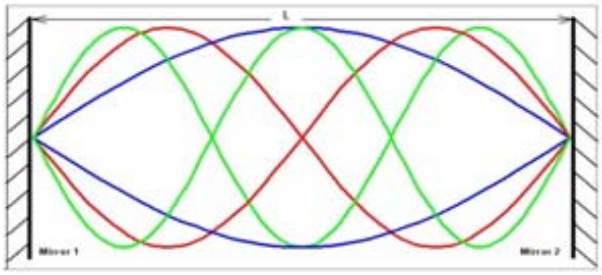

Fig.7.1.Schematic representation of various longitudinal modes in a laser cavity

Longitudinal modes refer to the simultaneous lasing at several discrete frequencies related to axial field distribution within the lasing cavity, all of which compete for gain dominance within the lasing medium. Each mode can be thought of as an intensity (Lorentzian) peak with a given frequency bandwidth characterized by the full width at half maximum (FWHM) of the peak. The free spectral range (FSR) is characterized by the frequency spacing between these neighbouring peaks and can be calculated in terms of wavelength as $\Delta\lambda = (\lambda_o)^2/2nL$,where L is the cavity length. It is the job of the extended cavity feedback to contribute to the reduction of the modality of the laser to single mode operation, to narrow the bandwidth of a single mode. The external cavity accomplishes this effect by helping to dictate what wavelengths of light have dominance in gain within the lasing cavity.

Fig.7.2, Fig.7.3 and Fig.7.4. show the gain selection of a single mode by gain profile of dye laser, extended cavity mode structure modulated by lasing cavity mode structure and single external cavity mode gain selected by gain profile and single lasing mode respectively.

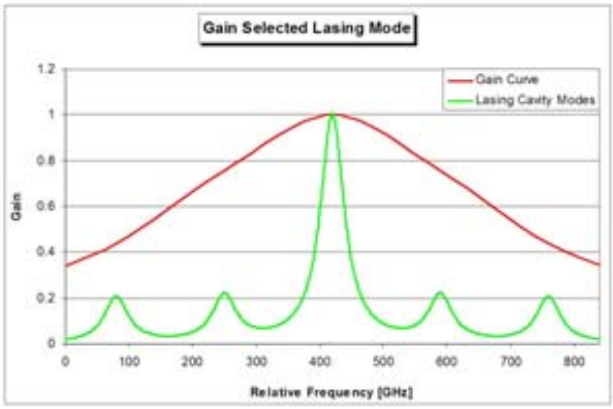

Fig.7.2.Gain selection of a single mode by gain profile of dye laser

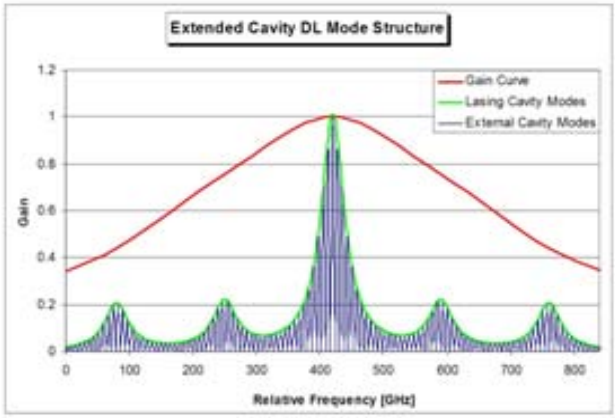

F.g.7.3.Extended cavity mode structure modulated by lasing cavity mode structure

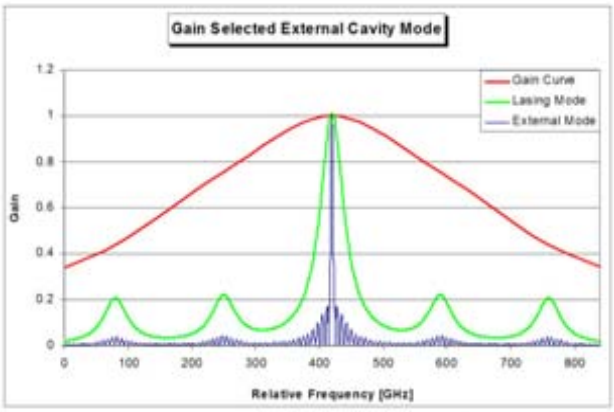

Fig.7.4. Single external cavity mode gain selected by gain profile and single lasing mode

As mentioned, the modes that have been discussed so far are referred to as longitudinal modes and correspond to the longitudinal direction of the resonating cavity. Notwithstanding, there also exist transverse modes that correspond to the spatial variation in the beam intensity cross section in the transverse direction of the lasing medium. These spatial variations are Gaussian in shape and are the result of the spatial variation of the electromagnetic field and the refractive index across of the lasing medium. Typically, modes of different orders with multiple peaks overlap, resulting in a complex output intensity profile with a given number of spatially separated and overlapping peaks.

In the present work, we have studied random laser emission in aqueous solutions of rhodamine 6G laser dye (R6G) mixed the conjugated polymer, polyaniline along with nano TiO_2. Studies were carried out at different dye concentrations of 10^{-3}, 10^{-4} and 10^{-5} M and pump power so as to get information regarding concentration dependence and pump power dependence on the lasing behaviour.

Experimental: Chemicals and Preparation:

Rhodamine 6G laser dye ($C_{28}H_{31}N_2O_3Cl$) with molecular weight 479.02 g/mol was supplied by Lambda Physics LC (5900), Aniline by (SD Fine Chemicals), Ammonium peroxodisulphate by (MERCK), Con.HCl (SDFCL).

Polyaniline was prepared via hydrothermal route. First aniline monomer was dissolved in 1M HCl and a 1M solution of the oxidant ammonium peroxodisulphate is added dropwise. The reaction proceeds in an ice bath under constant stirring. The resulting black precipitate thus obtained was sonicated for about one hour. The mixture was then transferred in to an autoclave and subjected to hydrothermal treatment at110^oC over night. It was

then filtered, washed with water and acetone to remove any unreacted monomer and dried at 110^{o}C to get polyaniline powder.

Experimental technique

In the experimental setup, the laser dye containing aqueous dispersion of polyaniline samples were placed in cuvettes of length of 3cm, and width of 1mm. The pumping source used was a frequency doubled Q-switched Nd: YAG laser (Spectra Physics, 532 nm, 10 Hz). A set of calibrated neutral density filters were used for varying the pump energy. The pump power was measured by using 'COHERENT Labmater Power meter' and it is varied from 6.5 to 7.5 mW. The laser emission was recorded using a collecting fiber coupled to a monochromator-CCD system (Spectra Pro) with a resolution of 0.03 nm. A high-speed photodetector and an oscilloscope (Tektronix) were used to measure the temporal intensity profile of the emitted laser pulse.

7.2. Results and Discussion:

Following studies were carried out.

1) Laser induced fluorescence emission and its amplification characteristics as a function of Rh 6G dye concentration.
2) Dependence of fluorescence emission characteristics of Rh 6G dye solution on pump power.
3) Influence of PANI, TiO_2 and PANI-TiO_2 on the lasing characteristics of Rhodamine 6G solution.

Fluorescence emission characteristics of Rhodamine 6G solution

Following are the main observations

a) Fluorescence emissions were observed when concentration was not raised to 10^{-5}M concentration. Emission was not observed at 10^{-5} M concentration

even at a pump power of 170mw.As the dye concentration is increased, spectral emission was broadened with enhancement in the emission.

b) When concentration was increased there was a concentration dependent red shift in the fluorescence emission due to overlap of absorption and emission spectra of the dye.

c) At a high concentration of 10^{-3}M concentration the long wavelength emission at 572 nm becomes prominent in comparison with that at 566 nm region. This is due to the fact that major component of emission was reabsorbed to emit fluorescence at long wavelength region. Due to the availability of large number of dye molecules in the medium, mode structure in the emission was also observed, with complex mode structure arising from the overlap of transverse and longitudinal modes.

In short, the dye solution shows longer wavelength amplified emission in comparison with that at shorter wavelength region. This is due to absorption and re emission of fluorescence emission.

When TiO_2 and PANI were introduced into the dye solution, the longer wavelength emission was found to get suppressed completely with enhancement in the shorter wavelength region. An important finding in the present study is that PANI can suppress the usual concentration dependent red shift and fluorescence quenching in the dye solution, details of which are given below.

Effect of PANI, TiO_2 and combination of PANI-TiO_2 on fluorescence emission of Rhodamine 6 G solution

1) At low dye concentration (10^{-4}M) presence of TiO_2, PANI and their mixture reduce the fluorescence emission intensity of Rhodamine 6G solution (Fig.7.6.).

2) In PANI-TiO_2 mixture in dye solution enhancement in the emission is observed by increasing the fraction of PANI. It should be noted that in all these cases the emission intensity does not exceed to that of dye solution alone (Fig.7.6.).

3) When dye concentration was increased to 0.5mM we find enhanced fluorescence emission around 565nm (Fig.7.5.) and on further increase in the concentration to 1mM and a pump power of 65mw (Fig.7.11.) enhancement in fluorescence emission due to PANI and TiO_2 was observed.

Dye solution in presence of PANI shows well defined longitudinal modes. However on reducing the pump power to 14mw at 1mM dye concentration (Fig.7.9) PANI generates well defined mode structure in the amplified emission.

The separation between the modes can be calculated using the formula

$\Delta\lambda = (\lambda_o)^2/2nL$, where 'n' is the refractive index (1.6) and 'L'is the length of the cell (1mm).

The calculated and observed mode separations were found to agree with each other within the constraints of accuracy in experimental method.

Studies show that PANI is a good component in the dye solution so as to get amplified emission around 566 nm region in the case of rhodamine 6G.TiO_2 unlike in the case of PANI does not exhibit mode structure in the fluorescence emission of rhodamine 6G solution. This is due to the fact that TiO_2 will broaden the emission spectrum due to multiple scattering thereby masking the mode structure.

1. Effect of dye concentration on lasing action

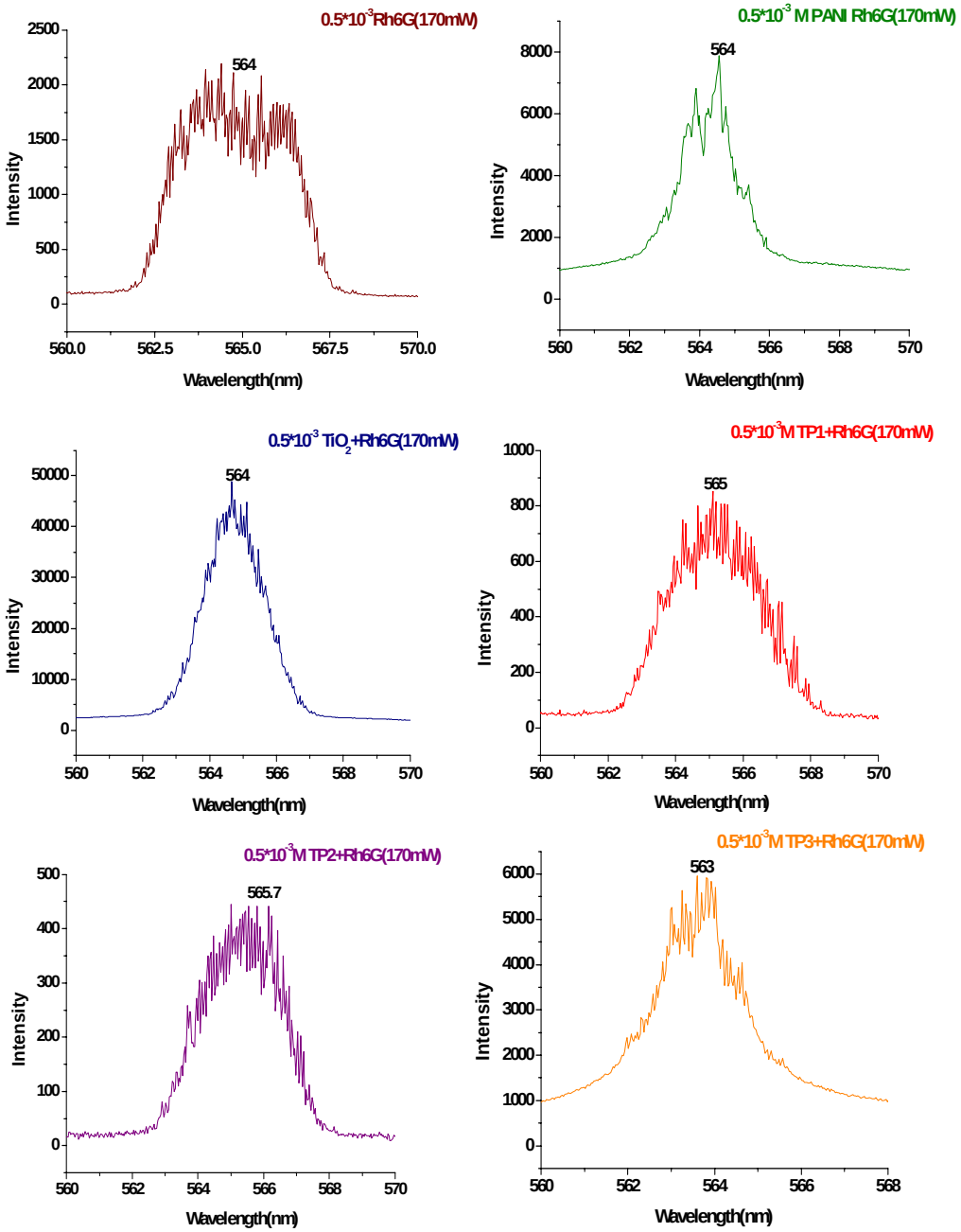

Fig.7.5. Fluorescence emission spectrum of Rh 6G,PANI,TiO_2 and TiO_2-PANI composites in 0.5 mM Rh6G dye solution (pump power is 170 mW)

For $0.5*10^{-3}$ M dye concentration, presence of TiO_2 in the dye solution was found to enhance the fluorescence of Rh 6 G dye solution with reference to that of the presence of PANI alone(Fig.7.5.). This enhancement is due to increase in the effective path length of the pump beam due to multiple scattering. However when the dye concentration is increased to 10^{-3} M, it was found that the emission intensity was more in the case of PANI rather than that of TiO_2.This is due to the fluorescence quenching arising from the increase in effective pump beam optical path length in the medium, as a result of increased scattering with TiO_2.

From our observations, it can be concluded that PANI acts as a sensitizer in the fluorescence emission of dye solution.

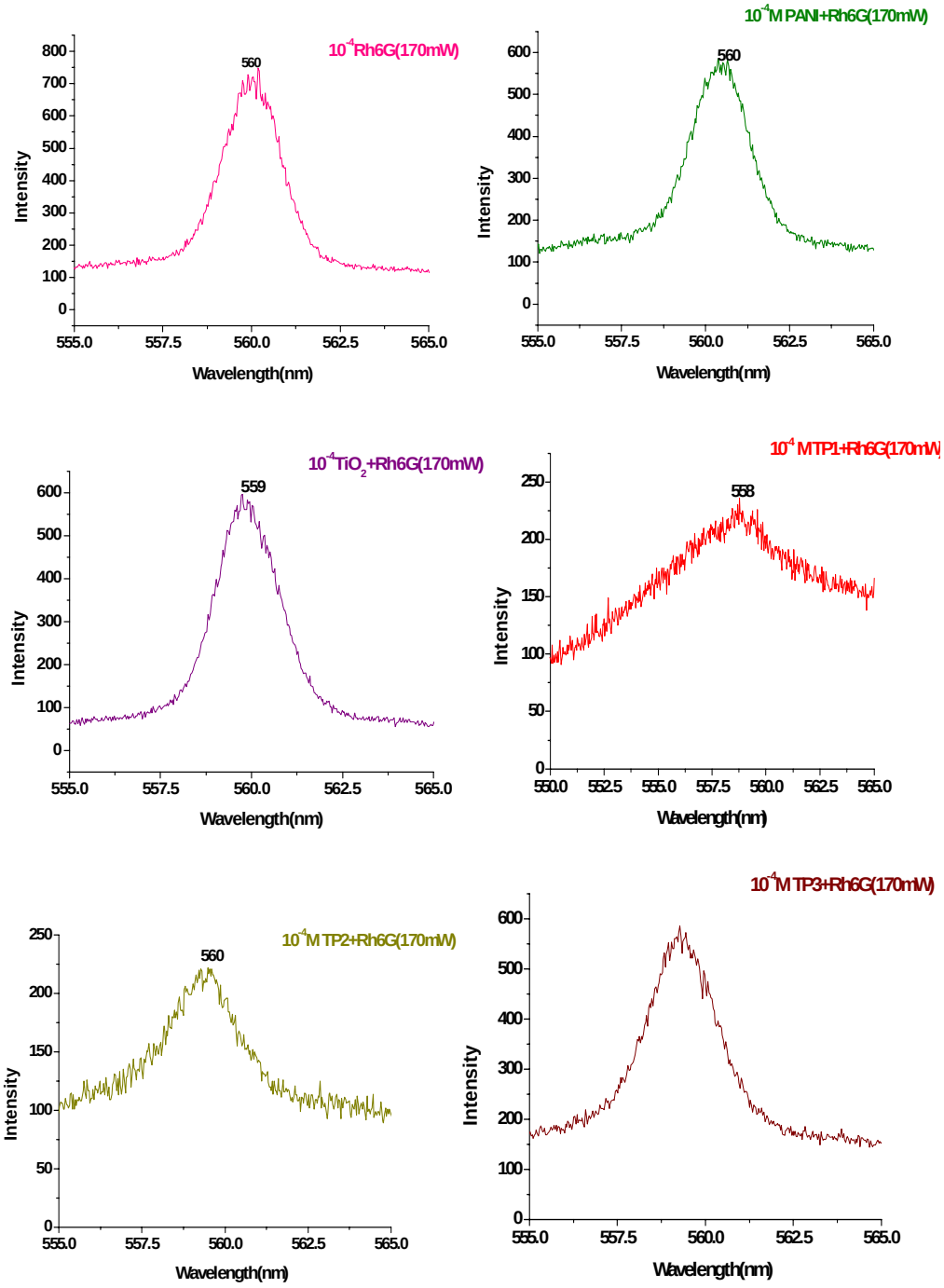

Fig.7.6. Fluorescence emission spectrum of Rh 6G, PANI, TiO_2 and TiO_2-PANI composites in 10^{-4} M Rh6G dye solution (pump power is 170 mW)

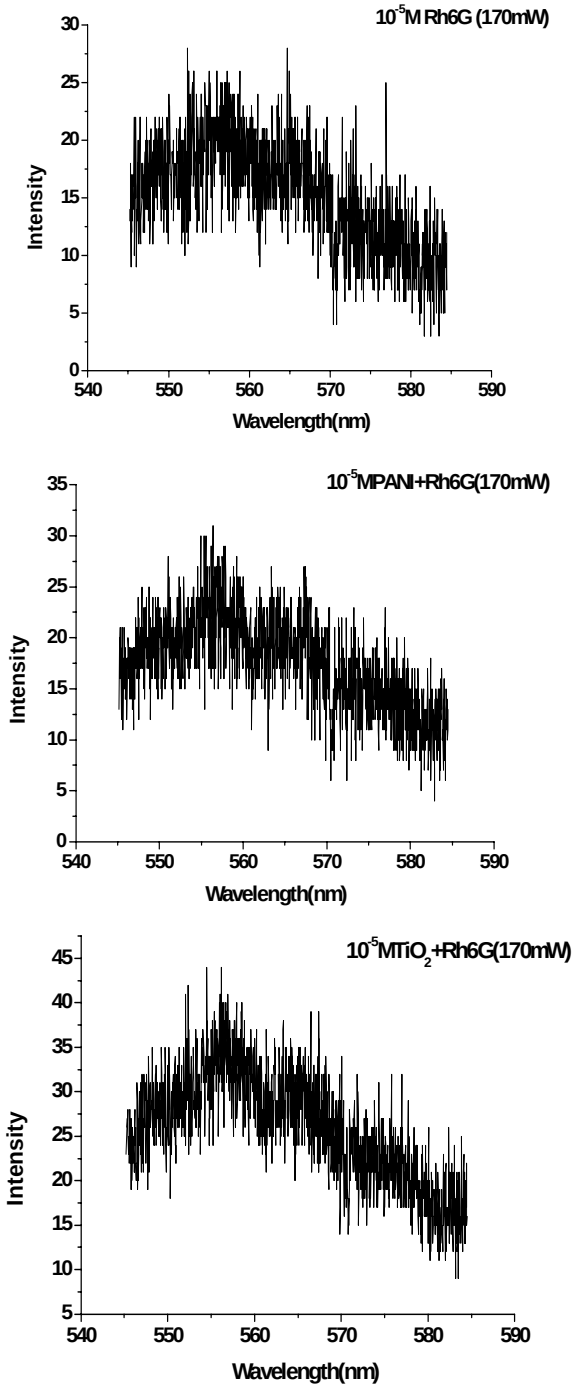

Fig.7.7. Fluorescence emission spectrum of Rh 6G, PANI, TiO_2 in 10^{-5} M Rh6G dye solution (pump power is 170 mW)

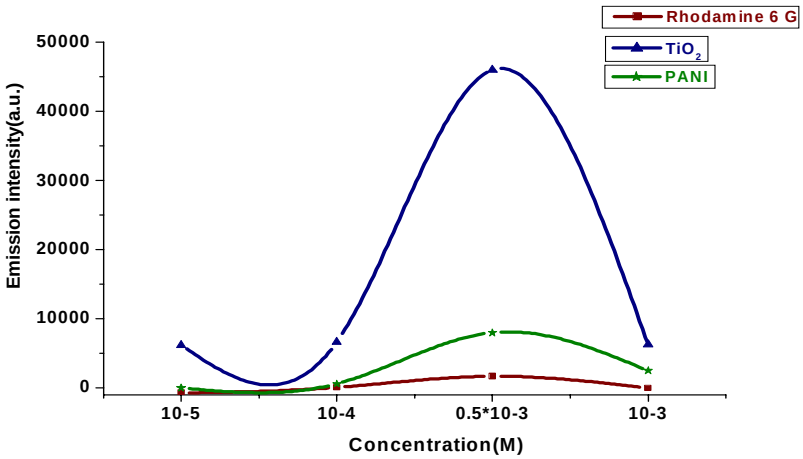

Fig.7.8.Concentration dependence on emission intensity

Fig.7.8. shows the Concentration dependence on emission intensity. From the figure (concentration dependence on emission intensity) we can draw the following conclusions.

The fluorescence emission intensity gets enhanced in the 560 nm region with complete quenching of the emission at around 570 nm. This confirms the fact that TiO_2/PANI will diminish the concentration quenching in dye solution due to the dye concentration. The fluorescence characteristics of the composite laser media show the similar behaviour of increase in emission at low concentration with concentration quenching after the optimum concentration of the fluorescence emission. However, the range of dye concentration where increase in fluorescence emission is found to get enhanced in presence of PANI and TiO_2.This is an important finding in the present study.

2. Effect of pump intensity on lasing action

Fig.7.9. to 7.11. shows the effect of pump intensity on lasing action.

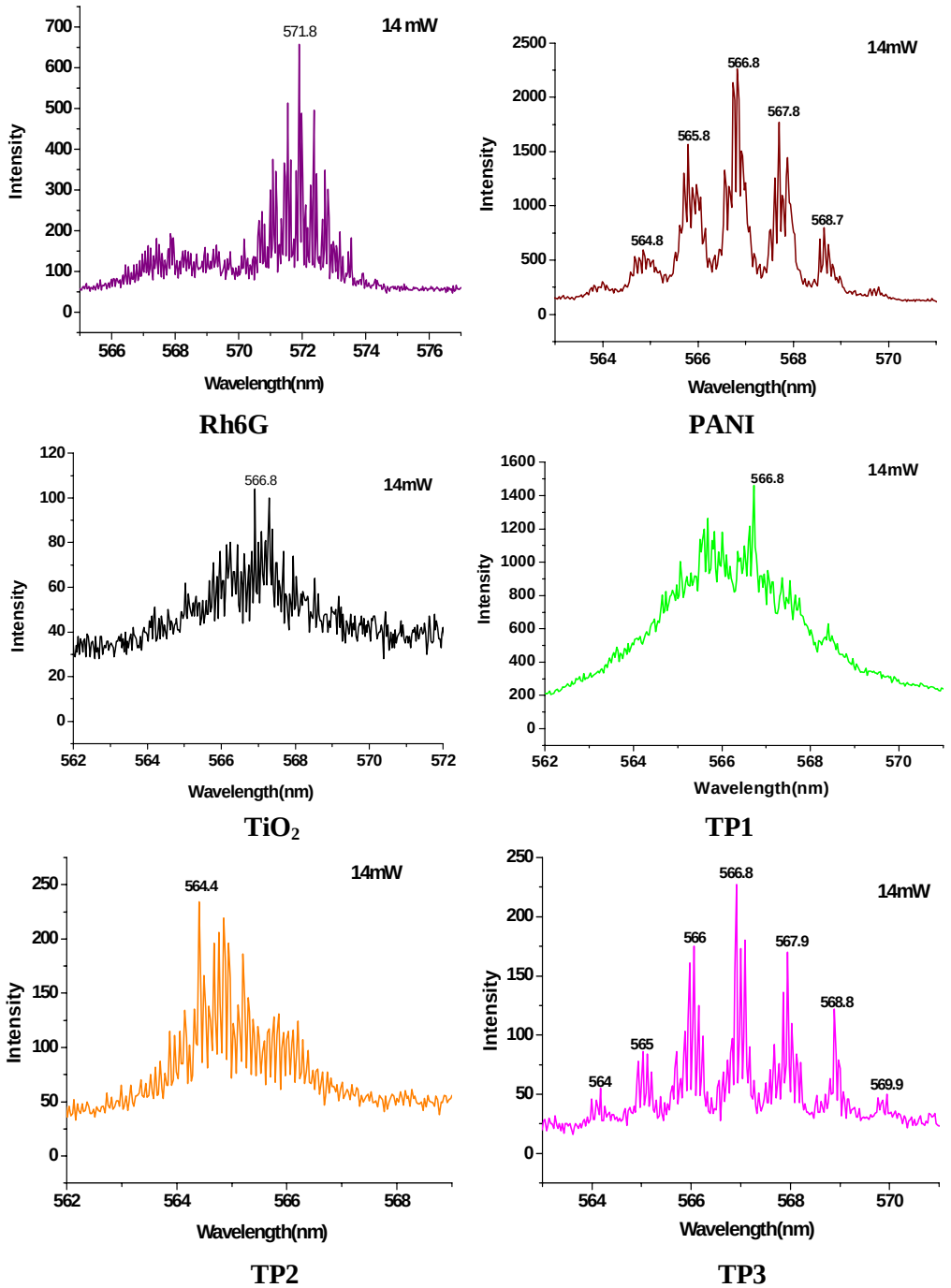

Fig.7.9. Fluorescence emission spectrum of Rh 6G, PANI, TiO_2 in 10^{-3} M Rh6G dye solution (pump power is 14 mW)

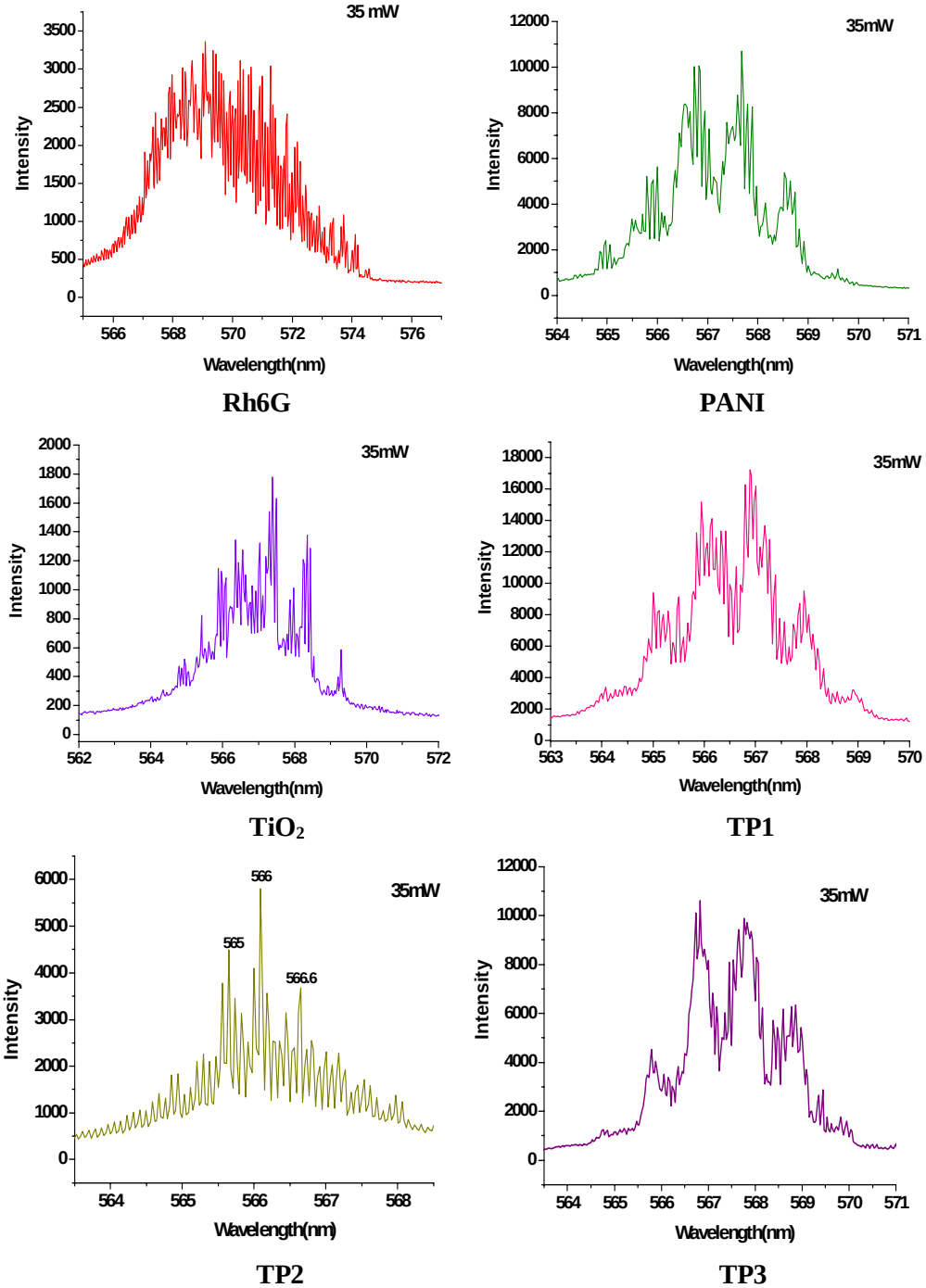

Fig.7.10. Fluorescence emission spectrum of Rh 6G, PANI, TiO_2 in 10^{-3} M Rh6G dye solution (pump power is 35 mW)

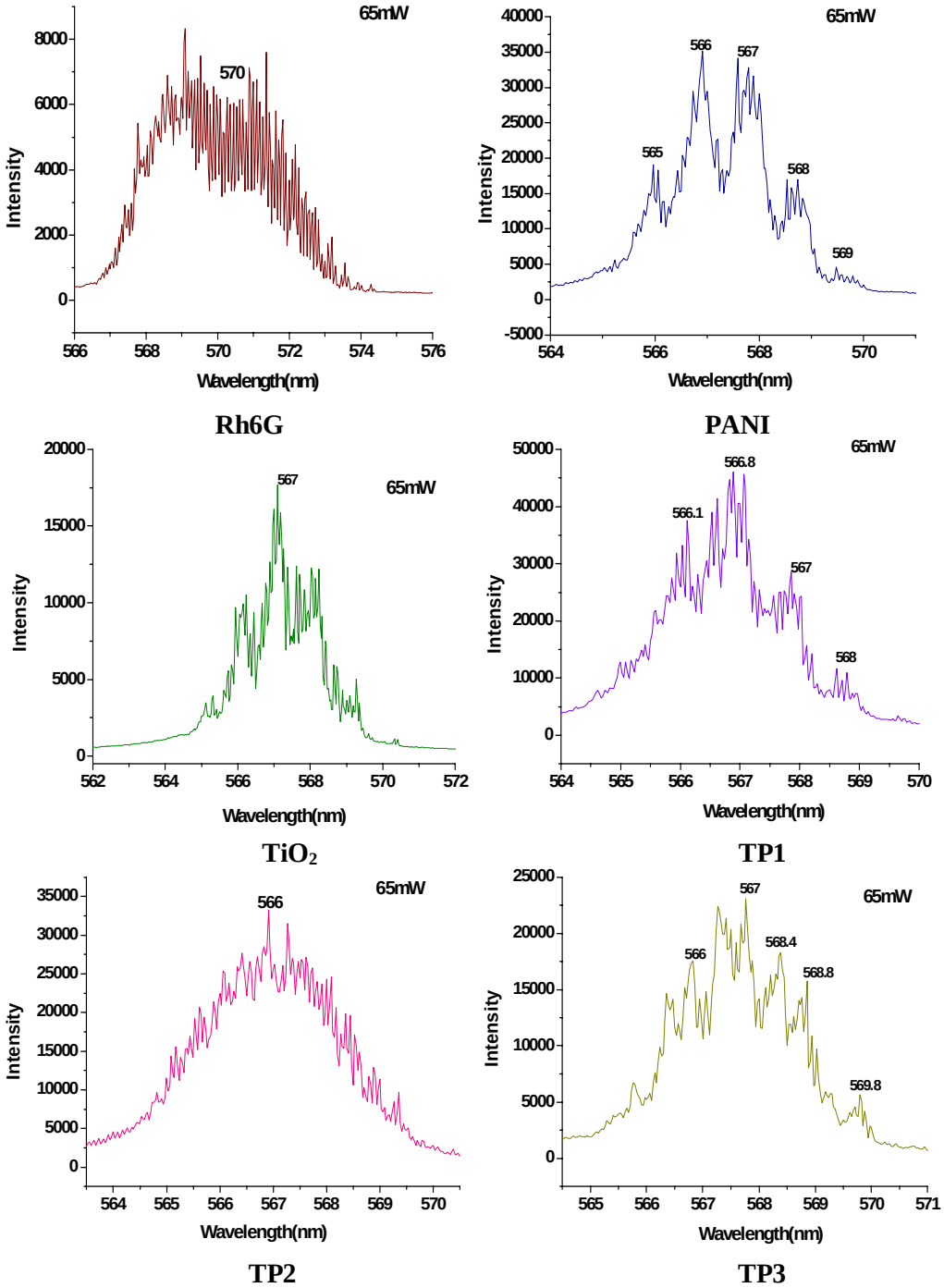

Fig.7.11. Fluorescence emission spectrum of Rh 6G, PANI, TiO_2 in 10^{-3} M Rh6G dye solution (pump power is 65 mW)

7.3 Conclusions:

Studies show that PANI and TiO_2 influence lasing characteristics of rhodamine 6G solution. The long wavelength emission of rhodamine 6G due to reabsorption and emission is suppressed by TiO_2 and PANI as clear from the figure. It was found that the line width of emission is reduced to very low values if we are able to select a particular longitudinal mode. All the studies were made in the liquid form. We can make thin films or thin rods, which will be useful in solid state laser medium.

References

[1]. Sajeev John, Physical review letters 58(1987)2486.

[2]. M. Storzer, P.Gross, C. M. Aegerter, G. Maret, Phys. Rev. Lett. 96 (2006) 63904.

[3]. H. Liu, X. Zhang, S.Jing, Z. Ren, Journal of Optics A: Pure and Applied Optics, J. Opt. 14 (2012) 055203

[4]. D. Anglos, A. Stassinopoulos, R. N. Das, G. Acharakis, M. Psyllaki, R.Jakubiak, R.A. Vaia, E. P. Giannelis, and S. H. Anastasiadis, J. Opt.Soc. Am. B 21(2004)208.

[5]. A. M. Brito-Silva, G. André, S. L. Anderson, J. J. Alcenisio, B. A.Cid, Appl. Phys. 108(2010) 033508.

[6]. G.Zacharakis, N. A. Papadogiannis, T. G. Papazoglou, Appl. Phys. Lett. 81(2002)2511.

[7]. R.C. Polson, A. Chipoline, Z. V. Vardeny, Adv. Mater. 13(2001)760.

[8]. H. Cao, Y. Ling, J. Y. Xu, C. Q. Cao, and P. Kumar, Phys. Rev. Lett. 86(2001)4524.

[9]. M. N. Shkunov, M. C. DeLong, M. E. Raikh, Z. V. Vardeny, A. A.Zakhidov, R. H. Baughman, Synthetic Met. 116(2001) 485.

[10]. D. Wiersma, and S. Cavalier, Nature 414(2001)708.

[11]. V.S.Letokhov, Sov. Phys. JETP 26(1968)835.

[12]. N. M.Lawandy, R. M Balachandran, A. S. L. Gomes, E.Sauvain, Nature 368 (1994) 436.

[13]. H.Cao, Y. G. Zhao, S. T. Ho, E. W. Seelig, Q. H. Wang, R. P. H. Chang, , Phys. Rev. Lett. 82(1999) 2278.

[14]. V S Letokhov, JETP Lett. 5 (1967)212.

[15]. V.M.Markushev, V.F. Zolin, C.M. Briskina, Sov. J. Quantum Electron. 16 (1986) 281.

[16]. M. A. Noginov, Solid-State Random Lasers (Springer, Berlin, 2005)

[17]. B. T. Chiad, M.A. Hameed, K. H. Latif, F. J. AL- Malikim, Journal of the European Optical Society - Rapid Publications 6(2011) 11049.

[18]. D. Wiersma, Nature, London, 406(2000)132.

[19]. D. S. Wiersma, Nature Physics 4(2008)359.

[20]. H. Cao, J. Waves Random Media 13(2003) R1.

Chapter 8

SUMMARY AND CONCLUSIONS

Contents

Significant scientific and technological interest has focused on polymer-inorganic nanocomposites (PINCs) over the last two decades. The use of inorganic nanoparticles into the polymer matrix can provide high-performance novel materials that find applications in many industrial fields. The integration of inorganic nanoparticles into a polymer matrix allows both properties from inorganic nanoparticles and polymer to be combined/enhanced and thus advanced new functions can be generated to the PINCs. Research in functional hybrid organic–inorganic materials is being mostly supported by the growing interest of chemists, physicists, biologists and materials scientists to fully exploit this opportunity for creating smart materials benefiting from the best of the three realms: inorganic, organic and biological. In addition to the high versatility in chemical and physical properties and shaping, hybrid nanocomposites present the paramount advantage to both facilitate integration and miniaturization, therefore opening a land of promising applications in many fields: optics, electronics, ionics, mechanics, membranes, functional and protective coatings, catalysis, sensors, biology, medicine, biotechnology, etc. The present work is mainly focussed on the synthesis, characterization and various application studies of conducting polymer modified TiO_2 nanocomposites.

8.1. Summary

The present thesis comprises of 8 chapters including introduction, experimental, physico chemical characterization and application studies.

Chapter 1 deals with a general introduction about hybrid nanocomposites, their different synthesis strategies and their properties and applications. Also contains a general introduction to photocatalysis by TiO_2, thermal diffusivity measurement by thermal lens technique, nonlinear optics, and lasing studies.

Chapter 2 describes the synthesis procedure of TiO_2 conducting polymer nanocomposites. This chapter also gives a brief description about the various techniques used for physico-chemical characterization. Pure TiO_2 was prepared via P123 assisted hydrothermal technique and the precursor used is titanium tetra isopropoxide. The polymer modified nanocomposites were also prepared via hydrothermal route. Prepared nanocomposite systems were characterized by XRD, UV-Vis.DRS, FT-IR Spectroscopy, SEM-EDX, Thermogravimetric analysis, Raman spectroscopy, TEM, XPS and BET surface area. Conductivity measurements of the prepared systems were done using standard 4-probe method.

Chapter 3 describes in detail the results of various physico-chemical characterizations of the prepared nanocomposite systems. The phase purity and crystalline nature of the prepared systems were obtained from XRD analysis. All the prepared systems contain TiO_2 in the anatase phase. This is also confirmed by Raman analysis. Low angle XRD pattern shows that pure TiO_2 is mesoporous in nature and the ordering of structure is retained only on forming composite with polyaniline. But on composite formation with polypyrrole

and polythiophene the structural order is destroyed. From UV-Vis.DRS analysis it is evident that the conducting polymers acts as good sensitizing material for TiO_2 and on composite formation the resulting nanocomposite photocatalyst can be activated by absorbing both the ultraviolet and visible light (λ = 190–800 nm) to give a maximum visible light harvesting, and is a promising photoelectric conversion and photocatalytic material for the efficient use of light, especially sunlight. FT-IR spectroscopy confirms the incorporation of polymer with TiO_2 .Thermal analysis TG-DTG reveals the thermal stability of the prepared nanocomposite systems. Surface morphology of the nanocomposite systems was obtained from SEM and TEM.N2 adsorption - desorption isotherms of all the samples show representative type IV isotherm which is characteristic of mesoporous materials. The elemental composition of the prepared systems was obtained from EDX and XPS analysis. In EPR analysis the TiO_2-conducting polymer composites, the spectrum shows a signal having 'g'value approximately equal to 2.004. Such a sharp symmetrical ESR signal, of which g value is close to that of free electron is typical in organic radicals or polaron species formed in conducting polymers.

Chapter 4 mainly discusses the photocatalytic degradation of cationic dyes such as Rhodamine B and malachite green **,** nitrophenol, phenol, endocrine disruptor bisphenol-A, antibiotic sulfamethoxazole and the photocatalytic antibacterial activity. In the degradation reaction reactions various reaction parameters such as effect of catalyst amount, effect of time, effect of lamp power and the effect of various catalytic systems were studied.

Chapter 5 discusses the thermal diffusivity measurements of TiO_2/polyaniline nanocomposite systems using thermal lens technique. The thermal lens technique is based on measurement of the temperature rise that is produced in an illuminated sample as a result of nonradiative relaxation of the energy absorbed from a laser. Because the technique is based on direct measurement of the absorbed optical energy, its sensitivity is higher than conventional absorption techniques. The composite material can be used as a good coolant material which will diffuse heat from the medium at faster rate as polyaniline component increases in the composite material.

Chapter 6 discusses the third order nonlinear properties of bare and polyaniline modified TiO_2 nanocomposite systems. Z scan technique is used to study the third order nonlinear optical properties. Thin films of the samples were prepared via tape casting technique. The polyaniline modified TiO_2 nanocomposites show reversible saturable absorption and they act as good optical limiting materials.

Chapter 7 presents the lasing applications of polyaniline modified TiO_2 systems. These nanocomposites act as a potential dye laser gain medium. The dye used is Rhodamine 6G.In this study lasing like sharp peaks are observed possibly due to the optical feedback process of the multiple light scattering induced by TiO_2 nanoparticles embedded within the hybrid polymer.

Chapter 8 presents the summary and major conclusions drawn from various investigations**.**

8.2. Conclusions

The conclusions of the present work are outlined below:

- Mesoporous TiO_2 was prepared by the cationic surfactant P123 assisted hydrothermal synthesis route and conducting polymer modified TiO_2 nanocomposites were also prepared via the same technique.
- All the prepared systems show XRD pattern corresponding to anatase phase of TiO_2, which means that there is no phase change occurring even after conducting polymer modification.
- Raman spectroscopy gives supporting evidence for the XRD results. It also confirms the incorporation of the polymer.
- The mesoporous nature and surface area of the prepared samples were analysed by N_2 adsorption desorption studies and the mesoporous ordering can be confirmed by low angle XRD measurement.
- The morphology of the prepared samples was obtained from both SEM & TEM. The elemental analysis of the samples was performed by EDX analysis.
- The hybrid composite formation is confirmed by FT-IR spectroscopy and X-ray photoelectron spectroscopy.
- All the prepared samples have been used for the photocatalytic degradation of dyes, antibiotic, endocrine disruptors and some other organic pollutants. Photocatalytic antibacterial activity studies were also performed using the prepared systems.

Polyaniline modified TiO_2 nanocomposite systems were found to have good antibacterial activity.

- Thermal diffusivity studies of the polyaniline modified systems were carried out using thermal lens technique. It is observed that as the amount of polyaniline in the composite increases the thermal diffusivity also increases. The prepared systems can be used as an excellent coolant in various industrial purposes.
- Nonlinear optical properties (3^{rd} order nonlinearity) of the polyaniline modified systems were studied using Z scan technique. The prepared materials can be used for optical limiting applications.
- Lasing studies of polyaniline modified TiO_2 systems were carried out and the studies reveal that TiO_2 - Polyaniline composite is a potential dye laser gain medium.

.....ꕥ.....

SEMINARS AND WORKSHOPS ATTENDED

[1]. International Conference on Materials for the new Millennium (MatCon2010); 13-1-2010.

[2]. UGC Sponsored National Seminar on Chemistry and Environment (Department of Chemistry, St.Pauls College Kalamassery) 2, 3, 4th September 2010.

[3]. Sandhya K.P., Suja Haridas, S.Sugunan- **A Comparative study of the Photocatalytic activity of supported and Non-supported Titania-polyaniline Composites under visible light irradiation**-International Conference on Advanced Oxidation Process (AOP 2010) September 18-21 (2010).

[4]. Sandhya K.P., Suja Haridas, S.Sugunan- **Effective photo degradation of various dyes by visible light sensitized Titania- Polyaniline composites**-20th National symposium on Catalysis IIT Madras December 2010(19-22 December 2010).

[5]. Sandhya K.P., Suja Haridas, S.Sugunan- **TiO_2 /WO_3 composites –An efficient photocatalyst for the degradation of Rhodamine B**-CTriC 2011 CUSAT March 2011 (4-5 March 2011)-National Seminar.

[6]. Sandhya K.P., S.Sugunan*- **Effect of Polypyrrole Content on the Photocatalytic activity of Titania**- CTriC 2012; CUSAT; January 2012(20-21 January 2012) -National Seminar.

[7]. Sandhya K.P., S.Sugunan*-**TiO_2-Polyaniline Composites –An Efficient Visible Light Photocatalyst for Sulfamethoxazole Degradation (Oral Presentation)**-21st National Symposium on Catalysis, (CATSYMP-21), "Catalysis for Sustainable Development, February10-13, 2013.

[8]. Sandhya K.P., S.Sugunan***TiO_2-Polyaniline Nano Composites –A Promising Visible light Photocatalyst for dye degradation**-National Seminar on Nanoscience and Technology, February15, 16-2013 Department of science and Humanities, Sree Narayana Gurukulam College of Engineering, Kolenchery.

[9]. Sandhya K.P., S.Sugunan -**Titania-Polyaniline Composite: An Efficient Photocatalyst for the Oxidation of Cyclohexene**-National Conference on Advances in Organic and Physical Chemistry (*AOPChem-2012)* 22 & 23 March 2012(University of Calicut).

[10]. Sandhya K.P., S.Sugunan- **TiO_2-Polypyrrole Composites –An Efficient Visible Light Photocatalyst for Phenol Degradation** -National conference on Emerging Technologies for the Processing and Utilization of Beach Sand Minerals (Reaindia) March 1-2,2013.

[11]. Sandhya K.P., S.Sugunan*-**Photocatalytic Degradation of Malachite Green with TiO_2- Polyaniline nanocomposite**.-CTriC 2013 CUSAT March 2013(22-23 March 2013) National Seminar.

[12]. Sandhya K.P., National seminar 2013 (12th Prof. K.V.Thomas Endowment Seminar) on Novel concepts in Computational and Supramolecular chemistry-Participation-Department of Chemistry, Sacred Heart College, Thevara.December 11-12 (2013)

[13]. K.P.Sandhya, Anju.K.Augustine, S. Mathew, S.Sugunan, V.P.N. Nampoori, **Modification of Optical limiting properties of Polyaniline with nano TiO_2 –**DAE-BRNS National laser Symposium,January8-11 (2014)

[14]. Sandhya K.P., S.Sugunan **Antibacterial activity Studies of TiO_2-Polyaniline Nanocomposites,** International Research Conference on Advanced Techniques in chemistry (IRCATC) 2014, Department of chemistry, St.Alberts College, Ernakulam.

[15]. Sandhya K.P., S.Sugunan*-**Visible light induced Photocatalytic degradation of 4-Nitrophenol by polyaniline sensitized TiO_2 nanocomposites,** CTriC 2014,CUSAT January 2014(17-18 January 2014) National Seminar.

Workshop attended

[1]. Orientation Programme in Catalysis Research -IIT Madras (17th November to 4th December) 2010

…..ൠ…..

PUBLICATIONS

[1]. Visible light induced photocatalytic activity of polyaniline modified TiO_2 and Clay- TiO_2 composites- **K.P.Sandhya**, Suja Haridas, S.Sugunan, Bulletin of Chemical Reaction Engineering & Catalysis, (2013) Vol.8 (2), 145-153.

[2]. Pd, N co doped visible light active TiO_2; A highly efficient photocatalyst for the conversion of Anthracene methanol to Anthraquinone- K M Mothi, **K P Sandhya**, A. H. Salim, S Sugunan**,** International Journal of Environmental Science and Engineering Research (2013) Vol 4(3)77-84.

[3]. Heterogeneous Photocatalytic degradation of 4-Nitrophenol by visible light responsive TiO_2-Polyaniline nanocomposites-**K.P. Sandhya**, S.Sugunan, Journal of Water Supply: Research and Technology – AQUA,IWA Publishing – Accepted.